THE UNIVERSITY of ADELAIDE

The effect of unsteady flow on wind turbine wake development and noise generation

Nima Sedaghatizadeh

School of Mechanical Engineering

The University of Adelaide

Adelaide, Australia

A thesis submitted in fulfilment of the requirements
for the degree of Ph.D. in Mechanical Engineering

In memory of my Father

To my hero

For her unconditional love, measureless support, and all the sacrifices she made throughout my entire life

To my Mother

Thesis Summary

The wake of a wind turbine is a low velocity region characterised by a complex flow structure and increased turbulence intensity. The interaction of the wake with downstream turbines not only results in power loss, it also increases the emitted noise level and fluctuating loads on the turbines blades. Due to their significant effect on wind farm performance and development, the study of wind turbines wake and the noise emitted from wind farms have been the focus of a great deal of research. However, the structure of the wake, its development and its effect on noise emission and propagation from wind turbines are still not well understood.

Aerodynamic noise emitted from wind turbines adversely affects the perception of communities towards wind energy development. Thus, it is vital to find the dominant noise generation mechanism and predict its propagation accurately. Most models developed to predict noise emission from wind turbines are semi-empirical and are based on airfoil noise prediction techniques. These models lack the ability to accurately model the propagation and refraction of the emitted noise, and hence the predicted directivity does not agree well with the observations in the field. In addition to the limitation of these models due to the assumptions they are based on, experimental investigation in this field which are also used to develop wake models, is expensive and difficult in terms of matching the boundary conditions of the experimental setup with the actual conditions in the field. The effect that wakes have on noise emission and performance of wind farms is another concern for the industry, especially during the planning design process. To address this concern, several semi-empirical and analytical models have been developed to predict the wake development, predominantly focused on estimating the velocity deficit in the wake region. Although these models are simple and can provide a reasonable estimation for calculating the power loss in

a wind farm, they are not able to accurately determine the effect of incoming instabilities, atmospheric boundary layer, yaw misalignment and wake interaction.

It is well known that sound is refracted through the interaction with vortices and shear layer in the flow. The wake of a wind turbine consists of complicated vortical structures accompanied with a shear between the low velocity region in the wake and free stream. Moreover, the wake of a wind turbine is highly affected by different parameters such as, instabilities in the incoming flow, wake interaction and the atmospheric boundary layer. Thus, in addition to the incoming flow condition which affects the noise generated by a turbine, the propagation of the noise signals from wind turbines is also affected by the wake behaviour and its development in different conditions.

This thesis commences with a meta-data analysis based on the reported noise perception surveys, combined with the publically available information on the directivity of the airfoil noise at different pitch angles. This approach was used to provide quantitative support for the hypothesised underlying physical mechanisms for noise generation which have been previously reported in literature. The results of this study show that underlying mechanism associated with the perceived noise in the far-field of the turbine blades is amplitude modulation due to partial stall on the blades or interaction of the blades with incoming turbulent structures. This is in contrast with the common belief of trailing edge noise to be the dominant source for the perceived noise and its amplitude modulation due to rotation of the blades. Moreover, it is observed that the majority of the locations in which the noise from whole turbines is perceived by the community, are in close proximity of the wake region. This shows the potential role of the wake on noise propagation patterns and should be accounted for.

To develop a detailed understanding about the noise generation mechanisms, especially stall noise, the aeroacoustic behaviour of an airfoil, which is the fundamental element of wind turbine blades, was investigated numerically. A 3D model of a NACA0012 airfoil in a wind tunnel was developed and the flow field was calculated using an embedded large eddy simulation technique. The flow field and aeroacoustic results were validated against experimental data available in published data. Using Ffowcs Williams and Hawkings analogy, the noise signals were calculated from the surface pressure data of the airfoil under different angles of attack. It was shown that the frequency of the noise decreases as the angle of attack increases and the blade experiences deep stall. On the other hand, the integral length scale of the separated vortices increases as the angle of attack increases, as does the noise level. Results show a perpendicular dipole directivity for the peak frequency when the blade is in stall conditions. However, at low angles of attack the peak frequency directivity shifts towards the leading edge of the airfoil. This is in contrast with the results obtained from the trailing edge noise theory and shows the existence of alternative noise sources near the trailing edge of the airfoil which cannot be predicted by the trailing edge noise theory.

A first step towards investigating the effect of wind turbine wake on the noise emission and propagation is to study the wake development and its structure. An embedded large eddy simulation model was developed and validated against experimental data. For studies conducted in wind tunnels, the simulated results show that vortical structures in the wake propagate to a distance of up to 20 diameters downstream of the wind turbine when the turbine is confined by wind tunnel walls. The distances that the vortical structures propagates reduces as the walls are eliminated from the computational domain. The length of the turbine wake significantly reduces when the turbine is located in an atmospheric boundary layer, where the wake breakdown occurs at 12 diameters downstream of the turbine with strong

downwash due to formation of the longitudinal vortices around the turbine and wake area in the atmospheric boundary layer. Strong downwash in the presence of the atmospheric boundary layer results in a higher velocity magnitude with less turbulence in the far-field region of the wind turbine in this case when compared with the wake formation in uniform flow. This new knowledge may assist wind farm developers in achieving higher turbine densities for future wind farms. The wake development and its structure varies as the terrain on which the turbines are erected varies. It is expected that higher turbulence intensity and shear within the incoming flow results in a reduction in the wake length and stronger downwash due to stronger longitudinal vortices.

To calculate the noise signature in far-field, the Ffowcs Williams and Hawkings (FW-H) aeroacoustic analogy was applied to the developed CFD model for wind turbine. Results revealed that, the highest noise level in the vicinity of a wind turbine corresponds to blade pass frequency and is due to amplitude modulation of the trailing edge noise caused by the rotation of the blade, as well as blade tower interaction. Results also showed that the emitted noise is refracted due to the wind shear in atmospheric boundary layer, as well as the wake and associated turbulent structures. The CFD outcomes showed that the wake breakdown occurs at a distance of 12 diameters downstream of the turbine with a strong downwash due to longitudinal vortices. Contours of sound pressure level at the breakdown location of the wake of the wind turbine showed refraction and modulation of the sound at this location. Results also revealed refraction of the noise towards the ground and wider areas due to existence of the longitudinal vortices.

Thesis Declaration

I certify that this work contains no material which has been accepted for the award of any other degree or diploma in my name, in any university or other tertiary institution and, to the best of my knowledge and belief, contains no material previously published or written by another person, except where due reference has been made in the text. In addition, I certify that no part of this work will, in the future, be used in a submission in my name, for any other degree or diploma in any university or other tertiary institution without the prior approval of the University of Adelaide and where applicable, any partner institution responsible for the joint-award of this degree.

I acknowledge that copyright of published works contained within this thesis resides with the copyright holder(s) of those works.

I also give permission for the digital version of my thesis to be made available on the web, via the University's digital research repository, the Library Search and also through web search engines, unless permission has been granted by the University to restrict access for a period of time.

_____

Nima Sedaghatizadeh

Acknowledgments

I would like to acknowledge the efforts of all the people who have made a contribution towards this thesis. I would cherish memories of all of them for the rest of my life. Many thanks to my mom and family, who has been so understanding throughout my study and always encouraged me to pursue my dreams. I am thankful to their unconditional love and support of all my undertakings, academic and otherwise.

I would also like to thank my wonderful supervisors and mentors Maziar Arjomandi, Richard Kelso, Benjamin Cazzolato, and Mergen Ghayesh for their great guidance, insightful inputs, encouragement, endless support and friendship. I could not possibly wish for a better supervisory board.

I would also like to give thanks to my friends Zahra Bagheri, Farzin Ghanadi, Pouria Aryan, Amir Arya, Maryam Yazdani, Mehdi Jafarian, Mahyar Silakhori, Nataliia Sergiienko and many more that I cannot list all of them who made my journey joyful and helped me through the dark moments of my study.

I am also indebted to the computing officer in Mechanical Engineering, Billy Constantine, and the “Phoenix HPC team”, Matt Westlake, Waseem Kamleh and Exequiel Sepulveda Escobedo for all their help with technical support for high performance computing system.

Contents

"Of all the forces of nature, I should think the wind contains the largest amount of motive power - that is, power to move things. Take any given space of the earth's surface - for instance, Illinois; and all the power exerted by all the men, and beasts, and running-water, and steam, over and upon it, shall not equal the one hundredth part of what is exerted by the blowing of the wind over and upon the same space. And yet it has not, so far in the world's history, become proportionably valuable as a motive power. It is applied extensively, and advantageously, to sail-vessels in navigation. Add to this a few wind-mills, and pumps, and you have about all. That, as yet, no very successful mode of controlling, and directing the wind, has been discovered; and that, naturally, it moves by fits and starts---now so gently as to scarcely stir a leaf, and now so roughly as to level a forest---doubtless have been the insurmountable difficulties. As yet, the wind is an untamed, and unharnessed force; and quite possibly one of the greatest discoveries hereafter to be made, will be the taming, and harnessing of the wind. That the difficulties of controlling this power are very great is quite evident by the fact that they have already been perceived, and struggled with more than three thousand years; for that power was applied to sail-vessels, at least as early as the time of the prophet Isaiah."[†]

Chapter 1 Introduction

1.1 Motivation and perspective

Since the application of fire during the early Stone Age, human beings have always relied on energy sources. With population growth and industrialisation the demand for energy increased dramatically and energy has now became one of the most important challenges that mankind currently faces. For centuries, finite fossil fuels reserves have been the main source of energy and driving force for industry. However, consumption of fossil fuels has resulted in degradation of the natural resources and accumulation of the greenhouse gases. These gases trap the thermal infrared radiation from the sun, which results in an increase in

[†] President Abraham Lincoln, "Discoveries and Inventions" 1860 lecture, New York Times, November 22, 1936.

the earth temperature, also called global warming (Ghosh and Prelas, 2011, Sawin, 2013, Wang and Wang, 2015).

With the current trend of global warming, it has been predicted that by 2047 the mean earth temperature will reach the critical value which is potentially dangerous for biodiversity and ecosystems and is a great threat to human life (Mora et al., 2013). Global warming has already resulted in a worldwide impact such as an increase in global rainfall, resulting in increased flooding in some parts of the world, while other parts are experiencing increased drought. The increase in temperature level has led to the increased melting of polar ice over last century and increasing global sea level. In addition, economic problems associated with the dependency on fossil fuels, and limited resources of fossil fuels have forced authorities to reduce their emissions of greenhouse gases and seek reliable sources of energy (Szulejko et al., 2017, Prasad et al., 2017). The Rio de Janeiro Earth Summit was the first universal agreement on this matter under the United Nations Framework Convention on Climate Change (UNFCCC) in 1992. This convention was ratified by 195 countries to reduce the emission of greenhouse gases and control the effects of climate change (Meakin, 1992). Later, in 1997, the Kyoto Protocol extended the UNFCCC agreement in Rio de Janeiro by legally forcing developed countries to reduce their emissions of greenhouse gases (Depledge, 2000). This protocol was followed by the recent agreement in Paris, which after ratification, will oblige the countries to reduce their greenhouse gases emissions in order to limit the global temperature rise below 2º Celsius (Web reference: http://unfccc.int/paris_agreement).

Since renewable energy from natural resources such as sunlight, wind, hydro, ocean tides, waves and geothermal heat does not emit any greenhouse gases, many countries are moving towards utilisation of these sources. A globally distributed abundant free resource, combined

with mature technology and relatively low construction cost, has made wind energy a reliable source of energy for most governments to meet both their obligations regarding the greenhouse gases emissions and their energy demands (Sawin, 2013). Wind power is widely used in Europe, Asia, the United States, Australia and New Zealand, with a worldwide installed capacity of 486,749 megawatts (MW) at the end of 2016, with a 13% increase compared to 2015 (Global Wind Energy Council, 2016). Furthermore, estimates of wind energy capacity and electricity usage, show that the total worldwide potential capacity for onshore wind energy alone can satisfy the global need for electricity.

Historically, the concept of extracting energy from wind goes back to early recorded history when ancient mariners used wind power for sailing their boats and ships at sea. It was also centuries ago (around 200 BC) when the first steps towards today's wind technology were made by Persians with their vertical axis windmills for grinding grains (Fleming and Probert, 1984, Pasqualetti et al., 2002, Musgrove, 2010). This wind energy extracting system was developed over the centuries and the first large wind electricity generator was installed in Cleveland, Ohio, in 1888 (Kaldellis and Zafirakis, 2011, Dodge, 2006). Figure 1.1 shows the evolution of the windmills from their ancient ancestors to the modern large wind turbines.

(a) (b) (c)

Figure 1.1 Evolution of the windmills from early stages in ancient Persia to Modern large wind turbines (Photos from left to right: Ghader Agheli, and web reference: www.flicker.com).

Studies show that despite having the lowest-cost among the renewable energy sources, there is a necessity to reduce the production cost of electricity cost efficient and comparable with

conventional energy resources in terms of levelized cost of electricity (LCOE) (Avia et al., 2013, van Kuik et al., 2016). One of the ways to reduce the net cost of the wind energy is to increase the amount of energy captured by a wind turbines. This can be achieved by using larger rotors which extract more energy from the wind over a larger swept area (Bolinger and Wiser, 2012, Møller and Pedersen, 2011). Adwen AD-180, which is the largest designed wind turbine with a rotor diameter of 180 meters, has the nominal capacity of 8 megawatts (Adwen webpage, 2016). This turbine itself, on average, can produce enough electricity for more than 6500 households in a year based on the averaged universal household electricity consumption. However, as the size increases the manufacturing process becomes more complex and costly. Another way to reduce the wind energy cost, is to locate wind turbines in a dense clusters to reduce the land area required by a wind farm. This is beneficial since the quality sites are limited and such arrangement can increase the productivity. Moreover, the costs associated with the construction, maintenance, and connection of the turbines to a smaller power grid decreases due to the concentration of all operations to the site area (Manwell et al., 2009).

On the other hand, grouping the wind turbines places the majority of the wind turbines in the wake of upstream ones, resulting in two main problems: loss of available kinetic energy for turbines located in the wake of other wind turbines; and reduction of the life span of the turbines due to the exposure of the turbine blades to an increased turbulence intensity. In addition, increased turbulence intensity not only results in higher fluctuating loads on the blades, which causes the fatigue, but also increases noise emissions (Crespo et al., 1999, Vermeer et al., 2003, Cleijne, 1993). Noise emission is one of the main technical challenges associated with wind farms, resulting in the negative perception of wind farms by communities and residents in their vicinity, thereby restricting the placement and

establishment of the farms (Kaliski and Neeraj, 2013, Walker et al., 2012). The noise emitted from wind turbines derives from a combination of different noise sources and can be divided into mechanical and aerodynamic noises. Generally four types of sound are generated by wind turbines during operation: tonal, broadband, low frequency or infrasound, and impulsive. The tonal sound is associated with mechanical noise, which is caused by the moving machinery, structural resonances or blunt trailing edge noise. Mechanical noise is not considered a concern for modern wind turbines because of advancements in the fabrication techniques and also its high frequency content which dissipates relatively quickly. The broadband sound is characterized by a distribution of frequencies above 100 Hz and is caused by the interaction of the turbulent boundary layer with the trailing edge of the blade. This mechanism is believed to be the cause of the "swishing" or "whooshing" noise from wind turbines (Doolan et al., 2012). Low frequency noise lies in the range of 20 to 100 Hz and is believed to be caused by the interaction of the blade leading edge with the flow perturbation as the blade passes the tower. This also could be caused by large turbulence structures in the incoming flow or stall on the blade (Jakobsen, 2005).

The total power produced by a wind farm is affected by the interaction of the wake with downstream turbines. Previous studies showed that the total power produced by a wind farm is 15-35% less than the total power produced by equal number of isolated turbines (Spera, 2009, Barthelmie et al., 2009). Accordingly, the most important and challenging goal of a wind farm design is to optimise the power production by selecting a more favourable layout. With an appropriately designed dense and staggered turbine arrangement for a wind farm, it is expected to yield a production similar to a sparse arrangement, which occupy less land (Ammara et al., 2002).

Wind turbines are large structures operating in the lowest parts of the atmospheric boundary layer. The atmospheric boundary layer (ABL) which envelopes the planet is a turbulent boundary layer with increasing wind velocity as the height from the earth surface increases. The turbulence intensity and its length scale also vary with height and different terrain topography. Hence, any large structure, which is placed in the ABL, such as tall buildings, skyscrapers, and bridges, are needed to be designed with a careful consideration of the ABL effect. In the case of wind turbines, varying velocity and incoming turbulence directly affects the performance, noise emission, fatigue loads, and consequently turbine life and maintenance cost (Krogstad and Eriksen, 2013, Bai and Wang, 2016). Therefore, in order to reach to an economically viable wind sector, the effect of features of atmospheric boundary layer must be thoroughly understood.

In this regard, this thesis focuses on investigation of the wake development in the atmospheric boundary layer and noise emission from a wind turbine exposed to a wind velocity gradient and turbulence.

In general, industrial wind farm and wind turbine designs do not account for the effects of the ABL and unsteady effects of wake of upstream turbines on downstream turbines. Varying wind velocity in the atmospheric boundary layer and unsteady structures in an incoming flow may cause additional cost to operation of a wind turbine. Dynamic loads exerted on the blades of a wind turbine due to operating in the atmospheric boundary layer, as well as interaction with the wake of upstream turbines may adversely affect their performance and reduce their life time and increase the maintenance cost associated with the wind turbines operation. In order to improve the energy output, life of the turbine, and reduce the emitted noise, a deep understanding of wake development under atmospheric boundary layer conditions is needed. Therefore, the primary motivation of this study is to develop a

well resolved model to study the effect of the atmospheric boundary layer on wake development and its subsequent breakdown. The research goals are not only to develop a model to study the wake but also to find out the effect of the ABL and turbine wake on noise propagation, and to identify the underlying mechanisms associated with the perceived noise from wind turbines.

1.2 Objectives of the research

The primary objective of this research is to improve the understanding and knowledge about wake and noise propagation from wind turbines operating in a variety of atmospheric boundary layers formed by different terrain categories. In order to accomplish this goal, it is first required to understand the underlying mechanisms associated with the perceived noise from wind turbines. Since noise is associated with fluctuating loads on the blade, it can be expected that designs with lower noise level emissions will have a longer life and lower maintenance cost, as well as a better performance.

Since wind turbines are often subjected to the wake of upstream turbines and turbulent atmospheric boundary layer, incoming turbulent structures in the wake and ABL, as well as wind shear, may result in sudden changes of angle of attack on some parts of the turbine blades. This sudden change in the angle of attack, in turn, can result in the partial and transitional stall on the blades which increases the fluctuating loads on the blade and the radiated sound power.

In order to be able to control the radiated noise and increase wind farm performance, it is essential to develop a deep knowledge about the aerodynamic noise and wake development themselves. Although extensive research has been carried out to study the wake development and noise emission from wind turbines, and several models have been developed to predict

the wake development and noise signature, some aspects still require further investigation. More specifically, the mechanism of the perceived noise downstream of a turbine is still open for discussion and there is no scientifically proven and documented link between the noise mechanisms and wind directivity. Although many noise models have been developed in order to predict the noise emission from wind turbines, most of them are based on experimental data and contain many assumptions and simplifications which affect their accuracy and limit their application in the investigation of noise propagation. Moreover, wind turbine wake affects both aerodynamic and aeroacoustic behaviour of a wind turbine. However, limited insight is available for the wind turbine wake development in the atmospheric boundary layer. The developed models, especially the ones commonly used in industry, provide an estimate for velocity deficit downstream of a turbine yet do not account for the effect of incoming turbulence, yaw misalignment, atmospheric boundary layer and wake interaction. Recently developed hybrid models in which the blades are modelled by replacing their effects through averaged forces over the rotor disk, can address some of these shortcomings, however since wind turbines have a wide range of geometries (i.e., height, blade shape, number of blades and upwind or downwind working condition) and the effect of different turbine parameters, especially the number of blades and their shape, on wake formation and structure have not been investigated. Although some efforts have been undertaken to consider the effect of these parameters using correction factors, they are not accurate and cannot be applied for all cases. Developing a high fidelity full CFD model can provide valuable information about the wake development, its breakdown, and surface pressure fluctuation on the blades in order to calculate the aerodynamic noise signature from wind turbines. This information, in addition to improving the knowledge about the wake structure, noise mechanisms and subsequent propagation, could be used by wind farm designers and developers to design an efficient layout with low noise emission.

1.3 Structure of the thesis

In this section a brief structure of the thesis is presented. This thesis is formatted as a collection of manuscripts that have been published or currently under review in peer-reviewed journals. These papers form the basis of this thesis and constitute its chapters which sequentially show the progress of the current study. This includes a meta-data analysis based on the reported noise surveys in order to find the relationship between wind direction and perceived noise from a wind turbine. The presented hypothesis is then followed and supported by a detailed study of the aeroacoustic behaviour of an airfoil at different angles of attack. An embedded large eddy simulation of the flow field around a wind turbine is developed, validated and its fidelity is compared with the current engineering wake models. The developed CFD model is then used to study the wake development of a wind turbine in the atmospheric boundary layer. Finally, using the developed model and based on the wake behaviour, the effect of the wake and the atmospheric boundary layer on wind turbine noise propagation using the FW-H analogy is investigated. The outline of the current thesis is presented briefly below.

In Chapter 2 of the thesis, based on literature review, a detailed framework for the study is established. Initially, the fundamentals of the aerodynamics of a wind turbine are presented, describing the wind turbine wake structure, its development and velocity profile downstream of a turbine. In addition, a collection of the known wake models, especially far-field engineering wake models, are presented and their advantages and limitations are discussed. Moreover, different noise generation mechanisms associated with wind turbines, their characteristics and directivity are presented and discussed. Several noise models which are frequently used for noise predication from airfoils and wind turbines are introduced and their

ability are explained. Finally, different parameters affecting the noise propagation and generation are specified and recent studies are introduced.

Chapter 3 includes a meta-data analysis of reported noise perception surveys conducted in the vicinity of wind farms in order to determine if there is any relationship between the noise propagation, wind direction and speed. In addition to its negative impact on public acceptance of wind farms, the choice of site is also limited by the noise emission from a wind farm which is another obstacle for wind farm development. Therefore, an investigation was conducted in an attempt to improve the knowledge about the origin of the perceived noise and to find a relationship between wind direction and speed and noise directivity. The results revealed that, while it is commonly believed that dominant noise generation mechanism is associated with the trailing edge noise mechanism, the characteristics of the perceived noise is more aligned with partial stall on the blade.

In Chapter 4, the aeroacoustic behaviour of an airfoil is studied using numerical modelling. For this study, a CFD model is developed and validated against published experimental data. The model is based on the modelling of the flow field surrounding an airfoil using Embedded Large Eddy Simulation (ELES). A Ffowcs Williams-Hawkings analogy is then applied to determine the far-field noise signals generated by the unsteady surface pressure fluctuations. As the main outcome of these studies the relationship between the aerodynamic noise emission from a NACA 0012 airfoil and its directivity at different angles of attack corresponding to shallow and deep stall was demonstrated. These results are used to support the hypothesis about the wind turbine noise mechanism associated with the perceived noise presented in Chapter 3, as well as choosing an appropriate noise control system based on the flow feature and noise characteristics. Aeroacoustics results revealed that the noise level increases and the dominant frequency decreases as the angle of attack increases. It was also

found that, in addition to trailing edge noise, there exists some noise sources which results in unconventional directivity patterns at some frequencies and cannot be explained by trailing edge noise theory.

Chapter 5 of this thesis focuses on developing a validated CFD model, as well as its comparison with some of the well-known engineering wake models used in industry. This study was performed to develop a well-resolved model for calculation of a wind turbine wake and the effect of different incoming flow features on the wake development. This is principally motivated by the earlier noise study presented in Chapter 5 which shows the significant effect of the flow pattern on noise propagation. Moreover, the validated model and its outcomes were compared with four engineering models used in industry for wind farm design. The CFD model revealed that the effect of wake can be extended up to 16D downstream of the turbine in uniform flow. It was shown that a combination of semi-empirical wake models can be used to provide more accurate information about wake expansion and velocity deficit in the wake.

The effect of the atmospheric boundary layer on the wake of a wind turbine is studied and explained in Chapter 6. This study is mainly motivated by the lack of information about the effect of the atmospheric boundary layer on wake development, which, in turn, has a significant effect on noise propagation from a wind turbine. The validated model in the previous chapter was used for modelling the flow field in the near-field region as well as in the far-field at the distances of up to 20 diameters downstream of the turbine. Vorticity patterns, wake breakdown, and velocity profiles at different distances downstream of the turbine were studied in detail. The effect of the atmospheric boundary layer on wake development and recovery is emphasised via the comparison of the results in the presence and absence of the atmospheric boundary layer. The fundamental mechanism responsible

for changes in wake development in the presence of the ABL is also explained in detail. It was found that a strong downwash occurs in the presence of the atmospheric boundary layer which results in shorter wake length and higher axial velocity in recovery region when compared with the uniform flow case.

In Chapter 7, a discussion is presented about the noise emission and propagation from a wind turbine in the presence of atmospheric boundary layer. Previous studies revealed that the wake is a low velocity region which consist of a complex system of vortices and turbulent structures. These structures, as well as the shear in the atmospheric boundary layer and the turbine wake, contribute to sound refraction by the wake. In addition, due to the shear in the atmospheric boundary layer, wind turbine blades experience different oncoming velocity during rotation which also changes the aerodynamic noise signature from the blades at different azimuthal angles.

In the final chapter, Chapter 8, a summary on the key findings and main conclusions of the studies undertaken during the course of this research is presented. Moreover, suggestions for future research are proposed for the researchers interested in this field.

1.4 Publications arising from this thesis

The research undertaken for this thesis has resulted in the publication of several articles in international journals and peer-reviewed conference proceedings. Following is the list of manuscripts, published and under-review that have been produced as part of current research.

1.4.1 Published Journal Articles

Sedaghatizadeh, N., Arjomandi, M., Cazzolato, B., & Kelso, R. 2017. Wind farm noises: Mechanisms and evidence for their dependency on wind direction. Renewable Energy, 109, 311-322.

Sedaghatizadeh, N., Arjomandi, M., Kelso, R., Cazzolato, B. S., & Ghayesh, M. H. 2018. Modelling of wind turbine wake using large eddy simulation. Renewable Energy, 115, 1166-1176.

1.4.2 Submitted Journal Articles

1) **Sedaghatizadeh, N.**, Laratro, A., Arjomandi, M., Cazzolato, B. S., & Kelso, R. 2017. Aeroacoustic behaviour of a NACA 0012 airfoil at moderate Reynolds number. Submitted to Journal of Vibration and Acoustics.
2) **Sedaghatizadeh, N.**, Arjomandi, M., Kelso, R., Cazzolato, B. S., & Ghayesh, M. H. 2017. Atmospheric boundary layer effect on the wake of a wind turbine. Submitted to the Journal of Wind Engineering and Industrial Aerodynamics.
3) **Sedaghatizadeh, N.**, Arjomandi, M., Kelso, R., Cazzolato, B. S., & Ghayesh, M. H. 2017. Wind turbine noise propagation operating in atmospheric boundary layer. Submitted to Renewable Energy.

1.4.3 Refereed Conference Articles

Sedaghatizadeh, N., Arjomandi, M., Kelso, R., Cazzolato, B. S., & Ghayesh, M. H. 2016. Effect of wall confinement on a wind turbine wake: 20th Australasian Fluid Mechanics Conference, Perth, Australia.

Sedaghatizadeh, N., Arjomandi, M., Kelso, R., Cazzolato, B. S., & Ghayesh, M. H. 2017 Effect of wake on wind turbine noise propagation: Wind Energy Science Conference 2017 (WESC-2017), Copenhagen, Denmark.

1.5 Thesis format

This thesis is based on the collection of the manuscripts produced during the course of the research and has been submitted according to the format approved by the University of Adelaide. The thesis is provided and available in both hard and soft copy which are identical. The soft copy is available online at the University of Adelaide Library and can be viewed by Adobe Reader.

1.6 References

Adwen 8 MW offshore wind turbine, 2016. Available: http://www.adwenoffshore.com, accessed: 2017.

NASA Report on Climate Change, 2017. Available: https://climate.nasa.gov, accessed: 2017.

Ammara, I., Leclerc, C. & Masson, C. 2002. A viscous three-dimensional differential/actuator-disk method for the aerodynamic analysis of wind farms. *Journal of Solar Energy Engineering*, **124**, 345-356.

Avia, F., Ahlgrimm, J., Kutscher, J., Gagliardi, F., Cruz, I., Hand, M., Holttinen, H., Horbaty, R., Kühn, M., Kühn, P., Musial, W., Peltola, E., Rodrigo, J. S., Schepers, G., Smith, B. & Weis-Taylor, P. 2013. Long-Term Research and Development Needs for Wind Energy. Ad Hoc Group Report prepared for International Energy Agency.

Bai, C.-J. & Wang, W.-C. 2016. Review of computational and experimental approaches to analysis of aerodynamic performance in horizontal-axis wind turbines (HAWTs). *Renewable and Sustainable Energy Reviews*, **63**, 506-519.

Barthelmie, R. J., Frandsen, S. T., Hansen, K., Schepers, J. G., Rados, K., Schlez, W., Neubert, A., Jensen, L. E. & Neckelmann, S. 2009. Modelling the impact of wakes on power output at Nysted and Horns Rev. European Wind Energy Conference. Marseille, France.

Bolinger, M. & Wiser, R. 2012. Understanding wind turbine price trends in the US over the past decade. *Energy Policy*, **42**, 628-641.

Cleijne, J. W. 1993. Results of Sexbierum Wind Farm; single wake measurements. TNO Institute of Environmental and Energy Technology, Technical report.

Crespo, A., Hernández, J. & Frandsen, S. 1999. Survey of modelling methods for wind turbine wakes and wind farms. *Wind Energy*, **2**, 1-24.

Depledge, J. 2000. Tracing the origins of the Kyoto Protocol: An article-by-article textual history. United Nations Framework Convention on Climate Change (UNFCCC) Technical paper.

Dodge, D. M. 2006. The illustrated history of wind power development. Littleton, Colorado: U.S. Federal wind energy program. Available: http://www.telosnet.com, Accessed January 2017.

Doolan, C. J., Moreau, D. J. & Brooks, L. A. 2012. Wind turbine noise mechanisms and some concepts for its control. *Acoustics Australia*, 40, 7-13.

Fleming, P. D. & Probert, S. D. 1984. The evolution of wind-turbines: An historical review. *Applied Energy*, **18**, 163-177.

Ghosh, T. K. & Prelas, M. A. 2011. Wind energy, Book chapter from Energy resources and systems, Volume 2: Renewable Resources, Springer, Netherlands.

Joselin Herbert, G. M., Iniyan, S., Sreevalsan, E. & Rajapandian, S. 2007. A review of wind energy technologies. *Renewable and Sustainable Energy Reviews*, **11**, 1117-1145.

Kaldellis, J. K. & Zafirakis, D. 2011. The wind energy revolution: A short review of a long history. *Renewable Energy*, **36**, 1887-1901.

Kaliski, K. & Neeraj, G. Prevalence of complaints related to wind turbine noise in Northern New England. ICA 2013 Montreal, 2-7 June 2013, Montreal, Canada.

Krogstad, P.-Å. & Eriksen, P. E. 2013. "Blind test" calculations of the performance and wake development for a model wind turbine. *Renewable Energy*, **50**, 325-333.

Kroldrup, L. 2010. Gains in global wind capacity reported.

Manwell, J. F., McGowan, J. G. & Rogers, A. L. 2009. Wind energy explained: Theory, design and application, Wiley Online Library.

Meakin, S. 1992. The Rio Earth Summit: Summary of the united nations conference on environment and development. November 1992, Government of Canada.

Møller, H. & Pedersen, C. S. 2011. Low-frequency noise from large wind turbines. *Journal of the Acoustical Society of America*, **129**, 3727-3744.

Mora, C., Frazier, A. G., Longman, R. J., Dacks, R. S., Walton, M. M., Tong, E. J., Sanchez, J. J., Kaiser, L. R., Stender, Y. O., Anderson, J. M., Ambrosino, C. M., Fernandez-Silva, I., Giuseffi, L. M. & Giambelluca, T. W. 2013. The projected timing of climate departure from recent variability. *Nature*, **502**, 183-187.

Musgrove, P. 2010. Wind power, Cambridge University Press.

Pasqualetti, M. J., Gipe, P. & Righter, R. W. 2002. A landscape of power. Book section from: Wind power in view. San Diego: Academic Press.

Prasad, P. V. V., Thomas, J. M. G. & Narayanan, S. 2017. Global warming effects. Encyclopedia of Applied Plant Sciences (second edition). Oxford: Academic Press.

Sawin, J. 2013. Renewables 2013: Global status report.

Spera, D. A. (ed.) 2009. Wind turbine technology: Fundamental concepts in wind turbine engineering, second edition, ASME.

Szulejko, J. E., Kumar, P., Deep, A. & Kim, K.-H. 2017. Global warming projections to 2100 using simple CO2 greenhouse gas modeling and comments on CO2 climate sensitivity factor. *Atmospheric Pollution Research*, **8**, 136-140.

Thor, S.-E. & Weis-Taylor, P. 2002. Long-term research and development needs for wind energy for the time frame 2000–2020. *Wind Energy*, **5**, 73 - 75.

Tonin, R. 2012. Sources of wind turbine noise and sound propagation. *Acoustics Australia*, 40, 20-27.

United Nations Framework Convention on Climate Change, 2016, UN Repoert on Paris agreement. Availabale: http://newsroom.unfccc.int, Accessed: 2017.

van Kuik, G. A. M., Peinke, J., Nijssen, R., Lekou, D., Mann, J., Sørensen, J. N., Ferreira, C., van Wingerden, J. W., Schlipf, D., Gebraad, P., Polinder, H., Abrahamsen, A., van Bussel, G. J. W., Sørensen, J. D., Tavner, P., Bottasso, C. L., Muskulus, M., Matha, D., Lindeboom, H. J., Degraer, S., Kramer, O., Lehnhoff, S., Sonnenschein, M., Sørensen, P. E., Künneke, R. W., Morthorst, P. E. & Skytte, K. 2016. Long-term research challenges in wind energy – a research agenda by the European Academy of Wind Energy. *Wind Energ. Sci.*, **1**, 1-39.

Vermeer, L. J., Sørensen, J. N. & Crespo, A. 2003. Wind turbine wake aerodynamics. *Progress in Aerospace Sciences*, **39**, 467-510.

Walker, B., Hessler, G. F., Hessler, D. M., Rand, R. & Schomer, P. 2012. A cooperative measurement survey and analysis of low frequency and infrasound at the Shirley Wind Farm in Brown County, Wisconsin, Report prepared for Public Service Commission of Wisconsin.

Wang, S. & Wang, S. 2015. Impacts of wind energy on environment: A review. *Renewable and Sustainable Energy Reviews*, **49**, 437-443.

Chapter 2 Literature Review

In this chapter a review of the literature and studies conducted in association with wind turbine wake and noise is presented. This is done in order to find the gaps and present the objectives of the current study.

2.1 Wind turbine operation, principals, and aerodynamics

Today's wind turbines have come a long way compared to the wind mills of old. The extracted energy in early windmills was typically used to grind grain or pump water, while in modern wind turbines it is used to generate electricity. Modern wind turbines are the largest rotating man-made structures, with rotor diameters nearly twice the wing span of an Airbus A-380. In addition to sitting large wind turbines in clusters, which are the commercial means of electricity generation, small scale wind turbines are also viable electricity generators for remote areas and enable decentralizing the energy supply in rural and urban areas (Peacock et al., 2008, Bai and Wang, 2016).

Based on the orientation of the rotation axis, wind turbines are classified as horizontal axis wind turbines (HAWT), in which the rotation axis is horizontal and perpendicular to the tower and vertical axis wind turbines in which the rotation axis is vertical and aligned with tower axis (VAWT). Figure 2.1 shows a three bladed horizontal axis wind turbine (Figure 2.1a) and a Darrieus vertical axis wind turbine (Figure 2.1b). Turbines can also be categorized based on the driving force as drag and lift type turbines. Due to limited application of the vertical axis wind turbines and drag type of wind turbines, the horizontal axis wind turbine is considered for the purpose of this study. Furthermore, horizontal axis

wind turbines can be also divided into upwind and downwind wind turbines based on the position of the rotor with respect to the tower (Hansen, 2008, Manwell et al., 2009, Neustadter and Spera, 1985).

(a) (b)

Figure 2.1 Two common types of wind turbines: a) A three bladed horizontal axis wind turbine, b) A Darrieus vertical axis wind turbine (right) in field (web reference: www.flicker.com).

Based on the control mechanisms for torque and rotational speed, the turbine rotor may also be categorised as either pitch regulated or stall regulated. Pitch regulated wind turbines utilise an active pitch control system, which controls the rotational speed of the rotor by changing the pitch angle of the blades (rotating the blades about their own axis) in order to prevent high rotational speeds and aerodynamic torques which can damage the turbine. On the other hand, the blades of stall regulated turbines, are designed in a way that their rotational speed and consequently power production of the rotor decreases above the certain wind speed (Joselin Herbert et al., 2007, Hansen, 2008). Active stall controlled wind turbines

are also another type of turbine which use a combination of the pitch and stall control mechanisms to control the power and prevent excessive load on the blades. These types of turbines use pitch control at low wind speeds to produce the maximum power, while the power at high wind speed is limited by the stall control mechanism (Barthelmie et al., 2009, Ahlstrom, 2005). The HAWT shown in Figure 2.1(a) is an upwind wind turbine since the rotor is located upstream of the tower. Most of today's commercial wind farms consist of upwind horizontal axis wind turbines with lift as their primary driving force for rotor. Due to their large application in commercial wind power generation this type of wind turbine is investigated in this study.

2.1.1 Wind turbine parts and working concepts

All wind turbines consist of several common parts. A generator which converts the rotary motion to electricity and a gearbox, which transmits the movement of rotating shaft to the generator, are common parts of all types of wind turbines. In HAWTs, the gear box, generator and yaw alignment system are placed in the nacelle (Ahlstrom, 2005, Joselin Herbert et al., 2007). Figure 2.2 shows a schematic view of a typical three bladed wind turbine and its components in the nacelle. The layout shown in the figure is not the only possible configuration used in industry. For example, in some configurations the gearbox is replaced by a number of generators (Hansen, 2008, Ahlstrom, 2005). A horizontal axis wind turbine has the best performance when the rotor axis of symmetry is parallel to the incoming wind. Therefore a yaw mechanism and wind vane are also embedded in the nacelle to change the orientation of the rotor to keep the rotor plane perpendicular to the flow. In addition to the mentioned parts, a horizontal axis wind turbine makes use of several other parts and components such as a foundation, bearings, a pitch control system, brakes, etc. Keen readers are referred to the references and company manuals which include detailed information

about parts and components of different wind turbines (Ghosh and Prelas, 2011, Ross and Altman, 2011).

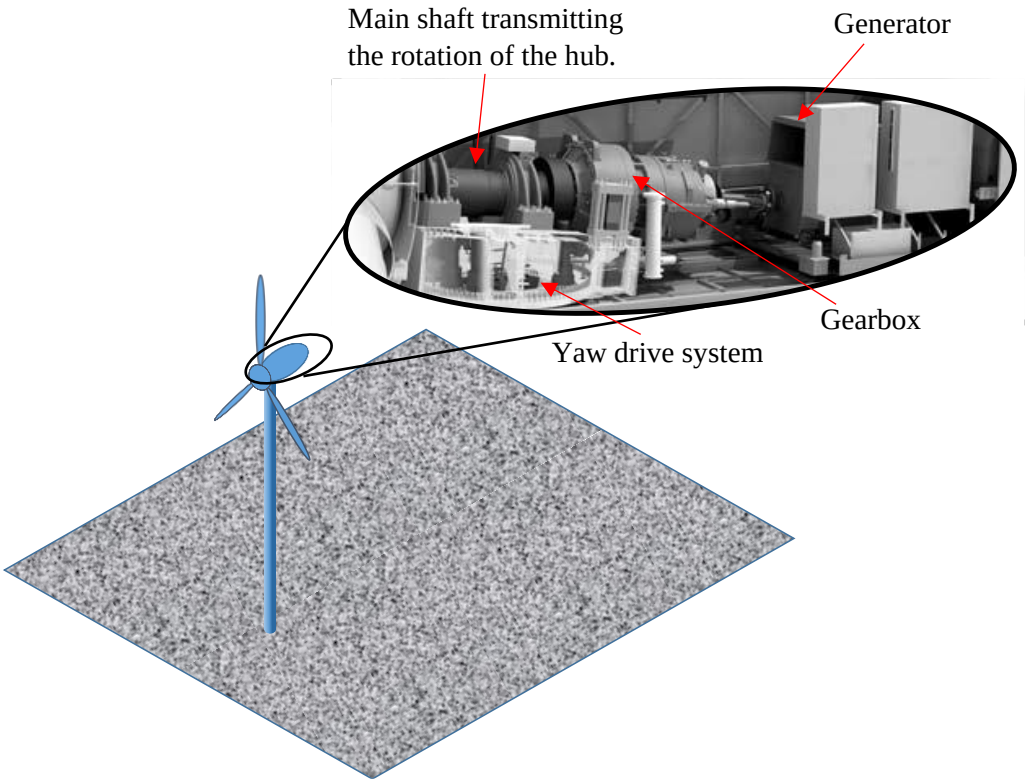

Figure 2.2 Schematic of a typical wind turbine and main components in the hub (permission is obtained from Siemens for the layout provided in this figure).

The early wind turbine blades in 80s were designed based on the airfoils developed for aircraft such as NACA airfoils. Since these blades were not designed to operate at pre-stall conditions at high angles of attack, which frequently happen during the operation of a wind turbine, the performance of the turbines were not optimum. Nowadays, blades of modern wind turbines are designed using tested and proven airfoils tailored for this specific application. In addition, different sections of the turbine blade experience different relative air velocity and hence require specific structural considerations (Singh et al., 2012, Bertagnolio et al., 2001, Fuglsang et al., 2004, Grasso, 2011). Hence, in order to design an efficient blade, several airfoil profiles are used along the blade. The fundamental parameter in rotor and blade design, in addition to careful consideration for structural strength, is the

aerodynamic performance of the rotor. This is usually represented by the ratio of lift to drag. Therefore, generally airfoils with high lift to drag ratio (usually $\frac{L}{D}$>30) are chosen for rotor design. Prior to moving into more details, it is necessary to introduce some basic definitions and design parameters of wind turbine (Ruano et al., 2012, Manwell et al., 2009, Dixon, 2008).

Tip speed ratio

Tip speed ratio is the ratio of blade velocity to the relative velocity of the flow and is an important parameter in designing wind turbines. It is given as,

$$\lambda = \frac{\Omega R}{U_w} \tag{2.1}$$

where λ is tip speed ratio and Ω, R, U_w, are rotational velocity of the rotor, rotor radius, and relative wind velocity, respectively. Operating conditions and other aspects such as efficiency, torque, mechanical stress, and noise of the wind turbine are directly affected by selected tip speed ratio (Sherry et al., 2013, McTavish et al., 2013). For example, increasing tip speed ratio can improve the efficiency of a rotor, however it may result in adverse effects such as increased unsteady aerodynamic loads and increased radiated noise.

Solidity

Turbine solidity represents the fraction of rotor swept area which is covered by the blades and is defined as the ratio between the total blade area to the area of the rotor disk,

$$\sigma = \frac{Bc(r)}{2\pi r} \tag{2.2}$$

where σ is the local solidity, B is the number of turbine blades, c is the chord length of the blade at a given section and r is the local radius of interest at given distance from the rotation axis of the blade.

Power coefficient

The power coefficient represents the amount of energy captured by the wind turbine from the maximum available energy in the incoming wind. Considering a tube of air with a speed of U approaching the rotor, one can calculate the maximum available kinetic energy (e) for a unit mass of the air as follows,

$$e = \frac{1}{2}U^2. \tag{2.3}$$

The available power, P_0, in the wind passing through a cross-section A can then be calculated using following expression,

$$P_0 = \dot{m}e = (\rho UA)e = \frac{1}{2}\rho U^3 A \tag{2.4}$$

where $\dot{m}$ is mass flow rate, and ρ is density. The power coefficient is defined as,

$$C_p = \frac{P}{\frac{1}{2}\rho U^3 A} \tag{2.5}$$

where P is the output power of the turbine.

Thrust coefficient

The thrust coefficient C_T is another non-dimensional parameter used to characterise the thrust of the turbine rotor and is defined as

$$C_T = \frac{\text{Thrust Force}}{\text{Dynamic Force}} = \frac{T}{\frac{1}{2}\rho A U^2} \tag{2.6}$$

where T is the thrust of the rotor.

Induction factor

According to Newton's third law, when the air exerts a force on the turbines blades, an equal and opposite force (and torque) is exerted to the air by the blades. This induces an axial velocity component to the air opposite to the direction of the wind and a tangential velocity component opposite to the rotation of the rotor blades. The effect of induced velocities on the relative velocity of the wind is represented through the axial and tangential induction factors (Sørensen, 2016, Wang, 2012, Sanderse, 2012). Figure 2.3 shows the relative velocity and the effect of induction factor on the angle of attack.

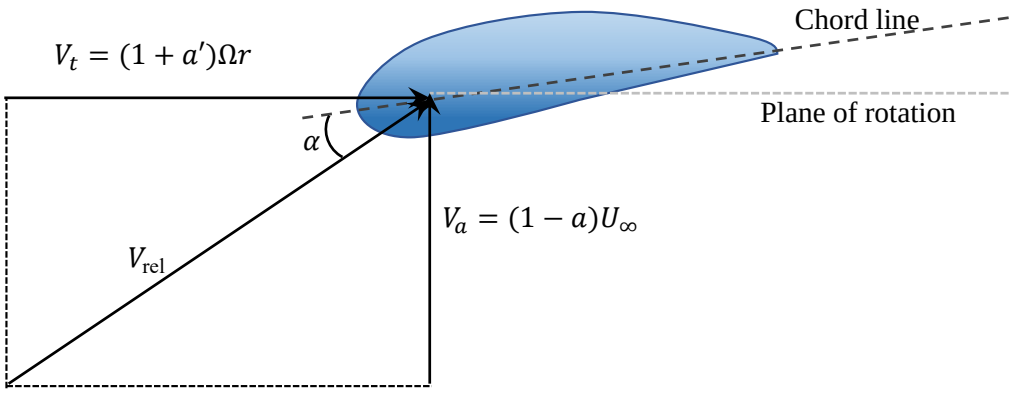

Figure 2.3 Schematic of a cross-section of a wind turbine blade showing the effect of induced velocity, relative velocity (V_{rel}) and angle of attack (α). V_t and $V_a$are the tangential and axial velocity respectively. Parameters a, a', α and U_∞ are axial induction factor, tangential induction factor, angle of attack and incoming wind velocity, respectively.

Twist angle

The blades of a wind turbine, are fabricated with twist and varying chord in the radial direction. This is done such that there is approximately a constant angle of attack along the span of the blade length in order to extract the highest rate of energy. A simple way to

calculate the twist and chord of a blade is based on the blade element method (BEM). In this method blade is divided into several elements along its length as shown in Figure 2.4.

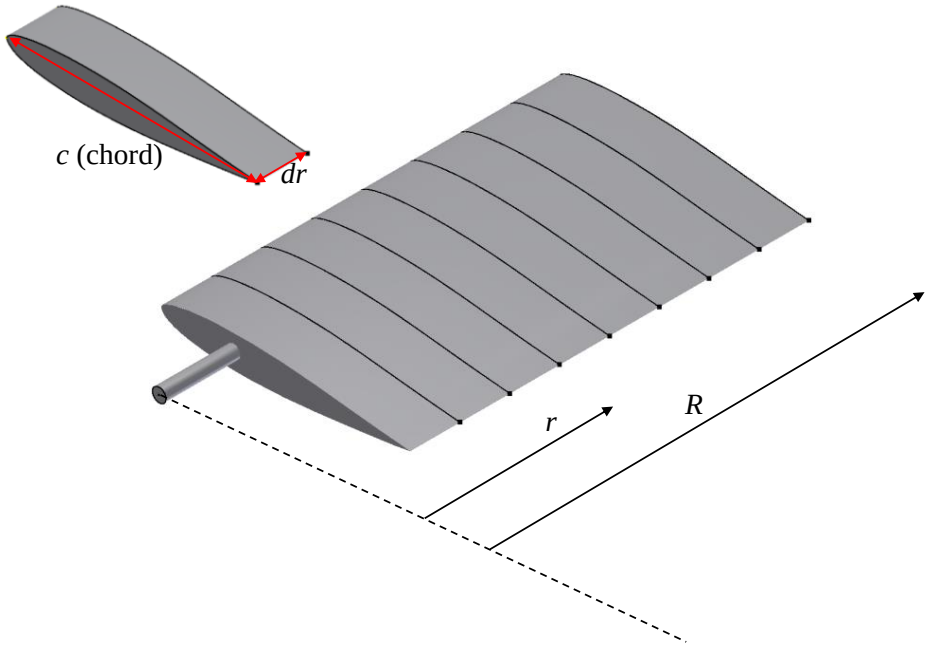

Figure 2.4 Schematic of the blade sections used in calculation of twist and chord by the Blade Element Momentum (BEM) method, where *r* is the radial distance, *dr* is radial element width, and *R* is the radius of the rotor.

The twist angle, φ, and chord length, c, in each section are calculated using the following equations (Manwell et al., 2009, Hansen, 2007),

$$\varphi = \tan^{-1}\left(\frac{2}{3\lambda_r}\right) \tag{2.7}$$

and

$$c = \frac{8\pi r \sin\varphi}{3BC_l\lambda_r} \tag{2.8}$$

where, λ_r, C_l and B are local tip speed ratio, lift coefficient and number of blades, respectively.

2.1.2 Wind turbine aerodynamics

Like any structure or object interacting with air, such as tall buildings, cars and airplanes, the aerodynamic behaviour, the forces and resulting motion of the wind turbine are of high importance. Since the turbine rotor is the driving part of a wind turbine and the primary component in the chain of power extraction from wind, it plays a vital role in determining of the performance of a wind turbine. Therefore to accurately predict the turbine performance it is of a great importance to understand its aerodynamics and flow field in its vicinity.

The first attempts to analyse wind turbine performance and aerodynamics were made by Betz and Glauert in the 1930s. Following their work, Wilson, Lissaman and Vries in 1970s further improved the Glauert and Betz approach (Betz, 1966, Glauert, 1926, Glauert, 1935, Wilson and Lissaman, 1974, Vries, 1979). These methods are all based on combining momentum theory and blade element theory into a strip theory to calculate the aerodynamic characteristics of an annular section of the turbine rotor. The characteristics of the entire rotor is then calculated by integrating and summing the calculated parameters for each section.

A simple approach to analyse the wind turbine performance is presented below to illustrate the basic concepts which are used in wind turbine aerodynamics (Vaz et al., 2011, Mikkelsen, 2003). In this approach, a control volume comprising a non-rotating streamtube of the wind approaching the rotor disk is considered. The rotor itself is considered as a porous disc which creates a discontinuity in pressure. As the flow reaches the turbine, the blocking effect of the disc results in the expansion of the streamtube as shown in Figure 2.5.

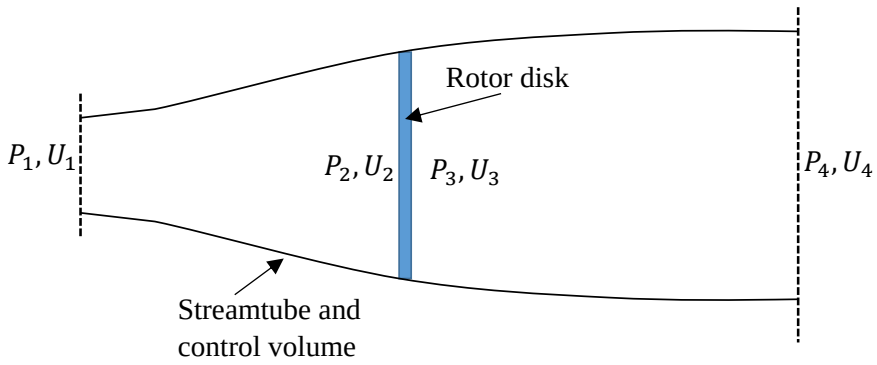

Figure 2.5 Control volume and flow feature for 1-D momentum theory analysis. $P_{1,2,3,4}$ is the pressure at each section, and $U_{1,2,3,4}$ is the air velocity at the associated sections.

Using Bernoulli's law, conservation of linear momentum and considering the axial induction factor, the equation for the output power of the rotor, *P*, may be derived as

$$P = \frac{1}{2}\rho A U^3 4a(1-a^2). \tag{2.9}$$

where a, A, and U represent axial induction factor, rotor swept area and wind velocity, respectively. Using the Equation (2.9) for output power, the power coefficient can be calculated using Equation (2.10) as,

$$C_P = 4a(1-a^2). \tag{2.10}$$

Differentiating C_P with respect to a, the maximum value of C_P for an ideal rotor may be obtained as $C_{P,max} = \frac{16}{27} = 0.5926$ for a value of $a = 1/3$. This means that for an ideal rotor maximum power is produced if it operates such that the air speed at the rotor is 2/3 of the free stream velocity (Vaz et al., 2011, Mikkelsen, 2003, Hansen and Butterfield, 1993).

The presented method, also known as the blade element momentum (BEM) approach, contains several assumptions, and in particular, it does not account for the effect of rotation of the flow due to interaction with the blades. As mentioned earlier, the rotational effect induces a tangential velocity which should be considered in more accurate analysis of the aerodynamic characteristics of the turbine rotor. In order to account for the effect of flow

rotation in the wake and consequent pressure drop, several variations of BEM have been developed. In the most simple and widely used approach the wake rotation is considered through a tangential induction factor without accounting for the pressure drop caused by the wake rotation. However, even with these modifications, the interaction of the flow with rotating blades results in a complex flow pattern, the analysis of which needs more accurate approaches with no or less simplifying assumptions. In addition to the complexities associated with the flow behaviour due to the interaction with the rotating blades, unsteady incoming structures result in unsteady loads on the blades and add to the inaccuracies in the calculations by these simple models.

2.1.3 Wind turbine operating environment

The characteristics of the incoming wind which provides driving force for a wind turbine has a significant effect on its aerodynamic performance. Unsteady structures in the wind generated due to surface roughness, upstream turbines and gusts, influence the forces on the turbine blade. The extent of these effects depends on the parameters of incoming structures and sometimes affect the entire blade. The spacing of the wind turbines in wind farms significantly affects the wind farm overall performance, noise emission and also construction and maintenance costs. Usually a distance of 5-7 diameters is considered when designing the layout of wind turbines in order to prevent negative effects of close proximity. Therefore, it is vital to have an understanding about the operating environment of a turbine (Ghadirian et al., 2014).

Similar to any large structure erected on the surface of the earth, wind turbines operate in the lower part of the atmospheric boundary layer (ABL). This part of the atmospheric boundary layer includes turbulent structures which is mostly associated with the surface

characteristics. In this region, mean properties of the flow such as velocity, temperature and humidity are significantly affected by ground surface characteristics and have their largest changes. Moreover, the existence of roughness elements such as hills, buildings and trees induces additional turbulences within the wind and also changes the gradient of the mean wind velocity profile. The flow in ABL is complex with a continuous spectrum of different flow related characteristics such as velocity, pressure and temperature. Considering all the spectrum in any wind engineering study is difficult and computationally expensive. A way around this is to use the simplified models based on the effective scales for a given application. Thus for wind engineering problems, usually simplified time averaged models with embedded turbulences (appropriate scales should be chosen based on the application and the parameter which is investigated) are utilised in order to account for the complex temporal and spatial nature of the ABL (Saurabh and Ramesh, 2014, Albertson et al., 1998).

The blades of a wind turbine also experience varying incoming wind velocity during every resolution due to the vertical gradient of wind speed, which consequently results in additional dynamic loads on the blades (Flay, 2015, Troldborg et al., 2007, Gómez-Elvira et al., 2005, Kasmi and Masson, 2008). Generally, two models of wind velocity profile are widely used in wind engineering applications: the log-law and the power-law. Although both models have uncertainties due to the turbulent nature of wind, they can be used to provide good estimates of the wind velocity variation with elevation in engineering applications. Studies on the accuracy of these models revealed that the log-law model produces more accurate wind profiles in comparison to the power-law model (Tian et al., 2014, Kircsi and Tar, 2008). However, due to its simplicity, the power-law model is more frequently used in engineering applications (Li et al., 2010, Mehta et al., 2014, Cheung et al., 2016, Newman, 1977).

The power-law and log-law profiles are given as:

$$V_w(h) = V_{w,h_0}\left(\frac{h}{h_0}\right)^e \qquad \text{(power-law)} \tag{2.11}$$

$$V_w(h) = \left(\frac{U_\tau}{\kappa}\right)\ln\left(\frac{h}{z_0}\right) \qquad \text{(log-law)} \tag{2.12}$$

where, $V_w(h)$ is the mean wind velocity at a height h, V_{w,h_0} is the wind velocity at a reference height h_0 (which is usually taken as 10 m or hub height), e is the power-law exponent, $U_\tau = \sqrt{\tau/\rho}$, $\kappa = 0.4$ is the von Karman constant, τ is the Reynolds shear stress at the surface, and z_0 is the surface roughness. The height of the ABL, as well as the power-law exponent, vary based on the category of the terrain categories. The validation of the exponent in power-law equation is based on the surface roughness and thermal stability in the ABL (Table 2.1 shows the power-law exponent for different terrain categories based on the surface roughness). Figure 2.6 shows different ABL velocity profiles for different terrain categories based on ANSI A58.1-1982 and ANSI/ASCE-7-1988 (American National Standards Institute & United States, Liu, 1990).

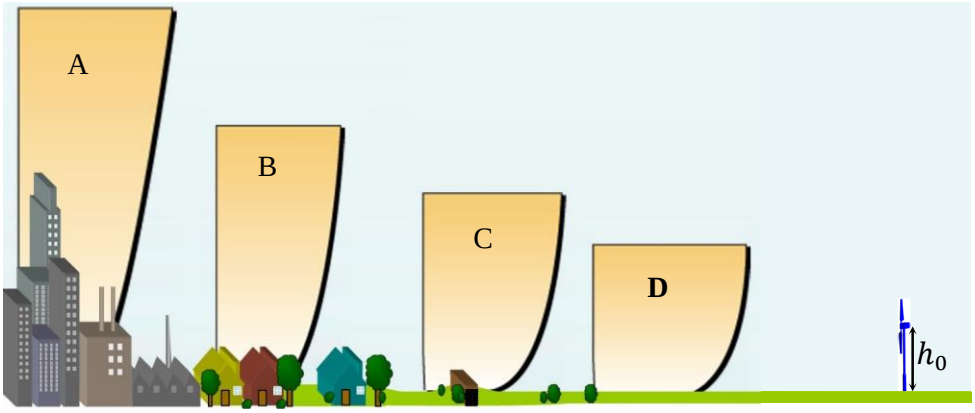

Figure 2.6 Different terrain categories and ABL velocity profiles, A: large cities and hilly terrains, B: suburban areas and terrains with forest, C: Open terrain or farmlands, D: Open coast or sea.

Table 2.1 Terrain roughness, power-law exponent, and ABL thickness (ANSI A58.1-1982 and ANSI/ASCE-7-1988 standard).

Terrain Category	Terrain Roughness (cm)	Power-Law Exponent	Atmospheric Boundary-Layer Thickness (m)
A (large cities)	80	1/3	457
B (suburban area)	20	2/9	366
C (open terrain)	3.5	1/7	274
D (open coast)	0.7	1/10	213

The other factor which plays an important role in the study of any structure in the turbulent boundary layer is turbulence intensity, which is a factor used to quantify the level of unsteadiness in the fluid flow defined as a system of stochastic and random eddies with different length scales added to the mean wind flow (Cheung et al., 2016, Bai and Wang, 2016, Tian et al., 2014). The main cause for formation of the turbulence in a wind are the ground obstacles and surface roughness such as hills, buildings and trees. The other mechanism which contributes in generation of the turbulence in the ABL is the natural convection due to solar heating which may result in movement of the large masses of air. In early wind turbine designs, the hub height turbulence was considered for design purposes. However, large rotors of modern wind turbines experience significant variation of turbulence during rotation. Thus an accurate estimation of the spatial distribution of turbulence intensity is required. The streamwise turbulence intensity (I_u) in ABL can be defined by the following expression (Wilcox, 1998, Lumley and Panofsky, 1964),

$$I_u(h,t) = \frac{u'_{rms}(h,t)}{\bar{U}(h)} \tag{2.12}$$

where $u'_{rms}(h,t)$ is the root-mean-square of the fluctuating component of the instantaneous wind velocity relative to the mean wind speed of $\bar{U}(h)$ at height h. Several models and expressions have been proposed to estimate the turbulent intensity, most of which are semi-

empirical and are based on the experimental data. A commonly simple model used in wind turbine design proposed by Panofsky (1967), is given by

$$I_u(h) = \frac{0.88}{\ln(h/z_0)}. \tag{2.13}$$

where z_0 is the roughness height. Panofsky model is a simple model which produces an estimation for the turbulence variation with height but it fails to account for the wind speed effect. Kaimal et al. (1976) presented a method to calculate the turbulence spectrum at a given wind speed, however their method does not provide any information about the spatial distribution of the turbulence. Recently, Cheung et al. (2016) proposed a framework to calculate the turbulence intensity across a rotor disk. They related the turbulent fluctuations to the mean shear profile, and then calibrated their model using LES data for various shear conditions. However, to apply their method one needs experimental data in order to calibrate the equation for the given conditions.

In addition to small scale turbulences which their effect is manifested via turbulence intensity and superposition to the mean wind velocity, wind gusts, which are the sudden change of the instantaneous speed of the wind over a specified period, also affect the performance of a wind turbine (Kristensen et al., 1991). Gusts are caused by turbulence due to friction, wind shear or solar heating of the ground. In comparison with small scale turbulences, wind gusts can sustain time-scales of up to several seconds and length scales of tens of meters. Due to their temporal and spatial distribution, gusts can affect the whole rotor area and result in severe unsteady loads on the turbine blade.

In order to determine the effect of gusts on aerodynamic loads on structures, the gust factor method, which relates the hourly mean wind speed to the maximum gust wind speed during

the gust period, is usually used (Ashcroft, 1994; Yu and Gan Chowdhury, 2009). While there is a relationship between the turbulence intensity and gust factor, since turbulence intensity is calculated using the root-mean-square of velocity fluctuations, it cannot be used for calculation of the maximum loads due to the wind gusts because it does not directly provide information about the gust peak. Attempts have been made to establish a relationship between turbulence intensity and gust peak using semi-empirical equations developed based on meteorological data (Ashcroft, 1994, Cook, 1997, Cook, 1985, Harstveit, 1996). Proposed semi-empirical models show a discontinuity near the ground surface and in the lower atmospheric layer where turbines operate, while in other parts they usually have an independent behaviour with respect to height (Harstveit, 1996). One of these models which relates the gust peak to turbulence intensity was proposed by Melbourne (1978). The experimental results revealed that the peak gust has a linear relationship with the turbulence intensity and mean wind velocity at a specific height and can be calculated by the following expression,

$$V_G = \overline{V_w(h)}\left(1 + 3.5 I_u(h)\right) \tag{2.14}$$

where the V_G, $\overline{V_w(h)}$, and $I_u(h)$ are gust peak velocity, mean wind velocity and streamwise turbulence intensity at height *h* over the averaging period, respectively.

Another environmental factor which should be considered for wind turbine aerodynamics is the change in wind direction (Kaimal et al., 1976, Barthelmie et al., 2008). Wind turbines can adjust themselves to the average wind direction by the means of a yaw system. The response time of a yaw system to a change in wind direction is about several minutes due to the significant gyroscopic loads and structural limitations caused by the rotation of the large rotor. Therefore, wind turbines cannot react to such sudden and sharp changes in wind

direction. Large turbulent structures can sometimes change the wind direction by $\pm 20° - 30°$, which can consequently result in a loss of performance and structural damage as a result of the temporary yaw misalignment (Hansen and Butterfield, 1993, Aditya and Sanjiva, 2015).

In addition to the parameters associated with ABL and its features, the interaction of wind turbines with each other in a wind farm should also be considered. Quality sites for wind farms are limited and their layouts and positions are heavily restricted by a variety of factors including legislation, construction and maintenance costs, terrain, and environmental aspects. Therefore, wind farms are usually tend to be built in dense clusters (Barthelmie et al., 2008). However, grouping the wind turbines may place the majority of the turbines in the wake region of the upstream ones resulting in two main problems: loss of available kinetic energy for turbines located in the wake of others and reduction of life span due to increased turbulence intensity. Increased turbulence intensity not only results in higher fluctuating loads on the blades, which can cause fatigue, but also increases noise emissions (Crespo et al., 1999, Vermeer et al., 2003, Cleijne, 1993). Noise emission from the wind turbines can be perceived at distances far from the wind turbines. It is one of the main issues related to wind farms and often results in the rejection of wind farms by communities and residents in their vicinity thereby restricting where they may be cited (Kaliski and Neeraj, 2013, Walker et al., 2012). In addition to an increased level of turbulence intensity in the wake, it is a low velocity region which results in power loss for the turbines placed in this region. Thus, the layout of a wind farm is very important in order to extract the maximum energy from a limited space available for construction.

Due to its significant effect on wind farm performance, noise emission, power production and even payback period, wind turbine wakes have been extensively investigated by

researchers and several models for prediction of the flow field in the wake region have been developed are discussed in the next section.

2.1.4 Wake of a wind turbine

The wake is a region of velocity deficit downstream of any object located in a fluid flow. In the case of wind turbines, the airflow downstream of a turbine has less momentum due to the transfer of energy from the flow to wind turbine blades (Whale et al., 2000). The wake of a wind turbine consists of a combination of different turbulent and vortical structures generated due to the interaction between the free stream, the moving blades and the generated vorticity sheets (Sezer-Uzol and Long, 2009, Whale et al., 2000). Since wind turbines consist of moving blades, a vortex system similar to a translating wing is expected to exist (Hansen, 2007). However, significant differences exist due to the effects of the blade rotation and the complex geometry of the blades (Sezer-Uzol and Long, 2006). According to the Newton's third law, the blades exert forces equal, but in the opposite direction to the fluid, forcing the airflow to move in the opposite direction.

The structure of the wind turbine wake is very complex due to the formation of induced tangential and radial velocity components of the air particles (Burton et al., 2001). Generally, the wake region comprises three types of vortices: the vortex sheet of bound lifting vortices, strong tip vortices at the edge of the rotor wake which forms the spiral (also called helical) structure downstream of the wind turbine; and the root or hub vortices which translate in a linear path along the rotor axis as shown in Figure 2.7 (Ivanell et al., 2009).

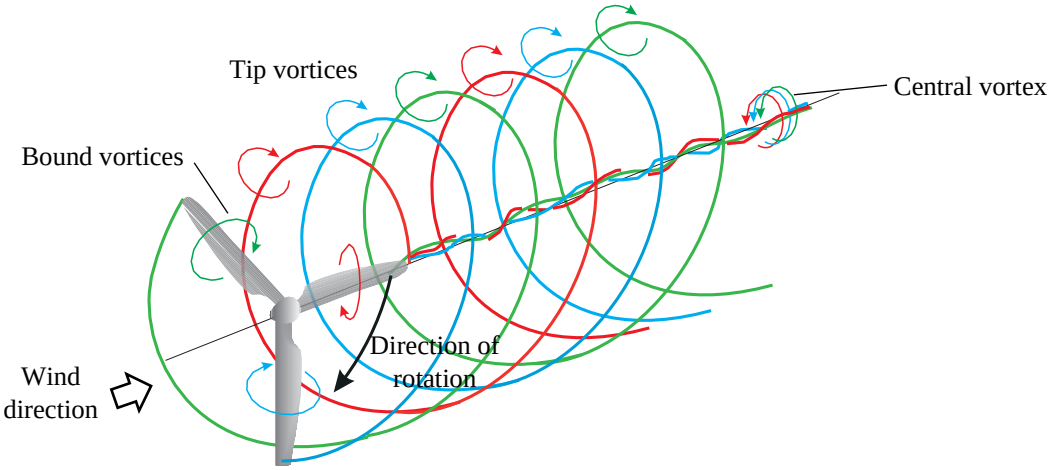

Figure 2.7 Schematic diagram of the typical vortex system downstream of a wind turbine (Ivanell et al., 2009).

The wake of a wind turbine can be categorised into two regions: near-wake and far-wake. The near-wake is the region immediately downstream of the turbine in which the effect of the rotating blades is dominant. This region is also characterised by helical tip vortices and high velocity deficit. The near-wake region is typically defined as $0 \leq x/D \leq 5$, where D is the rotor diameter and x is the downstream distance (Vermeer et al., 2003, Schepers, 2003, Ainslie, 1988, et al., 2008, Crespo et al., 1999). On the other hand, the far-wake commences where the actual rotor shape is less important and the flow is characterised by a significant velocity deficit and increased turbulence. In this region, the convection and turbulent diffusion are two main mechanisms which in addition to the ambient turbulence and topographic effects determine the flow condition (Vermeer et al., 2003, Sanderse, 2012, Mo et al., 2013). Figure 2.8 schematically shows the typical wake expansion and velocity profiles downstream of a wind turbine. It can be seen that due to the velocity difference between the wake and the free stream, a shear layer including tip vortices is created between the free flow and wake region (Crespo et al., 1999, Blomhoff, 2012). Further downstream, the induced turbulent eddies inside the shear layer mix with the free stream and with the low-velocity flow in the wake causing the shear layer to expand. The near-wake ends where the shear layer spreads inwards and reaches the wake axis. At this point the tip vortices

breakdown and the static pressure reaches the atmospheric pressure (Mo et al., 2013, Crespo et al. 1999). Mo et al. (2013) defined different locations for the boundary between near and far-wake regions in regard to the different wind speeds. Their study further showed that as the wind speed increases, the length of near-wake also increases (Mo et al., 2013). They suggested average location between start of the wake instability and its complete breakdown as the boundary of distinction between the near and far-wake regions of a turbine (Mo et al., 2013). Based on their finding the wake region of a wind turbine can be divided into three regions: (i) near wake with a strong and stable system of helical vortices, (ii) transition region in which instabilities are initiated by tip vortices and ends as they break down, (iii) far wake region which starts when the helical vortices have collapsed. Collapse occurs as the helical tip vortices break down and start to mix by the strong vortical structures in the wake.

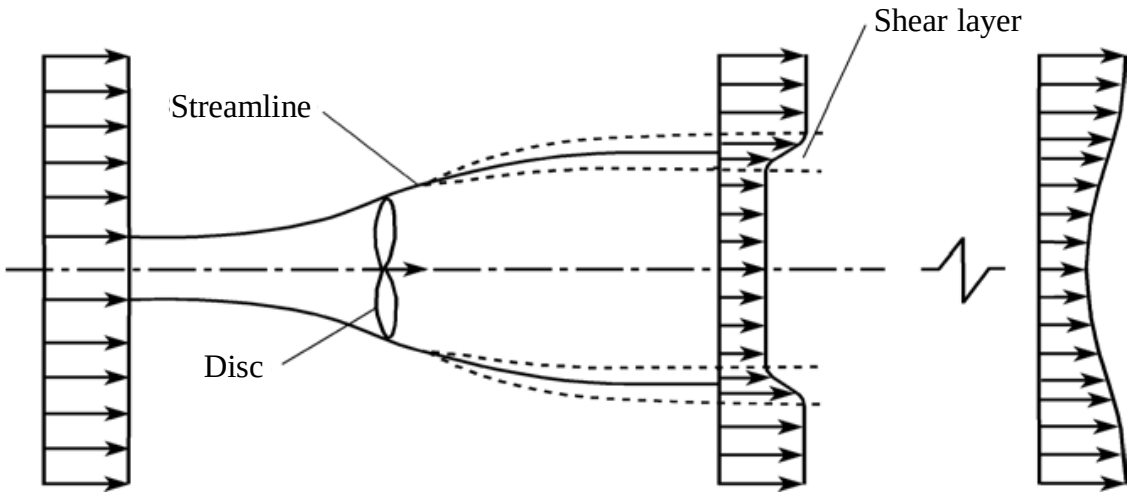

Figure 2.8 Schematic representation of the velocity profile: wind turbine wake (Jimenez et al., 2008).

Most experimental studies on the wake of a wind turbine are limited to the near wake region due to the difficulties in data collection in the far-wake. This is applied to both explained the field and laboratory measurements due to the limited length of wind tunnels. One of the highly-cited experiments on wind turbine wake, its aerodynamic performance and pressure distribution on the blades was performed by Hand et al. (2001) using the NREL Phase VI

wind turbine with a rotor diameter of 10.058 m in a large wind tunnel with a blockage ratio of less than 9%. They measured the aerodynamic performance and loading on the blades, along with some qualitative visualisation of the tip vortices using smoke. Although the results of this study have been used by other researchers as a means for validation of wake models, their experiment does not provide sufficient information about the velocity field in the wake region (the interested reader is referred to Bai and Wang (2016) for more information regarding the experimental studies on the wind turbine wake). Another experimental study in which the velocity distribution in the wake region was measured, conducted by Schümann et al. (2013). Using hot wire anemometry and a five-hole probe they measured the velocity distribution in the wake of a HAWT with a rotor diameter of 0.9 m and were able to provide detailed information about the wake rotation. Their results showed a low velocity region in the wake downstream of the wind turbine surrounded by the tip vortices. It was also found that there are strong vortical structures in the central area of the wake. The wake of the tower is deflected by due to the interaction with the rotating flow field in the near wake. In addition, they showed tower effects result in the deformation of the wake and the movement of the axis of rotation; it also changes the distribution of turbulence intensity (Schümann et al., 2013).

Experimental studies can provide viable information which can be used directly or indirectly to investigate the wake behaviour and aerodynamic performance of a wind turbine, however, they possess some limitations such as being limited to specific conditions, limitation of measurement devices and techniques etc. In addition to difficulties associated with data measurement in the field, one of the limitations in the study of the wind turbine wake is the effect of confinement on the wake when conducting experiments in a wind tunnel. McTavish et al. (2013) stated that the wind turbine wake formation and its expansion are not affected

by the tunnel walls when the blockage ratio is less than 10%. However, the blockage effect in wind turbine wake studies is a function of several parameters such as the blockage ratio (based on rotor swept area), tip speed ratio, number of blades, pitch angle and even the shape of the blades. This effect is discussed in more details in Appendix A of this thesis, where the impact of confinement on wake development is numerically investigated.

The shape, structure and breakdown distance of the wake are also highly affected by different factors such as: (i) atmospheric turbulence, (ii) topological effects, and (iii) velocity gradients in the atmospheric boundary layer (ABL) (Liu et al., 1983, Sanderse, 2012). A laminar ABL with a low turbulence level results in a longer far-wake region and larger velocity deficit which leads to a lower available energy for downstream wind turbines. On the other hand, a higher turbulence intensity results in shorter far-wake distance and higher fatigue loads due to the fluctuating forces (Elliott, 1991).

In addition to experimental studies, several theoretical studies has been carried out to investigate the wind turbine wake which resulted in the development of different wake models (Vermeer et al., 2003, Sørensen et al., 1998). Wake models usually are based on experimental data and utilise numerous assumptions. According to the development of the wake and their capabilities in predicting the flow field in different regions of the wake, these models can be divided into near-wake models and far-wake models. Near-wake models are mainly used to calculate the flow-induced forces acting on the blade in order to predict the output power of a turbine. Thus, the shape of the rotor blades plays an important role and near-wake models should be able to account for this factor. The shape of the rotor blades loses its significance in the far-wake region. Far-wake models are generally used to calculate the velocity deficit and wake expansion in order to estimate the power output of the wind

farm and the power loss for turbines located in the wake region (Kloosterman, 2009, Sanderse, 2012). In the following sections, some of these models and methods are presented.

2.1.4.1 Near-wake models

The "near-wake" is the region behind wind turbine in which the effect of rotor geometry (number of blades, tip vortices, flow separation, etc.) is dominant and the shear layer is not fully developed (Vermeer et al., 2003). Thus, it is important for near-wake models that the aerodynamic properties of the blades are accurately modelled, whereas for far-wake models this is of lesser importance. Most popular near-wake models are based on the Blade Element Method (BEM), actuator disk, or vortex models. The BEM is a semi-empirical inviscid method based on momentum theory (Hansen, 2008). Although a large number of methods and different approaches have been introduced that are more accurate than BEM, it still is the most common technique for approximation of the lift forces acting on the wind turbine rotors. In BEM the rotor is assumed as a disc and aerodynamic forces are calculated using tabulated data for sectional airfoils and induction theory by dividing the blades into discrete elements (Ghadirian et al., 2014).

The simplicity of BEM is its main advantage, however, it cannot account for effects of unsteadiness and non-uniform flow features, atmospheric turbulence, the velocity gradient in the ABL, deep stall and the effect of neighbouring turbines (Sant, 2007, Vermeer et al., 2003, Sørensen, 1986).

The actuator disc theory can be described as a development of the BEM method. The classic BEM is limited to the steady state condition where a wind turbine exposed to a uniform flow, which is not a representative of the operating conditions for most wind turbines. Generalized actuator-disc models have less limitations than BEM since the flow around a turbine is

modelled using Computational Fluid Dynamics (CFD) methods. However, some inaccuracies arise since the flow around the blades is not resolved numerically and the lift and drag forces are derived from the sector-wise characteristics of the airfoils without any correction for 3D effects (Sørensen and Myken, 1992, Sørensen et al., 1998). The traditional actuator disc model does not account for the effect of blade rotation on the 3D lift characteristics. In addition, the partial stall due to wind gusts are not currently considered in actuator disc models. Moreover, a full CFD calculation of the surrounding flow is time-consuming and therefore less feasible for large wind farms.

Solving the full Navier-Stokes equations for the domain around a wind turbine rotor could give an accurate prediction of the flow structures surrounding the rotor blades and in the near-wake. However, since the computational cost to perform a full viscous and turbulent simulation (Direct Numerical Simulation) is too high it is necessary to use a simplified solution of the Navier-Stokes equations. This, however, can be a difficult exercise since too much simplification may reduce the accuracy of the solution of the unsteady flow which is formed in the vicinity of the rotor. Several of these techniques are discussed below.

(i) Reynolds Averaged Navier-Stokes (RANS): A method recommended for avoiding the need for solving the fully-turbulent Navier-Stokes equations is to assume that a turbulent flow consists of a mean flow and a fluctuating part (Kundu and Cohen, 2004). The fluctuating components of the velocity result in an additional term in Navier-Stokes equations, called Reynolds stresses which itself need to be modelled to close the set of Navier-Stokes equations. Popular Reynolds averaged models (e.g. k-ε and k-ω) use the Boussinesq hypothesis to model the Reynolds stress terms, assuming an isotropic turbulent diffusion which is not a valid assumption in atmospheric flows (Mehta et al., 2014). On the other hand, model constants in RANS turbulent approaches are highly dependent on

aerodynamic data from field studies and lack of data for every condition reduces the accuracy of RANS models. These models also are not able to resolve the low frequency and large scale unsteadiness in highly separated flows (Sanderse, 2012).

(ii) Large Eddy Simulations (LES): Wind turbines operate at large Reynolds numbers (based on chord length) in the order of 10^6. Hence, there is a significant difference between the smallest and largest length scales of the vortices or eddies in the flow. It is therefore not possible to perform a full Navier-Stokes simulation due to high computational cost associated with the required grid size. A LES takes into account only the eddies in the flow that are larger than the grid size. In this way, the large scale turbulent motions that govern diffusion, momentum and energy exchange are calculated explicitly and only the dissipative small scale motions have to be modelled with a turbulence model. Interesting features of the flow such as turbulence intensity, axial momentum loss, flow separation and spatial coherence of turbulence can be modelled with a LES (Jimenez et al., 2007 and Mo et al., 2013). However, LES calculations are computationally expensive since they need a high resolution mesh, especially in the boundary layer of the wind turbine blade to yield accurate results.

It can be concluded that the semi-empirical near-wake models such as BEM and actuator disc models are primarily developed to provide an approximation of the aerodynamic forces acting on the rotor of a wind turbine, and are unable to reveal flow features. They also do not take into consideration the effect of different conditions such as yaw misalignment, wake of other turbines, ABL and turbulence in the atmospheric boundary layer. The anisotropic nature of turbulent structures in the ABL and wind farms also reduces the accuracy of the RANS CFD models. The LES approach has proved to give reliable results, however requires

significantly more computational power than RANS and due to its sensitivity to the grid size, especially in the boundary layer region of a blade.

2.1.4.2 Far-wake models

The far-wake commences after the breakdown of the near-wake. At these distances, the aerodynamic properties of the rotor are no longer discernible. In a wind farm, turbines are spaced such that they are in the far-wake region of other turbines. Thus, far-wake models play an important role in modelling the interaction of the wind turbines with wakes and prediction of power loss resulted from the momentum deficit in the wake. In the early days of wind farm modelling, a wind farm was mostly seen as distributed roughness elements that interacts with the atmospheric flow (Templin, 1974, Newman, 1977). Thus, the early models were not capable of providing a distinct wake region for each wind turbine in a wind farm. Following this, further studies were carried out in order to develop models for the prediction of a wind turbine wake development and the velocity distribution in the wake region. Far-wake models can be divided into kinematic wake models (also called explicit models) and field models (also called implicit models or boundary layer models) (Kloosterman, 2009, Vermeer et al., 2003).

Kinematic models

Kinematic models, also known as explicit models, are relatively simple wake models that can be solved analytically; making them suitable for the evaluation of wind speed deficits in large wind farms. These models use only the momentum equation to model the velocity deficit of the wake behind a turbine. In these models, the wake descriptions do not consider the initial expansion region of the wake. Due to their simplicity, the models are not able to calculate the increase in turbulence intensity which occurs in the wake and therefore must be coupled with a separate turbulence model, while, in reality, the velocity deficit and

increased turbulence intensity are connected. Three well-known kinematic models are the solutions presented by Jensen, Larsen and Frandsen. These models are described briefly below. The governing equations and some additional information are presented in Chapter 5.

(i) Jensen model: One of the oldest and most commonly used wake models is the model developed by Jensen (1983). It is a simple wake model, assuming a linearly expanding wake with a velocity deficit which is only dependent on the distance from the rotor and the coefficient of thrust. The velocity in the wake only depends on the downstream distance and not on the radial position in the wake, which results in a so-called hat shaped velocity profile with a uniform velocity within the wake (see Figure 2.9). In reality, however, the velocity profile varies across the plane of the rotor.

A modified version of the Jensen model is capable of considering different turbines (i.e., varies in terms of the number of blades, and hub height); however, it is still incapable of accounting for the effect of the ABL and existing turbulence, wake interaction and yaw misalignment (Thøgersen, 2005, Katic´ et al., 1986).

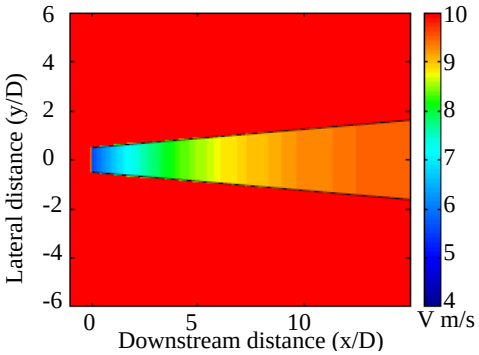

Figure 2.9 Velocity distribution in the wake of a turbine based on Jensen model (Renkema (2007)).

(ii) Larsen model: Larsen model (also known as the EWTSII model) is a semi-empirical method which uses the Prandtl turbulent boundary layer equations (Larsen, 1988). Assuming

incompressible, stationary and self-similar velocity profile along with applying the Prandtl mixing length theory, a closed solution for the width of the wake and mean velocity can be presented. Compared to the Jensen model, the Larsen model is based on a Gaussian distribution of the wind speed deficit profile in the wake (see Figure 2.10) and also depends on the ambient turbulence intensity, thrust coefficient, rotor diameter and hub height. This semi-analytical model enables a quick assessment of the velocity-deficit as a function of axial and radial positions. However, it still fails to reveal the structure of the wake, the effect of the ABL interaction and neighbouring turbines.

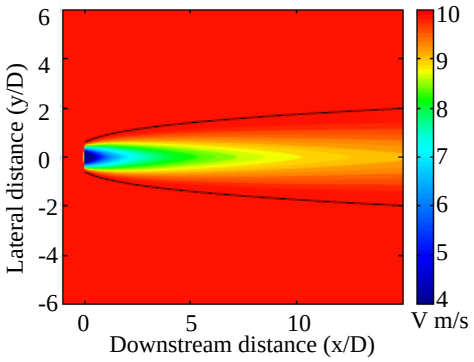

Figure 2.10 Velocity contour in the wake of a turbine using Larsen model (Renkema, 2007).

(iii) Frandsen model: More recently Frandsen et al. (2006) presented their Storkpark analytical wake model for offshore wind farms. The so-called SAM (Storkpark Analytical Model) was first designed to calculate the wake region in large offshore wind farms with a rectangular grid and constant spacing between rows. The Frandsen model is similar to the Jensen model, with respect to wind velocity deficit. However, the Frandsen model can accommodate the interaction of multiple wakes by dividing the potential wake interaction into several regions with a constant but different velocity deficit for each one (Kloosterman, 2009, Rathmann et al., 2006).

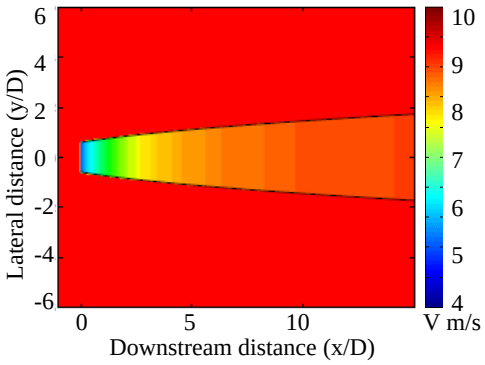

Figure 2.11 Velocity contour in the wake region of a turbine using Frandsen model (Renkema, 2007).

(iv) Ishihara's Model: Ishihara's model is designed to account for variable wake recovery rates, which is normally assumed to be a certain value defined by the model (Ishihara et al., 2004). The wake recovery rate is different for each case and depends upon the turbulence intensity in the wake (Wu and Porté-Agel, 2012). The turbulence intensity in the wake is divided into two components; the ambient turbulence intensity, and the machine generated turbulence intensity. The model uses a similar approach to other Kinematic models in far wake where the turbulence generated by the turbine is highly dissipated and atmospheric turbulence is the dominant source of the turbulence.

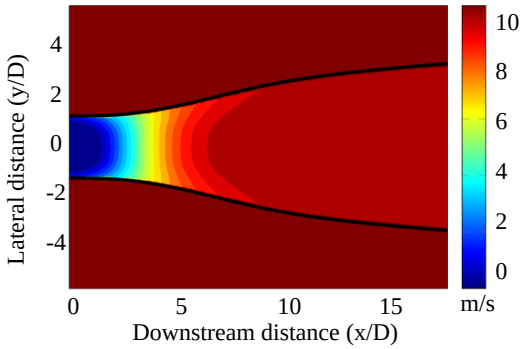

Figure 2.12 Contour plot of a wind turbine wake according to Ishihara's model (Kloosterman, 2009).

Field models

Compared to kinematic methods which use simple correlations for wake expansion and velocity deficit, field models are more advanced since they involve solving RANS equations with turbulence models but, they are more computationally expensive. To solve RANS

equations, different profiles are assumed for initialization of the models. The initial velocity profile is the main difference between the developed field models, which are discussed below.

(i) Ainslie model (two-dimensional field models): Ainslie (1988) proposed a 2D eddy viscosity model for the far-wake region of a wind turbine assuming axisymmetric flow with a steady and uniform incoming flow. Without taking into account the streamwise pressure gradient and interaction with ABL, the model is initialised using a Gaussian wind speed deficit profile. An example of the axial velocity development downstream of a turbine based on Ainslie model is given in Figure 2.13 (Medici, 2005, España et al., 2011).

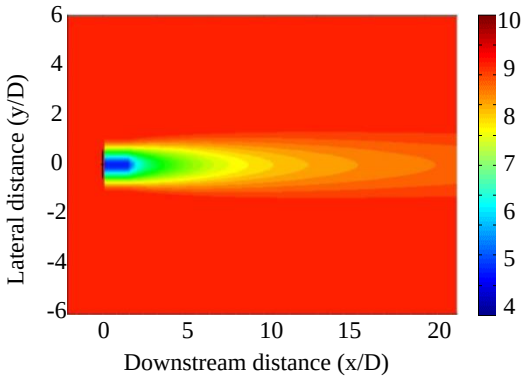

Figure 2.13 Calculated flow field in the wake of a turbine at hub height using the Ainslie model (Thøgersen, 2005).

Although the Ainslie model can model wake meandering (see Figure 2.13), it assumes that the size of large eddies increases linearly downstream of the wind turbine (Ainslie, 1988), and it cannot incorporate the general anisotropic turbulences inside the atmospheric boundary layer.

(ii) UPMWAKE: The UPMWAKE code is based on the 3D parabolized RANS equations as developed by Crespo (1985), with k-ε as turbulence model. ECN (Energy research Centre of the Netherlands) implemented this code in the Wakefarm program, initializing the wake with a Gaussian wind speed deficit profile (Schepers, 2003). The execution of the code in a

cluster of wind turbines is relatively fast due to the parabolic equations since only upstream effects are modelled.

UPMWAKE is able to incorporate 3D effects such as the downward deflection of the wake centreline and wake meandering. To model the wake meandering effect, an accurate wind rose is required as an input. Incorporation of wake meandering in this case means that several steady calculations are performed for different wind directions, and their average is taken. Validation studies for both wind speed deficit and turbulence intensity show good agreement, but the simulation results are very sensitive to input parameters and high quality measurements are required for a reliable comparison with simulations (Schepers, 2003).

(iii) Elliptic field models: Several elliptic field models have been developed to study the flow around wind turbines and through wind farms. In these techniques wind turbines are modelled either using actuator discs or actuator lines (Ammara et al., 2002, Mikkelsen, 2003, Troldborg et al., 2007). Though these models are able to calculate the details of the flow in the near wake, they are computationally very intensive. Mikkelsen only studied a single wind turbine, Troldborg et al. (2007) a row of 3 turbines and Ammara a large wind farm with periodically distributed wind turbines (Ammara et al., 2002, Mikkelsen, 2003, Troldborg et al., 2007). As mentioned, these studies could provide quality data in near-wake, however their accuracy reduces when considering the atmospheric turbulence due to the inhomogeneous nature of the turbulent atmospheric boundary layer. The Robert Gordon University (RGU) used a fully elliptic three-dimensional Navier-Stokes code with a turbulent k-ε closure during the ENDOW project. High computational costs with very low improvement in results limited the usage of these models (Schepers, 2003).

Combined models

A way to overcome the limitations of different wake models is to use the models in the region of the wake where they are most applicable. Using this approach, models can be combined in a smart way such that the entire flow field from the rotor to the far field region is resolved.

(i) Hybrid model by Voutsinas: To model the whole domain of the wind turbine wake, Voutsinas (1992) suggested to divide the computational domain into three regions. Each region is resolved using an existing wake model. The rotor region within $0.05D$ downstream is modelled using a vortex wake code. Using the results from the first region, viscous RANS equations with a k-ε turbulent model are solved for modelling the flow field in the region of up to $4D$ downstream. Taking these results as the boundary conditions for the last region and assuming a self-similar velocity profile, boundary layer equations are solved to provide the velocity deficit for the distances greater than $4D$ downstream. The model is capable of handling different initial velocity profiles, however the effect of yaw misalignment and turbulence in the incoming flow is not considered in the model. The anisotropic nature of atmospheric turbulences is also a source of error since this model uses k-ε RANS equations which are based on isotropic turbulence diffusion.

(ii) Hybrid model by Kasmi: Kasmi and Masson (2007) applied the classic BEM approach to model the rotor region. Again, the RANS approach is used to model the transition region from near-wake to far-wake, as well as the far-wake itself. Adding the effect of the turbine nacelle and a term for describing the energy transfer between the large and small scale turbulence led to more accurate results compared to the k-ε model developed by Crespo et al. (1985).

The Kasmi hybrid model requires development and modification in order to handle complex terrains. However, there are other shortcomings associated with using this model such as using RANS models for atmospheric turbulent boundary layer and the effect of misalignment on wake development and recovery length.

Engineering wake models which are used when designing wind farms, are simple semi-empirical models which provide an insight to velocity deficit behind an individual wind turbine located in a uniform incoming flow. These models also use a simple superposition of velocity decay associated with the wake interaction. Detailed information about these models and their applications are presented in Chapter 5 of this thesis.

Another shortcoming of the engineering models is their inaccuracy in the case of atmospheric boundary layer, which has a significant effect on the wake development. Accurate prediction of the wake development in atmospheric boundary layer is critical for a wind turbine operating in the wake of another wind turbine, noise studies and also optimisation of the layout of wind farms (Porté-Agel et al., 2011, Dörenkämper et al., 2015). Porté-Agel et al. (2011) used an actuator disc model combined with a LES turbulent model to calculate the flow field in the wake of a wind turbine in atmospheric boundary layer. Figure 2.15 shows the streamwise velocity contours for a wind turbine wake in an atmospheric boundary layer with three different stability conditions. As shown, the wind turbine wake length decreases as the atmospheric boundary layer becomes more unstable. While the atmospheric boundary layer has a significant effect on wake development, the models usually used in industry are based on empirical data and are not able to directly calculate the effect of atmospheric boundary layer and flow features on the turbine. The effect of atmospheric boundary layer and the fundamental mechanism of wake development are described in details in Chapter 6 of this thesis. Another method which has attracted

attentions of many researchers due to its capabilities in providing detailed information is the Embedded LES (ELES). ELES is a hybrid CFD model which benefits from the accuracy of LES model in regions of interest with a high turbulent content and a reduced computational cost in other regions of the domain.

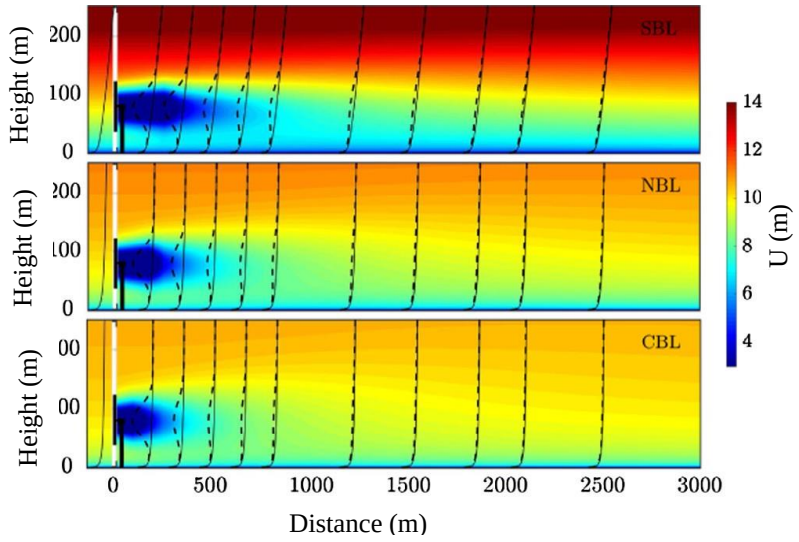

Figure 2.14 Contours of streamwise velocity in the vertical mid-section showing the effect of different atmospheric boundary layer conditions on wake of a wind turbine. Top: stable condition, middle: neutral condition, and bottom: unstable condition (Porté-Agel et al., 2011).

2.2 Wind turbine noise

Noise emission is one of the main issues associated with wind farms, and a major concern about their development (Kaliski and Neeraj, 2013, Walker et al., 2012). Serious concerns have been raised about wind turbines noise emission due to their effects on public health and consequently public acceptance of wind energy. Sleep disturbance, annoyance and distress have been reported as major effects of wind turbine noise on individual's health (Seong et al., 2013, Paller et al., 2013, Bakker et al., 2012, Zosuls et al., 2013). In addition, the formation of thermal inversion layer during the night, especially in a quiet environment with low background noise (e.g. rural areas) intensifies noise perception and its effect (Thorne, 2011, Møller and Pedersen, 2011). Studies showed that wind turbine noise is not masked easily in the presence of other noise sources due to its varying feature and frequency content

(see Figure 2.15). Interestingly, in most communities wind turbine noise has resulted in more complaints than traffic (Janssen et al., 2011, Pedersen et al., 2009). This is due to the fact that the negative effect of noise is magnified when the scenic stimuli and psychological factors are involved (Pawlaczyk-Luszczynska et al., 2013, Pedersen et al., 2007, Kuwano et al., 2013). Thus, a wide variety of factors should be taken into account, when investigating the wind farm noise and its impacts on communities.

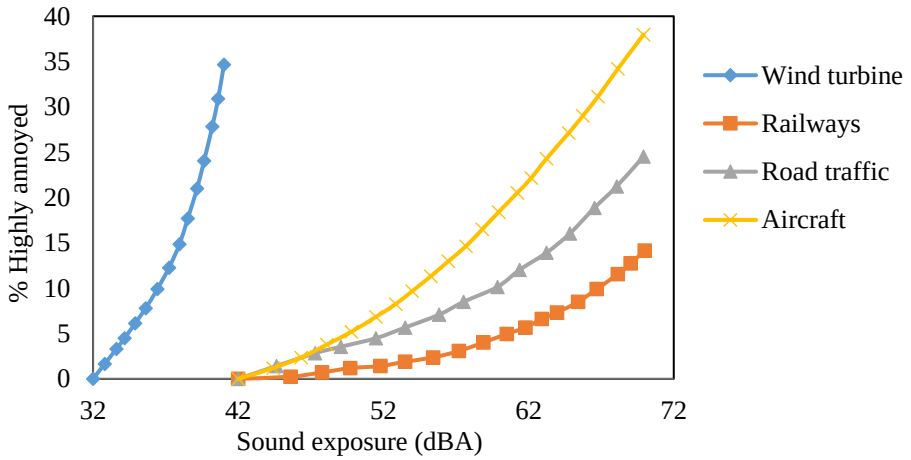

Figure 2.15 Comparison between annoyance feature of different source of noise (Pedersen and Waye, 2004)

In addition to personal attitude towards the sound source and the effect of environment, frequency content of the sound and its quality have a significant effect on noise perception. Studies on the noise effects on humans show that in certain frequency conditions and noise quality, the annoyance level increases (Nobbs et al., 2012). Among all characters and special qualities reported by individuals living in the vicinity of wind farms, “swishing”, and “thumping” are described as most annoying qualities which, often occur at blade pass frequencies (Waye and Öhrström, 2002, Leventhall, 2006, Bolin et al., 2011, Pedersen et al., 2008). Noises emitted from wind turbines include wide range of frequencies, from infrasound (i.e. sound waves below 20 Hz) and low frequency noise (i.e. sound with frequencies in the range of 20-200 Hz) to high frequencies (2000-20000 Hz) (Jakobsen, 2005, Evans, 2013, Thorne, 2011, Oerlemans et al., 2007). Another important factor which

affects the noise frequency is the size of wind turbines; the larger the wind turbine is, the smaller the dominant frequency becomes, resulting in lower absorption through atmosphere and dwellings' structures (Bolin et al., 2011).

2.2.1 Different noise mechanisms

Wind turbine noise can be divided into two categories with respect to its generating mechanism: mechanical noise and aerodynamic noise (Stewart, 2002, Moorhouse et al., 2007, Oerlemans, 2009):

2.2.1.1 Mechanical noise

Mechanical noise is generated by the interaction of moving components of a wind turbine, which is usually accompanied with high frequencies and prominent tonal characteristics (Oerlemans and Schepers, 2009). Improvement of turbine design and application of advanced technologies in wind turbine manufacturing have almost eliminated machinery noise; thus, this noise is not a major concern in modern wind turbines (Meir et al., 1996, Moorhouse et al., 2007, Bolin et al., 2011). In addition, high frequency noise from the moving turbine components of a turbine such as the gearbox is dissipated by atmosphere, ground, and obstacles in short distances from a wind turbine (Oerlemans et al., 2007).

2.2.1.2 Aerodynamic noise

Aerodynamic noises is generated by fluctuating forces acting on the blades and consists of infrasound to moderate frequency sounds (Oerlemans, 2011, Oerlemans and Schepers, 2009). Due to very low frequencies, aerodynamic noise is not dissipated by atmosphere and ground, hence it travels much longer distances compared to those of mechanical noise (Timmerman, 2013, Bellhouse, 2004). Different parameters such as wind conditions (speed and direction), wind shear, temperature, humidity, inversion layer, and topography of the

area affect the aerodynamic noise and its propagation and hence its perception (Shepherd et al., 2012).

The frequency of the generated noise on the blades is directly proportional to wind speed and has an inverse relationship with the size of turbulent structures (i.e.$f \propto U / \Lambda$), where Λ is the length scale of eddies and U is the mean flow velocity (Moorhouse et al., 2007); thus, smaller eddies produce higher frequency noise.

The fluctuating forces, are the main cause of aerodynamic noise and are generated on the blade surface due to its interaction with the eddies. As shown in Figure 2.16, four types of vortices interact with different parts of the blade resulting in different noise characteristics. The major interacting eddies with the turbine blade are: (a) eddies in the incoming turbulent flow; which consist of a wide range of length scales and are usually dependent on the surface roughness, topography of the ground, and the upstream obstacles. These eddies usually interact with the leading edge of the turbine blade and part or its entire chord length; (b) eddies in the turbulent boundary layer formed on the blade surface; the length scale of these eddies is in the order of turbulent boundary layer thickness and they usually interact with the trailing edge of the blade; (c) Separation eddies; these eddies are generated due to adverse pressure gradients and their size can be comparable with the blade chord; (d) tip vortices; these vortices are generated at the tip of the blade due to the pressure difference between the pressure and the suction sides of the blade. Previous studies show that the core size of these vortices are approximately 10% of the chord and they interact with the tip part of the blade (Ebert and Wood, 1999, Sherry et al., 2013).

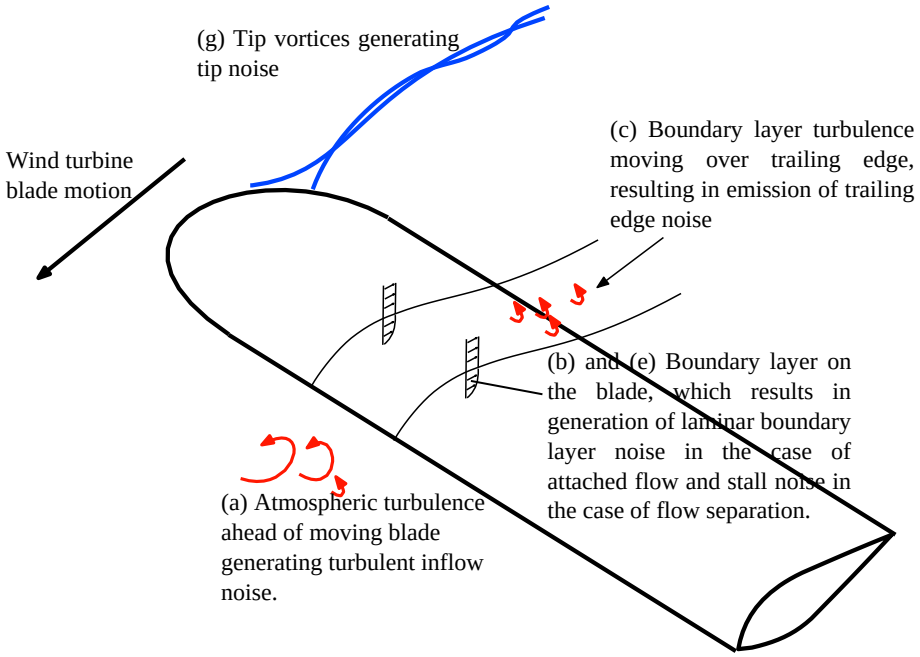

Figure 2.16 The flow over a wind turbine blade tip and flow features associated with aerodynamically generated noise (Doolan, 2011).

The noise signature of a wind turbine spans a wide range of frequencies. Major acoustic emissions from a wind turbine with disturbing influences are related to noise with frequencies below the moderate range (Pedersen and Waye, 2004, Bolin et al., 2011). Low frequency noises can travel far, penetrate houses and dwellings, and can cause resonances leading to increased annoyance levels (Hansen et al., 2012, Bellhouse, 2004, Stewart, 2002). Studies show that even infrasound and low frequency sound from a wind turbine with low-pressure levels can be perceived via the vestibular and the hearing systems (Schomer, 2013, Lichtenhan and Salt, 2013, Berg, 2004). However, noise perception and its effect on health is a multi-parameter function, and so more studies are required to be conducted in the field to determine the importance of each parameter.

According to flow pattern over wind turbine blade, aerodynamic noises can be divided into the following groups:

(a) Unsteady turbulent-inflow: When the blade interacts with turbulent eddies from incoming flow (usually Reynolds number around million based on the rotor diameter), the

fluctuating forces on the blade surface result in noise generation. If the diameters of the vortices are larger than the chord length of the airfoil, unsteady lift is generated on the blade which results in low frequency (around 10 Hz) noise which radiates as a compact dipole at the leading edge. However, it should be noted that the frequency of the emitted noise is also a function of other parameters such as Reynolds Number (Oerlemans, 2011, Doolan et al., 2012).

(b) Stall noise: Stall occurs when flow separates from the suction side of an airfoil at a large enough angle of attack. Stall and consequent vortices result in fluctuating loads on the airfoil and if a deep stall occurs, large eddies form the suction surface of the airfoil result in a significant increase in noise level of low frequency ranges (Oerlemans, 2011, Moreau et al., 2009). Study conducted by Oerlemans (2011) showed that the stall noise is a minor source of noise in pitch regulated wind turbines.

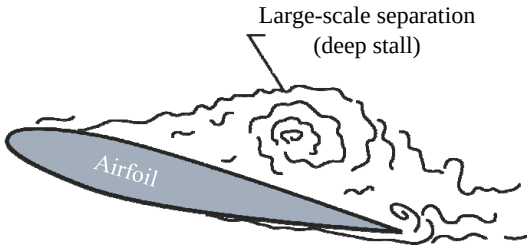

Figure 2.17 Large eddies separated from airfoil interacting with the surface generating low frequency noise (brooks et al., 1989).

(c)Trailing edge noise: For $Re > 10^6$ and attached flow condition, a turbulent boundary layer is formed on the blade which includes turbulent eddies in the vicinity of the blade surface. Eddies in the scale of the boundary layer displacement thickness at the edge and outer part of the blade cause a fluctuating force at a moderate frequency on the trailing edge and hence generate noise (Moorhouse et al., 2007, Oerlemans, 2011). This type of noise is broadband with higher frequencies compared to other aerodynamic noises (500-1000 Hz)

(Berg, 2005). The swish sound is often generated by this mechanism at the outer part of the blade and a higher sound level is perceived in cross-wind direction as the blade moves toward the observer (Oerlemans, 2011). It was believed that the thumping noise which is perceived at distances far from a wind turbine is due to the directivity of trailing edge noise and its convective amplification, however recent investigations and observations contradict this hypothesis (Oerlemans, 2011, Madsen et al., 2015). As seen in Figure 2.18 (b), the trailing edge noise propagates perpendicular to the blades and towards the leading edge of the turbine blade (Lee et al., 2013).

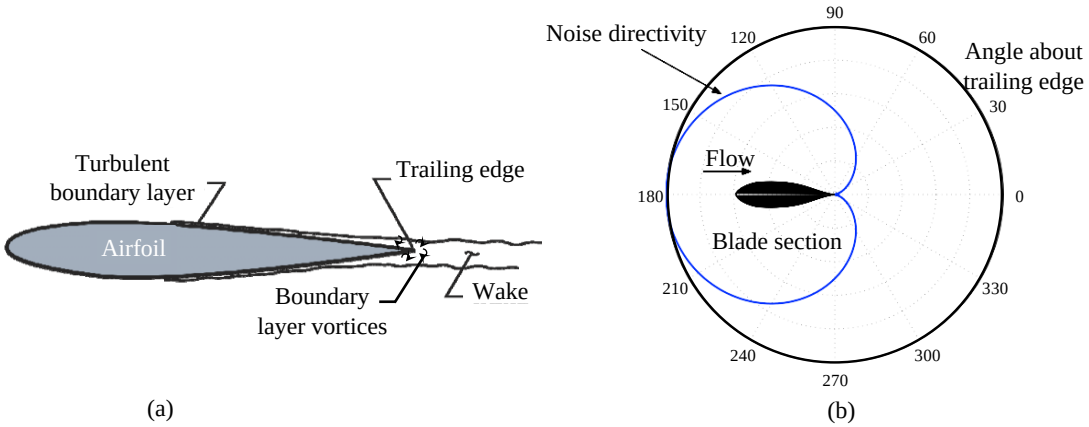

Figure 2.18 a) Turbulent eddies in the turbulent boundary layer interacting with trailing edge, causing broadband trailing edge noise, b) Directivity of the trailing edge noise (Brooks et al., 1989).

(d) Blunt trailing edge noise: As shown in Figure 2.19 bluntness of the blade trailing edge may cause vortex shedding downstream of the turbine blade provided that the thickness of the trailing edge exceeds a critical value (Oerlemans, 2011). Pressure fluctuations created by Von Karman vortices result in the generation of tonal noise which radiates similar to a sharp edge noise source for the wavelength smaller than chord; whereas, it behaves as a compact dipole for wavelength larger than chord length. Since the wind speed varies along the wind turbine blade, the wavelength of blunt trailing edge noise varies and it may appear as a broadband spectral increase in the noise spectrum (Oerlemans, 2011). The blunt trailing edge noise can be prevented by improving the manufacturing quality and fabricating sharp enough

trailing edges. This type of noise is not a concern for noise emission from wind turbines as the frequency content is large and because the noise is dissipated in short distances (Rogers, 2002, Moorhouse et al., 2007, Oerlemans, 2011).

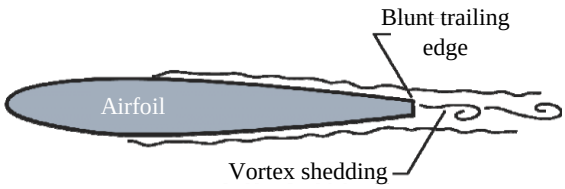

Figure 2.19 Vortex shedding due to blunt trailing edge which generates tonal noise radiation from blade.

(e) Laminar-boundary-layer-vortex-shedding-noise (airfoil tonal noise): When the flow condition results in the formation of a laminar boundary layer on both sides of an airfoil (i.e. $Re < 10^6$), the trailing edge noise which radiates upstream may cause boundary layer instabilities (i.e. Tollmien-Schlichting waves) which, in turn, radiate as tonal noise from the trailing edge (Oerlemans, 2011, Doolan et al., 2012). Recently, it has been found that this aeroacoustic feedback is not necessarily the cause of the generation of tonal noise. It was shown that an inflectional mean velocity profile in the separated shear layer just upstream of the trailing edge strongly amplifies the TS waves and generates a tonal noise (Doolan et al., 2012). The laminar-boundary-layer-vortex-shedding noise has a similar directivity pattern to trailing edge noise and radiated from the trailing edge portion of the airfoil as shown in Figure 2.23(b). The effect of laminar-boundary-layer-vortex-shedding noise can be observed through spectral peaks in the noise signature which their frequency increases with wind speed (Oerlemans, 2011b, Zhu, 2004). This tonal noise is not a major problem in large wind turbines because they work at high Reynolds number conditions (i.e. $Re > 10^6$).

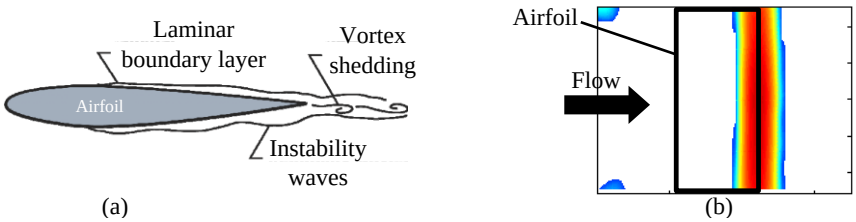

Figure 2.20 a) Vortex shedding due to the resonant interaction of the unsteady laminar-turbulent transition with the trailing edge noise (Brooks et al., 1989). b) Acoustic source mapping of an airfoil in clean flow with $Re=0.5\times10^6$ corresponding to the laminar-boundary-layer-vortex-shedding noise (Oerlemans, 2011).

(f) Blade-tower interaction noise: This type of noise was reported as the dominant noise source for downwind turbines because of significant impulsive and thumping noise generated due to the interaction of the blade and vortices shed from the turbine tower (Kelley et al., 1985, Jakobsen, 2005, Ellenbogen et al., 2012). In the case of upwind turbines the interaction of the blades with the deformation of the flow caused by tower stagnation in its upstream region (see Figure 2.21), results in low level of impulsive noise at the blade pass frequency (1-30 Hz) radiating with a dipole pattern (Doolan et al., 2012, Berg, 2005). Studies show that blade tower interaction does not have a significant effect on blade loading compared to the wake interaction because of the negligible effect the tower has on the upstream wind velocity (Kim et al., 2011). Thus, the resulting pressure fluctuations on the blade surface is not comparable with other noise mechanisms in wind turbines. Moreover, studies on the directivity of the noise show that the radiation pattern of this noise is not aligned with the reported noise data.

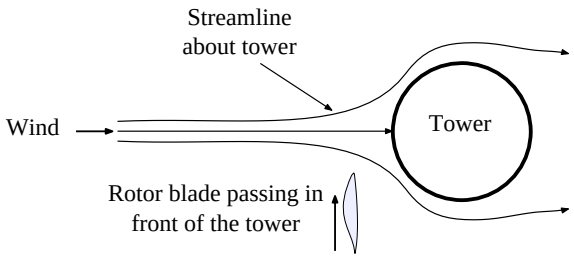

Figure 2.21 Blade-tower interaction noise generation mechanism due to interaction of the blade with the deflected flow in front of the tower in up-wind wind turbine configuration (Doolan et al., 2012).

(g) Tip noise: The differences between the pressure on the upper and lower surfaces of the

blade at the tip may result in the generation of tip vortices. Interactions of tip vortices with the blade tip generate a noise signature similar to the trailing edge noise because of the similarity in the generation mechanism (see Figure 2.16). The spectral content of tip noise depends on the length scale of the tip vortices and the flow velocity at the tip, which itself is related to the shape of the blade tip, load on the blade and strength of the tip vortices. This noise has a broadband and a high frequency character, but is not considered as significant source of noise for modern wind turbines because of its frequency content and level (Doolan et al., 2012, Oerlemans, 2011).

2.2.2 Airfoil noise prediction models

For the prediction of wind turbine noises airfoil noise models are usually used. Several empirical and analytical approaches have been developed to investigate and predict the noise generated by an airfoils. One of the first attempts for prediction of the aerodynamically-generated noise was conducted by Powell (1959), who reported that the surface pressure fluctuation near the trailing edge is the main contributor to noise generation by an airfoil. Based on his study, the trailing edge noise is dipolar in nature and its power varies with U^5 (with U being the free stream velocity) (Powell, 1959, Powell, 1990). The semi-empirical model developed by Powel is based on the acoustic and aerodynamic measurement of airfoil sectional data of pressure fluctuation in an anechoic wind tunnel. In another attempt, using the collected data and amplitude scaling laws proposed by Ffowcs Williams and Hall (1970), an empirical model was developed for all airfoil self-noise mechanisms. The directivity pattern was calculated using the directivity function of the trailing edge noise for an attached flow and a compact dipole in the case of stall. Comparison of the results from the developed models with experimental data showed that the trend of the noise spectrum for most mechanisms were in good agreement. The models showed a strong dependency to the size

of the airfoil and the angle of attack, but their accuracy decreased significantly with increasing angle of attack. The model proposed by Brooks et al. (1981) is based on experimental dataset for NACA 0012 or similar airfoils. Later, the TNO-Blake model was proposed in order to account for more general airfoil cross-sections (Jianu et al., 2012, Kamruzzaman et al., 2011). This model uses more accurate boundary layer characteristics and is less dependent on experimental data than the model propose by Brooks et al. (1981).

While these models have proven to be acceptable for the prediction of the noise for some given cases, in others they have given inaccurate results. For instance, Leloudas et al. (2007) used the Brooks et al. (1989) model for the calculation of the emitted noise from a wind turbine and found that the model cannot accurately predict the blunt-trailing-edge noise for the frequencies above 3 kHz. In another work by Moriarty and Migliore (2003), the predictions by the model were compared to the wind tunnel test data for a NACA 0012 and a S822 airfoils at different Reynolds numbers in the range of 2×105 to 1×106 and it was shown that the accurate prediction by the proposed model is limited to a moderate angle of attack and high frequency noise. However, the discrepancy between the measured and theoretical data exceeded 6 dB for the frequencies less than 2 kHz, especially for angles of attack larger than 7°.

Recently, with the advances in computational aeroacoustics, accurate CFD methods have been used for the prediction of the flow field, pressure fluctuation, and noise signature from an airfoil. Computational aeroacoustics (CAA) can be performed using the following two main techniques: **(i) direct computational aeroacoustics**: in which flow-filed and acoustic pressure are modelled simultaneously and computationally. In order to obtain high fidelity data using this method, a fine grid is required to capture all noise sources and calculate their directivity pattern which makes this method computationally expensive. **(ii) Coupling CFD**

with acoustic analogies or hybrid methods: in which the flow field is computed of a high resolution and the sound pressure level in far-field is calculated using acoustic analogies such as TNO-Blake, Linearized Euler, Ffowcs Williams and Hawkings (FW-H), acoustic/viscous splitting, the acoustic perturbation equation method, the parabolic equation method, and the non-linear disturbance equation method (Kamruzzaman et al., 2011, Bailly and Juvé, 2000, Hardin and Pope, 1994, Ewert and Schröder, 2003, Morris et al., 1997). Sandberg et al. (2008) computationally investigated the airfoil noise signature using direct numerical simulations combined with a direct aeroacoustic approach. Their results revealed that at some frequencies, the directivity of the emitted noise is not in agreement with the directivity predicted by the trailing edge noise theory (see Figure 2.22). However, the computational domain used in their simulations consisted of 17×10^9 grid points which required a high performance computing system to perform the large amount of calculations necessary in a reasonable time frame.

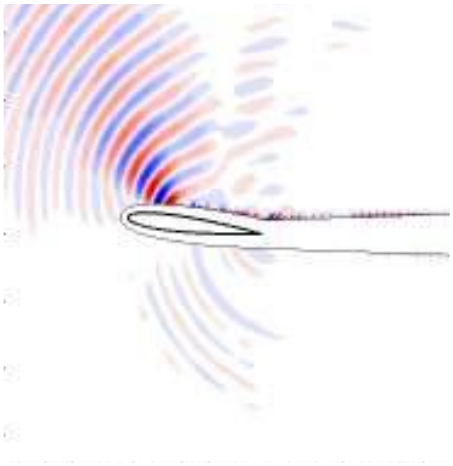

Figure 2.22 Iso-contours of the acoustic pressure computed using DNS and reported by Sandberg et al. (2008).

Hybrid models, on the other hand, benefit from solving the fluid flow and acoustic propagation separately, which reduces the computational cost. Linearized Euler methods are based on the solution of the linearized Euler equations for sound propagation, incorporating

the flow velocity obtained from the CFD (Bailly and Juvé, 2000). The main advantage of the Euler methods is their ability to consider the effect of the flow field on scattering and propagation of the sound (Renterghem, 2014). Hardin and Pope (1994) proposed a flow/acoustic splitting technique based on the concept of calculation of acoustic flow field for low Mach number flows. This approach is based on two steps: initially the transient viscous flow field is calculated and then the acoustic field is obtained using the equations describing the decomposition of the variables into incompressible and perturbed compressible parts. Parabolic equation (PE) method is another approach which has been attracted researchers because of its ability to account for the effect of the flow field. This method was first applied to propagation of radio waves in the atmosphere (Leontovich and Fock, 1946) and then improved and introduced to underwater acoustics by Hardin and Tappert (Hardin and Tappert, 1973). Among aforementioned methods, Ffowcs Williams and Hawkings (FWH) is one of the most commonly used analogies in combination with CFD (Williams and Hawkings, 1969). This method is based on the Curle's model which is an expanded version of Lighthill's acoustic analogy (Casalino et al., 2003, Williams and Hawkings, 1969). However, while this method provides a flexibility in selecting the control surfaces, it does not account for the effect of flow on noise propagation. Moreover, FWH method requires a fine mesh inside the control surface as well as a small time step in order to calculate the acoustic field with a high resolution, which, in turn increases the computational cost of the calculations. The models briefly described in section 2.2.3 are some of the most frequently used hybrid models in airfoil noise studies. Information about other methods and their details can be found in related references.

2.2.3 Wind turbine noise prediction models

One of the first models developed for wind turbine noise prediction was proposed by Grosveld in 1985. The semi-empirical wind turbine noise model developed by Grosveld (1985) is capable of predicting three separate noise mechanisms of trailing edge noise, blunt trailing edge noise, and turbulent inflow noise. He used the approach proposed by Schlinker and Amiet (1981) for the prediction of the trailing edge noise mechanism and a model based on Brooks' scaling law and Howe's directivity function for estimation of the blunt trailing edge noise. Turbulent inflow noise in Grosveld model is based on the assumption that the blade is a line of low frequency dipole sources according to Lighthill's model (1952) and Amiet's theory (1975) for low frequency sound. The model was validated against the experimental data from three downwind wind turbines and an upwind wind turbine. Although the model was not able to predict the noise from some mechanisms (such as laminar-vortex-shedding-trailing-edge noise, and stall noise) and used a simple inflow turbulence model, the predicted spectral shape was in a good agreement with the experimental measurements and the predicted sound pressure level was generally within 4 dB offset range from the experimental data.

Lowson (1993) proposed a semi-empirical model based on the strip theory in which the turbine blade is discretised into several segments. The noise of the blade was predicted based on the angle of attack and the inflow conditions for each segment. The total noise from the blade is then calculated using superposition of the noise levels from each segment. The Lowson model accounted for the effect of all five self-noise mechanisms, with a special focus on the turbulent inflow noise. The turbulent inflow noise in the Lowson model is assumed to be generated by the pressure fluctuations at the blade surface due to the velocity fluctuations. The noise generated by pressure fluctuations on the blade surface is then

assumed to propagate as a distribution of dipoles based on Curle theory (1955). The frequency of the radiated noise is determined by $f = U_c/\lambda_t$ where U_c is the convective velocity of the incoming turbulence and λ_t is its length scale. Especial attention should be paid to the variation of the velocity of the blade segments along the blade span, which, in turn, results in variation of the frequency and wavelength of the emitted noise. Lowson also noted that the rotor and its induction effect increase the turbulence intensity in the incoming flow, however, he did not consider this effect in the model. Lawson tuned his model with the experimental data collected from a noise study of three upwind wind turbines by a single microphone measurement. Comparison of the results provided by Lowson (1993) with the ones predicted by Grosveld (1985) using the same data set, shows a more balanced contribution for the physical mechanisms of the noise generation by a wind turbine.

Although the Lowson model provides more accurate data and includes all aerodynamic noise generation mechanisms in the prediction, it does not account for the finite thickness of the airfoil nor the variation of the angle of attack. Another source of inaccuracy arises from the prediction of the boundary layer thickness, which in Lowson model is based on a flat plate boundary layer calculation. To better estimate the required boundary layer parameters for the model, CFD codes were used, such as the XFOIL code (Moriarty and Migliore, 2003, Moriarty et al., 2004). However, these models still need accurate experimental data for validation and are sensitive to incoming flow features such as turbulence intensity and turbulent length scale (Moriarty, 2004, Moriarty and Migliore, 2003, Buck, 2017).

2.2.4 Recent research on wind turbine noise

As mentioned in the previous section, wind turbine noise prediction models are tunned using experimental data. In many of these models a single microphone is used for measuring the data which does not provide enough information for tunning the model for all self-noise

mechanisms because there are more unknowns than there are sources of information (Buck, 2017). One of the attempts for providing detailed information about the noise source and its directivity was carried out by Oerlemans (Oerlemans et al., 2007, Oerlemans and Schepers, 2009). A 148-element microphone array was utilised in an experiment to identify the noise source while the directivity of the emitted noise was assessed by 8 single microphones located at 240 m distance around the wind turbine. The effects of surface treatment (i.e., cleaning the blade surface) and tripping the boundary layer on the noise emission were also investigated (Figure 2.26).

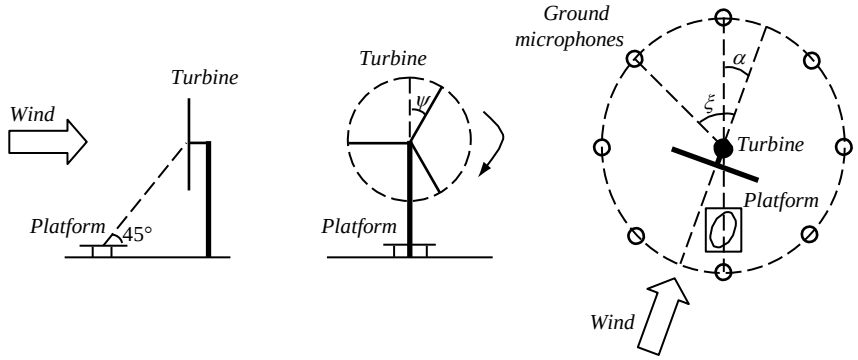

Figure 2.23 Test set-up in Oerlemans experiment: side view (left), front view (middle), top view (right) (Oerlemans and Schepers, 2009).

The experimental investigation by Oerlemans et al. (2007) showed an increased level of noise for the tripped surface, while the surface treatment did not have a major effect on the level of emitted noise. Based on the directivity pattern and the noise source map (Figure 2.27), Oerlemans concluded that the convective amplification of the trailing edge noise is the dominant noise generation mechanism. In order to test this hypothesis, the results from the trailing edge noise model developed by Brooks et al. (1985) with a modified directivity pattern were compared with the experimental data; and as a good agreement was observed, the model was broadly validated. Their study showed that the model proposed by Brooks et al. (1985) can predict the trailing edge noise without requiring much tuning. However, the directivity pattern was modified based on the smoothed version of the high frequency

analytical directivity pattern. Although this experiment provided useful information about the noise source and its directivity, the measurements were carried out in the near-field and at upwind locations and no information was provided for the low frequency range and the downwind noise.

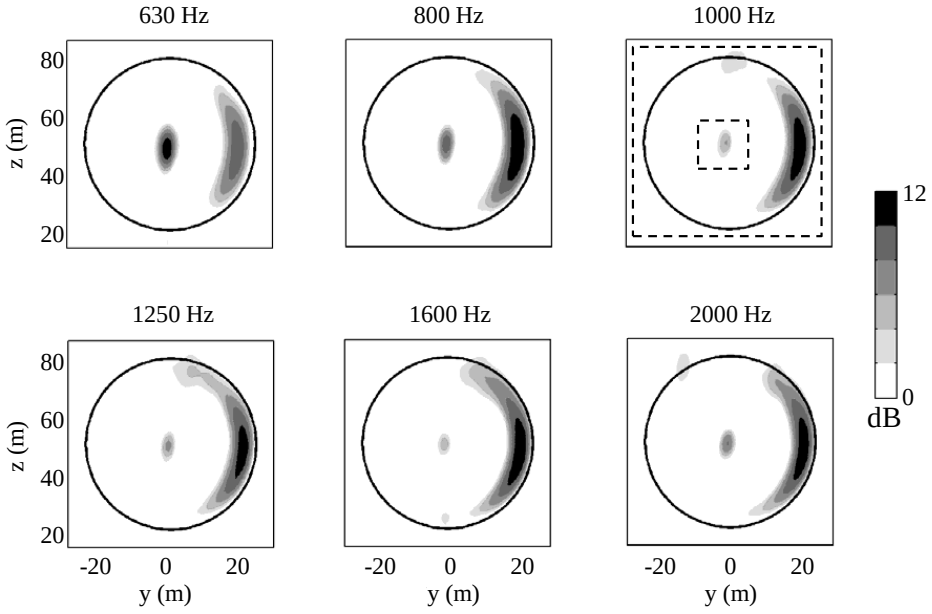

Figure 2.24 Average distribution of noise source in the rotor plane at different frequencies (Oerlemans et al., 2007).

In addition to the noise generation mechanisms, discussed in previous sections, wind turbine noise possesses a unique varying feature called amplitude modulation (AM) (Oerlemans and Schepers, 2009, Napoli, 2011). The varying characteristic of the noise augments the noise perception by human and has been reported as one of the major concerns by communities in the vicinity of the wind farms (Lee et al., 2011, Pedersen et al., 2009). Although the amplitude modulation has been reported by several researchers, its main source is still a topic of discussion. There are two features attributed to the amplitude modulation from wind turbines, namely “swishing” and “thumping” sound. The “swish”, also known as normal amplitude modulation, is attributed to the directive amplification of trailing edge noise while the “thumping” is still somehow unknown. Several hypotheses have been proposed by researchers to explain this phenomenon such as partial stall due to incoming gusts or high

shear in atmospheric boundary layer (Madsen et al., 2013, Madsen et al., 2014, Oerlemans, 2011a). These features and associated mechanism are discussed in more detail in Chapter 3.

2.2.5 Wind turbine noise propagation

Motion of the turbine blade in a flow with varying speed due to wind shear, atmospheric turbulence, and the wake of other turbines results in a wide range of frequencies in the emitted noise from a wind turbine. Studies by Choudhry et al. (2014) showed that a turbine operating in the wake of an upstream turbine at a distance as far as 15 rotor diameters is more susceptible to stall and flow separation can occur on more than 30% of its blade. Due to different frequency bands in noise signature of a wind turbine, aerodynamic noises can undergo amplitude modulation which may lead to an increased level of annoyance (Lichtenhan and Salt, 2013, Berg, 2004a). Even infrasound by a wind turbine may cause an amplitude modulation of audible sound (Lichtenhan and Salt, 2013). Rotation of wind turbines with the same phase in a wind farm can also increase the average sound level and make the turbine noise level more audible at larger distances (Berg, 2004b).

In addition to the complex noise signature of a turbine due to the interaction of the rotating blade with the incoming wind, propagation of the generated noise is also affected by different parameters. The other factors which affect the sound propagation is refraction due to the shear in the atmospheric boundary layer, the wake of the wind turbine, air absorption, temperature gradient, and sound reflection.

Energy of sound waves are dissipated in the air due to two main mechanisms: (i) viscous losses represented as heat due to molecular friction (also called classical absorption); (ii) relaxation of molecules which is manifested through vibration or rotation of the molecules by sound waves energy (Kinsler et al., 2012). The sound absorption by air has been

extensively studied and standard codes such as ANSI Standard S1-26:1995 and ISO 9613-1:1996 have been developed for its quantification. In addition to sound absorption, wind velocity gradient in the atmospheric boundary layer results in noise refraction which alters sound level at different locations. As shown in Figure 2.25, the sound rays travelling downwind are bent towards the ground due to velocity gradient and then reflected upward and then refracted towards the ground again (Schepers and Hubbard, 1985). Thus, an observer located far from the source on the ground surface may experience different sound conditions based on the sound ray path. Refraction of the sound in the atmospheric boundary layer and reflection from the ground also may result in an intersection of different sound rays at the observer location resulting in constructive or destructive effects (Schepers and Hubbard, 1985). On the other hand, when propagating upwind, the sound rays are bent away from the ground and hence the effect of velocity gradient on the sound propagation may result in the formation of shadow zone. A region where no or very low sound wave penetration and is bounded by the sound ray which just touches the ground without being reflected. The shadow zone is not a sound free zone, as the noise is refracted into this zone due to inhomogeneities in the atmospheric flow. Moreover, beyond this zone, upstream of the noise source the sound pressure level attenuates more effectively, especially at higher frequencies (Schepers and Hubbard, 1985).

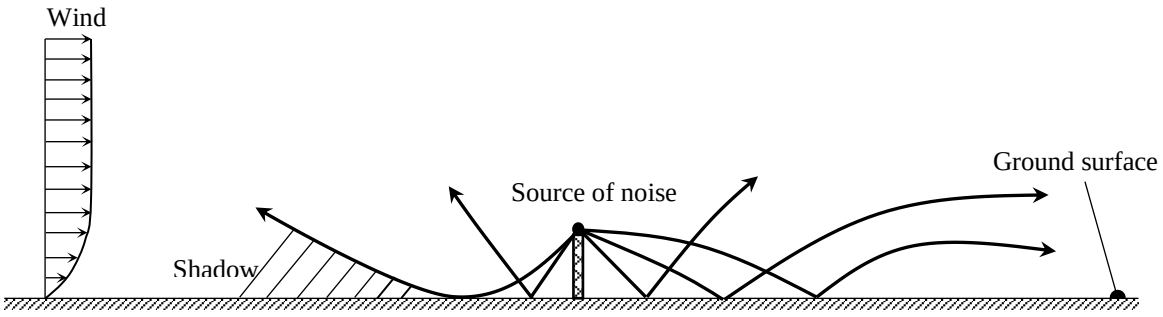

Figure 2.25 Effect of wind gradient and ground reflection on noise directivity (Schepers and Hubbard, 1985).

Temperature gradients also affects sound propagation by refracting sound waves in the

direction of lower temperatures. Figure 2.26 shows sound refraction from a point noise source located in a medium with decreasing and increasing temperature with respect to height. The typical temperature gradient in atmosphere during the day is such that the temperature decreases with increasing altitude. In this situation, the sound waves tend to bend upward from the source and thus forming a circular shadow. Whereas the reverse condition often occurs at night, when the air close to the surface cools rapidly and results in positive temperature gradient, such that the sound waves bend towards the ground (Friman, 2011).

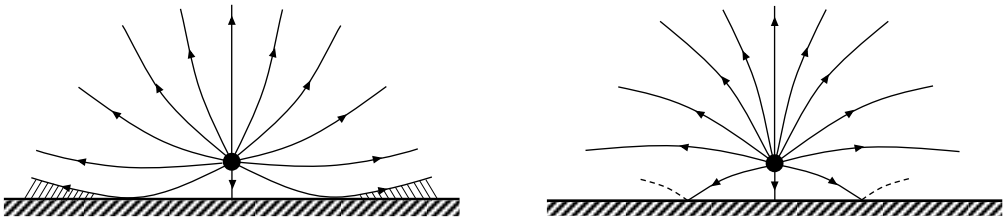

Figure 2.26 Effect of temperature gradient on sound refraction, a) negative temparature gradient, b) inversion or positive temperature gradient (Friman, 2011).

Flow passing through the wind turbine results in a flow field which consists of a vortex street of bound and tip vortices. In addition to streamwise structures, it contains spanwise structures which have refracting effect on the sound and alters the noise propagation direction. The explanation of the interaction of the sound with the vortices can best be explained using the ray-tracing analogy. Figure 2.21 shows the effect of a finite-circulation 2D vortex on ray paths of a plane sound wave. As can be seen the ray paths are bent due to the circular motion of the vortex and the directivity pattern of the sound changes, resulting in the higher sound intensity in some regions of the medium (Colonius et al., 1994).

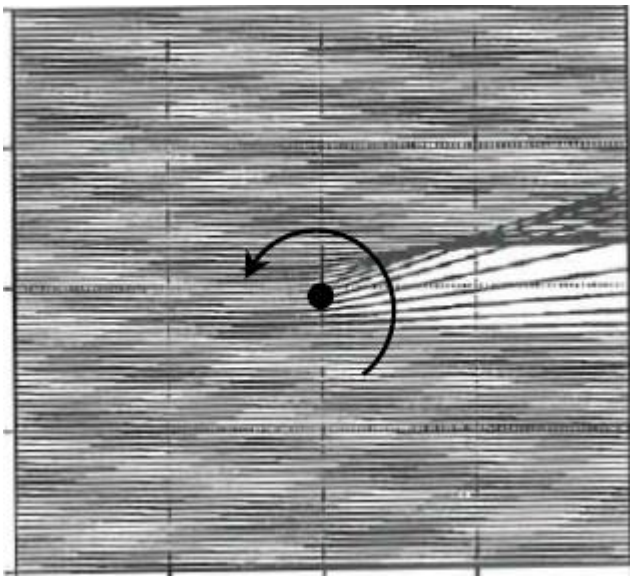

Figure 2.27 Effect of vortex on ray paths of planar sound wave (Colonius et al., 1994)

Moreover, the low velocity region in the wake surrounded with strong tip vortices can act as a conduit which ducts the sound energy downstream of the turbine up to the breakdown point. At this point the sound rays are refracted towards the ground resulting in a higher sound pressure level at the breakdown location (see Figure 2.22) (Heimann et al., 2011, Barlas et al., 2017).

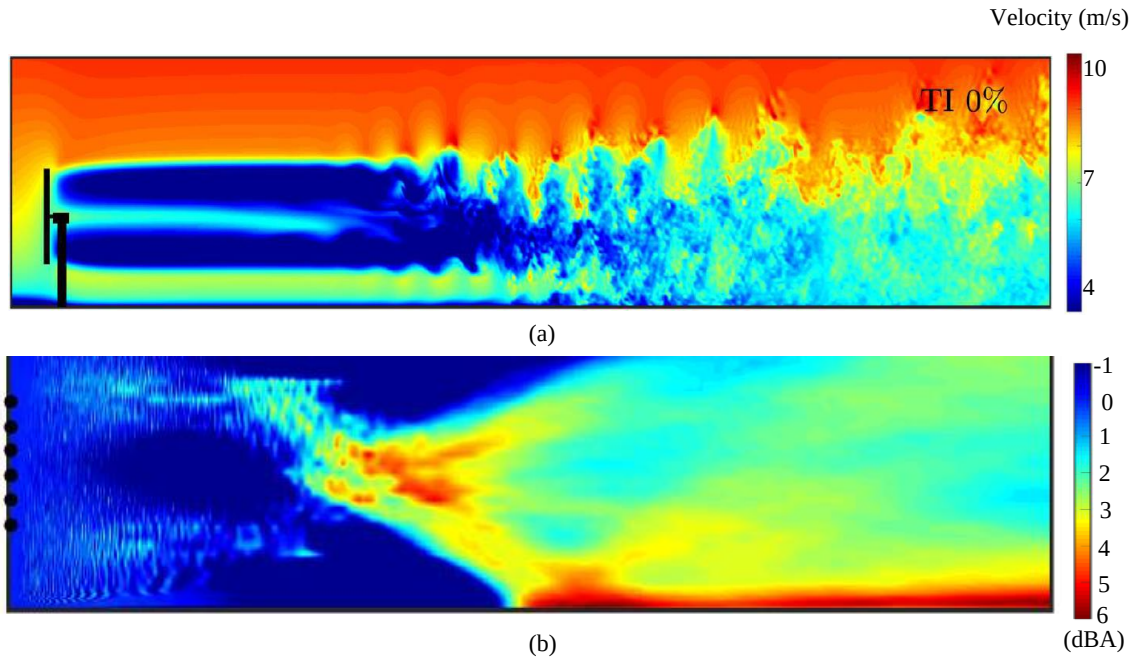

Figure 2.28 a) Instantaneous velocity contour in a wake of a wind turbine at zero turbulence intensity, b) Contour of differential sound pressure level (Reproduced from Barlas et al., 2017).

Using the parabolic equation (PE) method, Barlas et al. (2017) studied the effect of the wake on sound propagation. The wind turbine in their study is a three bladed Vestas turbine with a rated power of 2.75 MW and 80 m rotor diameter. Parabolic equation reduces the computational cost significantly compared to direct aeroacoutic computations since the scattering and propagation of the sound due to flow field are calculated indirectly. The governing equation is based on a sound field in an inhomogeneous moving medium as follows:

$$\left[\nabla^2 + k^2(1+\epsilon) - \frac{2i}{\omega}\frac{\partial v_i}{\partial x_j}\frac{\partial^2}{\partial x_i \partial x_j} + \frac{2ik}{c_0} v.\nabla\right] P'(r) = 0 \tag{2.15}$$

Here, ω is the radian frequency of sound, c_0 is the reference speed of sound, $P'(r)$ is the monochromic sound field, $k = \omega/c_0$ is the wave number, and $\epsilon = (c_0/c)^2 - 1$. The model was applied to a velocity field which was calculated by hybrid LES-actuator line model. As seen in Figure 2.29, the effect of wake is clearly visible through the peak at around 1300 m downstream of the wind turbine. Thus, it can be concluded that the far-field noise can be under-predicted if the correct flow field is not considered when calculating the sound propagation for a wind turbine.

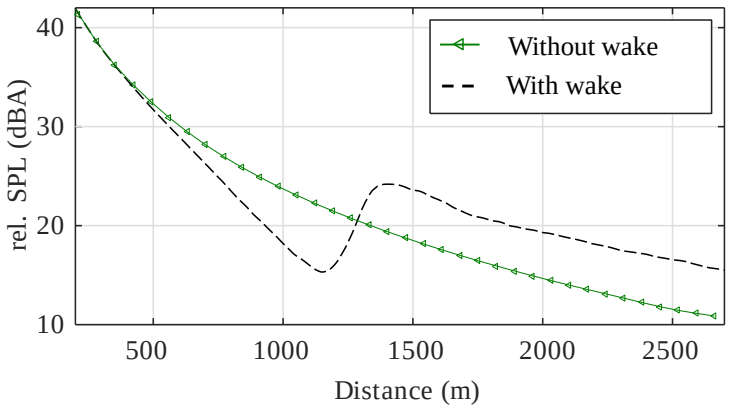

Figure 2.29 Effect of wake on sound pressure level downstream of the wind turbine for an observer at 2 m height. Modulation of sound is visible in the diagram when the effect of wake is considered (reproduced from Barlas et al., 2017).

2.3 Concluding Remarks

This literature review has been carried out in order to show that strong evidence exists that the noise perception at distances far from a wind turbine is associated with aerodynamically generated noise and there is a dependency between the noise direction, perceived noise and direction of the wind. Mechanisms associated with the aerodynamic noise emission from wind turbines are: i) unsteady turbulent-inflow noise; ii) stall noise; iii) trailing-edge (TE) noise; iv) blade-tower interaction noise; v) tip noise; vi) laminar-boundary-layer vortex-shedding noise. The last three mechanisms were found to have a negligible contribution in the emitted noise from modern wind turbines based on their frequencies and levels. Therefore, most studies were focused on the trailing edge noise, stall noise, and turbulent inflow noise, and their corresponding characteristics. The literature review presented in this chapter, revealed that, although the amplitude modulation of the trailing edge noise is suggested to be the main mechanism of the perceived noise, its characteristics and features do not completely match the underlying mechanism for the perceived noise.

After establishing that the modern wind turbines emit noise, which affects the residents even at significant distances from the turbines and specifying the main possible mechanisms for noise perception, every mechanism was discussed in details. Moreover, the parameters which significantly affect the noise generation, such as the incoming flow and wake interaction, have been identified. Similar to the effect on the generated noise, the propagation of the noise is also affected by the flow field and the topography of the terrain. It was found that, the noise propagation from a wind turbine changes if it operates in of the wake of another wind turbine. The wake of a wind turbine acts as a channel which ducts the energy of the sound up to the breaking point of the wake. The sound waves are then radiated towards the ground resulting in the amplitude modulation of the noise at this location.

To better understand the aerodynamics of a wind turbine and the effect of its wake on both noise generation and its propagation, the wind turbine wake development and models for its prediction were also reviewed. The models of the wake are divided into two categories based on the region they analyse: near-wake models which mainly are used to calculate the flow-induced forces acting on the rotor in order to predict the power generated by a wind turbine; and far-wake models which are used to calculate the flow field in the far-wake region. Wind turbines in a wind farms are usually located in the far-wake regions of upstream turbines and hence it was shown that most far-wake models are used to calculate the velocity deficit based on empirical data. The wake interaction in these models is usually taken into account by linear superpositioning of the flow field in the wake of each turbine; however, a wind turbine in a wind farm is exposed to different incoming flow features and its wake also possesses complex turbulent and vortical structures, which are not considered in engineering wake models.

In the light of the literature review, the primary objectives of this research are as follows:

- To establish a relationship between the wind turbine noise perception and wind direction using statistical analysis of the noise perception. This also helps to find out the underlying noise generation mechanism and effective parameters on the noise generation and its propagation. Furthermore, it allows to narrow down the noise mechanisms with the most significant impact on the noise perception for further investigations. The outcomes of this study can help wind farm designers and developers to design a layout which has less effect on the residents in their vicinity.
- To develop a validated model for the investigation of the aeroacoustic behaviour of an airfoil as the fundamental element of wind turbine blades. A deeper insight into the stall

noise which is hypothesised as the potential mechanism of noise perception, may facilitate finding ways to control and mitigate the noise.

- To develop a well-resolved validated wake model and its comparison with the existing engineering far wake models in order to evaluate the fidelity of engineering models and their applicability for wind turbine wake studies. The wake has a significant effect on noise propagation and its interaction with downstream turbines, which may result in increasing the noise level, reducing the power, and increasing the fatigue loads. Therefore, developing a well-resolved model is an essential step towards the investigation of the wake effect.
- To develop a well-resolved validated model for the investigation of the effect of the atmospheric boundary layer on wind turbine wake development and its breakdown. A wind turbine operates in the atmospheric boundary layer, hence its wake is affected by the flow features in the atmospheric boundary layer. The velocity and vorticity pattern downstream of a wind turbine operating in the ABL vary significantly from the one exposed to a uniform flow and since wake has a significant effect on wind farm performance and both noise generation and its propagation. Thus, developing this model and investigation of wind turbine wake in ABL is of high importance.
- To investigate the wind turbine noise propagation in the presence of an atmospheric boundary layer and the wake of an upstream turbine. As mentioned in the literature review, the wake of a wind turbine affects the noise propagation. This study can reveal the regions of the turbine wake which are most susceptible to noise perception.

Towards these objectives, **Chapter 3** of the thesis presents an investigation of the correlations between the potential noise generation mechanisms and perceived noise by residents in the vicinity of a wind turbine. A metadata analysis was carried out in order to

identify the noise generation mechanisms perceived by the residents. Further to aerodynamic noise, **Chapter 4** focuses on the aerodynamic noise generated by a NACA 0012 airfoil. For this study, a numerical method was used to determine the flow field in the selected flow domain and pressure fluctuation on the airfoil surface. A Fowcs-Williams and Hawkings analogy was applied to calculate the sound signature in the far-field. Moreover, directivity of the noise emitted from the airfoil under pre-stall, light-stall and deep-stall was investigated. This research provides information regarding the noise characteristics such as changes in the directivity and noise level as a function of the angle of attack changes. In **Chapter 5**, a numerical model of wind turbine aerodynamics was developed and validated against experimental data. The outcomes of four engineering models of turbine wakes were then compared with the well resolved data and their accuracy and ability to provide useful data for wake and noise studies were assessed. The numerical and validated model was used to study the effect of the atmospheric boundary layer on the wind turbine wake in **Chapter 6**; where the fundamental mechanism of wake development and its breakdown in the atmospheric boundary layer were studied. The change in the wake behaviour were highlighted through comparing the results in the presence and absence of the atmospheric boundary layer. Previous research by Barlas et al. (2017) showed that the wake of a wind turbine has a significant effect on the propagation of a monopole sound source immediately upstream of the turbine wake. The wake acts like a duct and conveys the noise energy downstream of the turbine up to the breakdown region. In order to investigate the effect of ABL and turbine wake on the noise emission from a wind turbine, a computational aeroacoustic model was developed and presented in **Chapter 7**. Finally, **Chapter 8** of this thesis provides concluding remarks and outlines the significant findings during the course of this research and introduces some aspects for further research in this field.

2.4 References

Aditya, G. & Sanjiva, K. L. 2015. A modeling framework for wind farm analysis: Wind turbine wake interactions. *33rd Wind Energy Symposium.* American Institute of Aeronautics and Astronautics.

Ahlstrom, A. 2005. *Aeroelastic simulation of wind turbine dynamics.* Doctoral Thesis, Royal Institute of Technology, Stockholm, Sweden.

Ainslie, J. F. 1988. Calculating the flow field in the wake of wind turbines. *Journal of Wind Engineering and Industrial Aerodynamics,* **27,** 213-224.

American National Standards Institute & United States. A58 1982, American national standard minimum design loads for buildings and other structures. National Bureau of Standards & American National Standards Committee on Building Code Requirements for Minimum Design Loads in Buildings, New York, N.Y.

Amiet, R. K. 1975. Acoustic radiation from an airfoil in a turbulent stream. *Journal of Sound and Vibration,* **41**, 407-420.

Ammara, I., Leclerc, C. & Masson, C. 2002. A viscous three-dimensional differential/actuator-disc method for the aerodynamic analysis of wind farms. *Journal of Solar Energy Engineering,* **124,** 345-356.

Ashcroft, J. 1994. The relationship between the gust ratio, terrain roughness, gust duration and the hourly mean wind speed. *Journal of Wind Engineering and Industrial Aerodynamics,* **53,** 331-355.

Bai, C.-J. & Wang, W.-C. 2016. Review of computational and experimental approaches to analysis of aerodynamic performance in horizontal-axis wind turbines (HAWTs). *Renewable and Sustainable Energy Reviews,* **63,** 506-519.

Bailly, C. & Juvé, D. 2000. Numerical solution of acoustic propagation problems using linearized Euler equations. *AIAA Journal,* **38**, 22-29.

Bakker, R. H., Pedersen, E., Berg, G. P. V. d., Stewart, R. E., Lok, W. & Bouma, J. 2012. Impact of wind turbine sound on annoyance, self-reported sleep disturbance and psychological distress. *Science of the Total Environment,* **425,** 42-51.

Barlas, E., Zhu, W. J., Shen, W. Z., Kelly, M. & Andersen, S. J. 2017. Effects of wind turbine wake on atmospheric sound propagation. *Applied Acoustics,* **122,** 51-61.

Barthelmie, R. J., Frandsen, S. T., Hansen, K., Schepers, J. G., Rados, K., Schlez, W., Neubert, A., Jensen, L. E. & Neckelmann, S. 2009. Modelling the impact of wakes on power output at Nysted and Horns Rev. *European Wind Energy Conference.* Marseille, France.

Barthelmie, R. J., Frandsen, S. T., Rathmann, O., Hansen, K., Politis, E. S., Prospathopoulos, J., Cabezón, D., Rados, K., Pijl, S. P. v. d., Schepers, J. G., Schlez, W., Phillips, J. & Neubert, A. 2008. Flow and wakes in large wind farms in complex terrain and offshore. *European Wind Energy Conference.* Brussels, Belgium.

Bellhouse, G. 2004. Low frequency noise and infrasound from wind turbine generators: A literature review. Prepared for: Energy Efficiency and Conservation Authority, New Zealand.

Berg, F. V. d. 2005. The beat is getting stronger: The effect of atmospheric stability on low frequency modulated sound of wind turbines. *Journal of Low Frequency Noise, Vibration & Active Control,* **24,** 1-24.

Berg, G. P. v. d. 2004a. Do wind turbines produce significant low frequency sound levels?, *11th International Meeting on Low Frequency Noise and Vibration and its Control*. Maastricht, Netherlands.

Berg, G. P. v. d. 2004b. Effects of the wind profile at night on wind turbine sound. *Journal of Sound and Vibration,* **277,** 955-970.

Bertagnolio, F., Sørensen, N. N., Johansen, J. & Fuglsang, P. 2001. Wind turbine airfoil catalogue. Denmark. Forskningscenter Risoe, Risoe-R: No. 1280(EN).

Betz, A. 1966. Section: 66 - wind-driven rotors. *Introduction to the theory of flow machines.* Pergamon.

Blomhoff, H. P. 2012. *An experimental investigation of wind turbine wakes.* Master of Science in Product Design and Manufacturing, Norwegian University of Science and Technology.

Bolin, K., Bluhm, G., Eriksson, G. & Nilsson, M. E. 2011. Infrasound and low frequency noise from wind turbines: Exposure and health effects. *Environmental Research Letters,* **6**, 035103.

Brooks, T. F. & Hodgson, T. H. 1981. Trailing edge noise prediction from measured surface pressures. *Journal of Sound and Vibration*, **78**, 69-117.

Brooks, T. F., Pope, D. S. & Marcolini, M. A. 1989. Airfoil self-noise and prediction. NASA Reference Publication, NASA. Document number: 1218.

Buck, S. 2017. An investigation into wind turbine acoustic noise variability. Thesis submitted in partial fulfillment of the requirements for the degree of Doctor of Philosophy, University of Colorado.

Burton, T., Sharpe, D., Jenkins, N. & Bossanyi, E. 2001. *Wind energy: Handbook*, Wiley Online Library.

Casalino, D., Jacob, M. & Roger, M. 2003. Prediction of rod-airfoil interaction noise using the Ffowcs-Williams-Hawkings analogy. *AIAA Journal*, **41**, 182-191.

Cheung, L. C., Premasuthan, S., Davoust, S. & Terzi, D. V. 2016. A simple model for the turbulence intensity distribution in atmospheric boundary layers. *Journal of Physics: Conference Series,* **753,** 032008.

Choudhry, A., Mo, J.-O., Arjomandi, M. & Kelso, R. 2014. Effects of wake interaction on downstream wind turbines. *Wind Engineering*, **38**, 535-548.

Cleijne, J. W. 1993. Results of Sexbierum Wind Farm; single wake measurements. TNO Institute of Environmental and Energy Technology, Reference number: 93-082, File number: 112324-22420.

Colonius, T., Lele, S. K. & Moin, P. 1994. The scattering of sound waves by a vortex: Numerical simulation and analytical solution. *Journal of Fluid Mechanics,* **260**, 271-298.

Cook, N. J. 1985. *The designer's guide to wind loading of building structures,* London, Boston, Butterworths, Building Research Establishment, Department of the Environment.

Cook, N. J. 1997. The Deaves and Harris ABL model applied to heterogeneous terrain. *Journal of Wind Engineering and Industrial Aerodynamics,* **66,** 197-214.

Crespo, A. 1985. Numerical analysis of wind turbine wakes. Proceedings of Delphi Workshop on "Wind turbine applications".

Crespo, A., Hernández, J. & Frandsen, S. 1999. Survey of modelling methods for wind turbine wakes and wind farms. *Wind Energy,* **2,** 1-24.

Dimitrov, N., Natarajan, A. & Kelly, M. 2015. Model of wind shear conditional on turbulence and its impact on wind turbine loads. *Wind Energy,* **18,** 1917-1931.

Dixon, K. R. 2008. *The near wake structure of a vertical axis wind turbine, including the development of a 3D unsteady free-wake panel method for VAWTs.* Thesis for fulfillment of the degree of Master of Science, Delft University of Technology.

Doolan, C. J., Moreau, D. J. & Brooks, L. A. 2012. Wind turbine noise mechanisms and some concepts for its control. *Acoustics Australia,* **40,** 7-13.

Ebert, P. R. & Wood, D. H. 1999. The near wake of a model horizontal-axis wind turbine—II. General features of the three-dimensional flow field. *Renewable Energy*, **18**, 513-534.

Ellenbogen, J. M., Grace, S., Heiger-Bernays, W. J., Manwell, J. F., Mills, D. A., Sullivan, K. A., Weisskopf, M. G. & Santos, S. L. 2012. Wind turbine health impact study: Report of independent expert panel. Prepared for Massachusetts Department of Environmental Protection, Massachusetts Department of Public Health.

Elliott, D. L. 1991. Status of wake and array loss research. *Windpower Conference*, Palm Springs 22-24 September, California.

España, G., Aubrun, S., Loyer, S. & Devinant, P. 2011. Spatial study of the wake meandering using modelled wind turbines in a wind tunnel. *Wind Energy*, **14,** 923-937.

Evans, T. 2013. Macarthur Wind Farm infrasound & low frequency noise, operational monitoring results. Resonate Acoustics, Technical report prepared for AGL Energy Limited.

Ewert, R. & Schröder, W. 2003. Acoustic perturbation equations based on flow decomposition via source filtering. *Journal of Computational Physics*, **188**, 365-398.

Flay, R. G. J. 2015. Model tests of wind turbines in wind tunnels. *Technical Transactions, Civil Engineering*, **12**, 63-81.

Frandsen, S., Barthelmie, R., Pryor, S., Rathmann, O., Larsen, S., Højstrup, J. & Thøgersen, M. 2006. Analytical modelling of wind speed deficit in large offshore wind farms. *Wind Energy*, **9,** 39-53.

Friman, M. 2011. *Directivity of sound from wind turbines: A study on the horizontal sound radiation pattern from a wind turbine.* Thesis for the degree of Master of Science, KTH Royal Institute of Technology.

Fuglsang, P., Bak, C., Gaunaa, M. & Antoniou, I. 2004. Design and verification of the Risø-B1 airfoil family for wind turbines. *Journal of Solar Energy Engineering,* **126,** 1002-1010.

Ghadirian, A., Dehghan, M. & Torabi, F. 2014. Considering induction factor using BEM method in wind farm layout optimization. *Journal of Wind Engineering and Industrial Aerodynamics,* **129,** 31-39.

Ghosh, T. K. & Prelas, M. A. 2011. Wind energy. *Energy Resources and Systems.* Springer Netherlands.

Glauert, H. 1935. Windmills and fans. *Aerodynamic theory.* Berlin: Julius Springer.

Glauert, H. 1926. The elements of airfoil and airscrew theory. *New York: Cambridge University Press*.

Gómez-Elvira, R., Crespo, A., Migoya, E., Manuel, F. & Hernández, J. 2005. Anisotropy of turbulence in wind turbine wakes. *Journal of Wind Engineering and Industrial Aerodynamics,* **93,** 797-814.

Grasso, F. 2011. Usage of numerical optimization in wind turbine airfoil design. *Journal of Aircraft,* **48,** 248-255.

Grosveld, F. W. 1985. Prediction of broadband noise from horizontal axis wind turbines. *Journal of Propulsion and Power,* **1**, 292-299.

Hand, M. M., Simms, D. A., Fingersh, L. J., Jager, D. W., Cotrell, J. R., Schreck, S. & Larwood, S. M. 2001. Unsteady aerodynamics experiment phase VI: Wind tunnel test configurations and available data campaigns. National Renewable Energy Laboratory.

Hansen, A. C. & Butterfield, C. P. 1993. Aerodynamics of horizontal axis wind turbines. *Annual Review of Fluid Mechanics,* **25,** 115-145.

Hansen, K., Henrys, N., Hansen, C., Doolan, C. & Moreau, D. 2012. Wind farm noise – what is a reasonable limit in rural areas?, *Acoustics 2012*, Fremantle.

Hansen, M. O. L. 2008. *Aerodynamics of wind turbines*, Earthscan, London. Sterling, VA.

Hansen, M. O. L., Sorensen, J. N., Michelsen, J. A. & Sorensen, N. N. 1997. A global Navier-Stokes rotor prediction model. *35th Aerospace Sciences Meeting & Exhibit*, AIAA.

Hardin, J. C. & Pope, D. S. 1994. An acoustic/viscous splitting technique for computational aeroacoustics. *Theoretical and Computational Fluid Dynamics*, **6**, 323-340.

Harstveit, K. 1996. Full scale measurements of gust factors and turbulence intensity, and their relations in hilly terrain. *Journal of Wind Engineering and Industrial Aerodynamics,* **61,** 195-205.

Ishihara, T., Yamaguchi, A. & Fujino, Y. 2004. Development of a new wake model based on a wind tunnel experiment. *Global Wind Power*. Chicago, Illinois, USA.

Ivanell, S., Sørensen, J. N., Mikkelsen, R. & Henningson, D. 2009. Analysis of numerically generated wake structures. *Wind Energy,* **12,** 63-80.

Jakobsen, J. 2005. Infrasound emission from wind turbines. *Journal of Low Frequency Noise, Vibration and Active Control,* **24,** 145-155.

Janssen, S. A., Vos, H., Eisses, A. & Pedersen, E. 2011. A comparison between exposure-response relationships for wind turbine annoyance and annoyance due to other noise sources. *Journal of the Acoustical Society of America,* **130,** 3746-3753.

Jensen, N. O. 1983. A note on wind generator interaction. Risø National Laboratory, Report number: Risø-M-2411.

Jianu, O., Rosen, M. A. & Naterer, G. 2012. Noise Pollution Prevention in Wind Turbines: Status and Recent Advances. *Sustainability*, **4**, 1104-1117.

Jimenez, A., Crespo, A., Migoya, E. & Garcia, J. 2007. Advances in large-eddy simulation of a wind turbine wake. *Journal of Physics: Conference Series,* **75**.

Joselin Herbert, G. M., Iniyan, S., Sreevalsan, E. & Rajapandian, S. 2007. A review of wind energy technologies. *Renewable and Sustainable Energy Reviews,* **11,** 1117-1145.

Kaimal, J. C., Wyngaard, J. C., Haugen, D. A., Coté, O. R., Izumi, Y., Caughey, S. J. & Readings, C. J. 1976. Turbulence structure in the convective boundary layer. *Journal of the Atmospheric Sciences,* **33,** 2152-2169.

Kaliski, K. & Neeraj, G. 2013. Prevalence of complaints related to wind turbine noise in Northern New England. *ICA 2013 Montreal*, 2-7 June 2013 Montreal, Canada.

Kamruzzaman, M., Lutz, T., Kraemer, E. & Wuerz, W. 2011. On the Length Scales of Turbulence for Aeroacoustic Applications. *17th AIAA/CEAS Aeroacoustics Conference (32nd AIAA Aeroacoustics Conference)*. American Institute of Aeronautics and Astronautics.

Kasmi, A. E. & Masson, C. 2008. An extended k-e model for turbulent flows through horizontal-axis wind turbines. *Journal of Wind Energy and Industrial Aerodynamics,* **96,** 103-122.

Katic´, I., Højstrup, J. & Jensen, N. O. 1986. A simple model for cluster efficiency. *European Wind Energy Association Conference and Exhibition.* Rome, Italy.

Kelley, N. D., McKenna, H., Hemphill, R., Etter, C., Garrelts, R. & Linn, N. 1985. Acoustic noise associated with the MOD-1 wind turbine: Its source, impact, and control. U.S. Department of Energy: Solar Energy Research Institute.

Kim, H., Potty, G. R., Miller, J. H. & Baxter, C. 2011. Modeling of offshore wind turbine noise radiation and propagation. *The Journal of the Acoustical Society of America,* **130,** 2332-2332.

Kinsler, L. E., Frey, A. R., Coppens, A. B. & Sanders, J. V. 2012. *Fundamentals of Acoustics*, John Wiley & Sons, Inc.

Kircsi, A. & Tar, K. 2008. Profile tests to optimize the utilization of wind energy *Acta Silvatica et Lignaria Hungarica*, **4**, 107-123.

Kloosterman, M. H. M. 2009. *Development of the near wake behind a horizontal axis wind turbine.* Master of Science, Delft University of Technology.

Kristensen, L., Casanova, M., Courtney, M. S. & Troen, I. 1991. In search of a gust definition. *Boundary-Layer Meteorology,* **55,** 91-107.

Kundu, P. K. & Cohen, I. M. 2004. *Fluid mechanics*, Elsevier Academic Press.

Kuwano, S., Yano, T., Kageyama, T., Sueoka, S. & Tachibana, H. 2013. Social survey community response to wind turbine noise. *Inter Noise.* Innsbruck, Austria.

Larsen, G. C. 1988. A simple wake calculation procedure technical report. RIS National Laboratory.

Lee, S., Kim, K., Choi, W. & Lee, S. 2011. Annoyance caused by amplitude modulation of wind turbine noise. *Noise Control Engineering Journal*, **59**, 38-46.

Lee, S., Lee, S. & Lee, S. 2013. Numerical modeling of wind turbine aerodynamic noise in the time domain. *The Journal of the Acoustical Society of America,* **133,** EL94-EL100.

Leloudas, G., Zhu, W. J., Sørensen, J. N., Shen, W. Z. & Hjort, S. 2007. Prediction and reduction of noise from a 2.3 MW wind turbine. *The Science of Making Torque from Wind, IOP Publishing, Journal of Physics, Conference Series*, **75**.

Leventhall, G. 2006. Infrasound from wind turbines – fact, fiction or deception. *Canadian Acoustics,* **34,** 29-36.

Li, Q. S., Zhi, L. & Hu, F. 2010. Boundary layer wind structure from observations on a 325 m tower. *Journal of Wind Engineering and Industrial Aerodynamics,* **98,** 818-832.

Lichtenhan, J. & Salt, A. Amplitude modulation of audible sounds by non-audible sounds: Understanding the effects of wind turbine noise. *ICA 2013 Montreal*, 2-7 June 2013 Montreal, Canada. Acoustical Society of America through the American Institute of Physics.

Lighthill, M. J. 1952. On sound generated aerodynamically. I. general theory. *Proceedings of the Royal Society of London. Series A. Mathematical and Physical Sciences*, **211**, 564-587.

Liu, H. 1990. *Wind engineering: A handbook for structural engineering*, Pearson Education.

Liu, M. K., Yocke, M. A. & Myers, T. L. 1983. Mathematical model for the analysis of wind turbine wakes. *Journal of Energy,* **7,** 73-78.

Lowson, M. V. 1993. Assessment and prediction of wind turbine noise. Bristol, United Kingdom: Flow Solutions Ltd., Technical report.

Lumley, J. L. & Panofsky, H. A. 1964. *The structure of atmospheric turbulence,* New York, Interscience Publishers.

Manwell, J. F., McGowan, J. G. & Rogers, A. L. 2009a. *Aerodynamics of wind turbines. Wind energy explained.* John Wiley & Sons, Ltd.

Manwell, J. F., McGowan, J. G. & Rogers, A. L. 2009b. *Wind energy explained: Theory, design and application*, Wiley Online Library.

McTavish, S., Feszty, D. & Nitzsche, F. 2013. An experimental and computational assessment of blockage effects on wind turbine wake development. *Wind Energy*, **17,** 1515-1529.

Medici, D. 2005. *Experimental studies of wind turbine wakes - power optimisation and meandering*. PhD, KTH Mechanics, Royal Institute of Technology.

Mehta, D., van Zuijlen, A. H., Koren, B., Holierhoek, J. G. & Bijl, H. 2014. Large eddy simulation of wind farm aerodynamics: A review. *Journal of Wind Engineering and Industrial Aerodynamics,* **133,** 1-17.

Meir, R., Legerton, M. L., Anderson, M. B., Berry, B., Bullmore, A., Hayes, M., Jiggins, M., Leeming, E., Musgrove, P., Spode, D. J., Thomas, H. A., Tomalin, E., Trinick, M. & Warren, J. 1996. The assessment and rating of noise from wind farms. Report prepared by ETSU for Department of Trade and Industry (DTI), Report number: ETSU-R-97.

Mikkelsen, R. 2003. *Actuator disc methods applied to wind turbines.* Doctoral dissertation, Technical University of Denmark.

Mo, J.-O., Choudhry, A., Arjomandi, M., Kelso, R. & Lee, Y.-H. 2013a. Effects of wind speed changes on wake instability of a wind turbine in a virtual wind tunnel using large eddy simulation. *Journal of Wind Engineering and Industrial Aerodynamics,* **117,** 38-56.

Mo, J.-O., Choudhry, A., Arjomandi, M. & Lee, Y.-H. 2013b. Large eddy simulation of the wind turbine wake characteristics in the numerical wind tunnel model. *Journal of Wind Engineering and Industrial Aerodynamics,* **112,** 11-24.

Møller, H. & Pedersen, C. S. 2011. Low-Frequency Noise from Large Wind Turbines. *Journal of the Acoustical Society of America,* **129**, 3727-3744.

Moorhouse, A., Hayes, M., Sabine von Hünerbein, Piper, B. & Adams, M. 2007. Research into aerodynamic modulation of wind turbine noise: Final report.

Moriarty, P. 2004. Development and validation of a semi-empirical wind turbine aeroacoustic code. *42nd AIAA Aerospace Sciences Meeting and Exhibit*. American Institute of Aeronautics and Astronautics.

Moriarty, P., Guidati, G. & Migliore, P. 2004. Recent improvement of a semi-empirical aeroacoustic prediction code for wind turbines. *10th AIAA/CEAS Aeroacoustics Conference.* American Institute of Aeronautics and Astronautics.

Moriarty, P. & Migliore, P. 2003. Semi-empirical aeroacoustic noise prediction code for wind turbines. National Renewable Energy Laboratory.

Morris, P. J., Long, L. N., Bangalore, A. & Wang, Q. 1997. A parallel three-dimensional computational aeroacoustics method using nonlinear disturbance equations. *Journal of Computational Physics*, **133**, 56-74.

Napoli, C. D. 2011. Long distance amplitude modulation of wind turbine noise. *Fourth International Meeting on Wind Turbine Noise*. Rome, Italy.

Neustadter, H. E. & Spera, D. A. 1985. Method for evaluating wind turbine wake effects on wind farm performance. *Journal of Solar Energy Engineering,* **107,** 240-243.

Newman, B. G. 1977. The spacing of wind turbines in large arrays. *Energy Conversion,* **16,** 169-171.

Nobbs, B., Doolan, C. J. & Moreau, D. J. 2012. Characterisation of noise in homes affected by wind turbine noise. *Acoustics 2012*, Fremantle, 21-23 November 2012, Australia.

Oerlemans, S. 2009. *Detection of aeroacoustic sound sources on aircraft and wind turbines.* PhD Thesis, University of Twente.

Oerlemans, S. 2011a. An explanation for enhanced amplitude modulation of wind turbine noise. National Aerospace Laboratory (NLR).

Oerlemans, S. 2011b. Wind turbine noise: Primary noise sources. Report prepared for National Aerospace Laboratory (NLR), Report number: NLR-TP-2011-066.

Oerlemans, S. & Schepers, J. G. 2009. Prediction of wind turbine noise and validation against experiment. National Aerospace Laboratory (NLR).

Oerlemans, S., Sijtsma, P. & López, B. M. 2007. Location and quantification of noise sources on a wind turbine. National Aerospace Laboratory (NLR).

Paller, C., Bigelow, P., Majowicz, S., Law, J. & Christidis, T. 2013. Wind turbine noise, sleep quality, and symptoms of inner ear problems. University of Waterloo.

Panofsky, H. A. 1967. A survey of current through on wind properties relevant for diffusion in the lowest 100 m. *Symposium on Atmospheric Turbulence and Diffusion.* Albuquerque, New Mexico: Sandia Laboratories.

Pawlaczyk-Luszczynska, M., Dudarewicz, A., Zaborowski, K., Zamojska, M. & Waszkowska, M. 2013. Assessment of annoyance due to wind turbine noise. *ICA 2013 Montreal*, 2-7 June 2013 Montreal, Canada. Acoustical Society of America through the American Institute of Physics.

Peacock, A. D., Jenkins, D., Ahadzi, M., Berry, A. & Turan, S. 2008. Micro wind turbines in the UK domestic sector. *Energy and Buildings,* **40,** 1324-1333.

Pedersen, E., Berg, F. v. d., Bakker, R. & Bouma, J. 2009. Response to noise from modern wind farms in the Netherlands. *The Journal of the Acoustical Society of America,* **126,** 634-643.

Pedersen, E., Bouma, J., Bakker, R. & Berg, F. V. D. 2008. Response to wind turbine noise in the Netherlands. *The Journal of the Acoustical Society of America,* **123,** 3536-3536.

Pedersen, E., Hallberg, L.-M. & Waye, K. P. 2007. Living in the vicinity of wind turbines — a grounded theory study. *Qualitative Research in Psychology,* **4,** 49-63.

Pedersen, E. & Waye, K. P. 2004. Perception and annoyance due to wind turbine noise—a dose–response relationship. *Journal of the Acoustical Society of America,* **116,** 3460-3470.

Powell, A. 1959. On the aerodynamic noise of a rigid flat plate moving at zero incidence. *The Journal of the Acoustical Society of America,* **31,** 1649-1653.

Powell, A. 1990. Some aspects of aeroacoustics: From Rayleigh until today. *Journal of Vibration and Acoustics,* **112,** 145-159.

Rathmann, O., Barthelmie, R. & Frandsen, S. 2006. Turbine wake model for wind resource software. *European Wind Energy Conference and Exhibition*.

Renkema, D. J. 2007. *Validation of wind turbine wake models, using wind farm data and wind tunnel measurements.* Master of Science, Delft University of Technology.

Renterghem, T. V. 2014. Efficient outdoor sound propagation modeling with the finite-difference time-domain (FDTD) method: a review. *International Journal of Aeroacoustics*, **13**, 385-404.

Rogers, A. L. 2002. Wind turbine acoustic noise. University of Massachusetts at Amherst: Renewable Energy Research Laboratory, Department of Mechanical and Industrial Engineering.

Ross, I. & Altman, A. 2011. Wind tunnel blockage corrections: Review and application to Savonius vertical-axis wind turbines. *Journal of Wind Engineering and Industrial Aerodynamics*, **99,** 523-538.

Ruano, C., Coin, K. & Roldan, L. 2012. Wind turbine model for wind tunnel testing. Senior design project, City College of New York.

Sandberg, R., Jones, L. & Sandham, N. 2008. Direct numerical simulations of noise generated by turbulent flow over airfoils. *14th AIAA/CEAS aeroacoustics conference (29th AIAA Aeroacoustics Conference).* American Institute of Aeronautics and Astronautics.

Sanderse, B. 2012. Aerodynamics of wind turbine wakes. Literature review report prepared for Energy Research Centre of the Netherlands.

Sant, T. 2007. *Improving BEM-based aerodynamic models in wind turbine design codes.* PhD Thesis, Delft University of Technology.

Schepers, J. G. 2003. Endow: Validation and improvement of ECN's wake model. Techincal report prepared for Energy Research Centre of the Netherlands.

Schlinker, R. H. & Amiet, R. K. 1981. Helicopter rotor trailing edge noise. United Technologies Research Center, Report prepared for Langley Research Center.

Schomer, P. 2013. Can wind-turbine sound that is below the threshold of hearing be heard? ICA 2013 Montreal, 2013 Montreal, Canada. Acoustical Society of America through the American Institute of Physics.

Schümann, H., Pierella, F. & Sætran, L. 2013. Experimental investigation of wind turbine wakes in the wind tunnel. *Energy Procedia,* **35,** 285-296.

Seong, Y., Lee, S., Gwak, D. Y., Cho, Y., Hong, J. & Lee, S. 2013, An experimental study on rating scale for annoyance due to wind turbine noise. *Internoise*, Noise Control for Quality of Life, 2013 Innsbruck, Austria.

Sezer-Uzol, N., Gupta, A. & Long, L. N. 2009. 3-D time-accurate inviscid and viscous CFD simulations of wind turbine rotor flow fields. *Parallel computational fluid dynamics 2007.* Springer Berlin Heidelberg.

Sezer-Uzol, N. & Long, L. N. 2006. 3-D time-accurate CFD simulations of wind turbine rotor flow fields. *American Institute of Aeronautics and Astronautics,* **394**.

Shepherd, D., Hanning, C. & Thorne, B. 2012. Noise: Windfarms. *Encyclopedia of Environmental Management*.

Shepherd, K. P. & Hubbard, H. H. 1985. Sound propagation studies for a large horizontal axis wind turbine. Hampton, Virginia, Technical report prepared for NASA.

Sherry, M., Nemes, A., Jacono, D. L., Blackburn, H. M. & Sheridan, J. 2013. The interaction of helical tip and root vortices in a wind turbine wake. *Physics of Fluids* (1994-present), 25, 117102-1-16.

Singh, R. K., Ahmed, M. R., Zullah, M. A. & Lee, Y.-H. 2012. Design of a low Reynolds number airfoil for small horizontal axis wind turbines. *Renewable Energy,* **42,** 66-76.

Sørensen, J. N. 1986. *Three-level, viscous-inviscid interaction technique for the prediction of separated flow past rotating wing.* PhD thesis, Technical University of Denmark.

Sørensen, J. N. 2016. *General momentum theory for horizontal axis wind turbines*, Springer.

Sørensen, J. N. & Myken, A. 1992. Unsteady actuator disc model for horizontal axis wind turbines. *Journal of Wind Engineering and Industrial Aerodynamics,* **39,** 139-149.

Sørensen, J. N., Shen, W. Z. & Munduate, X. 1998. Analysis of wake states by a full-field actuator disc model. *Wind Energy,* **1,** 73-88.

Spera, D. A. (ed.) 2009. *Wind turbine technology: Fundamental concepts in wind turbine engineering, second edition*, ASME

Stewart, J. 2002. Location, location, location, an investigation into wind farms and noise by the noise association. The Noise Association, London: The Noise Association.

Stull, R. B. 1988. *An introduction to boundary layer meteorology*, Springer.

Templin, R. J. 1974. An estimation of the interaction of windmills in widespread arrays. National Aeronautical Establishment.

Tennekes, H. & Lumley, J. L. 1972. *A first course in turbulence,* Massachusetts, The MIT Press.

Thøgersen, M. L. 2005. Windpro / park - introduction to wind turbine wake modelling and wake generated turbulence. EMD International A/S.

Thorne, B. 2011. The problems with "noise numbers" for wind farm noise assessment. *Bulletin of Science, Technology & Society,* **31,** 262-290.

Tian, W., Ozbay, A. & Hu, H. 2014. Effects of incoming surface wind conditions on the wake characteristics and dynamic wind loads acting on a wind turbine model. *Physics of Fluids,* **26,** 125108.

Timmerman, N. S. 2013. Wind turbine noise. *Acoustics Today,* **9,** 22-29.

Troldborg, N., Sørensen, J. N. & Mikkelsen, R. 2007. Actuator line simulation of wake of wind turbine operating in turbulent inflow. *Journal of Physics: Conference Series,* **75**.

Vaz, J. R. P., Pinho, J. T. & Mesquita, A. L. A. 2011. An extension of BEM method applied to horizontal-axis wind turbine design. *Renewable Energy,* **36,** 1734-1740.

Vermeer, L. J., Sørensen, J. N. & Crespo, A. 2003. Wind turbine wake aerodynamics. *Progress in Aerospace Sciences,* **39,** 467-510.

Voutsinas, S. G., Rados, K. G. & Zervos, A. 1992. Investigation of the effect of the initial velocity profile on the wake development of a wind turbine. *Journal of Wind Energy and Industrial Aerodynamics,* **39**, 293-301.

Vries, O. D. 1979. Fluid dynamic aspects of wind energy conversion. Technical report prepared for National Aerospace Laboratory (NLR).

Walker, B., Hessler, G. F., Hessler, D. M., Rand, R. & Schomer, P. 2012. A cooperative measurement survey and analysis of low frequency and infrasound at the Shirley Wind Farm in Brown County, Wisconsin, Report number: 122412-1.

Wang, T. 2012. A brief review on wind turbine aerodynamics. *Theoretical and Applied Mechanics Letters,* **2,** 062001.

Waye, K. P. & Öhrström, E. 2002. Psycho-acoustic characters of relevance for annoyance of wind turbine noise. *Journal of Sound and Vibration,* **250,** 65-73.

Whale, J., Anderson, C. G., Bareiss, R. & Wagner, S. 2000. An experimental and numerical study of the vortex structure in the wake of a wind turbine. *Journal of Wind Engineering and Industrial Aerodynamics,* **84,** 1-21.

Wilcox, D. C. 1998. *Turbulence modeling for CFD*, DCW Industries.

Wilson, R. E. & Lissaman, P. B. S. 1974. Book, *Applied aerodynamics of wind power machines,* Corvallis, Oregon State University.

Wu, Y.-T. & Porté-Agel, F. 2011. Large-eddy simulation of wind-turbine wakes: Evaluation of turbine parametrizations. *Boundary-Layer Meteorology,* **138,** 345-366.

Yu, B. & Chowdhury, A. G. 2009. Gust factors and turbulence intensities for the tropical cyclone environment. *Journal of Applied Meteorology and Climatology,* **48,** 534-552.

Zosuls, A., Kelley, R. M., Mountain, D. & Grace, S. 2013. Generation of wind turbine noise signature for use in lab environment. *The Journal of the Acoustical Society of America,* **133,** 3419-3419.

Chapter 3 Mechanism of perceived noise from wind turbine

3.1 Chapter overview

In this chapter the possible wind turbine noise mechanisms associated with the perceived noise by the communities in the vicinity of the wind farms are discussed and the noise mechanisms associated with the wind turbine operation was identified and presented. To find a relationship between wind direction, noise directivity and location of the perceived noise several noise reports and surveys were analysed. The possible noise mechanisms were specified by eliminating the noise generation mechanisms, characteristics of which do not match the features of the perceived noise such as the distance and wind conditions during the noise perception period. Results from source mapping and recorded pressure fluctuations on the turbine blade in the field were also used to support and verify the hypothesis on the relationship between the wake and noise signatures.

The details of the methodology, location of the wind farm sites, supporting evidences and data are presented and explained in the following sections of this chapter. This section is published in the Journal of Renewable Energy and permission to reproduce the article has been obtained from the publishing authority.

Statement of Authorship

Title of Paper	Wind farm noises: Mechanisms and evidence for their dependency on wind direction
Publication Status	☑ Published ☐ Accepted for Publication ☐ Submitted for Publication ☐ Unpublished and Unsubmitted work written in manuscript style
Publication Details	Sedaghatizadeh, N., Arjomandi, M., Cazzolato, B., & Kelso, R. 2017. Wind farm noises: Mechanisms and evidence for their dependency on wind direction. Renewable Energy, 109, 311-322.

Principal Author

Name of Principal Author (Candidate)	Nima Sedaghatizadeh		
Contribution to the Paper	- Research - Providing the data, writing of the manuscript and production of original figures - Correspondence with editor and reviewers including the production of all cover letters and rejoinder		
Overall percentage (%)	80%		
Certification:	This paper reports on original research I conducted during the period of my Higher Degree by Research candidature and is not subject to any obligations or contractual agreements with a third party that would constrain its inclusion in this thesis. I am the primary author of this paper.		
Signature		Date	14/09/2017

Co-Author Contributions

By signing the Statement of Authorship, each author certifies that:

i. the candidate's stated contribution to the publication is accurate (as detailed above);

ii. permission is granted for the candidate in include the publication in the thesis; and

iii. the sum of all co-author contributions is equal to 100% less the candidate's stated contribution.

Name of Co-Author	Maziar Arjomandi		
Contribution to the Paper	- Supervision of the work, including the production of the manuscript - Participation in the development of the concepts and ideas presented in the manuscript - Evaluation and editing of the manuscript prior to submission		
Signature		Date	15/09/2017

Name of Co-Author	Benjamin Cazzolato		
Contribution to the Paper	- Supervision of the work, including the production of the manuscript - Participation in the development of the concepts and ideas presented in the manuscript - Evaluation and editing of the manuscript prior to submission		
Signature		Date	14/09/2017

Name of Co-Author	Richard Kelso		
Contribution to the Paper	- Supervision of the work, including the production of the manuscript - Participation in the development of the concepts and ideas presented in the manuscript - Evaluation and editing of the manuscript prior to submission		
Signature		Date	14/9/2017

Wind farm noises: Mechanisms and evidence for their dependency on wind direction

Nima Sedaghatizadeh, Maziar Arjomandi, Benjamin Cazzolato and Richard Kelso

School of Mechanical Engineering, the University of Adelaide, SA 5000, Australia

Published: Sedaghatizadeh, N., Arjomandi, M., Cazzolato, B., & Kelso, R. 2017. Wind farm noises: Mechanisms and evidence for their dependency on wind direction. Renewable Energy, 109, 311-322.

3.2 Abstract

The mechanisms responsible for swishing and thumping noises generated by wind turbines are unclear and the existence of which have significantly affected the perception of wind energy by the community. To better understand the nature of this noise source, this study, for the first time, investigates the correlation between the potential noise generation mechanisms in wind farms and the characteristics of the perceived noise reported by residents in the vicinity of the farms in survey data. Published reports and measurements show that in addition to the perceived noise near the turbines, the thumping noise, in general, is perceived far downstream of the turbines. Normal swish perceived in a short distance from a wind turbine, especially in the cross-wind directions, can be explained by the convective amplification and directivity of the trailing edge noise. As will be discussed in this article, there exists strong evidence that the dominant mechanism of wind farm noise is associated with amplitude modulation of the aerodynamic noise by the eddies generated when the turbine blade partially stalls or due to an interaction with the turbine wake. This hypothesis is primarily based on the low frequency characteristics of the stall and also the distance and direction of the noise propagation. Moreover, it is hypothesised that the wake supplements this effect as it results in refraction and modulation of the emitted noise.

3.3 Introduction

Wind energy has had the fastest growth rate among the renewable sources of energy over the past few decades due to its competitive price and mature technology. This has resulted in the widespread deployment of wind turbines in rural communities, which, despite resulting in some economic and environmental benefits, has led to negative community impact, such as health concerns, which in turn, are hypothesised to be related to the wind

turbine noise (Sawin, 2014, Nobbs et al., 2012, Bakker et al., 2012, Meunier, 2013, Crespo et al., 1999).

Wind turbine noise can be categorised into two groups (Stewart, 2002, Moorhouse et al., 2007, Ellenbogen et al., 2012, Oerlemans and Schepers, 2009): a) mechanical noise, which is well studied and understood, can be easily mitigated and can usually be perceived only in the vicinity of a turbine (Katinas et al., 2016); b) aeroacoustic or aerodynamic noise which is generated due to fluctuating forces interacting with the blades of the wind turbines. There exist several mechanisms contributing to the generation of aerodynamic noise from a wind turbine such as: turbulent inflow, turbine blade stall, blade trailing edge, blade-tower interaction, blade tip and laminar boundary layer vortex shedding (Oerlemans, 2011). The last two mechanisms are predominantly high frequency signatures and are unlikely to play significant roles in perceived noise far from the wind turbines. While blade-tower interaction has been reported as a major noise source for downwind turbines due to interaction of the blade and vortex shedding from the tower, studies show that the effect of perturbed flow upstream of the towers of modern upwind turbines is not significant in generation of unsteady loads on the blade compared to the load variation due to interaction of the blade with the incoming turbulence (Kim et al., 2011). Moreover, the level of noise generated by the blade-tower interaction also decreases as the mean wind speed and yaw error increase, while the level of noise generated by other mechanisms increases under these conditions (Kim et al., 2011, Laratro et al., 2014). In addition, the noise generated due to the blade-tower interaction occurs at the blade pass frequency and may contribute to the infrasound (frequency less than 16 Hz) (Timmerman, 2013, Lenchine and Song, 2014), hence it is not the objective of this study which investigates only the audible sound.

To explain the mechanisms which are believed to be the main sources of the noise generated by wind turbine blades, a schematic of the flow over a blade is shown in Figure 3.1. When the blade encounters turbulence eddies from incoming flow, fluctuating forces on the blade surface result in noise generation. The frequency of the emitted noise has an inverse relationship with the size of the incoming eddies such that the larger eddies generate noise at lower frequencies compared with the noise generated due to interaction of the blade with smaller eddies (Berg, 2005, Doolan et al., 2012). Trailing edge noise is generated by the eddies in the scale of boundary layer displacement thickness at the trailing edge of the airfoil, which results in fluctuating forces at a moderate frequency (400-1000 Hz) (Moorhouse et al., 2007, Oerlemans, 2011). Stall and consequent vortices generated due to the flow separation also result in fluctuating load on the airfoil and if the deep stall occurs large eddies will form on the suction of the airfoil which result in a significant increase in noise level at an audible lower range of frequency (100-400 Hz) (Oerlemans, 2011, Moreau et al., 2009).

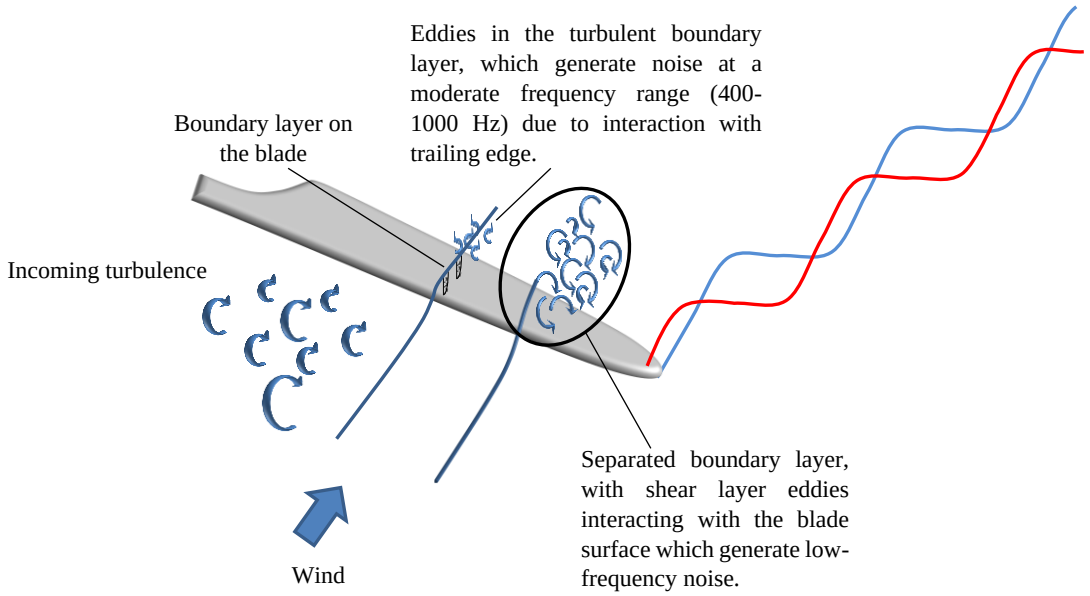

Figure 3.1 Incoming flow features and different noise generation mechanisms.

Amplitude modulation is also another mechanism, which affects the emitted noise from wind farms and has been reported to be one of the reasons of perceived annoying noise

(Oerlemans, 2011, Madsen et al., 2014). Amplitude modulation is characterised by a variation of the level and character of noise in time. The normal amplitude modulation is caused due to variation in noise level due to movement of the source of the trailing edge noise during the rotation of the blade. Normal amplitude modulation of broadband trailing edge noise occurs at blade pass frequency with the fluctuation of a few decibels and is perceived in close distance of wind turbines (Oerlemans, 2011). There exists another type of amplitude modulation, so called Other Amplitude Modulation (OAM) or Enhanced Amplitude Modulation (EAM), which has stronger low-frequency content and increased depth of the modulation (6-12 dB) (Oerlemans, 2011, Smith, 2012). EAM can be caused by the partial or transient stall on the blade when the blade interacts with incoming eddies, turbine wake or inclined flow. Since most of the survey data are collected far downstream of the turbines it can be concluded that EAM or OAM can be the underlying mechanism for perceived noise. As will be discussed further in the text and in section 3.5,

Two main features of the aerodynamic noise are noticeable: a) "***swish"*** which has broadband content and directed towards the leading edge, generated primarily due to turbulent boundary layer interaction with the trailing edge of the turbine airfoil; b) "***thumping"*** at the blade pass frequency which travels a few kilometres and is known to have the most annoying effect on people (Waye and Öhrström, 2002, Leventhall, 2006, Bolin et al., 2011, Pedersen et al., 2009, Oerlemans and Schepers, 2009). This article investigates the above sources of noise with a focus on thumping as explained above.

In the past decades a large number of scientific articles have been published on the mechanisms of noise generation from wind turbines with the main focus on reporting the outcomes of laboratory experiments and numerical modelling (Alvarez, 2011, Madsen et al., 2013, Oerlemans, 2011, Ghasemian and Nejat, 2015, Lee et al., 2013, Lichtenhan and Salt,

2013). In contrast to the published literature, this article for the first time is based on the statistical analysis of the recorded complaints by the residences in the vicinity of wind farms. This has been done in an attempt to draw a correlation between the sound directivity, the prevailing wind direction and the blade angle of attack. In this paper, a meta-data analysis has been conducted based on the reported noise perception surveys combined with the publically available information on the directivity of the airfoil noise at different pitch angles. This approach is used in order to provide a quantitative support for the hypothesised underlying physical mechanisms for noise generation. This can contribute significantly to the field, since the outcomes of this work can be used by wind farm designers and decision makers to identify the source of the noise observed at residences, which potentially can be used in the design of future wind farms. In the following section, the main mechanisms for airfoil noise are described and the survey data from the residents in the vicinity of four wind farms are analysed to establish a relationship between the perceived noise and the associated mechanisms. A data analysis approach is utilised in the next section to determine the dominant underlying mechanism for wind turbine noise. This section is followed by a discussion and summary of the outcomes from the statistical analysis of the survey data to conclude the possible noise generation mechanism.

3.4 Directivity of the perceived noise

Figure 3.2 (a) shows a typical wind turbine. The turbine blade is generally twisted such that the airfoil reaches its maximum pre-stall angle of attack along its span when it rotates at its nominal rotational speed (Sherry et al., 2013, Schubel and Crossley, 2012). The directivity of the trailing edge and stall noise is shown at three segments of the blade in Figure 3.2 (b). As shown on Figure 3.2 (b), the trailing edge noise is largest along the airfoil chordline and towards the leading edge, which means it tends to be perceived at the locations

approximately perpendicular to the relative wind direction (Oerlemans, 2007, Doolan et al., 2012). Due to higher attenuation rate of the high frequency trailing edge noise, the direction of the highest sound level is considered in this study as the main direction of propagation of trailing edge noise. In contrast, the noise perceived downstream of the wind turbine and parallel to the wind direction is unlikely to be associated with the trailing edge. Hence, the source of the perceived noise is hypothesised to be related to the blade operation at stall (Oerlemans, 2011, Moreau et al., 2009) and near stall (Waye and Öhrström, 2002, Oerlemans and Schepers, 2009, Madsen et al., 2013). Stall conditions on the blade can result from sudden changes of the angle of attack due to interaction with the inclined and turbulence inflow arising from the topographic roughness or tandem positioning of the turbines (Choudhry et al., 2014, Laratro et al., 2014, Poggi and Katul, 2008). Length scale of the incoming turbulences also has a significant effect on the pressure fluctuation on the blade, as well as the local angle of attack of the airfoil and hence, it can significantly change the noise emission. The length scale of the eddies is partially associated with the topography and roughness of the terrain, as well as the height and the location of the turbine. In complex terrains, these eddies in addition to the acceleration and deceleration of the flow, change the local angle of attack on some parts of the turbine blade, resulting in partial or transient stall. Moreover, partial and transient stall of the blade can result in amplitude modulation of the noise which can be perceived as thumping noise downstream of the wind turbine with up to 6 to 10 dB modulation depth (Oerlemans, 2011, Madsen et al., 2014). This will be further discussed in the following sections.

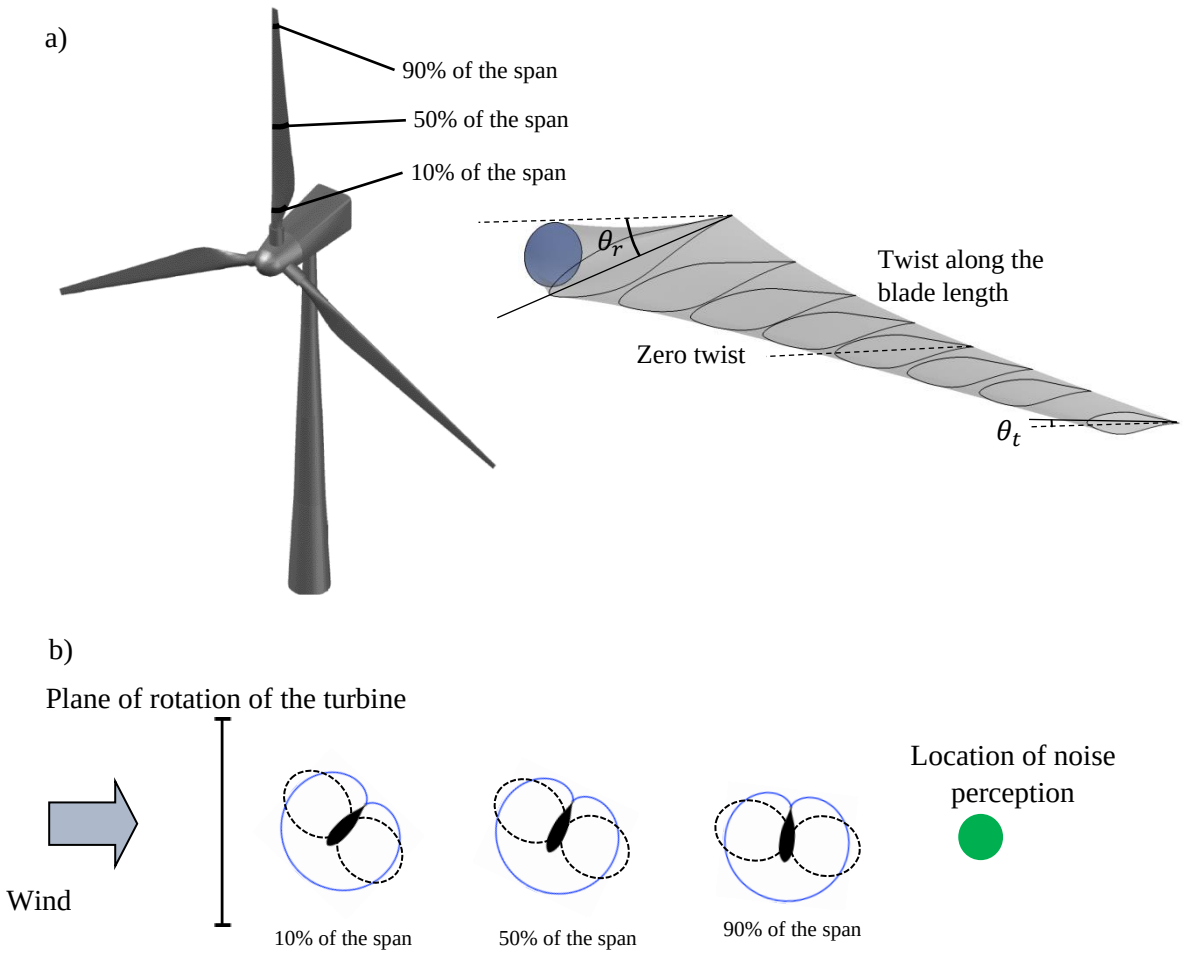

Figure 3.2 a) Schematic of wind turbine and orientation of blade due to twist ($\boldsymbol{\theta_r}$ is the blade twist angle at the root and $\boldsymbol{\theta_t}$ is the blade twist angle at the tip), b) Directivity of trailing edge noise (solid line) and stall or turbulent inflow noise (dotted line).

Four sites have been studied in an attempt to correlate the noise directivity and wind direction with the reported complaints from residents in the areas surrounding wind farms. The four sites of Makara (New Zealand), Waterloo (Australia), Bears Down (United Kingdom) and Te Rere Hau (New Zealand) were chosen as the residences in the vicinity of these farms were formally surveyed and the results have been published in peer reviewed articles (EPA, 2013, Stewart, 2002, Moorhouse et al., 2007, Thorne, 2011). The direction of the wind and the perception of noise have been assessed based on the reported residents' surveys, in addition to the associated wind conditions using meteorological databases. An investigation has been carried out to correlate the wind directions with the largest number of complaints. Then the correlation between different sources of noise and their characteristics at the

perceived locations were used to understand the mechanisms responsible for the greatest number of complaints.

3.4.1 Site 1

Waterloo Wind Farm located in South Australia, comprises thirty seven Vestas V90/3000 wind turbines, mounted on 80-metre towers, providing a generating capacity of 111 MW. The turbines rotate clockwise and are placed on a low ridge in a relatively flat terrain.

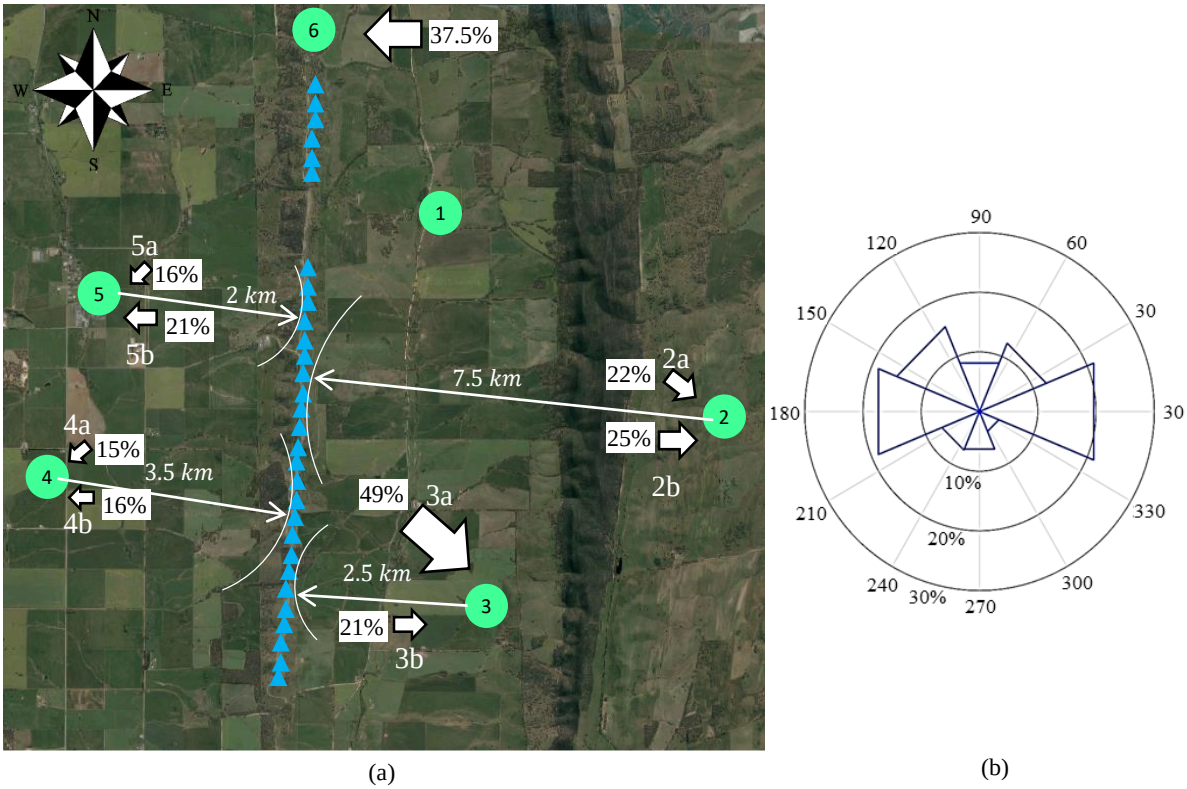

(a) (b)

Figure 3.3 a) Site map of Waterloo Wind Farm showing the dominant wind directions associated with highest occurrence of noise perception in different locations (bigger arrows show the higher percentage of complaints at the associated location). Triangles represent turbine locations and the percentage of the complaints associated with each direction is represented next to each arrow. It should be noted that the remaining directions are attributed to less than 5% of complaints for each location, b) Wind-rose during the period of the noise study. The wind velocity at hub height was in the range of 6-9.2 m/s at the time of noise perception.

Since the beginning of the wind farm's operation, a significant number of complaints about the turbines noise have been received from local residents. The South Australian Environment Protection Authority (EPA) conducted an investigation on noise perception by residents at six locations around this wind farm (EPA, 2013). Figure 3.3 illustrates the wind-

rose during the investigation period and results of completed surveys about wind farm noise for different locations, showing the dominant wind direction at the time when complaints were registered. Hereafter, the green circle will be used to indicate the noise perception location and the blue triangles represent the wind turbines. Each green circle represents the central location of different groups of residences that completed the noise survey. It should be noted that most of the complaints were received from residents in location 2, 3, 4 and 5 and the results are presented as percentage of the dominant wind direction to the total number of complaints for each location. Data were selected from the surveys completed for a week which the wind blew in all directions and residents mostly perceived the noise in particular directions. A total of 296 complaints were received during this period from these four locations. Among the recorded complaints, the wind direction associated with the highest number of complaints and with the thumping quality is selected and shown in Figure 3.4 (the other directions which correspond to less than 10% of the total complaints are not shown on the figure).

Residents located on the north-east of the wind farm complained while the wind was from west or north-west. It should be noted that the distance of location 2 from the nearest wind turbine is about 7.5 km. Considering that the trailing edge noise is broadband and radiates in a cross-wind direction it can be concluded that the perceived noise at this location is unlikely to be associated with this noise generation mechanism. On the other hand, the resultant noise from turbulent inflow and stall has low frequency content which can travel longer (Laratro et al., 2014). Moreover, the directivity of the perceived noise is aligned with the direction of the radiation of the turbulent inflow and stall noise and not trailing edge noise. Considering the closest turbines to the dwellings of the remaining locations which reported the highest rate of complaint, it can be seen that noise is perceived behind the rotor plane which again is in accordance with directivity of the turbulent inflow or stall noise.

In order to better understand the directivity of the radiated noise, the angle between chord normal and the line which connects each location to nearest wind turbine, is considered. A distance weighted approach is used to calculate the distance from main source of noise, allocating the highest share to the nearest wind turbine (a conservative approach) since the share of the nearest wind turbine among all turbines is the greatest. Taking the twist angle from root to tip into account one can calculate the range of variation for this parameter. Figure 3.5 illustrates this angle for four locations for the dominant wind direction with largest number of complaints. Since $\beta = 90°$ represent the radiation of the noise in the rotor plane, it can be concluded that the noise is mostly perceived behind the rotor plane and in the downstream direction, not in rotor plane. This pattern is mostly aligned with stall or turbulent inflow noise. This trend is also illustrated in Figure 3.5. The smaller angles for β show that the noise is radiated normal or close to normal direction to the chord line. It should be noted that for all residential locations, except location 2, "b" direction is the direction that attributes to the largest number of the complaints (see Figure 3.3 (a)). This behaviour is more likely associated with the stall or turbulent inflow noise and large angles are related to trailing edge noise. Further discussion about the relevant noise mechanisms and their relationship with wind direction is presented in Section 3.5.

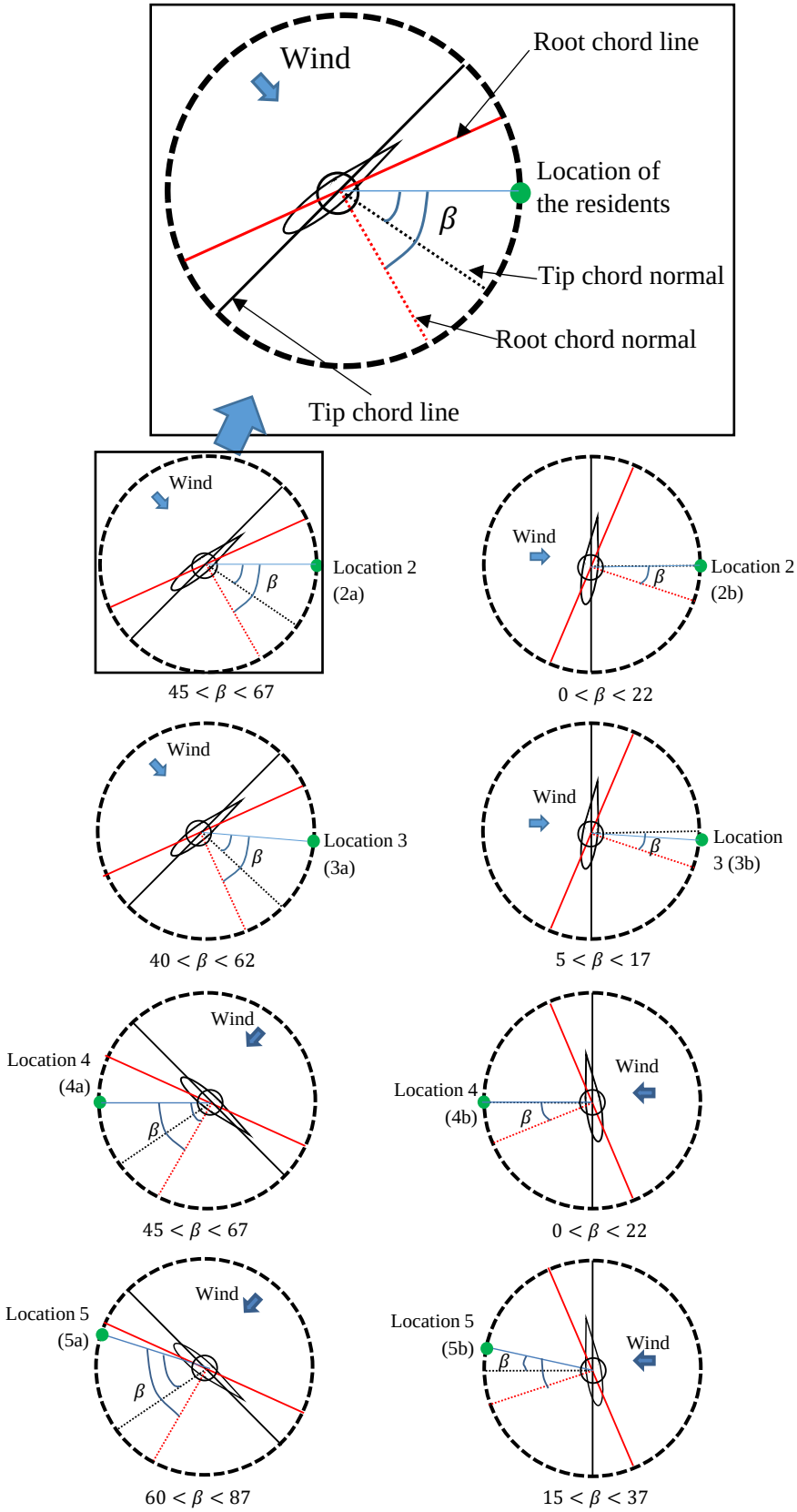

Figure 3.4 Directivity of the noise with respect to location of the residents near the Waterloo Wind Farm. The angle β represents the range of the angles formed between the noise perception location and the normal to the blade chord. Only airfoil at 80% of the span has been shown as representative to prevent confusion and lines show the root and tip limits. Hereafter, red and black colours stand for root and tip respectively. Chord lines are determined by solid lines and dashed lines show chord normal (the other directions which correspond to less than 10% of the total complaints are not shown on the figure).

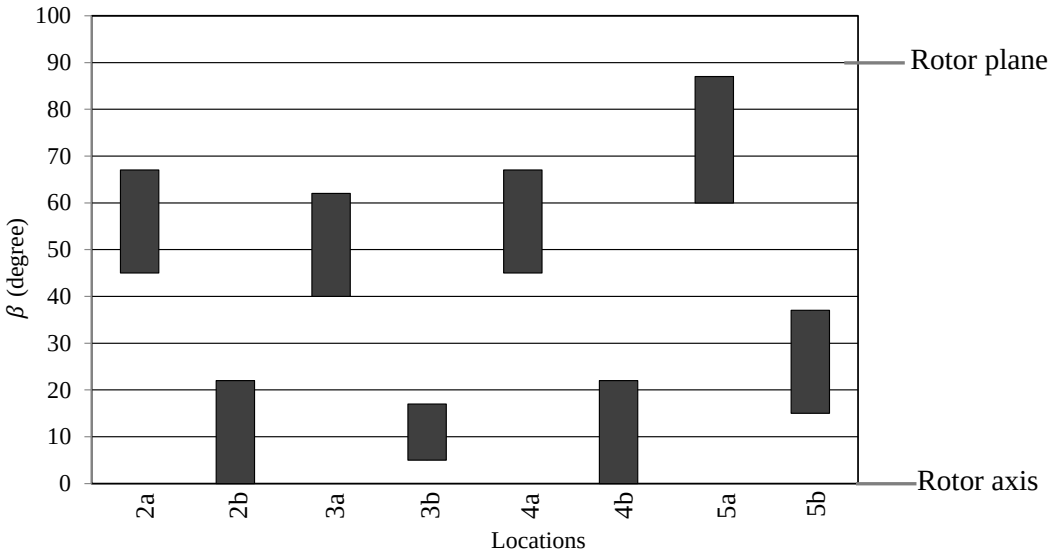

Figure 3.5 Range of the β (angle of noise radiation based on chord normal of the blade and relative position of the residents). Each bar shows the range of angle in which the most complaints has been received.

3.4.2 Site 2

The West Wind Wind Farm, located in Makara region in New Zealand, was chosen as the second site for this study. Sixty-two Siemens wind turbines rotating in clockwise direction, with a total nominal power generation of 142.6 MW, are located at an average height of 170 m on a hilly terrain near the sea (Fig. 6). The survey data collected from the Makara Valley residents and other residents in the vicinity (for more information about the residents location refer to Thorne, 2011) of the wind farm shows that the dominant wind directions for noise perception are from the north-west (Thorne, 2011). The distance of the residents from closest wind turbine ranged from 1.250 km to 2 km. The white arrow in Figure 3.6 displays the dominant wind direction for the perceived noise which was described as rumble, hum or annoying thumping sound. Figure 3.7 shows the relative position of the noise perception locations with respect to nearest wind turbine and the direction of the wind when the noise was perceived. Considering the relative position of the noise perception locations, it can be seen that the noise is mostly perceived behind the rotor plane. Being constructed on hilly terrain, and also located in the wake of the upstream wind turbines, the incoming flow has

relatively high turbulence intensity compared to a flat terrain (Kloosterman, 2009). Moreover, flow features such as velocity magnitude and components over hills and inclined surfaces significantly changes due to the effect of inclined surface and acceleration near the hill and deceleration on the lee side of the hill (Poggi and Katul, 2008, Emeis et al., 1995, Bowen and Lindley, 1977). Interaction of the blades of wind turbines with the incoming flow that has been affected by the hills (wind velocity direction and its magnitude changes as the flow passes over a hill) results in the changes of angle of attack and consequently increased noise level due to the partial stall on the blade as well as the turbulent inflow mechanism. However, for the cases in which $\beta > 70$, the trailing edge noise can also be one of the possibilities due to the close proximity of the residents (less than 2km).

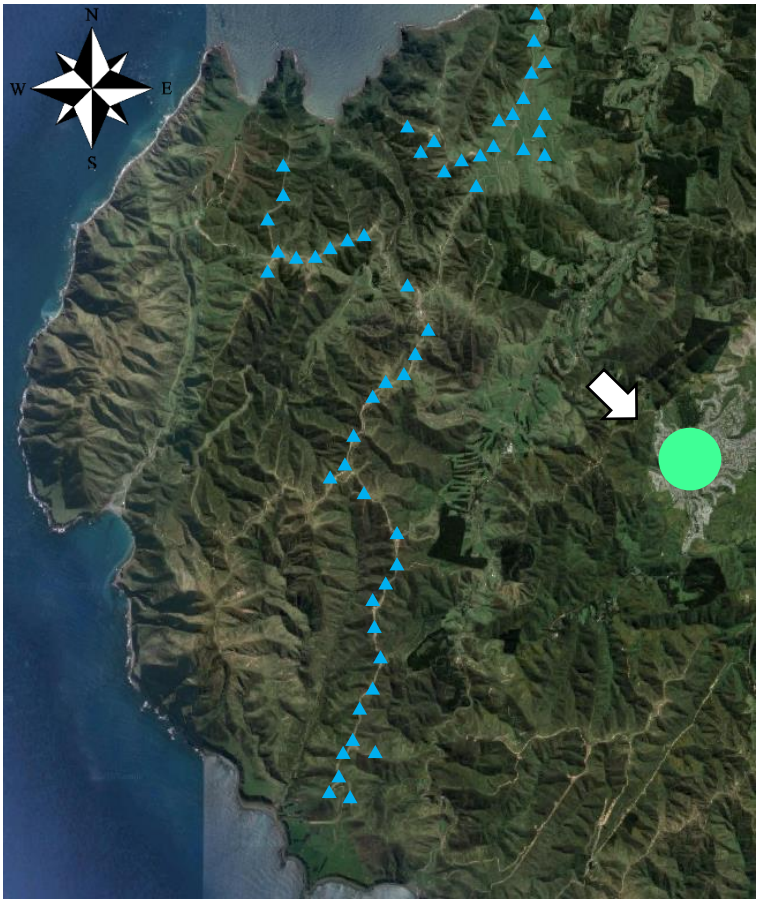

Figure 3.6 Aerial photograph of the location of the West Wind Wind Farm and the residents of Makara and dominant wind directions. Triangles represent the turbine locations. The arrow shows the wind direction associated with the highest percentage of complaints.

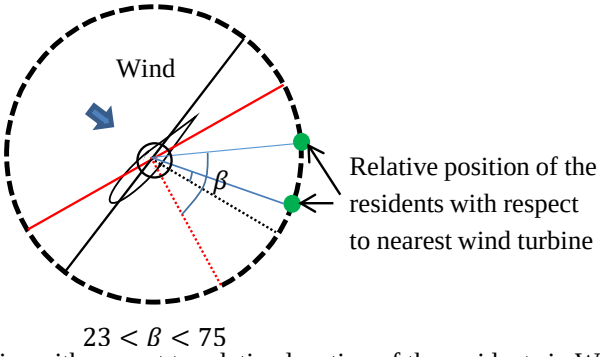

Figure 3.7 Directivity of the noise with respect to relative location of the residents in West Wind Wind Farm.

3.4.3 Site 3:

Site 3 is the Bears Down Wind Farm located in Cornwall area in England (see Figure 3.8). The site consists of sixteen 0.6 MW Bonus wind turbines providing 9.6 MW in total, located in an almost flat area. In this study consideration was made of the nearest residents influenced by the wind farm noise and their reports (Stewart, 2002). The distance of the dwellings in this area from nearest wind turbine is approximately 1.1km.

Figure 3.8 Aerial photograph of the Bears Down Wind Farm showing the location of residents (googlemap.com). Triangles represent wind turbines and arrows show the wind direction associated with noise perception.

As can be seen in Figure 3.8, most of the complaints were claimed for wind directions from south to south-westerly. Reports reveal that 73% of the "swish" or "whoosh" noise perception occurred for the small arc from southerly to south-westerly (Moorhouse et al., 2007). Figure 3.9 shows the directivity of the perceived noise with respect to relative position of the residents. As can be seen the noise is perceived mostly in rotor plane or slightly in

upwind direction aligned with chord line. Considering the proximity and direction of propagation, it can be concluded that the trailing edge noise is the underlying noise generation mechanism in this case.

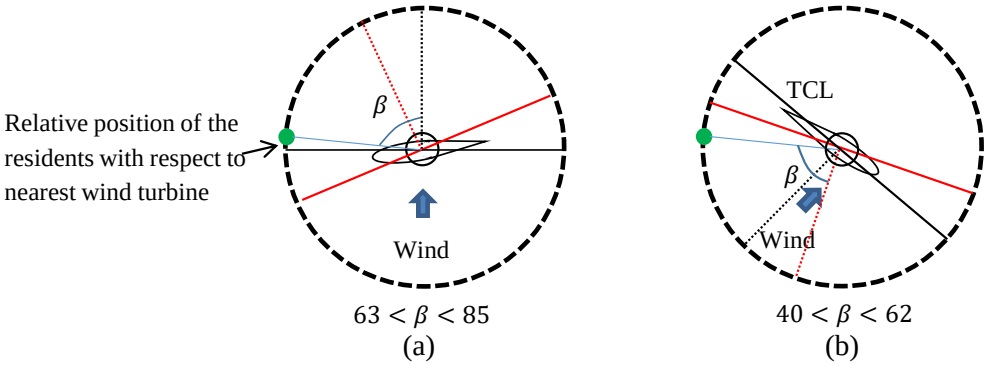

Figure 3.9 Directivity of the noise with respect to relative location of the residents in Bears Down Wind Farm. a) Southerly wind direction, b) South-Westerly wind direction.

3.4.4 Site 4

Figure 3.10 shows the Te Rere Hau Wind Farm in New Zealand, consisting of ninety-seven two-bladed Windflow 500 turbines, generating a total power output of 48.5 MW. The turbines rotate clockwise and are located on relatively hilly ground. Results gathered from residents' diaries around the wind farm show that thumping and pulsing noise was perceived for the easterly and south-easterly winds (Thorne, 2011).

For the easterly wind direction, the noise perception occurred in the location behind the rotor plane of most of the working turbines. Located in a hilly environment in a relatively dense cluster, the blades of the turbine are facing relatively turbulent flow. As shown in Figure 3.11 the noise is mostly perceived behind the rotor plane. The incoming wind is highly turbulent containing eddies with different varying turbulent length scales, which can result in change of angle of attack on the blades and consequently cause partial or transient stall. The acceleration of the wind as well as the change in flow direction (because of the change in velocity components as the wind climbs the hill) due to inclined surface of the hill also

can cause partial or transient stall on the blades. Thus, the noise generation mechanism is likely to be the stall or turbulent inflow noise. Thumping noise can also be explained by the partial stall due to sudden change of angle of attack when the blades interact with eddies in incoming flow (S. Oerlemans, 2011). Figure 3.11 also reveals that for south-easterly wind the locals are relatively close to rotor plane. In this case, trailing edge noise can also be the noise generation mechanism since the dwellings are close to wind turbines. This statement is also supported by the swishing feature of the perceived sound by some of the residents.

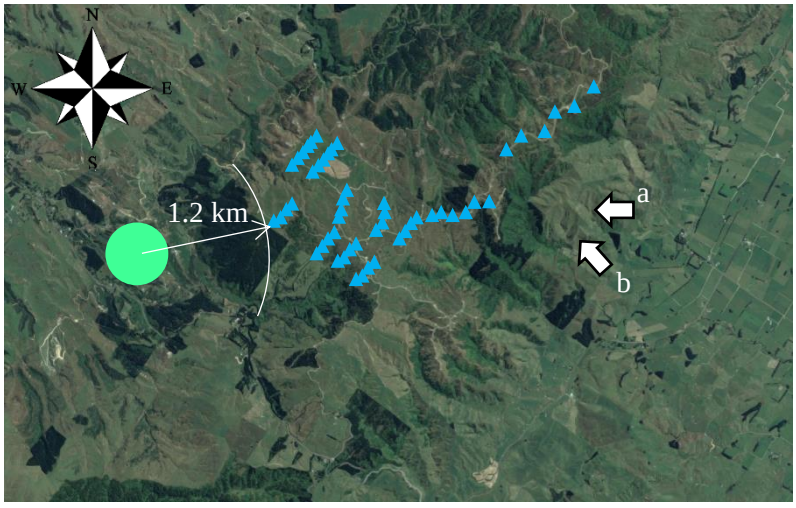

Figure 3.10 Aerial photograph of the Te Rere Hau Wind Farm and locations of noise perception (green circle show the noise perception locations. Triangles represent the wind turbines' locations and and white arrows show the dominant wind direction associated with largest number of reported noise perception).

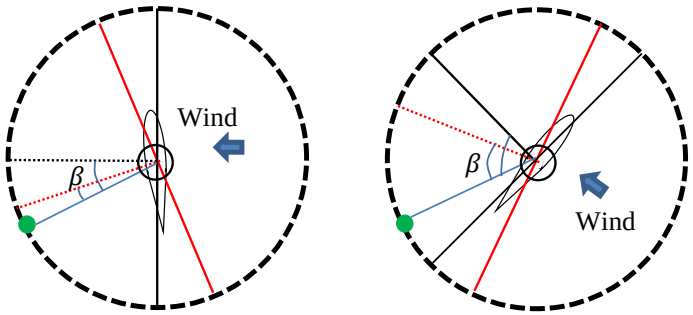

$8 < \beta < 30$ (a) $53 < \beta < 75$ (b

Figure 3.11 Directivity of the noise with respect to relative location of the residents (green circle) in Te Rere Hau. . a) Easterly wind direction, b) South-Easterly wind direction.

3.5 Summary and discussion on the underlying mechanism

As previously described in Section 3.3, each aerodynamic noise mechanism has characteristics which can be used to differentiate from one another. Based on the experimental study conducted by Oerlemans (2011), the trailing edge noise has higher sound level at the outer part of the blade during its descent (see Figure 3.12). Thus in all analysis the foil orientation at 80% of the span is used for directivity analysis. As shown in Figure 3.2, the trailing edge noise is strongest towards the leading edge. Hence it is expected to be better perceived in rotor plane or crosswind direction. On the other hand, stall or turbulent inflow noise are stronger normal to the chordline of the airfoil. Considering the orientation of the airfoil this noise is likely to be perceived behind the rotor plane. The frequency content of these noise sources are also different, with trailing edge noise containing higher frequency content which attenuates faster compared to stall and turbulent inflow noise. Moreover, measurements and qualitative descriptions of the noise at residents downstream of the wind turbine show evidences of an enhanced amplitude modulation different from normal amplitude modulation (which is perceived in a cross-wind direction due to rotation of the blades). This phenomenon can be explained by amplitude modulation due to partial stall which is supported by the directivity characteristics of the stall noise and its lower dominant frequency content when compared to normal amplitude modulation.

Figure 3.12 Noise emission from a large wind turbine in the rotor plane, measured by microphone arrays at 1D upstream of the turbine. As seen, the noise is mostly produced at the outer part of the blade during its descent

Figure 3.13 shows the directivity angle (β) of the perceived noise with regard to chord line normal. Larger angles mean that the noise perception locations are close to rotor plane, and due to close proximity to wind turbines for this case it can be concluded that the perceived noise is broadband trailing edge noise. However, for the cases with small angles, residents are close to the normal plane, and considering the large distance from wind turbine, it can be concluded that the turbulent inflow or stall noise is the underlying mechanism. The presented evidence shows that the dominant direction for noise radiation is downstream of the wind turbine, which is in agreement with the study conducted by Cooper et al. (2014). The dominance of the downstream direction becomes more distinct as the distance from wind turbines increases. The swish noise generated by trailing-edge noise, mostly includes high-frequency signatures and radiates in the cross-wind direction. Noise perception and measurements at large distances downstream of the wind farms suggest that directly propagated trailing edge noise is not the underlying mechanism of the disturbing noise.

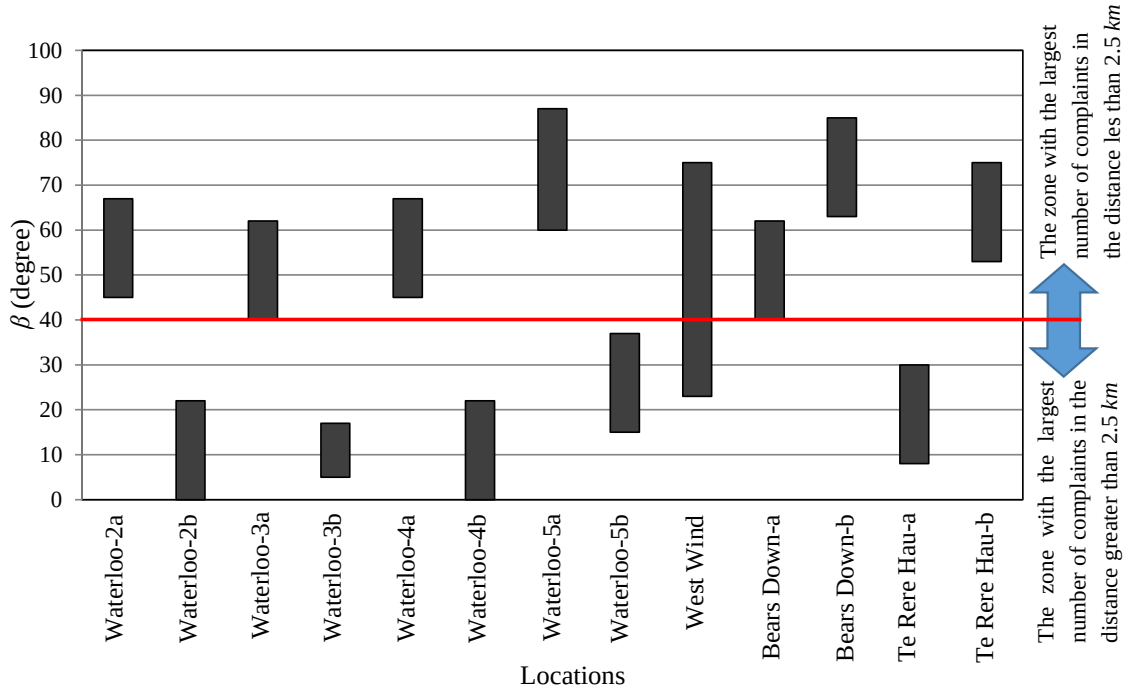

Figure 3.13 Summary of the directivity angle (β) of the noise with respect to relative location of the noise perception. In this figure the closest wind turbine is identified by the shortest straight line connecting the wind turbine to the location of the residents.

To explain the underlying mechanism of emitted aerodynamic noise, the flow interaction with blade should be considered. Flow characteristics over rotor blades significantly affects the aeroacoustic noise emitted from the wind turbines. Madsen et al. (2013) investigated the noise radiated from the blade of a NM80 turbine for various angles of attack. Figure 3.14 shows the acoustic power spectral densities for a segment of the blade at angles of attack from 8° to 13°. The low-frequency noise (LFN, i.e., $f < 200$ Hz) levels suddenly increases when the angle of attack (AoA) changes from 12 to 13 degrees, which is the onset of stall on the blade. It is hypothesised that this increase could be the main contributor for periods of reported increased swish and thumping sound in far field, which is also denoted as enhanced amplitude modulation (EAM) in literatures (Oerlemans, 2011).

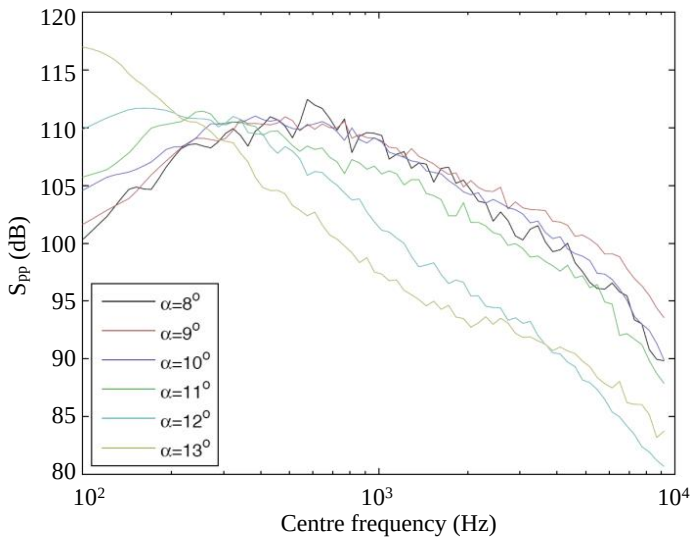

Figure 3.14 Effect of AoA on narrow band spectra of surface pressure (Madsen et al., 2014, permission has been obtained to use this figure).

High shear in the atmospheric boundary layer, turbulent vortices due to the ground topography and working in the wake of an upstream turbine, can result in changes to the angle of attack and consequently stall the blades of a turbines. Studies show that stall can occur on more than 30% of the blade of the downstream turbine even with 15 diameters separation (Choudhry et al., 2014). Tip vortices and vortical structures can suddenly change the angle of attack at the outer parts of the blades, causing partial stall and increased noise level near the blade tips. Partial stall on the turbine's blade due to incoming turbulences, inclined flow, gusts and wind shear generates amplitude modulation of the sound signature in the far field.

Aerodynamic noise emission from wind turbines is a complicated phenomenon, compounded by the movement of the noise source and the effect of the flow on noise radiation. Variations of the velocity in the atmospheric boundary layer and ground reflection also affect the noise propagation.

The flow over the blades of wind turbines is complex, containing turbulent structures due to the wakes of other wind turbines or turbulence in atmosphere (Sedaghatizadeh et al., 2016).

Bound vortices, ring of tip vortices and other vortical structures in the wake region can affect the noise propagation from blades. Colonius et al. (1994) investigated the effect of a single vortex on noise propagation. They found that it has significant effect on directivity of a planar sound wave. This type of behaviour would be expected to occur for sound generated by turbine blades. Rotating blades also exert centrifugal forces on the flow over the blade surfaces, causing the flow to move toward the tip of the blade. This phenomenon also affects the noise propagation and noise emission from blades (Dowling, 1975, Colonius et al., 1994).

Figure 3.16 shows the wake vortex structure system behind a wind turbine. Tip vortices are generated at the tip of the blade due to pressure difference between the suction and pressure side of the blade. Rotation of the blade results in the formation of the helical structures when the tip vortices propagate downstream with the flow. Emitted noise from the blade enters the wake region, which is surrounded, by helical tip vortices. Studies show that the wake of a wind turbine acts like a duct for the sound waves enter in this region and results in refraction of the sound signals (Barlas et al., 2016). Barlas et al. (2016) used parabolic equation method to study the effect of wake and velocity deficit in the wake region on the noise propagation. They found that wake acts like a duct for noise source on the blade and constrains the acoustic energy and affects its directivity. Their results show the considerable effect of the wake on the noise level in the far field when compared with no-wake condition such that the far field noise level can be increased by 7.5 dB at the wake centre in a stable atmospheric boundary layer. Moreover, interaction of the sound waves with the wavelength in the same order of the vortices, results in refraction of the sound towards the downstream direction (Colonius et al., 1994). Nevertheless, the effect of vortices in the wake region on noise

propagation has not been fully understood yet, due to the complexity of the flow and turbulent structures in this region.

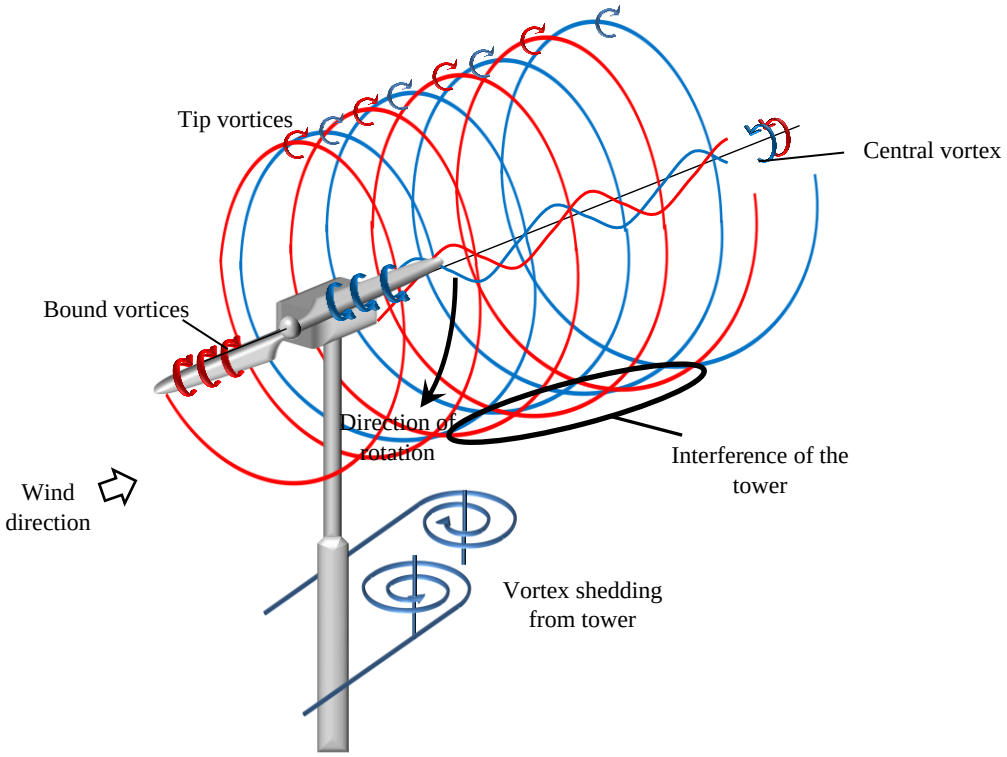

Figure 3.15 Schematic diagram of the typical vortex system downstream of a wind turbine. In addition to tip, bound and root vortices, vortical structures and turbulences in the wake region and velocity deficit can result in refraction of the generated noise from turbine blades.

3.6 Conclusion

Noise propagation from wind farms depends on source directivity, geometric spreading and atmospheric absorption, ground reflections and absorption, meteorological effects such as refraction and convection, terrain complexity and wind direction. According to extant literature, the dominant source of noise is the railing edge noise, which occurs on the outer part of the blade. This sound radiates toward the observer in the rotor plane and it is strongest towards the leading edge. Trailing edge noise directivity and its varying location due to blade rotation, results in a specific type of amplitude modulation referred to as normal amplitude modulation, heard as a swish sound in the cross-wind direction. However, analysing the noise perception data from the residents in the vicinity of several wind farms revealed that

noise is mostly perceived in downwind locations. The evidence also revealed the existence of amplitude modulation far from the wind turbines.

Based on the direction and the distance of noise propagation, and its swish and thumping characteristics, it is concluded that the increased noise levels far downstream of the wind turbines is caused by stall or turbulent inflow mechanisms. Transient or partial stall on the blade is caused by sudden changes in the angle of attack due to incoming turbulence, strong wind shear, sudden gusts, tripped oncoming flow and yaw misalignment. In stable conditions with a relatively flat ground surface, the incoming turbulence and non-uniform flow due to the wakes of other turbines could be the reason for local stall and turbulent-induced noise. Local stall and turbulent-inflow noise have lower frequencies compared with trailing edge noise and can travel greater distances downwind. Interaction of sound waves with helical tip vortices and other vortical structures in the wake region results in higher noise perception in the wake-affected zone and its vicinity. Moreover, the wake acts as a conduit directing the noise energy downstream up to up to the point of the breakdown of the wake vortex resulting in higher noise level at the wake centre and in far-field region. This effect is supplemented with amplitude modulation by the cyclic augmentation in noise level due to partial stall. Based on the directivity pattern of the aerodynamic noise mechanism, it can be concluded that the stall noise ducted by the wake results in higher noise level at the break-down point. This mechanism explains the measured and perceived increase in noise in locations far behind wind turbines.

3.7 References

Albertson, J. D., Katul, G. G., Parlange, M. B. & Eichinger, W. E. 1998. Spectral scaling of static pressure fluctuations in the atmospheric surface layer: The interaction between large and small scales. *Physics of Fluids,* **10,** 1725-1732.

Alvarez, E. 2011. *Block Island Wind Farm and its potential effect on tourism*. Thesis in Bachelor of Arts-Environmental & Architectural Studies, Brown University.

Bakker, R. H., Pedersen, E., Berg, G. P. V. d., Stewart, R. E., Lok, W. & Bouma, J. 2012. Impact of wind turbine sound on annoyance, self-reported sleep disturbance and psychological distress. *Science of the Total Environment*, **425**, 42-51.

Barlas, E, Zhu, W. J., Shen, W. Z., & Andersen, S. J., 2016, Wind Turbine Noise Propagation Modelling: An Unsteady Approach, *Journal of Physics: Conference Series*, **753**, 2, 022003.

Bowen, A. J., & Lindley, D., 1977, A wind-tunnel investigation of the wind speed and turbulence characteristics close to the ground over various escarpment shapes, *Boundary-Layer Meteorology*, **12**, 3, 259-271.

Van der Berg, F. 2005. The beat is getting stronger: The effect of atmospheric stability on low frequency modulated sound of wind turbines. *Journal of Low Frequency Noise, Vibration & Active Control*, **24**, 1-24.

Bolin, K., Bluhm, G., Eriksson, G. & Nilsson, M. E. 2011. Infrasound and low frequency noise from wind turbines: Exposure and health effects. *Environmental Research Letters*, **6**, 3, 035103.

Choudhry, A., Mo, J.-O., Arjomandi, M. & Kelso, R. 2014. Effects of wake interaction on downstream wind turbines. *Wind Engineering*, **38**, 535-548.

Colonius, T., Lele, S. K. & Moin, P. 1994. The scattering of sound waves by a vortex: Numerical simulation and analytical solution. *Journal of Fluid Mechanics*, **260**, 271-298.

Cooper, J., Evans, T. & Alamshah, V., 2014. Influence of non-standard atmospheric conditions on turbine noise levels near wind farms. Inter-Noise 2014, 16-19 November 2014 Melbourne, Australia.

Crespo, A., Hernández, J. & Frandsen, S. 1999. Survey of modelling methods for wind turbine wakes and wind farms. *Wind Energy*, **2**, 1-24.

Doolan, C. J., Moreau, D. J. & Brooks, L. A. 2012. Wind turbine noise mechanisms and some concepts for its control. *Acoustics Australia*, **40**, 7-13.

Dowling, A. P. 1975. The refraction of sound by a shear layer made up of descrete vortices. Aeronautical Research Council Reports and Memoranda, Research Report.

Ellenbogen, J. M., Grace, S., Heiger-Bernays, W. J., Manwell, J. F., Mills, D. A., Sullivan, K. A., Weisskopf, M. G. & Santos, S. L. 2012. Wind turbine health impact study: Report of independent expert panel. Massachusetts Department of Environmental Protection, Massachusetts Department of Public Health.

Emeis, S, Frank, H. P., & Fiedler, F., 1995, Modification of air flow over an escarpment — Results from the Hjardemål experiment', *Boundary-Layer Meteorology*, **74**, 1, 131-161.

Environment Protection Authority (EPA), 2014, Web refernce: http://www.epa.sa.gov.au/

Ghasemian, M. & Nejat, A. 2015. Aerodynamic noise prediction of a horizontal axis wind turbine using improved delayed detached eddy simulation and acoustic analogy. *Energy Conversion and Management*, **99**, 210-220.

Katinas, V., Marčiukaitis, M. & Tamašauskienė, M. 2016. Analysis of the wind turbine noise emissions and impact on the environment. Renewable and Sustainable *Energy Reviews,* **58**, 825-831.

Kim, H., Lee, S. & Lee, S. 2011. Influence of blade-tower interaction in upwind-type horizontal axis wind turbines on aerodynamics. *Journal of Mechanical Science and Technology*, **25**, 1351-1360.

Kloosterman, M. H. M. 2009. *Development of the near wake behind a horizontal axis wind turbine*. Master of Science, Delft University of Technology.

Laratro, A., Arjomandi, M., Kelso, R. & Cazzolato, B. 2014. A discussion of wind turbine interaction and stall contributions to wind farm noise. *Journal of Wind Engineering and Industrial Aerodynamics,* **127**, 1-10.

Lee, S., Lee, S. & Lee, S. 2013. Numerical modeling of wind turbine aerodynamic noise in the time domain. *The Journal of the Acoustical Society of America,* **133**, EL94-EL100.

Leventhall, G. 2006. Infrasound from wind turbines – fact, fiction or deception. *Canadian Acoustics,* **34**, 29-36.

Lichtenhan, J. & Salt, A. Amplitude modulation of audible sounds by non-audible sounds: Understanding the effects of wind turbine noise. ICA 2013 Montreal, 2-7 June 2013 Montreal, Canada. Acoustical Society of America through the American Institute of Physics.

Lenchine, V. V. & Song, J. 2014, Infrasound and Blade Pass Frequency Levels in Areas adjacent to Wind Farms, paper presented at INTER-NOISE 2014, Melbourne, Australia, 16-19 November.

Madsen, H. A., Bertagnolio, F., Fischer, A. & Bak, C. 2014. Correlation of amplitude modulation to inflow characteristics. Proceedings of 43rd International Congress on Noise Control Engineering. The Australian Acoustical Society.

Madsen, H. A., Fischer, A. & Kragh, K. A. 2013. Mechanisms and causes of amplitude modulation (AM) and other amplitude modulation (OAM) of aeroacoustic wind turbine noise inflow measurements. Technical Report prepared for RenewableUK.

Meunier, M. 2013, Wind farm - long term noise and vibration measurements. ICA 2013 Montreal, 2-7 June 2013 Montreal, Canada. Acoustical Society of America through the American Institute of Physics.

Moorhouse, A., Hayes, M., Sabine von Hünerbein, Piper, B. & Adams, M. 2007. Research into aerodynamic modulation of wind turbine noise: Final report. University of Salford, Research Report Prepared for Defra.

Moreau, S., Roger, M. & Christophe, J. 2009. Flow features and self-noise of airfoils near stall or in stall. 15th AIAA/CEAS Aeroacoustics Conference (30th AIAA Aeroacoustics Conference). Miami, Florida.

Nobbs, B., Doolan, C. J. & Moreau, D. J. 2012, Characterisation of noise in homes affected by wind turbine noise. Acoustics 2012 - Fremantle, 21-23 November 2012 Fremantle, Australia.

Oerlemans, S. 2011. An explanation for enhanced amplitude modulation of wind turbine noise. National Aerospace Laboratory NLR, Technical Report.

Oerlemans, S. & Schepers, J. G. 2009. Prediction of wind turbine noise and validation against experiment. National Aerospace Laboratory NLR, Technical Report.

Oerlemans, S., Sijtsma, P. & López, B. M. 2007. Location and quantification of noise sources on a wind turbine. National Aerospace Laboratory NLR, Technical Report.

Pedersen, E., Berg, F. v. d., Bakker, R. & Bouma, J. 2009. Response to noise from modern wind farms in the Netherlands. *The Journal of the Acoustical Society of America*, **126**, 634-643.

Poggi, D. & Katul, G. G. 2008. Turbulent intensities and velocity spectra for bare and forested gentle hills: Flume experiments. *Boundary-Layer Meteorology*, **129**, 25-46.

Saurabh, S. P. & Ramesh, O. N. 2014. Scaling of pressure spectrum in turbulent boundary layers. *Journal of Physics: Conference Series,* **506,** 012011.

Sawin, J. 2014. Renewables 2014: Global status report. REN21, Paris, France.

Schubel, P. J. & Crossley, R. J. 2012. Wind turbine blade design. *Energies*, **5**, 3425-3449.

Sedaghatizadeh, N., Arjomandi, M., Kelso, R.M., Cazzolato, B.S., Ghayesh, M.H., 2016, Effect of wall confinement on a wind turbine wake, 20th Australasian Fluid Mechanics Conference, Perth, Australia.

Sherry, M., Sheridan, J. & Jacono, D. 2013. Characterisation of a horizontal axis wind turbine's tip and root vortices. *Experiments in Fluids*, **54**, 1-19.

Smith, M. G., 2012, Wind Turbine Amplitude Modulation: Research to Improve Understanding as to its Cause & Effect, Consultancy Report submitted to RenewableUK.

Stewart, J. 2002. Location, location, location, an investigation into wind farms and noise by the noise association. The Noise Association, London, Research Report.

Thorne, B. 2011. The problems with "noise numbers" for wind farm noise assessment. Bulletin of Science, *Technology & Society*, **31**, 262-290.

Timmerman, N. S. 2013. Wind turbine noise. *Acoustics Today*, **9**, 22-29.

Waye, K. P. & Öhrström, E. 2002. Psycho-acoustic characters of relevance for annoyance of wind turbine noise. *Journal of Sound and Vibration*, **250**, 65-73.

Chapter 4 Aerodynamic noise generation by a NACA 0012

4.1 Chapter preview

Aerodynamic noise from a wind turbine is generated due to the interaction of the blade sections (airfoils) with an incoming wind. Due to the varying nature of the wind in the atmospheric boundary layer, different flow structures are generated (e.g. gusts and turbulent structures in the incoming flow), which with the moving blade of a wind turbine may result changes in the angle of attack of the blade sections and partial stall on the blade. Occurrence of the stall on the blade changes the characteristics of the noise emitted from the blade which also may lead to amplitude modulation of the sound with a potential to be perceived in far-field.

In this section, the aeroacoustic behaviour of an airfoil when undergoes pre-stall, shallow-stall, and deep-stall due to different angles of attack is discussed. Pressure fluctuations on the surface of the blade was obtained by means of computational fluid dynamics using an Embedded Large Eddy Simulation (ELES) approach. The noise directivity and sound pressure level in far-field were calculated using the Ffowcs Williams and Hawkings approach.

The following section is presented in a paper format submitted to the Journal of Vibration and Acoustics.

Statement of Authorship

Title of Paper	Aeroacoustic behaviour of a NACA 0012 airfoil at moderate Reynolds number
Publication Status	☐ Published ☐ Accepted for Publication ☑ Submitted for Publication ☐ Unpublished and Unsubmitted work written in manuscript style
Publication Details	Submitted to the Journal of Vibration and Acoustics ASME

Principal Author

Name of Principal Author (Candidate)	Nima Sedaghatizadeh		
Contribution to the Paper	- Research - Providing the data, writing of the manuscript and production of original figures - Correspondence with editor and reviewers including the production of all cover letters and rejoinder		
Overall percentage (%)			
Certification:	This paper reports on original research I conducted during the period of my Higher Degree by Research candidature and is not subject to any obligations or contractual agreements with a third party that would constrain its inclusion in this thesis. I am the primary author of this paper.		
Signature		Date	14/09/2017

Co-Author Contributions

By signing the Statement of Authorship, each author certifies that:

i. the candidate's stated contribution to the publication is accurate (as detailed above);

ii. permission is granted for the candidate in include the publication in the thesis; and

iii. the sum of all co-author contributions is equal to 100% less the candidate's stated contribution.

Name of Co-Author	Alex Laratro		
Contribution to the Paper	- Providing experimental data - Editing of the manuscript prior to submission		
Signature		Date	14/09/2017

Name of Co-Author	Maziar Arjomandi		
Contribution to the Paper	- Supervision of the work, including the production of the manuscript - Participation in the development of the concepts and ideas presented in the manuscript - Evaluation and editing of the manuscript prior to submission		
Signature		Date	15/09/2017

Name of Co-Author	Benjamin Cazzolato		
Contribution to the Paper	- Supervision of the work, including the production of the manuscript - Participation in the development of the concepts and ideas presented in the manuscript - Evaluation and editing of the manuscript prior to submission		
Signature		Date	14/09/2017

Name of Co-Author	Richard Kelso		
Contribution to the Paper	- Supervision of the work, including the production of the manuscript - Participation in the development of the concepts and ideas presented in the manuscript - Evaluation and editing of the manuscript prior to submission		
Signature		Date	14/9/2017

Aeroacoustic behaviour of a NACA 0012 airfoil at moderate Reynolds number

Nima Sedaghatizadeh, Alex Laratro, Maziar Arjomandi, Benjamin Cazzolato, Richard Kelso

School of Mechanical Engineering, the University of Adelaide, Adelaide, SA, 5005

Paper submitted to: Journal of Vibration and Acoustics (ASME).

4.2 Abstract

In this study, the aeroacoustic behaviour of a NACA 0012 airfoil at different angles of attack corresponding to shallow and deep stall, is investigated using an embedded LES technique to compute the flow field, pressure fluctuations and aerodynamic forces. The Ffowcs-Williams and Hawkings analogy is used to calculate the far-field noise signatures emitted from the airfoil. The results of aeroacoustic modelling show that as the angle of attack increases and the blade experiences stall, the peak frequency of the noise signal decreases due to the generation of large eddies on the suction side of the airfoil. Narrowband spectra show that the highest noise level occurs at a reduced frequency of 1.9 in the light stall condition (18 degrees angle of attack), while the reduced frequency associated with the highest noise level is almost double (3.58) for an angle of attack of 5 degrees. The directivity diagrams of total sound pressure level for both conditions form dipoles with their axes of symmetry perpendicular to the chord line. However, the directivity patterns of peak frequencies show strong dipole behaviour aligned in a direction normal to the chord line when in stall, while the results for the pre-stall condition show a stronger signature towards the leading edge, resulting in a dipole which is aligned more in the direction of the chord line. The directivity pattern at this particular frequency shows that, in addition to trailing edge noise, other noise sources are present which cannot be explained by trailing edge noise theory.

Nomenclature

x, y, z	Cartesian coordinate system	S_{ij}	Strain rate tensor (s^{-1})
c	Airfoil chord (m)	ρ	Fluid density ($kg.m^{-3}$)
U_i & u_i	Velocity component (ms^{-1})	μ	Dynamic viscosity (Pa.s)
k	Turbulent kinetic energy (m^2s^2)	μ_t	Subgrid turbulent viscosity (Pa.s)
L_{vK}	von Karman length scale (m)	υ	Kinematic viscosity (m^2s^{-1})
L_t	Turbulence length scale (m)	L_s	Mixing length scale (m)
p	Pressure (Pa)	α	Angle of attack (°)
$\acute{p}$	Gauge hydrodynamic pressure (Pa)	f	Frequency (Hz)
ζ	Model constant	κ	von Karman factor
$\bar{u}$	Resolved velocity (ms^{-1})	C_s	Smagorinsky factor
τ	Subgrid scale stress (Nm^{-2})	δ_{ij}	Kronecker delta function
σ	Stress tensor (Nm^{-2})	$\bar{x}$	Normalised chord-wise distance
ε	Dissipation rate (m^2s^{-3})	a_0	Speed of sound (ms^{-1})

4.3 Introduction

Airfoils are a known source of aerodynamic noise, consequently investigation of the noise generation mechanisms, and techniques to control them have been an ongoing endeavour for researchers and engineers for the last 30 years (Kim et al., 2015, Laratro et al., 2016). Airfoil noise is mainly generated by fluctuating surface forces exerted by turbulent eddies and instabilities in the flow which interact with different parts of an airfoil (Kim et al., 2014, Brooks et al., 1989). The spectral content of the aerodynamic noise from an airfoil is primarily related to the size of the eddies, with larger eddies producing lower frequencies (Moorhouse et al., 2007). Based on the source of the eddies and the part of the airfoil with

which they interact, the generated noise can be divided into four main categories: unsteady turbulent-inflow; stall noise; trailing-edge (TE) noise; and laminar-boundary-layer vortex-shedding noise (Sedaghatizadeh et al., 2017, Brooks et al., 1989). Among these mechanisms, TE noise has been the focus of researchers, since it is the dominant broadband mechanism in aerodynamic and hydrodynamic applications, where the airfoil operates at low angles of attack (Sandberg, 2015, Jianu et al., 2012). However, there is evidence that in some applications, such as wind turbines which operate in unsteady inflow conditions, the airfoil undergoes partial or dynamic stall, which results in increased noise levels and amplitude modulation (Madsen et al., 2014, Laratro et al., 2014). Figure 4.1 illustrates the mechanisms of noise generation and associated eddies on the blade of a wind turbine constructed from airfoil sections. Trailing-edge noise is generated by eddies of the scale of the turbulent boundary layer thickness at trailing edge of the airfoil. This has a dominant mid to high-frequency content (around 500 Hz to 1600 Hz) which is attenuated within shorter distance from its source compared to low frequency noise sources (frequencies below 200 Hz) (Doolan et al., 2012, Oerlemans and Schepers, 2009). However, recent studies and reports from residents around wind farms show observations of low-frequency noise at distances far downstream (distances larger than 10 diameters downstream) of wind turbines (Pedersen and Waye, 2004). It is hypothesised that this noise is generated due to stall on the blade (Oerlemans, 2011, Moreau et al., 2009).

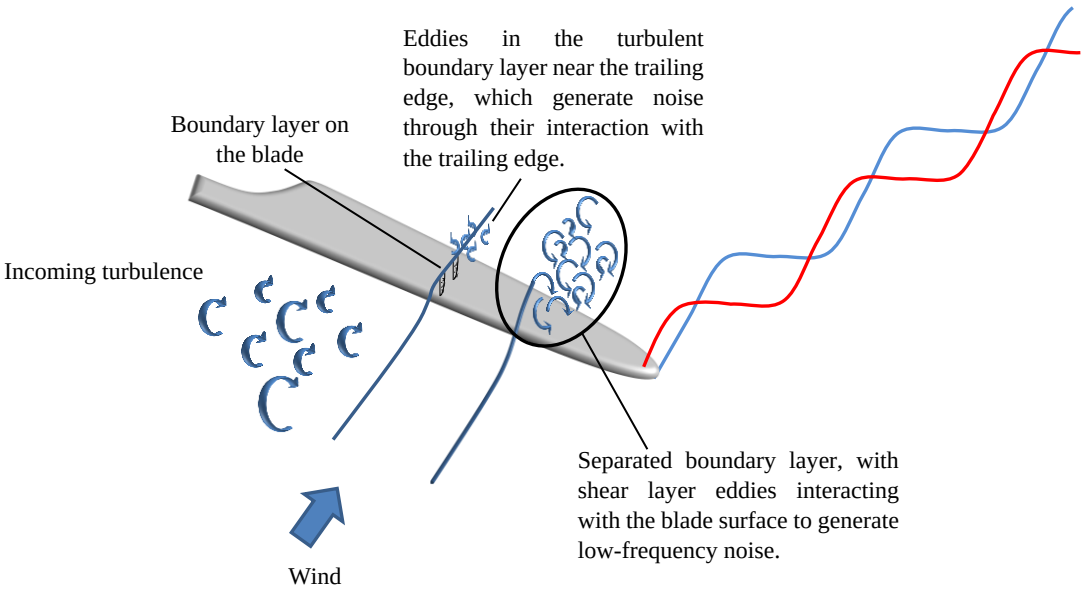

Figure 4.1 Incoming flow features and different noise generation mechanisms. Small eddies in the turbulent boundary layer interacting with trailing edge generate broadband trailing edge noise, large separated eddies are responsible for low frequency stall noise, and incoming turbulence interact with the blade to generate turbulent inflow noise, with larger eddies generating lower frequency noise (Sedaghatizadeh et al., 2017).

Several empirical and analytical approaches have been developed to investigate and predict the noise generated by airfoils. One of the first attempts for predicting aerodynamically-generated noise was conducted by Powell (1959). He introduced three main sources of noise from a flat plate moving at zero incidence: layer noise; edge noise; and wake noise. He reported that the main contributor to noise generation is the surface pressure fluctuation near the trailing edge. Based on his study, edge noise is dipolar in nature and its power varies with U^5, where U is the free stream velocity (Powell, 1959, Powell, 1990). The other two mechanisms have quadrupole directivity and their power depends on the eighth power of the velocity (Powell, 1959). By combining analytical models with experimental methods, several researchers have proposed semi-empirical models to predict the aeroacoustic signature of airfoils. While these models have proven to be acceptable for the prediction of the noise for some given cases, in some others they have given inaccurate results. Leloudas et al. (2007) used the Brooks et al. (1989) model to calculate the emitted noise from a wind turbine and found a systematic problem with the prediction of blunt-trailing-edge noise for

frequencies above 3 kHz. In the work of Moriarty and Migliore (2003), the predictions were compared to wind tunnel test data from NACA 0012 and S822 airfoils with the Reynolds number in the range of 2×10^5 to 1×10^6. Their model showed the best performance for NACA 0012 at moderate angle of attack and high frequency noises. However, the difference between the measured and predicted data exceeded 6 dB for the frequencies less than 2 kHz and large angle of attack.

Faster and multi-processor computers have enabled researchers to model the flow field around an airfoil with the required accuracy determination of noise signals (Sandberg et al., 2008, Sandberg, 2015). However, accurate CFD methods are computationally expensive, while simpler models are incapable of providing accurate results with sufficient spectral content to allow accurate acoustic calculations. The use of hybrid models such as Embedded Large Eddy Simulation (ELES) has opened the door to resolving the flow field with high resolution in desired zones, while using simpler models in other zones to reduce the computation cost (Gritskevich et al., 2012, Menter and Egorov, 2010).

The present study investigates the aerodynamic noise generated by a NACA 0012 airfoil using the ELES technique for the computation of the flow field. A dynamic Smagorinsky-Lilly model with a central-differencing scheme for momentum discretisation was used to capture small instabilities in the flow near the surface of the airfoil. The acoustic signatures of the interaction between the airfoil and fluid flow for 5°, 18°, and 40° angles of attack were numerically predicted to better understand the noise generation mechanism of an airfoil at stall. Three different angles of attack (AoA) were chosen to create pre-stall, light stall, and deep stall conditions and the pressure fluctuations at several receiving locations were calculated using the Ffowcs-Williams and Hawkings (FW-H) analogy. Moreover, the effect

of change in angle of attack on flow features and their correlation with directivity of the noise is analysed and discussed.

4.4 Numerical Modelling Methodology

In this study an ELES approach is used to calculate the flow field around a NACA 0012 airfoil, implemented using ANSYS Fluent software (version 17.0). ELES is a multi-domain approach which benefits from the accuracy of LES technique in the regions of interest and the lower computational demand of RANS in other regions. In this work, the computational domain was divided into two regions: a cylindrical region around the airfoil where LES is used, and the rest of the domain where Scale-Adaptive Simulation (SAS) is performed. SAS was chosen because it performs similarly to a standard Reynolds-Average Navier-Stokes (RANS) model in steady flows, but allows the formation of broadband turbulence for unstable flows. This model is able to provide sufficient spectral content for acoustic computations, in contrast to RANS models which are unable to do so due to their time-averaged nature (Menter and Egorov, 2010). As shown in Figure 4.2, SAS can capture more details of instabilities in the flow compared to RANS models. Thus, it is possible to capture a large range of frequencies of the instabilities and fluctuations in the flow.

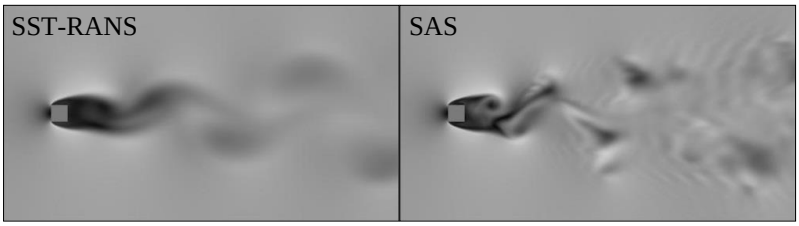

Figure 4.2 Comparison of instantaneous velocity field over a square cylinder at Re=11000 by SST-RANS (left) and SAS (right), showing more details and instabilities when SAS was applied (Maliska et al., 2012).

The main difference between the SAS and standard RANS models lies in how the scale-defining equations are formulated and treated. The original SAS model (Menter and Egorov,

2010) was formulated as a two-equation model, with the variable $\varphi = \sqrt{k}L_t$ for the scale equation:

$$\frac{\partial(\rho k)}{\partial t} + \frac{\partial\left(\rho\overline{U_j}k\right)}{\partial x_j} = P_k - c_\mu^{\frac{3}{4}}\rho\frac{k}{\varphi^2} + \frac{\partial}{\partial x_j}\left(\frac{\mu_t}{\sigma_k}\frac{\partial k}{\partial x_j}\right) \tag{4.1}$$

$$\frac{\partial(\rho\varphi)}{\partial t} + \frac{\partial\left(\rho\overline{U_j}\varphi\right)}{\partial x_j} = \frac{\varphi}{k}P_k\left(\xi_1 - \xi_2\left(\frac{L_t}{L_{vK}}\right)^2\right) - \xi_3\rho k + \frac{\partial}{\partial x_j}\left(\frac{\mu_t}{\sigma_\varphi}\frac{\partial\varphi}{\partial x_j}\right) \tag{4.2}$$

$$L_{vK} = \kappa\left|\frac{\overline{U'}}{\overline{U"}}\right|; \quad U' = S = \sqrt{2S_{ij}S_{ij}}\,; \quad \overline{U"} = \sqrt{\frac{\partial^2\overline{U_i}}{\partial x_j\partial x_j}\frac{\partial^2\overline{U_i}}{\partial x_k\partial x_k}} \tag{4.3}$$

$$S_{ij} = \frac{1}{2}\left(\frac{\partial\overline{U_i}}{\partial x_j} + \frac{\partial\overline{U_j}}{\partial x_i}\right); \quad L_t = \frac{\varphi}{\sqrt{k}}; \quad P_k = \overline{-u'v'}\frac{\partial U}{\partial y} \tag{4.4}$$

where ρ is fluid density, k is turbulent kinetic energy, Lt is turbulent length scale, U is the resolved velocity, $\xi_{1,2,3}$ and c_μ are model constants, U' is the first derivative of the velocity, κ is von Karman constant, P_k is the production term, μ_t is the turbulent viscosity, and S is the shear strain. As shown in the SAS model, the main new term that appears in the transport equation (Equation 2) is the inclusion of the von Karman length scale L_{vK}, which does not appear in a standard RANS model. Using the second derivative of velocity (U'') in calculation of length scale enables the model to match its length scale with the turbulent structures which already been modelled in the flow. This functionality is not present in a standard RANS model. This leads to more LES-like behaviour, which can capture a wider range of instability length scales and therefore agrees more closely with the experimental observations.

The interface between the LES and SAS regions is treated such that the consistency between two regions is maintained. To do so, synthetic turbulence is introduced at the interface

between the two regions with two different approaches. The LES part of the computations is formulated as below (Wilcox, 1998):

$$\frac{\partial \rho}{\partial t} + \frac{\partial}{\partial x_i}\left(\rho \overline{u_i}\right) = 0 \tag{4.5}$$

$$\frac{\partial(\rho \overline{u_i})}{\partial t} + \frac{\partial(\rho \overline{u_j}\,\overline{u_i})}{\partial x_j} = \frac{\partial \sigma_{ij}}{\partial x_j} - \frac{\partial \overline{p}}{\partial x_i} - \frac{\partial \tau_{ij}}{\partial x_j} \tag{4.6}$$

In above equations, $\bar{u}$ is the resolved velocity, σ is the stress tensor due to molecular viscosity (obtained from resolved velocity) and $\tau_{ij}$is the subgrid-scale stress, defined as $\tau_{ij} = \rho\overline{u_i u_j} - \rho\overline{u}_i\overline{u}_j$. To close the set of equations, the Boussinsque hypothesis is used for the calculations as described below (Wilcox, 1998, Menter and Egorov, 2010):

$$\tau_{ij} - \frac{1}{3}\tau_{kk}\delta_{ij} = -2\mu_t \overline{S_{ij}} \tag{4.7}$$

where $\mu_t$is the subgrid turbulent viscosity, calculated using Smagorinsky-Lilly model as $\mu_t = \rho L_s^{\,2}\left|\bar{S}\right|$. Here $\bar{S}$ is the resolved strain rate as presented in Equation (4) and L_s is the mixing length for subgrid length-scale computed by:

$$\left|\bar{S}\right| \equiv \sqrt{2\overline{S_{ij}}\,\overline{S_{ij}}}, \quad L_s = \min\left(\kappa d, C_s V^{1/2}\right) \tag{4.8}$$

where κ is the von Karman factor, d is the closest distance to the airfoil surface, C_s is the Smagorinsky factor, and V is the volume of the computational cell. The value of C_s has a significant effect on large-scale fluctuations in the mean shear and in the regions close to solid boundaries. To address this problem, Germano et al. (1991), and subsequently Lilly (1992), proposed a method by which the Smagorinsky constant is calculated dynamically using the resolved motion data.

The noise signature used in the model presented in this paper is computed based on coupling the CFD for the aerodynamic calculations with the Ffowcs-Williams and Hawkings (FW-H) model. One of the main advantages of using the FW-H analogy compared to direct aeroacoustic computation is the ability to calculate the sound signature indirectly from the CFD results, which significantly reduces the computational demand. The FW-H model is essentially an extension to Lighthill's theorem, which takes into account the noise source related to surfaces in a relative motion. The FW-H equation is written as (Williams and Hawkings, 1969):

$$\frac{1}{a_0^2}\frac{\partial^2 \acute{p}}{\partial t^2} - \nabla^2 \acute{p} = \frac{\partial^2}{\partial x_i \partial x_j}\{T_{ij}H(f)\} - \frac{\partial}{\partial x_i}\{[P_{ij}n_j + \rho u_i(u_n - v_n]\delta(f)\} + \frac{\partial}{\partial t}\{[\rho_0 v_n + \rho(u_n - v_n]\delta(f)\} \tag{4.9}$$

where ρ_0 is the fluid density at the state of equilibrium, ρ is the instantaneous fluid density, u_i is the fluid velocity component in x_i direction, u_n is the fluid velocity component normal to the surface ($f = 0$), v_i is the surface velocity component in x_i direction, and v_n represents the velocity component normal to the surface. The terms $\delta(f)$ and $H(f)$ in the FW-H equation are the Dirac delta and Heavyside functions, respectively, where $f = 0$ corresponds to the source surface and $f > 0$ denotes the exterior flow region. Here $\acute{p}$ is defined as the gauge hydrodynamic pressure, while a_0, P_{ij} and T_{ij} represent speed of sound, compressive stress tensor and Lighthill's stress tensor, respectively. Equation (9) reduces to Lighthill's theorem if there is no surface (i.e., $H = 1$).

The FW-H equation can be integrated analytically assuming a free-space flow without any obstacles between the sound source and the receiver. The solution to this is given in Equation (10), broken into quadrupole, dipole and monopole terms.

$$H(f)\acute{p}(x,t) =$$

$$\underbrace{\frac{1}{4\pi}\int_V \frac{\partial^2}{\partial y_i \partial y_j}\left[\frac{1}{|1-M_r|}T_{i,j}\left(y,t-\frac{r}{a}\right)\right]\frac{dy}{r}}_{\text{Quadrupole}} +$$

$$+\underbrace{\frac{1}{4\pi}\int_{f=0}\frac{\partial}{\partial y_i}\left[\frac{1}{|1-M_r|}F_i\left(y,t-\frac{r}{a}\right)\right]\frac{dy}{r|\nabla f|}}_{\text{Dipole}} + \tag{4.10}$$

$$+\underbrace{\frac{1}{4\pi a_0}\int_{f=0}\frac{\partial}{\partial t}\left[\frac{1}{|1-M_r|}Q_i\left(y,t-\frac{r}{a}\right)\right]\frac{dy}{r|\nabla f|}}_{\text{Monopole}}$$

where $F_i = P_{i,j}n_j + \rho u_i(u_n - v_n)$ and $Q_i = \rho v_n + \rho(u_n - v_n)$. The quadrupole term, which is represented by a volume integral, contributes to the unsteady stresses in the region outside the source surface, while surface integrals represented by the dipole and monopole terms are respectively related to the flow interaction with moving bodies and body thickness respectively. The monopole part of the formulation contributes to the thickness noise or volume displacement noise, which originates from the relative motion of the air and surface. This explanation has been added to the text. Since the airfoil is stationary, the contribution of the monopole term is just associated with the relative motion of the fluid over the airfoil surface. Monopole noise source is significantly affected by the compressibility of the medium. However, the effect of compressibility on the monopole term in the current study was neglected due to non-compressibility of the fluid medium. The quadrupole term is often negligible compared to the other two terms and becomes close to zero for subsonic flows. Thus the FW-H model in this study utilises the monopole and dipole terms to calculate the noise emission from the airfoil.

4.5 Computational Domain and Grid Specification

The computational domain was constructed based on the experiment conducted by Moreau et al. (2009) as shown in Figure 4.3. Figure 4.4 shows the corresponding computational domain and its dimensions. This geometry was selected because of the availability of experimental data required for validation. The dimensions of the airfoil and Reynolds number for each case are similar to the ones used by Moreau et al. (2009). A NACA 0012 airfoil with with 10 cm chord length and 13 cm span (aspect ratio =1.3) is placed in jet flow with 20 m/s uniform velocity resulting in Reynolds number of 1.3×10^5.

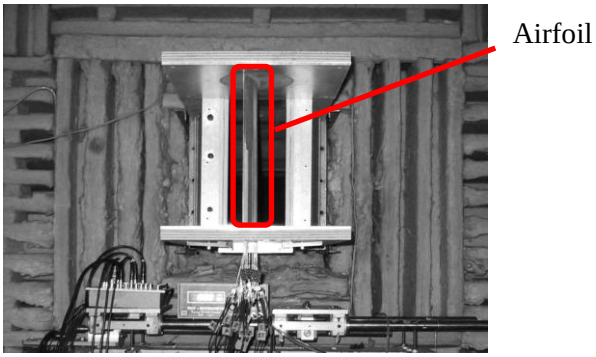

Figure 4.3 Experimental setup at Ecole Centrale de Lyon (Moreau et al., 2009)

A uniform velocity field with low turbulent intensity ($TI = 1\%$) was selected for the inlet and a pressure outlet with zero gauge pressure was chosen for the outlet boundary condition. The front and back sides of the domain are treated as the symmetry boundary condition, except the limiting sheets which were chosen as a wall as suggested by Moreau et al. (2009). The computational domain was extended compared to the experiment to eliminate the effect of reverse flow at the outlets, to improve the stability of the computations and accuracy of the results.

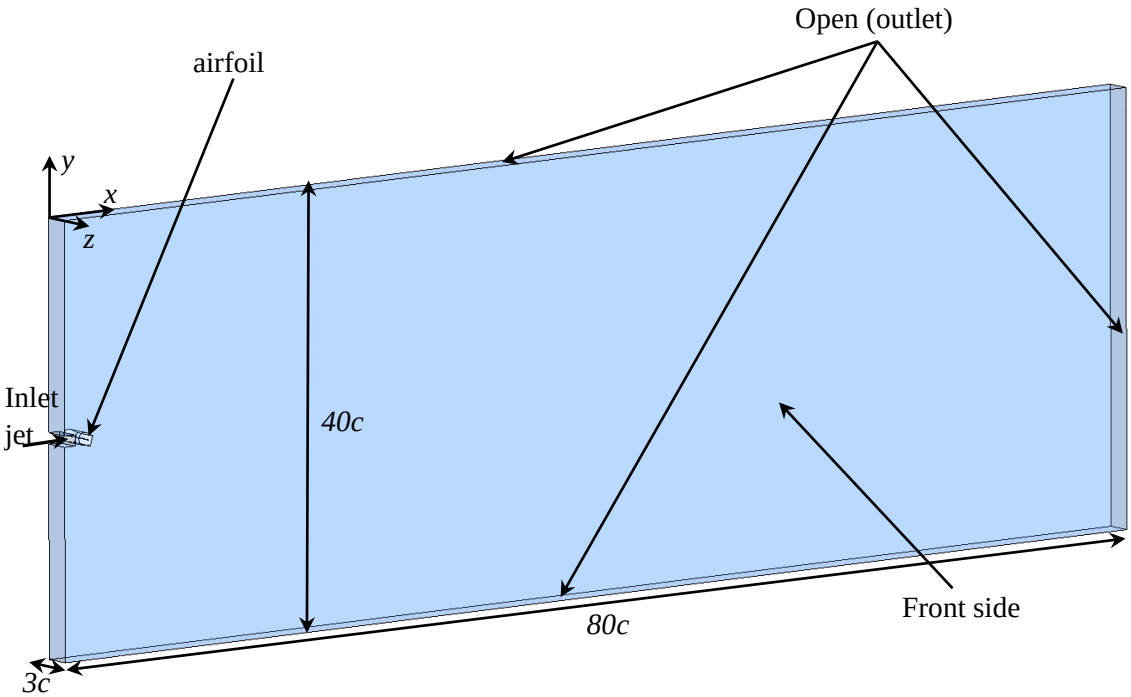

Figure 4.4 Computational domain used for current simulations. The large domain size is chosen to eliminate any reverse flow at outlets.

Figure 4.5 shows the mesh and domain used in the simulation. The LES zone around the airfoil consists of two million cells and the total number of elements in the domain is approximately 3.5 million. The domain consists of hexahedral elements with growth rate of 1.1 in near field and 1.2 far from airfoil. The non-dimensional y^+ (which represents the distance from the solid surface) is set to one, in order to capture the boundary layer at the required accuracy.

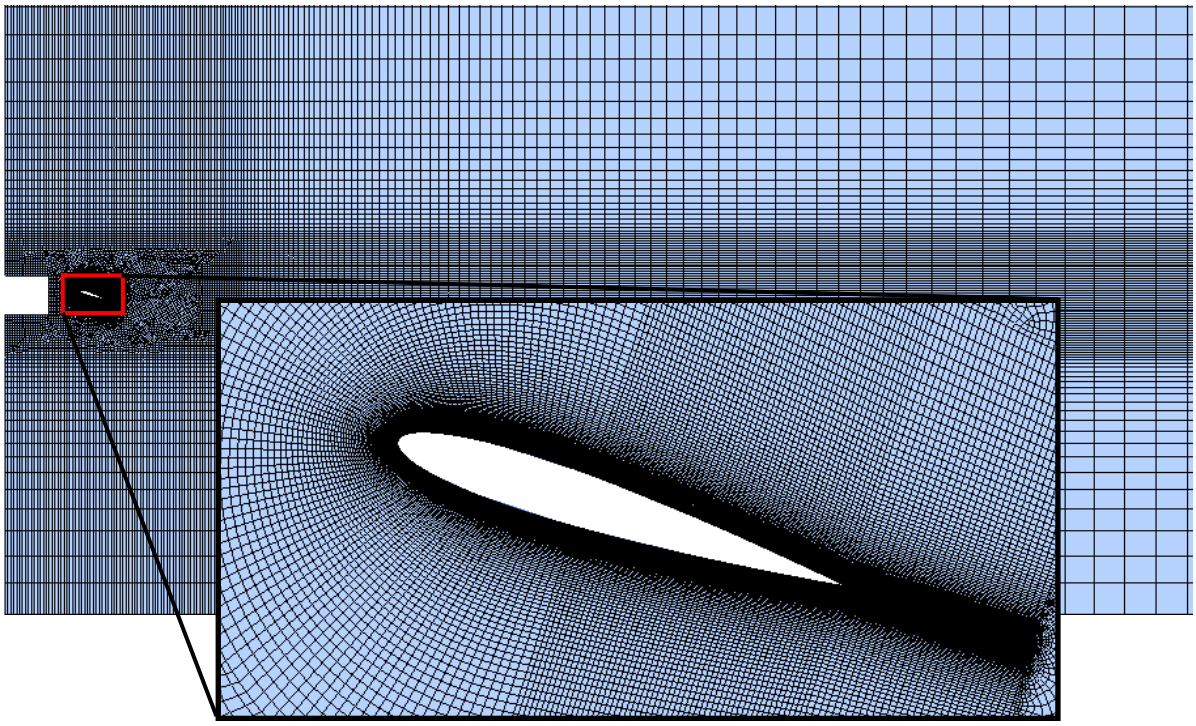

Figure 4.5 Generated mesh in the computational domain and zones. The airfoil area is magnified to show the grid around the airfoil.

A time step of $\Delta t=1\times10^{-5}$ s was used to ensure that the maximum Courant–Friedrichs–Lewy (CFL) number lies in the range of unity for most of the domain, especially in the wake region. The blade and associated mesh are rotated together when the angle of attack is changed such that same mesh structure is maintained.

4.6 Validation

For validation purposes, the model was solved at a Reynolds number of 1.34×10^{5} and at an angle of attack of 18°, such that the results could be compared with the experimental results of Moreau et al. (2009). Figure 4.6 shows the comparison of the pressure coefficient distribution obtained from the CFD simulation with the experimental results. The comparison shows good agreement, with a maximum deviation of 7%. It should also be noted that there were only 16 measurement points on the airfoil surface in the experiment and at both the leading and trailing edges the experimental data are sparse due to the physical size limitations of the pressure sensors. This limited the ability of the measurements to

resolve the details of the pressure distribution, especially at the leading edge where large pressure gradients occur.

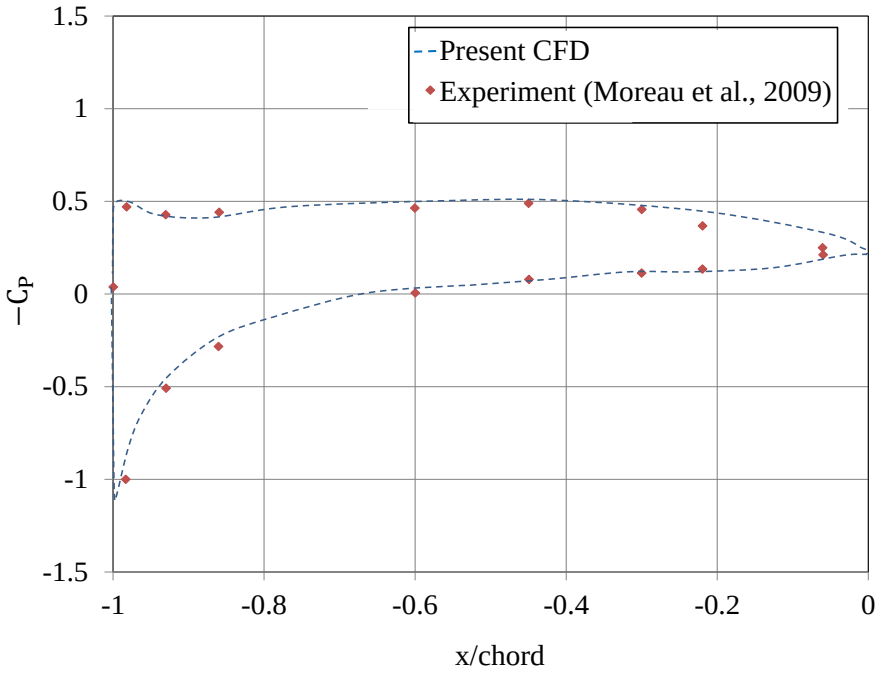

Figure 4.6 Comparison of computational results and experiment a pressure coefficient obtained by Moreau et al. (2009.).

To further evaluate the validity of the model, the lift coefficient has been recorded at each time-step (Figure 4.7). The presented lift coefficient corresponds to 0.15 seconds of the simulation during which the data was collected after transient period of the simulation. Figure 7 (b) shows the Fast-Fourier Transform of the lift coefficient which is used to identify the frequency of the vortex shedding. The dominant frequency of the lift coefficient fluctuation is approximately 118Hz, which corresponds to Strouhal number of St=0.59. This is close to the experimental Strouhal number of St=0.58 by Moreau et al. (2009) and St=0.63 by Suzuki et al., (2006) at 18° angle of attack and Reynolds number of 1.3×10^5 which shows the ability of the model to capture the instabilities in the flow. The slight difference between the current results and experimental data can be explained by the difference in blockage ratio

between the two experimental setups. The effect of blockage will be discussed later in Section 4.5.

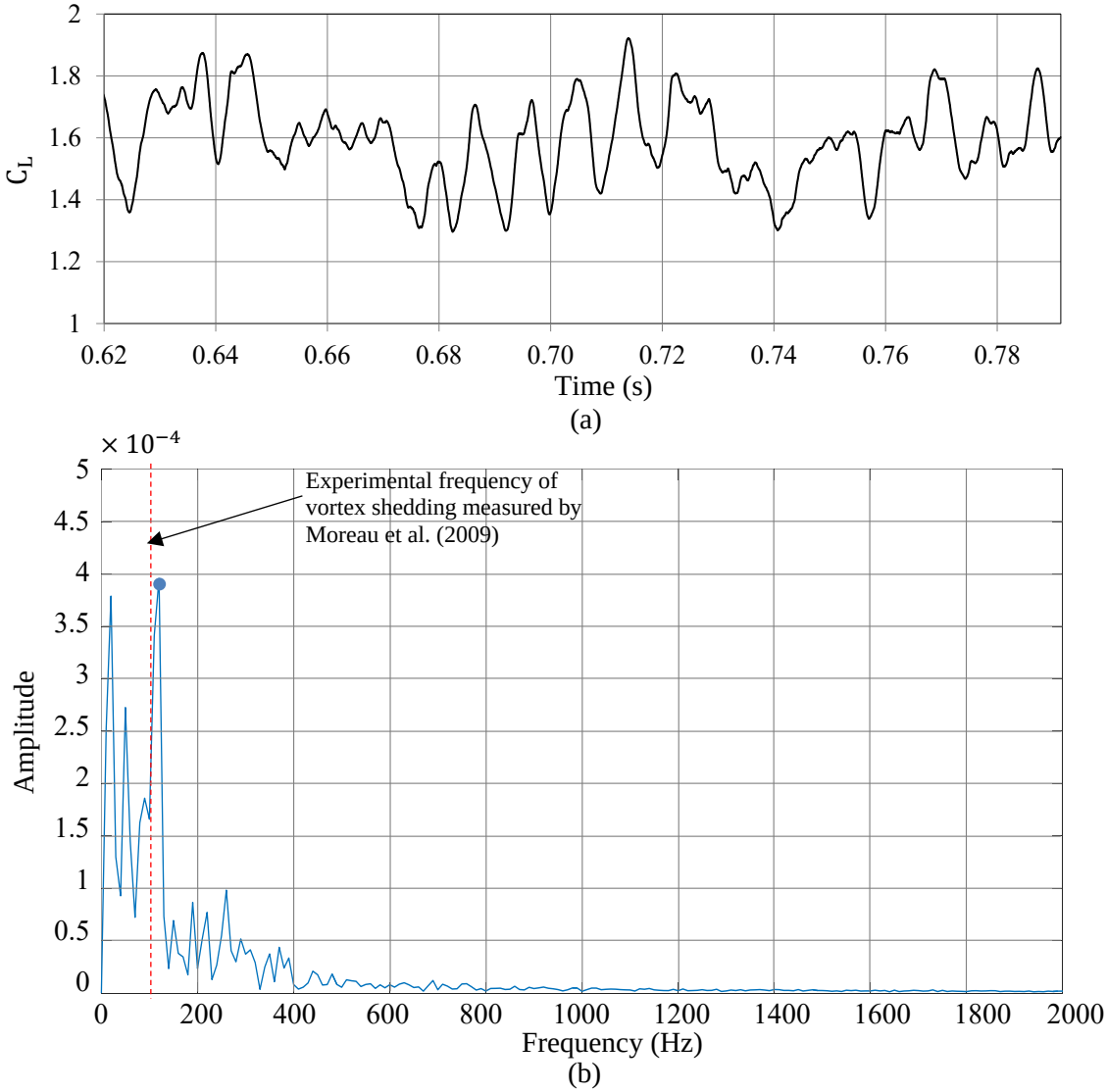

Figure 4.7 (a) Variation of the lift coefficient of the airfoil with time, used to calculate the frequency of the vortex shedding. (b) FFT of the lift coefficient over 0.15 seconds of the data collection with the first frequency around 118 Hz compared with Moreau et al. (2009).

To evaluate the accuracy of the aeroacoustic model, the results are compared with the data of experiment for a similar geometry by Moreau et al. (2009). Figure 4.8 illustrates the comparison of the predicted noise signal at 70 chords downstream of the airfoil with the experimental data for the geometry described in Section 3. In general, the model provides a good agreement about the trend of the noise with the experimental data, however, a shift in amplitude is evident. This may be partially attributed to the lack of information about the

location of the microphone in the experimental setup. In addition, as shown in Figure 4.8, the frequency of the calculated first peak is 11% lower than the experimental data which is believed to be associated with the uncertainties due to setup and measurement at low frequencies (Moreau et al., 2009). The discrepancies between the computed and measured noise signals can be explained by: i) numerical errors, ii) background noise and experimental uncertainties associated with the measurement (especially noise generated by the support tower and the jet exit which add to the discrepancies between the predicted and measured data which should be considered in analysing the data). To eliminate the effect of the background noise, form the measured noise signals, the sound spectral in the test section with no airfoil installed is determined and subtracted from the total noise signature. However, this cannot completely eliminate the effect of the test rig due to the change in the flow behaviour in the presence and absence of the airfoil. Based on the reasonable agreement between the trend and behaviour of the noise signature for measured and calculated data, it can be concluded that the aeroacoustic model presented in this work can be further used for investigation of the noise directivity and level of a NACA 0012 at different angles of attack.

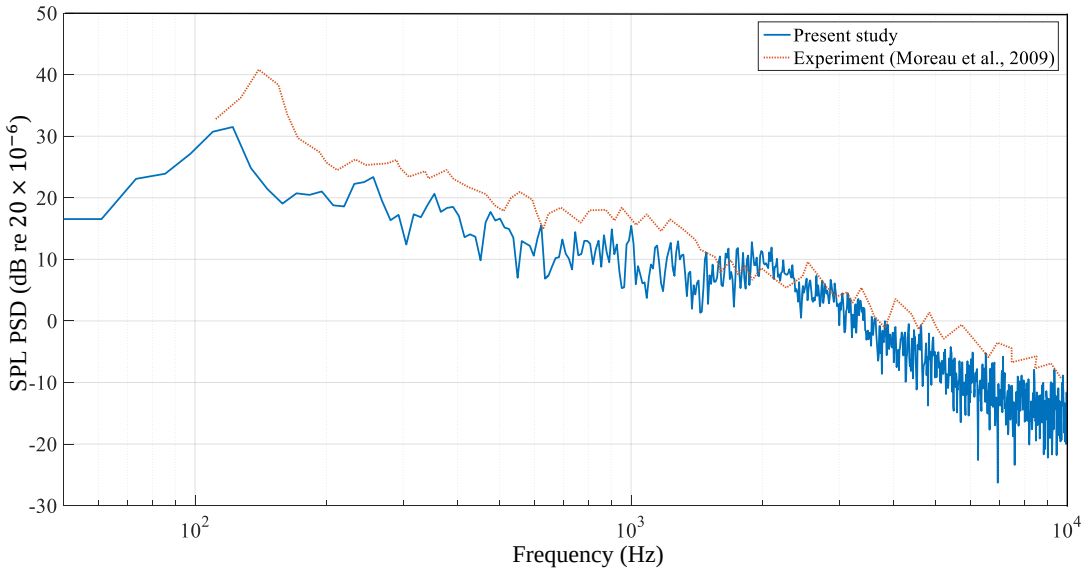

Figure 4.8 Comparison of the predicted and measured noise signature from a NACA 0012 airfoil. Experimental data is reproduces from the data provide by Moreau et al. (2009).

4.7 Results and Discussion

4.7.1 Flow Structure Results

Figure 4.9 shows a snap shot of the turbulence in the flow using the Q-criteria. It can be seen that the boundary layer is separated from the suction surface at high angles of attack when the airfoil experiences stall. At an AoA of 40º, the existence of high level turbulence and large eddies in the flow indicates that the airfoil is in the deep stall condition. In addition, there are some other unsteady flow structures associated with shear layer roll-up generated due to the jet flow and high blockage ratio caused by the airfoil at a high angle of attack. This effect is enhanced as the blockage ratio increases, which results in the formation of vortices shed from the edge of the nozzle. Separated flow structures, with smaller eddies, can be also seen in the 18° AoA case. Figure 4.9 also shows that the size of the eddies correlates with the angle of attack, with eddies becoming larger and stronger as the angle of attack increases. This can be explained by the increase in the size of the projected frontal area of the airfoil, hence the width of the wake. It can be also seen from the turbulent eddies that the flow separates close to the leading edge for angles of attack greater than 18°. Under these conditions the large-scale turbulence can be seen to interact with the whole surface of the airoil, which is expected to result in higher noise levels and lower frequencies compared to the 5° degree AoA case.

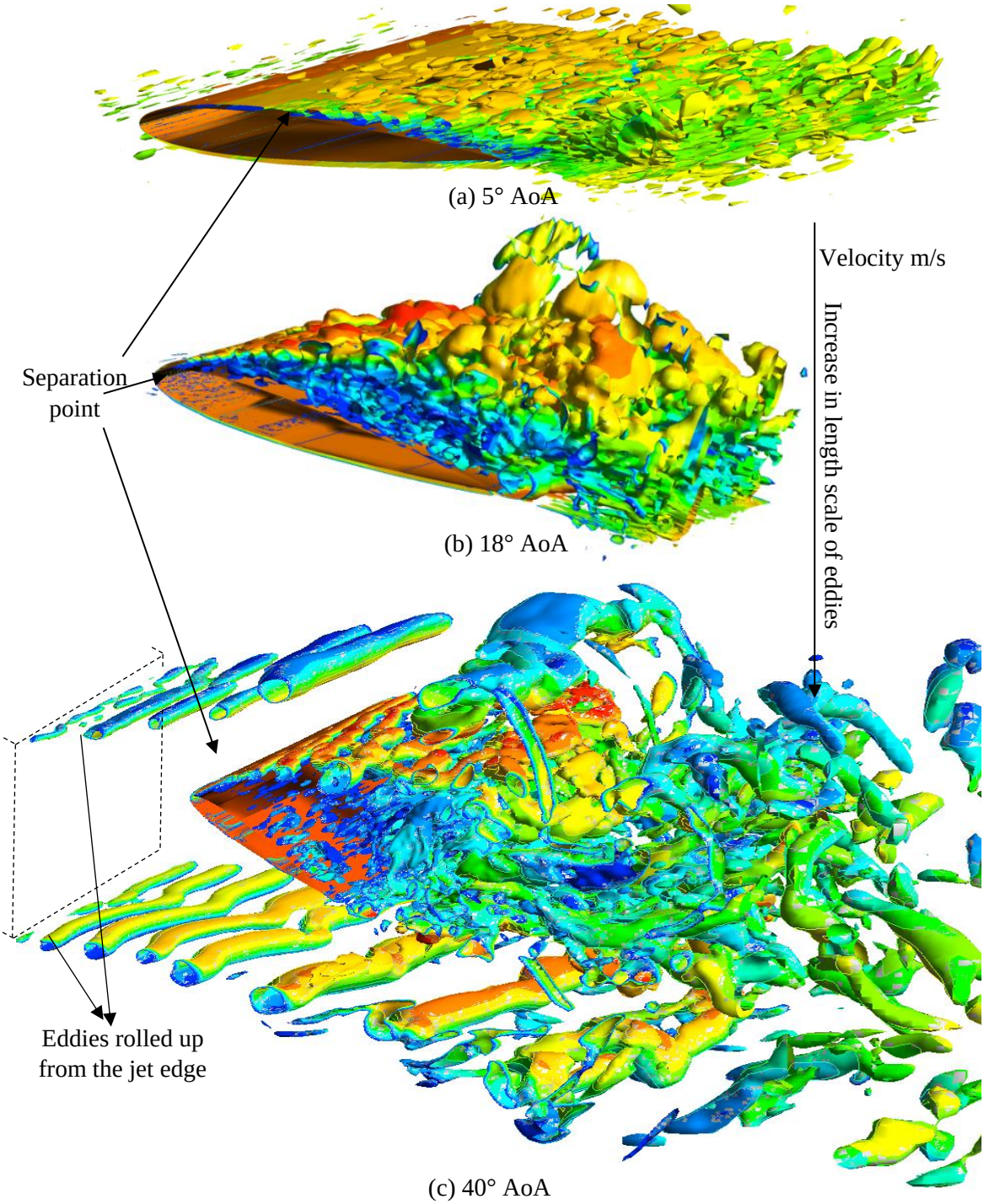

Figure 4.9 Velocity contour on iso-surface of Q-criterion showing the turbulent structures separated from the airfoil surface; a) AoA=5°, b) AoA=18°, c) AoA=40°.

Knowledge of the length scales of turbulent structures in the flow is important in aeroacoustics since turbulence length scales have a significant effect on the far-field noise spectra and noise source parameter modelling (Kamruzzaman et al., 2011). An estimate of the length scale can also help to identify the underlying noise generation mechanism, since

the larger eddies interact with larger surfaces and result in lower frequency noise emission. The integral length scale is calculated using the turbulent kinetic energy, k, and its dissipation rate, ε, is given by $l = \frac{k^{3/2}}{\varepsilon}$ (Tennekes and Lumley, 1972, Wilcox, 1993). The integral length scale qualitatively shows the distance in which the fluid elements are moved by large turbulent structures (Ni et al., 2003). To compare the integral length scales of the studied cases, its evolution along the horizontal axis (see Figure 4.11) is calculated and depicted in Figure 10. The integral length scale generally increases as the angle of attack increases. For both stall conditions shown in Figure 4.9, a peak exists in length scale of the turbulent structures which is associated with the shed vortices downstream of the airfoil. This means that it is expected that the frequency of the noise signals in the far field decreases when the size of eddies increases in the wake.

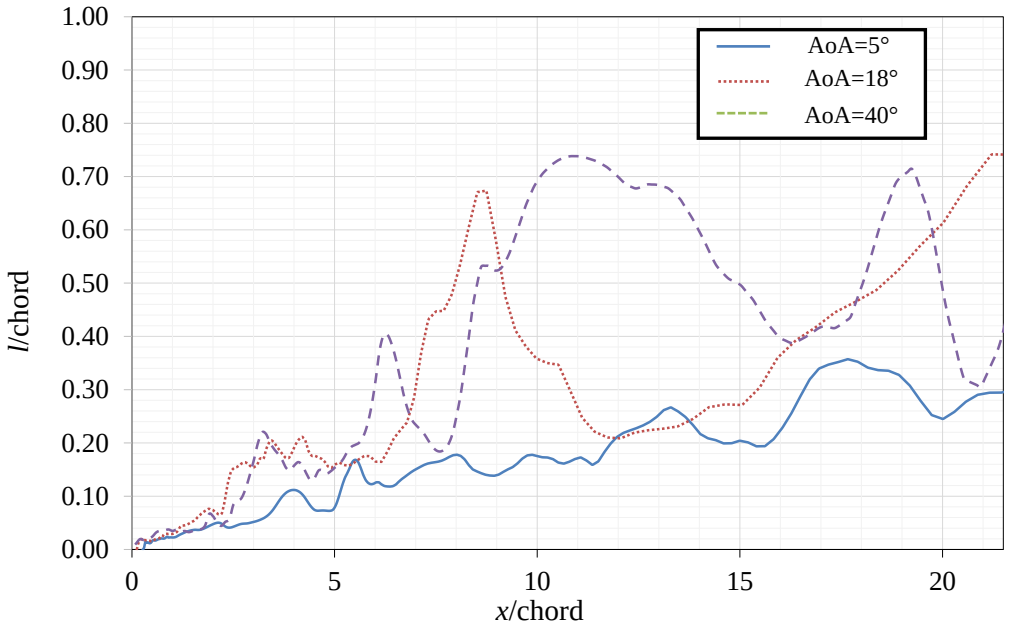

Figure 4.10 Integral length scale downstream of the airfoil for 3 angles of attack. Large peaks correspond to the large eddies separated from the airfoil at stall.

Streamlines on the mid-section plane of the flow are presented in Figure 4.11 which show several vortical structures separating from the airfoil surface. It can be seen that the separation starts at the leading edge for the AoA 18º and 40º degree cases, whereas at 5°

AoA there is laminar flow separation from the airfoil surface at the mid-chord which forms a turbulent shear layer at the trailing edge. For 5° and 18° AoA, the separated shear layer becomes turbulent as a consequence of the instabilities developed by the action of a Kelvin-Helmholtz mechanism. These high-frequency fluctuations in the velocity field grow in magnitude as the distance from the leading edge increases and eventually cause the shear layer to roll up and undergo transition to turbulence (Prasad and Williamson, 1997, Rodriguez et al., 2011a). At high angles of attack the airfoil acts like a bluff body, with large separation zone and the formation of a Karman vortex street. As can be seen in Figure 4.11 (a) small eddies for low angles of attack interact with the airfoil close to the trailing edge, while for higher angles of attack the whole suction surface is influenced by generated eddies. Thus, it is expected that the source of noise for low angles of attack is in the vicinity of the trailing edge, while for the high angles of attack the whole airfoil surface is the source of noise generation. The size of the eddies significantly increases when angle of attack changes from 18° to 40°, whilst the number of turbulent eddies decreases. Based on the size of the eddies and surface with which they interact, it is expected that the whole surface of the airfoil produces noise in these cases. Consequently, the dominant noise frequency decreases as angle of attack increases.

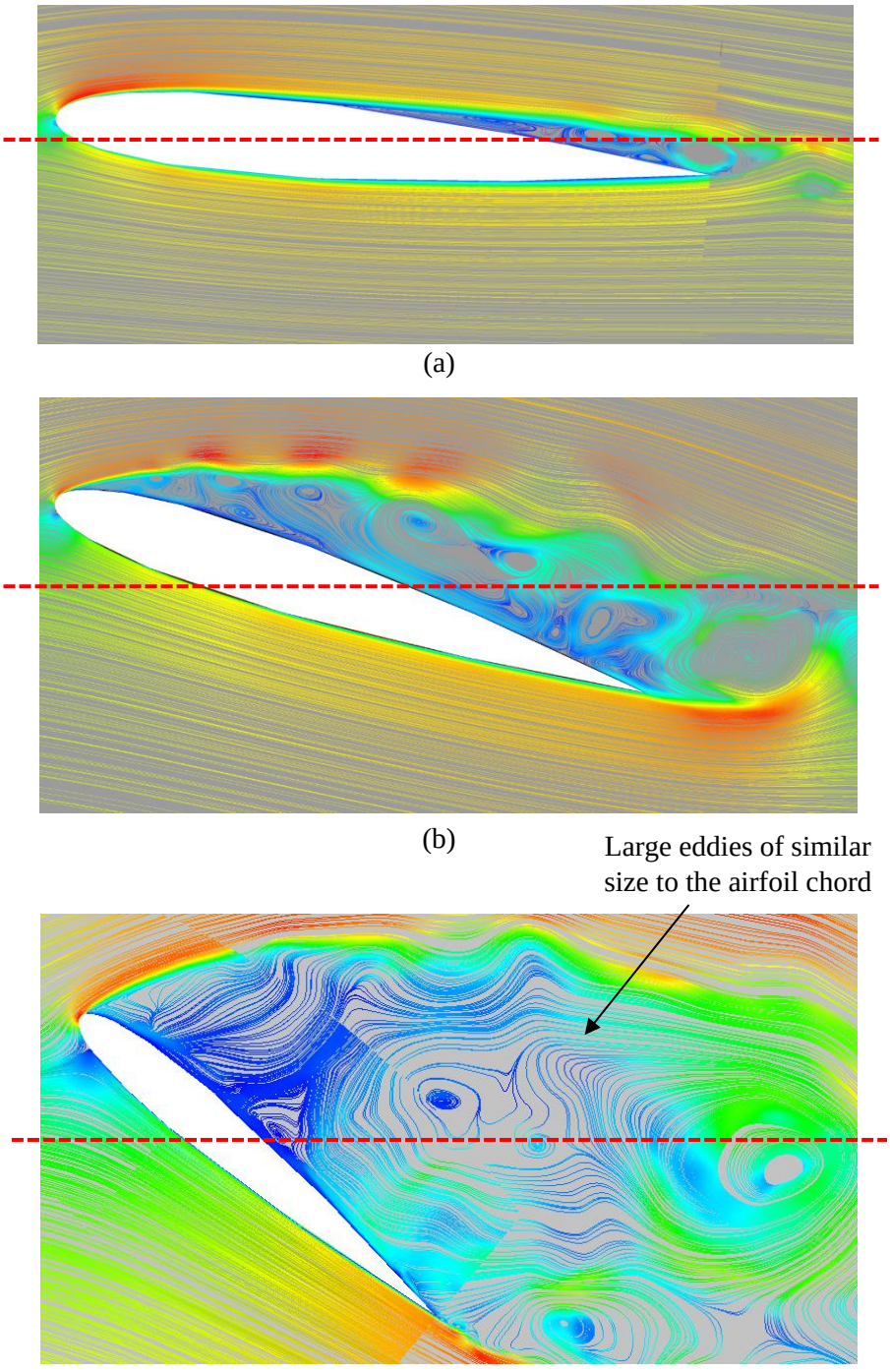

Figure 4.11 Instantaneous streamlines for different cases, which illustrate the size of the vortices separated from the airfoil surface and their interaction with the airfoil surface further downstream, (a) AoA= 5°, (b) AoA= 18°, (c) AoA= 40° (the discontinuity in streamlines is caused by post processing program during visualisation due to the existing interface). Dashed red lines shows the line on which the integral length scale is calculated.

4.7.2 Aeroacoustic Results

As mentioned in the Section 4.4, the quadrupole term in FW-H analogy is neglected in the governing equations. Thus, the noise signatures are associated with flow-surface

interactions, and vortex-vortex interactions are not considered in the calculations. The instantaneous local pressure fluctuations on the mid-section plane at the final time step are displayed in Figure 4.12. As can be seen, the plot shows dipole characteristics for the pressure field. These pressure dipoles are aligned with the chord line for 18° and 5° angles of attack, however they are not aligned for the 40º case. This behaviour can be explained by the large separation and bluff body behaviour of the airfoil at this angle of attack. The magnitude of the pressure fluctuations also increases significantly at this AoA.

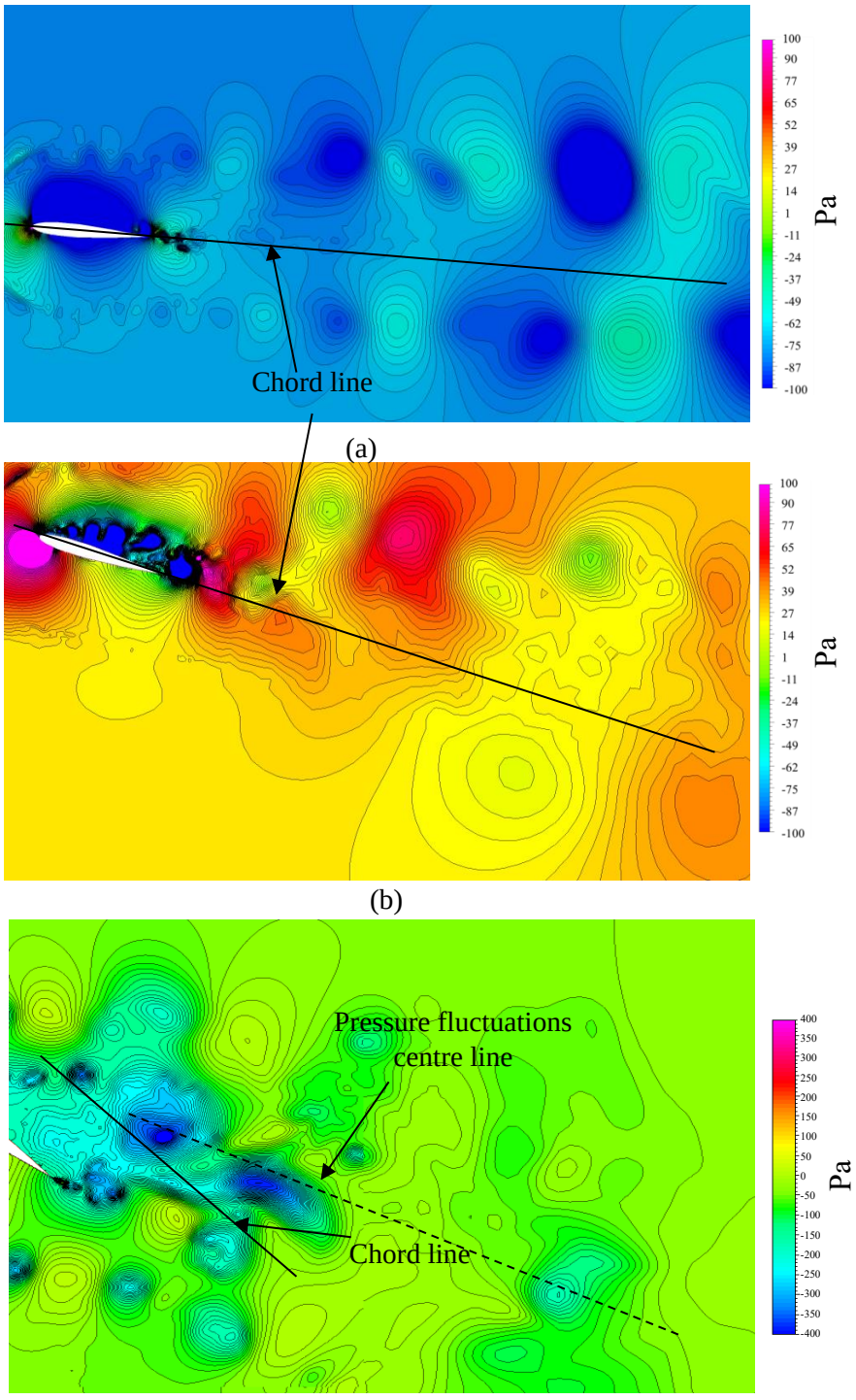

Figure 4.12 Deviation of the local pressure with respect to atmospheric pressure, a) AoA=5°, b) AoA=18°, and

Over 7500 samples of surface pressure on the airfoil were collected during the period of final 0.15 seconds of the simulation, and the data were used to calculate the far-field sound pressure using FW-H analogy. Recording the data at each time step resulted in a frequency resolution of about 6 Hz. Considering the vortex shedding frequency of 117 Hz for 18º angle

of attack, which corresponds to a 0.0085 second shedding period, the 0.15 seconds time span can provide sufficiently accurate resolution for the acoustic study. Sixteen receivers, located symmetrically around the airfoil located 70 chords away from the airfoil centre (see Figure 4.13), such that the chord-line passes through a pair of receivers. Using the Ffowcs-Williams and Hawkings analogy, the far-field noise signatures at the receiver locations were calculated. The spectra densities of these noise signatures are presented in Figure 4.14. As can be seen in Figure 14, the peak in the SPL of the noise shifts to lower reduced frequencies as the AoA increases. Since the frequency of the generated noise depends on the size of the turbulent eddies, and generally $f \propto U/l$, where l is the integral length scale and U is mean flow velocity, these results are consistent with the increase in turbulence length scales shown in Figure 4.10.

The sound pressure spectra in the far field for 18° angle of attack shows different behaviour at some receivers. The sound spectra for receivers 1 and 9 have a relative minimum at the reduced frequency of 6, while other receivers have their relative peaks at reduced frequency around 2. Reduced frequency is defined as $k = f \times b/V$ where f, b, and V are frequency of the noise, aifoild chord and flow velocity, respectively. It should be noted that these receivers are located on the chord line direction. Higher frequency content at these locations compared to the rest of the receivers suggests that the noise is generated by smaller eddies interacting with the smaller surface at the leading or trailing edge of the airfoil. The peak of the noise signature slightly decreases as the airfoil undergoes a deep stall condition at 40° angle of attack. Similar to light stall at 18° angle of attack, the calculated far-field sound pressure at deep stall condition shows lower sound pressure level for the receivers located on the chord line direction. However, unlike the 18° angle of attack, the peak frequency for all locations are the same. This behaviour shows that the noise is associated with the large eddies

separated from the airfoil, with lower sound energy propagation in chord line direction. The noise level on the chord line direction is generally lower than other receivers, suggesting lower sound energy transmission in this direction.

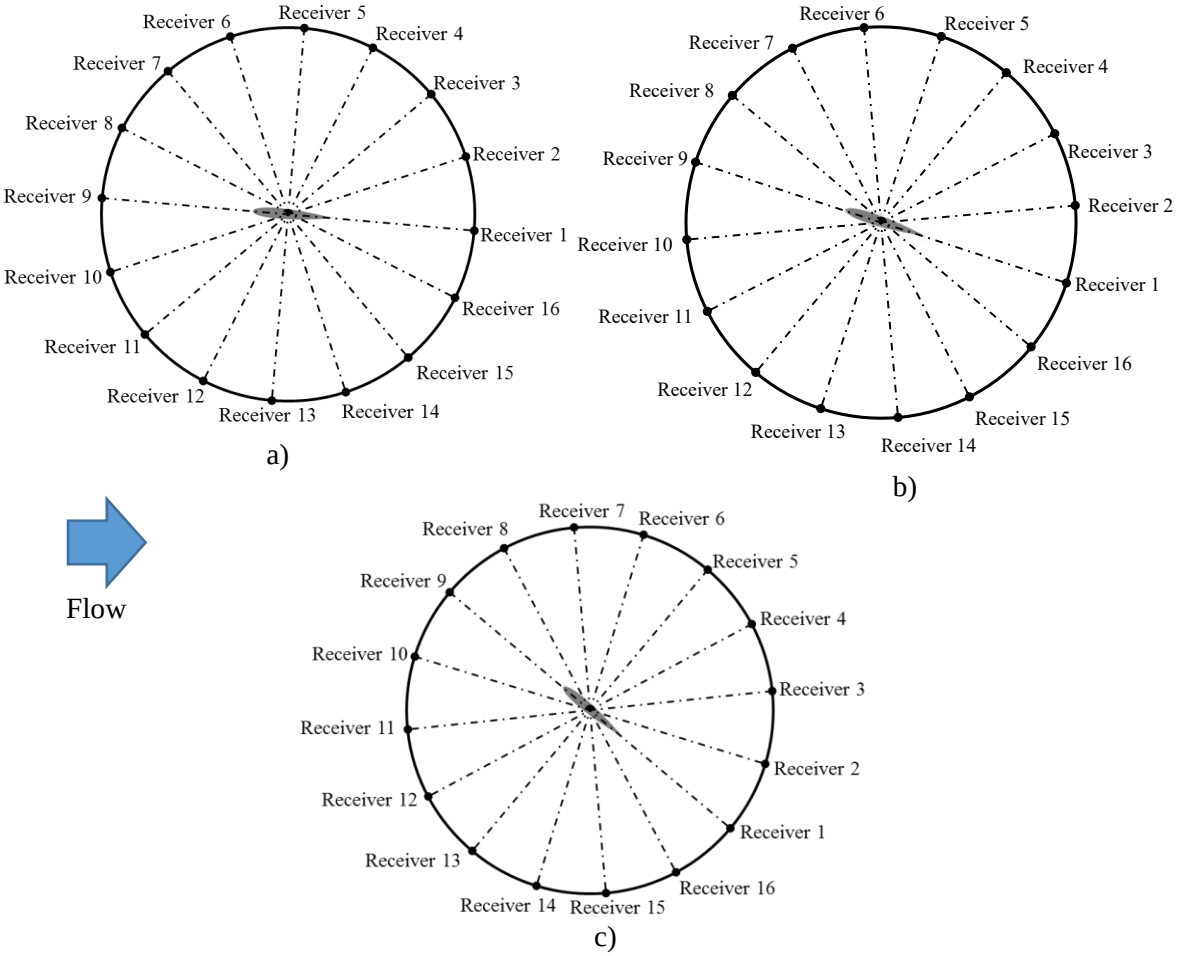

Figure 4.13 Relative locations of the receivers with respect to the airfoil, a) 5º AoA, b) 18º AoA, and c) 40º

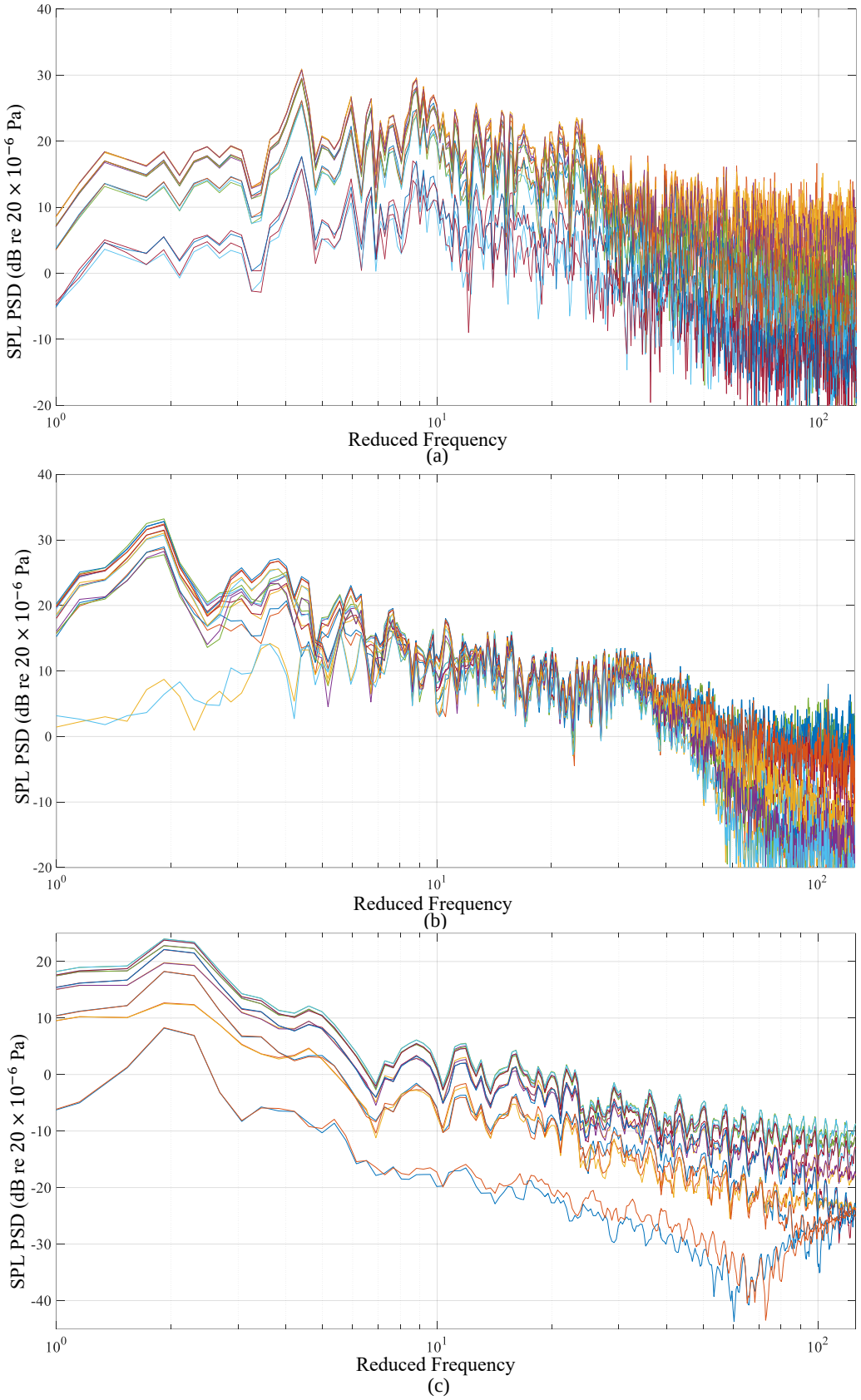

Figure 4.14 Sound pressure level at a distance of 70 chords from airfoil, a) AoA=5°, b) AoA=18°, c) AoA=40°. The frequency content of the noise decreases as the angle of attack increases.

The change in narrowband spectra at a distance of 70 chords downstream of the airfoil for

the three angles of attack at the receiver locations, is presented in Figure 4.14. As shown, the dominant frequency decreases as the AoA increases. The shift of the dominant frequency towards the lower frequency range with an increase in the angle of attack is caused by the increase in size of the vortices separated from the airfoil surface (see Figure 4.9 and 4.10). The SPL of the peak for highest angle of attack is slightly smaller than the light stall case (22.3 vs 23.3 dB re 20 μPa). However, the frequency content significantly drops for the 40° angle of attack when compared to the case at 18° angle of attack.

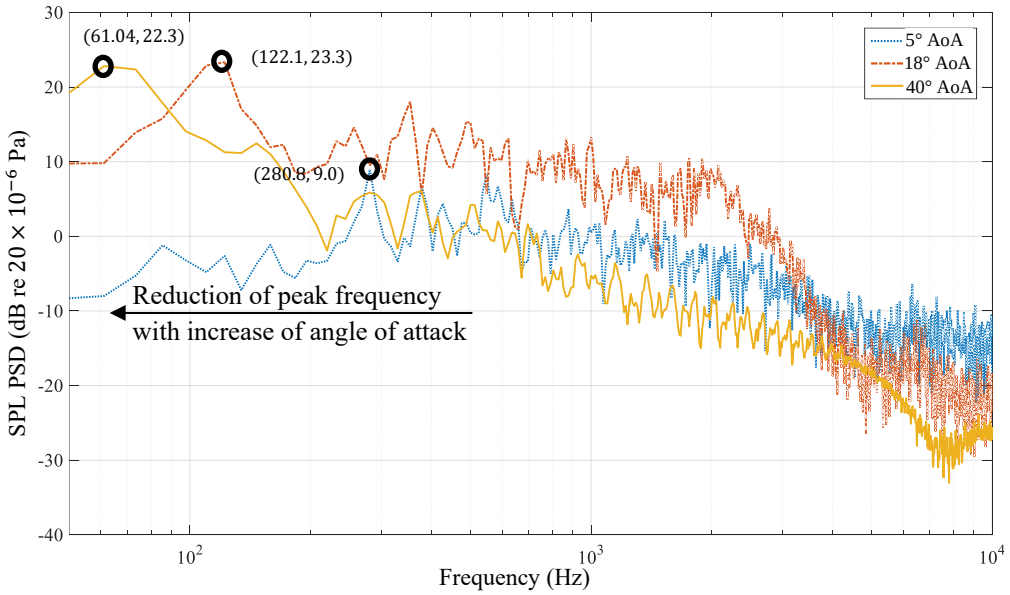

Figure 4.15 Comparison of narrowband spectra for 3 different angles of attack. As expected the frequency content of the noise decreases as the AoA increases and separation occurs on the blade surface.

Figure 4.16 shows contours of surface pressure level on the airfoil surface at peak frequencies for each case. The surface pressure here denotes the transient flow pressure on the surface of airfoil, characterized by the reference pressure of 20 μPa. As can be seen, the dominant noise source is located near the trailing edge for 5º AoA, consistent with Figure 4.10(a) which shows distinct vortices only near the trailing edge. In contrast, there is no distinct source location with higher acoustic pressure level at the onset of stall for 18˚ AoA. This confirms the interaction of the shear layer eddies along the entire length of the suction surface of the airfoil, as illustrated in Figure 4.10 (b). Interaction of large eddies formed in

the deep stall condition at 40˚ AoA with the airfoil surface, also results in noise emission from the surface of the airfoil. However, due to the presence of a strong vortex roll-up at the trailing edge, the amplitude of the pressure fluctuation is slightly higher at this location. These results confirm that the interaction of the large-scale stall vortices, with a size proportional with the entire suction surface of the foil, is the main mechanism responsible for noise generation from the foil.

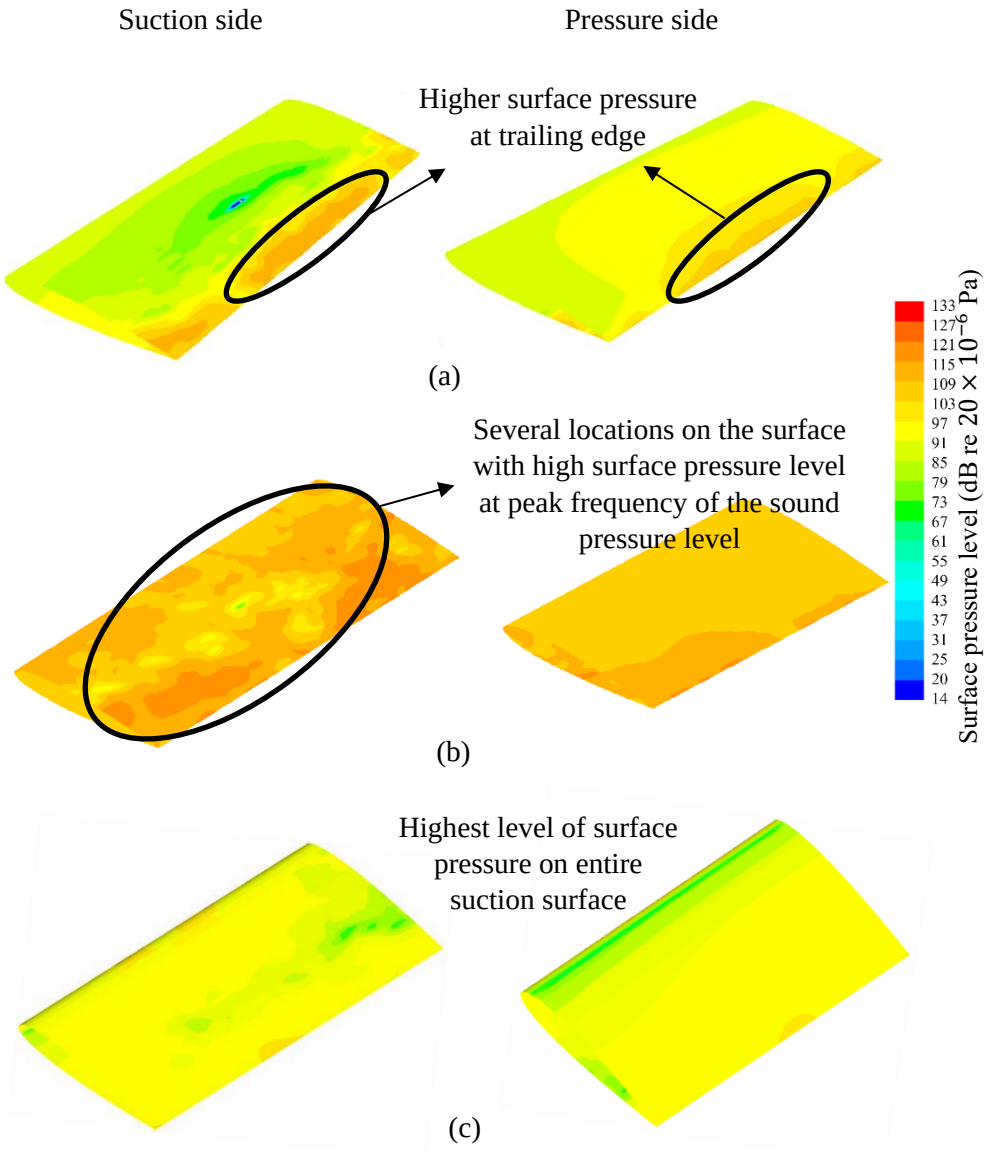

Figure 4.16 Surface pressure level contours at peak frequencies for 3 angles of attack; a) AoA=5° and *f*=280.03 (Hz), b) AoA=18° and *f*=122.1 (Hz), c) AoA=40° and *f*=61.04 (Hz).

The directivity of the noise was investigated by calculating the overall sound pressure level at receiver locations. It should be noted that, since the implemented FW-H analogy in this study does not take into account the quadrupole sources, it is expected to only exhibit the monopole and dipole like behaviours in the noise propagation results. The overall sound pressure level for all cases is dipolar, with directivity normal to the chord line. However, for 18˚ AoA the overall sound pressure level shows a stronger monopole component to the directivity.

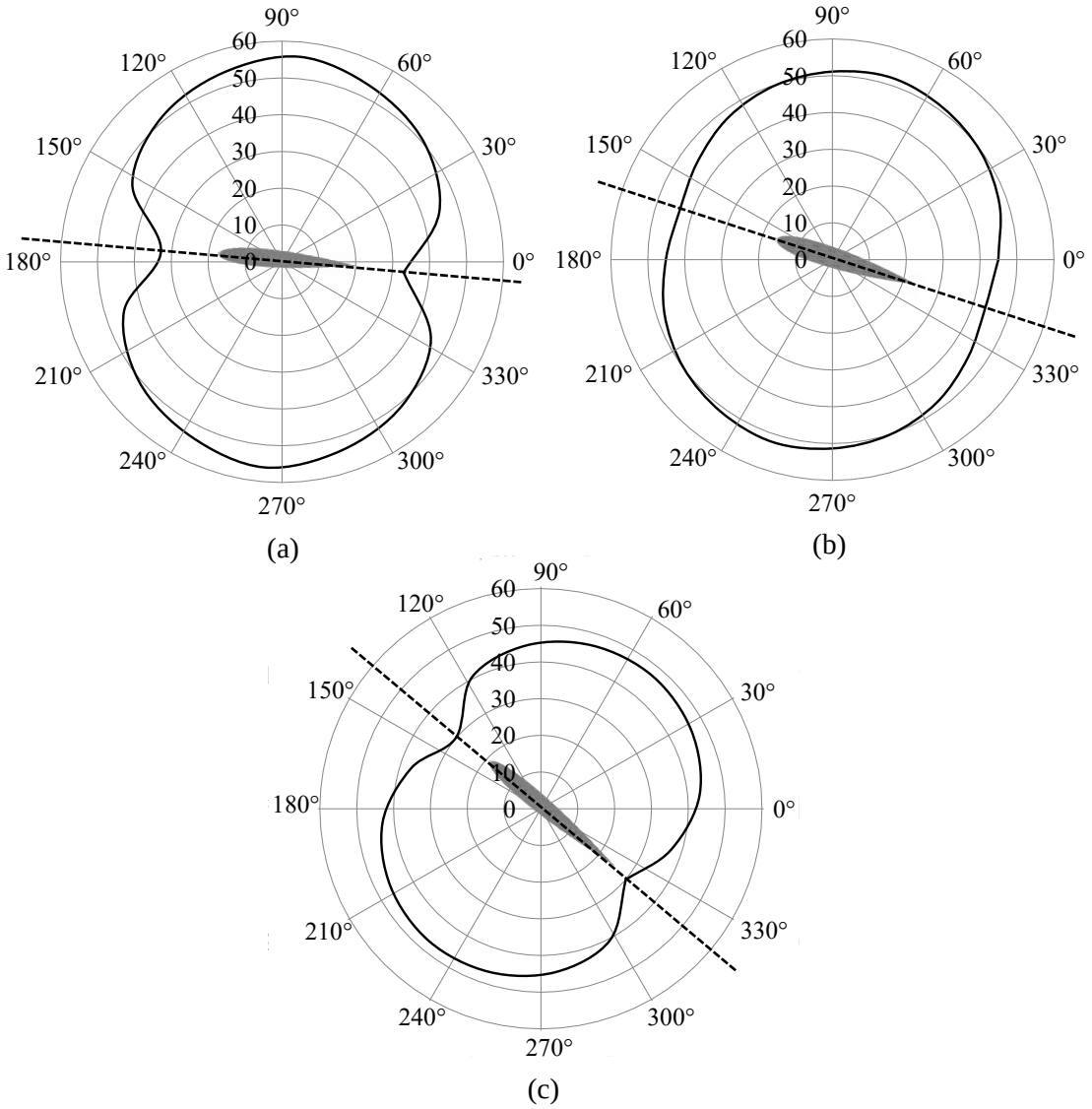

Figure 4.17 Directivity of the overall sound pressure level (dB re $\mathbf{20 \times 10^{-6}}$ Pa) at 70 chords around the airfoil at: a) AoA=5°, b) AoA=18°, c) AoA=40°.

The directivity of the noise at the peak frequencies is also shown in Figure 18. The directivity of the peak for 5˚ AoA shows dipole directivity with higher noise level toward the leading edge of the airfoil. This behaviour is in contrast with the directivity of the noise predicted by trailing edge noise theories. This could be caused by existence of the additional noise sources close to trailing edge of the blade. These sources can result in unorthodox radiation pattern, of the sound in specific frequencies, which has been observed previously in direct numerical simulation studies (Sandberg and Jones, 2010). Higher peak frequency for the noise signature at 5° in comparison with angles of attack at 18° and 40°, is hypothesised to be related to the interaction of smaller eddies with a small portion of the airfoil close to its trailing edge. The surface pressure fluctuations show that the highest level of fluctuations occurs at the part of the airfoil surface adjacent to its trailing edge. These fluctuations are higher on the suction side and could be the source of the unique radiation pattern of the sound at this angle of attack. Further investigation is required to determine the underlying mechanism for this behaviour. The dipole directivity of the stall noise can be clearly seen for the stall condition at 18º AoA. As can be seen, for the highest noise levels for the stall conditions, the noise is stronger perpendicular to the chord line. To better illustrate the directivity pattern of the peak frequency, the variation of the angle between the chord-normal and the peak-to-peak direction (β) versus angle of attack is shown in Figure 4.18 (d). The diagram shows that the angle β is the highest when the angle of attack is small, decreasing as the AoA increases up to 40°, at which point the chord-normal and peak-to-peak direction coincide. This shows that at deep-stall condition the whole airfoil surface is a noise source, and noise is radiated perpendicular to the airfoil chord-line.

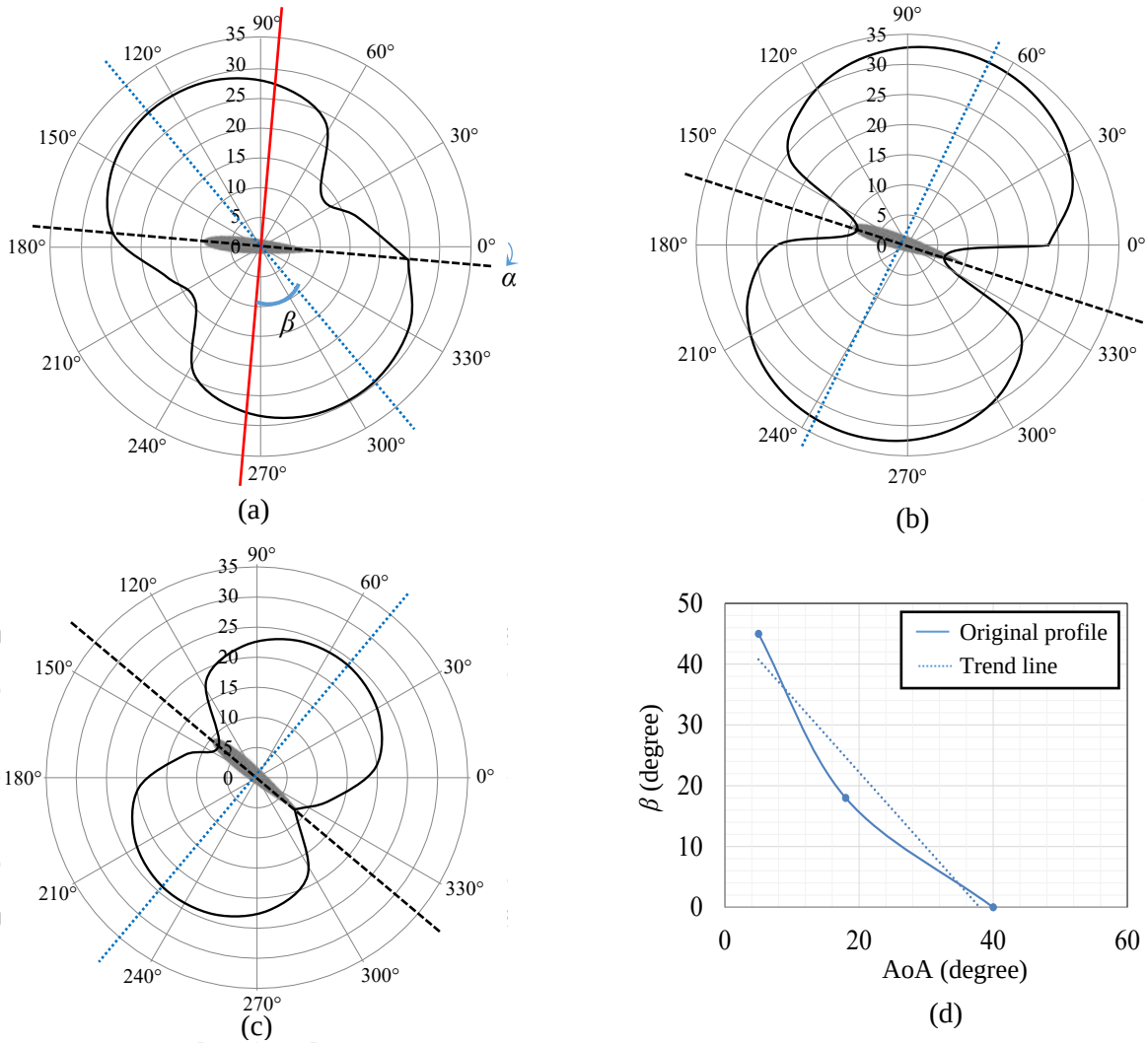

Figure 4.18 Directivity of the peak frequencies for the 3 angles of attack: (a) AoA=5°, Peak at *f*=280.8 (Hz), (b) AoA=18°, Peak at *f*=122.1 (Hz), (c) AoA=40°, Peak at *f*=61.0 (Hz), (d) variation of β (angle between chord normal and peak direction) versus angle of attack.

4.7.3 Experimental uncertainty

It is expected that the large blockage ratio at 40º angle of attack has an effect on the flow structures and consequently on the noise spectra in comparison to the low blockage ratio cases. For further validation and investigation of the effect of blockage ratio an experiment was conducted at the University of Adelaide with lower blockage ratio in comparison to the experiment conducted by Moreau et al. (2009). Experiment were conducted using a NACA 0012 airfoil with a chord of 50 mm and a span of 73 mm span which is half of the size of the airfoil used in Moreau et al.'s experiment (100 mm × 130 mm). This was done to achieve a

smaller blockage ratio (23% of the blockage ratio in the experiment conducted by Moreau et al. (2009)). Figure 4.19(a, b) shows the experimental setup and the location of the microphones Figure 4.19(c) shows the predicted and measured noise signature at the location of the microphone (microphone 2). Considering that the wind tunnel is anechoic at the frequencies above 200 Hz (Leclercq et al., 2007), a good agreement is seen between calculated and measured noise signatures, especially for the peak frequencies. Two peaks at low frequency are observed in Figure 4.19 (c), which correspond to the stall signature. Sound pressure level decreases at higher frequencies, which shows the dominancy of the stall noise due the large eddies interacting with the blade surface.

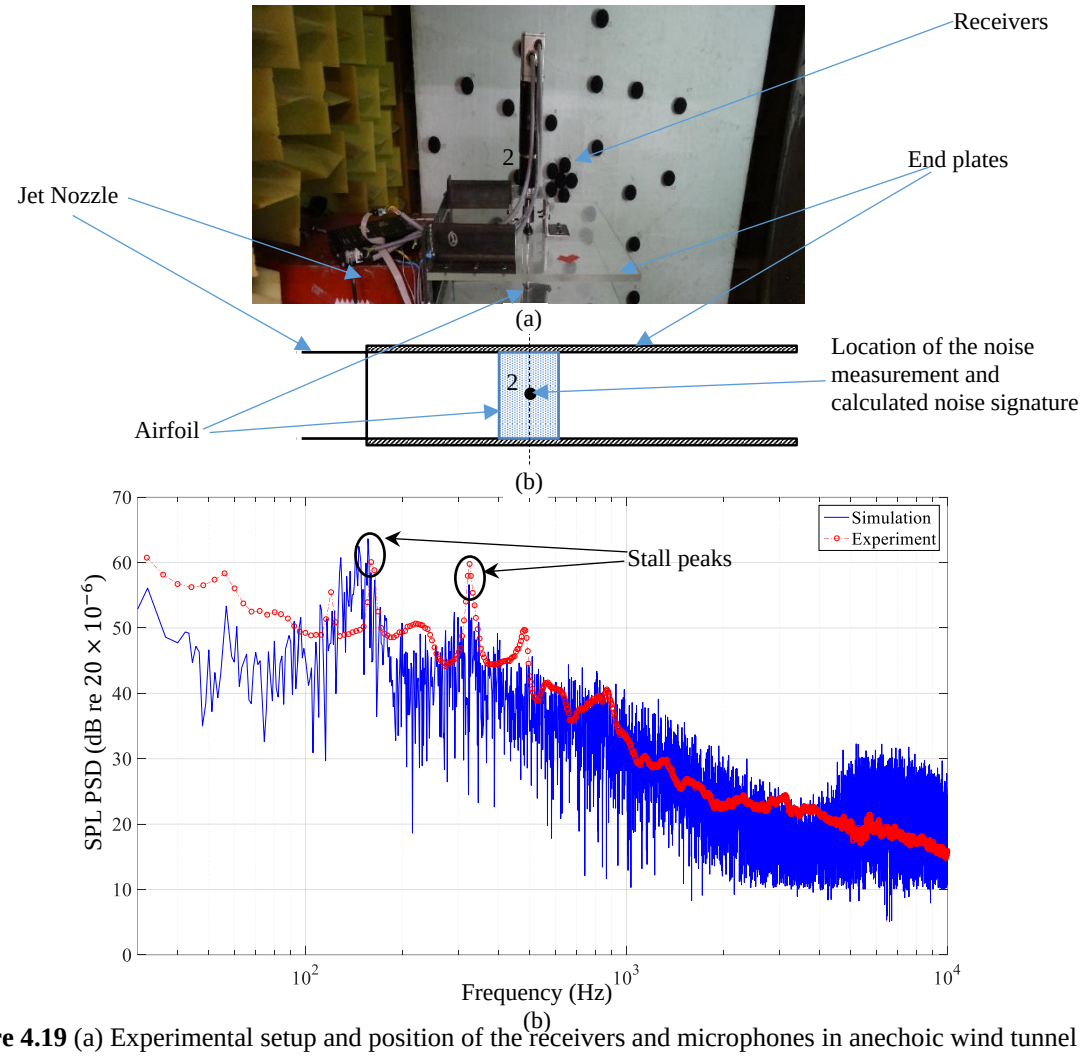

Figure 4.19 (a) Experimental setup and position of the receivers and microphones in anechoic wind tunnel at the University of Adelaide, (b) Schematic of the experiment, the noise signature is calculated at the location of the shown microphone (microphone 2), (c) Comparison of the predicted noise signature from CFD simulation (FW-H analogy). The trend along with the first and second peaks, are predicted with reasonable agreement with measured noise signature. Experimental data is obtained from the receiver 2 location.

Figure 4.20 shows the sound signature for both blockage ratios at 70 chords downstream of the airfoil. Frequencies of both peaks are doubled for the larger airfoil while the associated sound pressure level is decreased. Higher peak frequency for the larger case can be explained by the large blockage ratio in this case which affects the eddies separated from the airfoil. As seen in Figure 4.21, the integral length scale for the experiment conducted at the University of Adelaide is larger than the experiment performed at Ecole Central de Lyon (Moreau et al., 2009). As mentioned before, the frequency of the emitted noise is proportional to the size of the eddies interacting with surface. Larger relative length scale

for the smaller blockage ratio case results in lower peak frequencies in comparison to the larger blockage ratio.

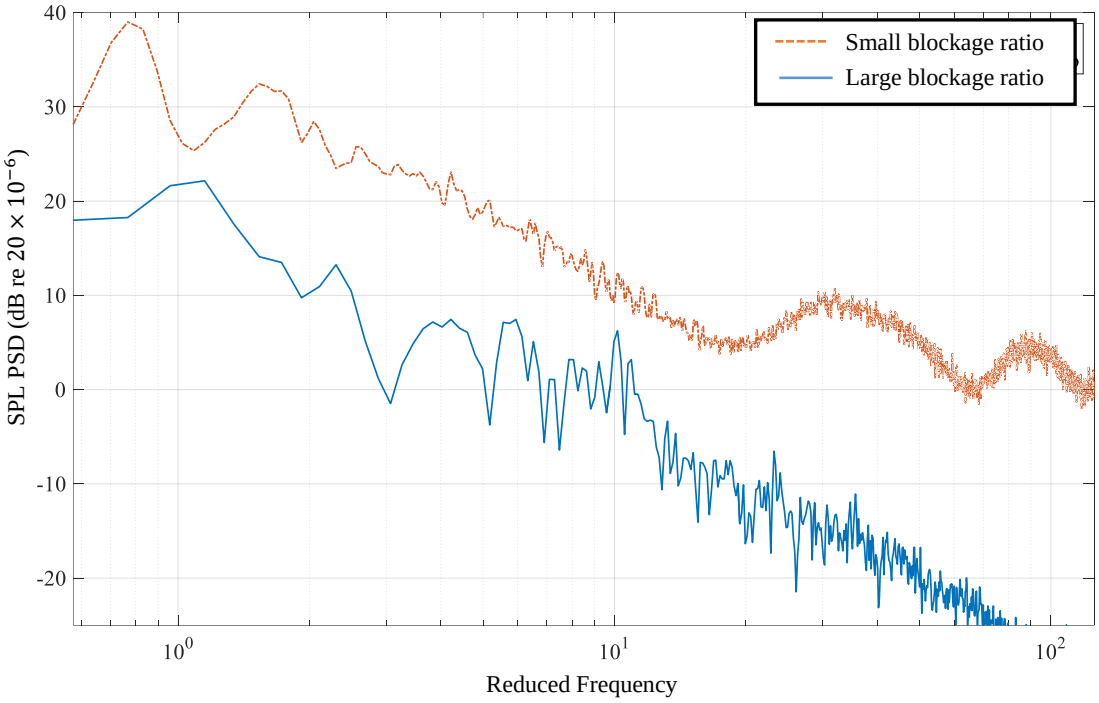

Figure 4.20 Sound signature 70 chords downstream of airfoils on the horizontal axis at each setup comparing the stall noise signature for two blockage ratios (50% vs 11%).

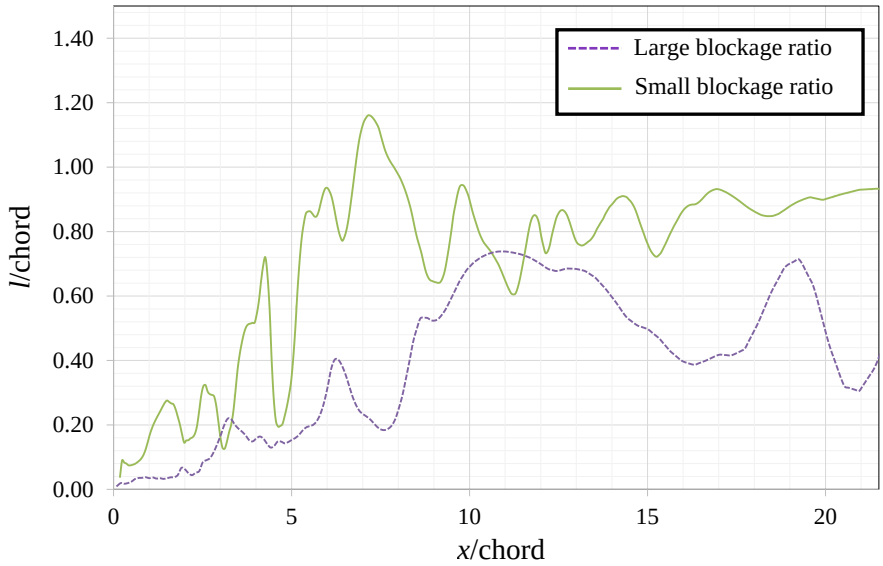

Figure 4.21 Integral length scale downstream of the airfoil for two setups and configurations, conducted at the University of Adelaide and Ecole Centrale de Lyon (Moreau et al., 2009). The blockage ratio in the setup of the experiment at the University of Adelaide is smaller and integral length scale is relatively larger than the setup at Ecole Centrale de Lyon.

Figure 4.22 shows the flow structure around the airfoil by the means of Q-criteria and streamline. Comparing these two cases show the effect of high blockage ratio (Figure 4.22 (b) and (d)) on the formation of the eddies. The size of the eddies for the setup with smaller blockage ratio is larger than the case with high blockage ratio when compared to the chord of the airfoil.

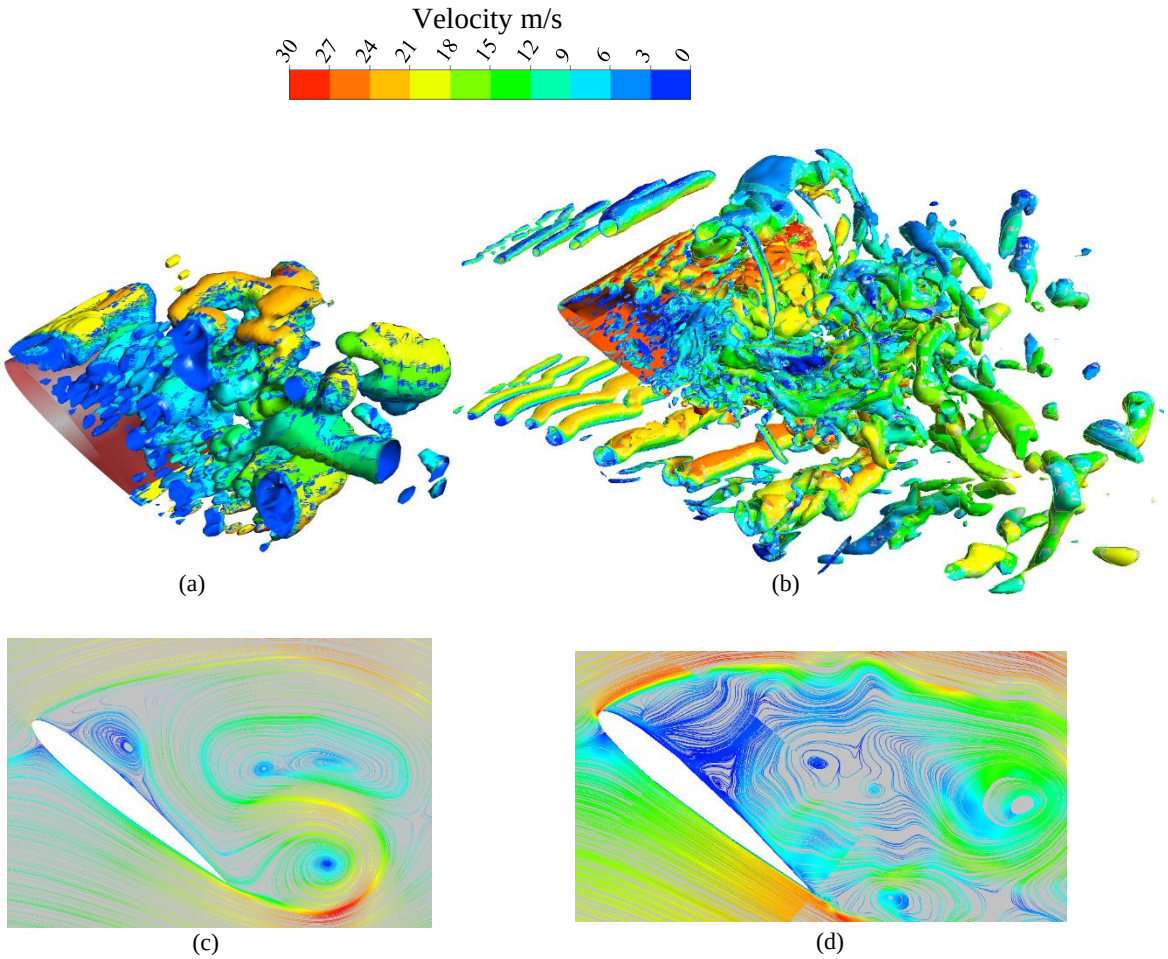

Figure 4.22 Flow structure around the airfoil showing different pattern for two different configurations; a) Q-criteria for the setup at the University of Adelaide, b) Q-criteria of the simulation for a configuration similar to the experiment conducted by Moreau et al. (2009), c) Streamline for the setup at the University of Adelaide, d) Streamline for the experiment conducted by Moreau et al. (2009).

4.8 Conclusion

The acoustic field generated by a NACA airfoil at 5º, 18º and 40º of angles-of attack and a Reynolds number of 1.3×10^5, corresponding to pre-stall, light or shallow stall and deep stall conditions respectively, was investigated using computational fluid dynamics. An

Embedded LES (ELES) method was used to calculate the flow field and a FW-H acoustic analogy for the acoustic pressure fluctuations in the domain. Results showed a good agreement between the computed and independently measured aerodynamic forces and vortex shedding frequency.

Results of the acoustic modelling showed higher level of surface pressure fluctuations at the trailing edge of the airfoil for the 5˚ angle of attack in comparison to other cases. On the other hand, the high-level regions of surface pressure are scattered on suction side of the airfoil at the light stall condition (18˚ AoA). Surface pressure level contours also revealed that the entire suction surface is acting as a sound source for the deep-stall condition. Aeroacoustic calculations showed dipole directivity for peak frequencies in all cases. These dipoles have peak directivity essentially perpendicular to chord line for both stall conditions, while they show higher noise level radiating towards the leading edge at the pre-stall condition. Trailing-edge noise, which is the dominant noise source from airfoils under pre-stall conditions, is dipolar and radiates perpendicular to chord line. However, this study shows that at some frequencies the airfoil noise radiates in other directions, which is in contrast with trailing-edge noise theory predictions. This contradiction has been also reported in previous literature using DNS simulations for low-Reynolds-Number flow over a NACA 0012 airfoil. This behaviour shows that at some frequencies there are other noise sources which cannot be explained by trailing-edge noise theory. The physical cause of this behaviour should be investigated further using experimental studies or direct aeroacoustic computations using accurate turbulence models.

Finally, it was shown that blockage ratio has a significant effect on the flow pattern and, consequently, noise generation. The size of the eddies separated from the airfoil decreases due to the blockage effect and consequently, the frequency of the peak signals reduces as the

blockage ratio decreases. These uncertainties are believed to be a reason of the discrepancies between different experimental and numerical investigations. In order to reduce the effect of blockage on the flow pattern and noise signals, it is suggested to keep the blockage ratio below 10%.

4.9 References

Brooks, T. F., Pope, D. S. & Marcolini, M. A. 1989. Airfoil self-noise and prediction. NASA Reference Publication 1218, Techincal information prepared for NASA.

Doolan, C. J., Moreau, D. J. & Brooks, L. A. 2012. Wind turbine noise mechanisms and some concepts for its control. *Acoustics Australia,* **40,** 7-13.

Germano, M., Piomelli, U., Moin, P. & Cabot, W. H. 1991. A dynamic subgrid-scale eddy viscosity model. *Physics of Fluids A* **3,** 1760-1765.

Gritskevich, M., Garbaruk, A., Schütze, J. & Menter, F. 2012. Development of DDES and IDDES formulations for the k-ω shear stress transport model. *Flow, Turbulence and Combustion,* **88,** 431-449.

Jianu, O., Rosen, M. A. & Naterer, G. 2012. Noise pollution prevention in wind turbines: Status and recent advances. *Sustainability,* **4,** 1104-1117.

Kamruzzaman, M., Lutz, T., Kraemer, E. & Wuerz, W. 2011. On the length scales of turbulence for aeroacoustic applications. 17th AIAA/CEAS aeroacoustics conference (32nd AIAA Aeroacoustics Conference). American Institute of Aeronautics and Astronautics.

Kim, D., Lee, G.-S. & Cheong, C. 2015. Inflow broadband noise from an isolated symmetric airfoil interacting with incident turbulence. *Journal of Fluids and Structures,* **55,** 428-450.

Kim, T., Jeon, M., Lee, S. & Shin, H. 2014. Numerical simulation of flatback airfoil aerodynamic noise. *Renewable Energy,* **65,** 192-201.

Laratro, A., Arjomandi, M., Cazzolato, B. & Kelso, R. 2016. A comparison of NACA 0012 and NACA 0021 self-noise at low Reynolds number. *In:* Zhou, Y., Lucey, A. D., Liu, Y. & Huang, L. (eds.) *Fluid-Structure-Sound Interactions and Control:*

Proceedings of the 3rd Symposium on Fluid-Structure-Sound Interactions and Control. Berlin, Heidelberg: Springer Berlin Heidelberg.

Laratro, A., Arjomandi, M., Kelso, R. & Cazzolato, B. 2014. A discussion of wind turbine interaction and stall contributions to wind farm noise. *Journal of Wind Engineering and Industrial Aerodynamics,* **127,** 1-10.

Leclercq, D., Doolan, C., Reichl, J. 2007, Development and validation of a small-scale anechoic wind tunnel, in 14th International Congress on Sound and Vibration 2007, ICSV 2007, pp. 556 – 563.

Leloudas, G., Zhu, W. J., Sørensen, J. N., Shen, W. Z. & Hjort, S. 2007. Prediction and reduction of noise from a 2.3 MW wind turbine. *The Science of Making Torque from Wind, IOP Publishing, Journal of Physics, Conference Series,* **75**.

Lilly, D. K. 1992. A proposed modification of the Germano subgrid-scale closure method. *Physics of Fluids A,* **4,** 633-635.

Madsen, H. A., Bertagnolio, F., Fischer, A. & Bak, C. 2014. Correlation of amplitude modulation to inflow characteristics. *Proceedings of 43rd International Congress on Noise Control Engineering.* The Australian Acoustical Society, Melbourne, 16-19 November.

Maliska, C., Paladino, E., Saltara, F., Contessi, B., Ataides, R. & Girardi Silva, V. 2012. A comparison of turbulence models for the computation of a detached flow around a square cylinder. *20th Annual Conference of the CFD Society of Canada*.

Menter, F. R. & Egorov, Y. 2010. The scale-adaptive simulation method for unsteady turbulent flow predictions. Part 1: Theory and model description. *Flow, Turbulence and Combustion,* **85,** 113-138.

Moorhouse, A., Hayes, M., Sabine von Hünerbein, Piper, B. & Adams, M. 2007. Research into aerodynamic modulation of wind turbine noise: Final report by University of Salford.

Moreau, S., Roger, M. & Christophe, J. 2009. Flow features and self-noise of airfoils near stall or in stall. *15th AIAA/CEAS Aeroacoustics Conference (30th AIAA Aeroacoustics Conference),* Miami, Florida.

Moriarty, P. & Migliore, P. 2003. Semi-empirical aeroacoustic noise prediction code for wind turbines, National Renewable Energy Laboratory.

Ni, X., Jian, H. & Fitch, A. 2003. Evaluation of turbulent integral length scale in an oscillatory baffled column using large eddy simulation and digital particle image velocimetry. *Chemical Engineering Research and Design*, **81**, 842-853.

Nobbs, B., Doolan, C. J. & Moreau, D. J. 2012, Characterisation of noise in homes affected by wind turbine noise. Acoustics 2012 - Fremantle, 21-23 November 2012 Fremantle, Australia.

Oerlemans, S. 2011. An explanation for enhanced amplitude modulation of wind turbine noise. National Aerospace Laboratory, Technical report prepared for Nationaal Lucht- en Ruimtevaartlaboratorium (NLR).

Oerlemans, S. & Schepers, J. G. 2009, Prediction of wind turbine noise and validation against experiment. *International Journal of Aeroacoustics*, **8**, 6, 555–584.

Pedersen, E. & Waye, K. P. 2004. Perception and annoyance due to wind turbine noise—A dose–response relationship. *Journal of the Acoustical Society of America,* **116,** 3460-3470.

Powell, A. 1959. On the aerodynamic noise of a rigid flat plate moving at zero incidence. *The Journal of the Acoustical Society of America*, **31**, 1649-1653.

Powell, A. 1990. Some aspects of aeroacoustics: From rayleigh until today. *Journal of Vibration and Acoustics*, **112**, 145-159.

Prasad, A. & Williamson, C. H. K. 1997. The instability of the shear layer separating from a bluff body. *Journal of Fluid Mechanics*, **333**, 375-402.

Rodríguez-Rodríguez, J., Marugán-Cruz, C., Aliseda, A. & Lasheras, J. C. 2011. Dynamics of large turbulent structures in a steady breaker. *Experimental Thermal and Fluid Science*, **35**, 301-310.

Sandbarg, R., Lloyd, J. & Neil, S. 2008. Direct numerical simulations of noise generated by turbulent flow over airfoils. *14th AIAA/CEAS Aeroacoustics Conference (29th AIAA Aeroacoustics Conference).* American Institute of Aeronautics and Astronautics.

Sandberg, R. D. 2015. Compressible-flow DNS with application to airfoil noise. *Flow, Turbulence and Combustion,* **95,** 211-229.

Sandberg, R. D. & Jones, L. E. 2010. Direct numerical simulations of airfoil self-noise. *Procedia Engineering*, **6**, 274-282.

Sedaghatizadeh, N., Arjomandi, M., Cazzolato, B., & Kelso, R. 2017. Wind farm noises: Mechanisms and evidence for their dependency on wind direction. *Renewable Energy*, **109**, 311-322.

Suzuki, Y., Miyazawa, M., Kato, C. & Fujita, H. 2007. Analysis of aerodynamic sound sources in a flow around a two-dimensional airfoil under stalled conditions. *INTERNOISE 2006*, Honolulu, Hawaii.

Tennekes, H. & Lumley, J. L. 1972. *A first course in turbulence*, Massachusetts, The MIT Press.

Wilcox, D. C. 1998. *Turbulence modeling for CFD*, DCW Industries.

Williams, J. E. F. & Hawkings, D. L. 1969. Sound generation by turbulence and surfaces in arbitrary motion. *Philosophical Transactions of the Royal Society of London A: Mathematical, Physical and Engineering Sciences*, **264**, 321-342.

Chapter 5 Wind turbine wake prediction

5.1 Chapter overview

In this chapter a well resolved CFD model for wind turbine wake study is presented and validated against experimental data. Large eddy simulation technique was utilised in order to obtain wake data such as velocity deficit, wake expansion and wake structure. Furthermore, three well-known engineering wake models were used to calculate the wake expansion and its development. This is followed by a discussion about the application and accuracy of the engineering wake models in predicting the wake development by comparing the results with the validated LES wake data. Through this comparison, it is illustrated that a combination of engineering models can be used to increase the accuracy of the predicted velocity deficit and wake expansion. It was alos found that engineering models cannot account for the effect of atmospheric boundary layer, and turbulent features of the incoming flow, hence, engineering wake models lack the temporal and spatial resolution in predicting the wake data required for the investigation of the interaction of wake with downstream turbines. This is a critical deficit in the application of semi-empirical low-fidelity wake models for investigation of fatigue loads on the blade and noise emission.

The detail of the CFD model, its validation, mesh characteristics, and engineering models are presented in the next section. The section is presented in the paper format submitted to the Journal of Renewable Energy.

Statement of Authorship

Title of Paper	A discussion on fidelity of wind turbine wake models and their application
Publication Status	☐ Published ☐ Accepted for Publication ☑ Submitted for Publication ☐ Unpublished and Unsubmitted work written in manuscript style
Publication Details	Sedaghatizadeh, N., Arjomandi, M., Kelso, R., Cazzolato, B., & Ghayesh, M. H., R. 2017. Wind farm noises: Modelling of wind turbine, wake using large eddy simulation. Renewable Energy, Accepted for publication.

Principal Author

Name of Principal Author (Candidate)	Nima Sedaghatizadeh		
Contribution to the Paper	- Research - Providing the data, writing of the manuscript and production of original figures - Correspondence with editor and reviewers including the production of all cover letters and rejoinder		
Overall percentage (%)	80%		
Certification:	This paper reports on original research I conducted during the period of my Higher Degree by Research candidature and is not subject to any obligations or contractual agreements with a third party that would constrain its inclusion in this thesis. I am the primary author of this paper.		
Signature		Date	14/09/2017

Co-Author Contributions

By signing the Statement of Authorship, each author certifies that:

i. the candidate's stated contribution to the publication is accurate (as detailed above);

ii. permission is granted for the candidate in include the publication in the thesis; and

iii. the sum of all co-author contributions is equal to 100% less the candidate's stated contribution.

Name of Co-Author	Maziar Arjomandi		
Contribution to the Paper	- Supervision of the work, including the production of the manuscript - Participation in the development of the concepts and ideas presented in the manuscript - Evaluation and editing of the manuscript prior to submission		
Signature		Date	15/09/2017

Name of Co-Author	Richard Kelso		
Contribution to the Paper	- Supervision of the work, including the production of the manuscript - Participation in the development of the concepts and ideas presented in the manuscript - Evaluation and editing of the manuscript prior to submission		
Signature		Date	14/9/2017

Name of Co-Author	Benjamin Cazzolato		
Contribution to the Paper	- Supervision of the work, including the production of the manuscript - Participation in the development of the concepts and ideas presented in the manuscript - Evaluation and editing of the manuscript prior to submission		
Signature		Date	14/09/2017

Name of Co-Author	Mergen H. Ghayesh		
Contribution to the Paper	- Supervision of the work, including the production of the manuscript - Participation in the development of the concepts and ideas presented in the manuscript - Evaluation and editing of the manuscript prior to submission		
Signature		Date	14/09/2017

Modelling of wind turbine wake using large eddy simulation

Nima Sedaghatizadeh, Maziar Arjomandi, Richard Kelso, Benjamin Cazzolato, Mergen H. Ghayesh

School of Mechanical Engineering, the University of Adelaide, Adelaide, SA, 5005

Paper accepted for publication: Sedaghatizadeh, N., Arjomandi, M., Kelso, R., Cazzolato, B., & Ghayesh, M. H., R. 2017. Wind farm noises: Modelling of wind turbine wake using large eddy simulation. Renewable Energy, Accepted for publication.

5.2 Abstract

In an array of wind turbines, the interaction of the downstream machines with the wakes from the upstream ones results in a reduction in the overall wind farm performance. Turbine wakes are a major source of turbulence which exerts fluctuating loads on the blades of the downstream turbines, resulting in the generation of noise and fatigue of the turbine blades. There are many *semi-empirical* wind turbine wake models in the literature. This paper, develops a fully *numerical* model of wind turbine wakes using CFD by means of a Large Eddy Simulation (LES). The new LES model is tested against experimental data, showing very good agreement. The advantages of the LES model compared to the available semi-empirical models in the literature are discussed and it is shown that the LES model is very accurate compared to the conventional semi-empirical wake models usually used in industry. Moreover, the LES model is used as a benchmark to compare the accuracy of these semi-empirical models; it is shown that the model proposed by Jensen can predict the velocity deficit most accurately among the semi-empirical models, while the highest degree of accuracy in the wake expansion is achieved by using the Larsen model.

Nomenclature

D_w	Wake diameter	A_w	Wake area
D	Rotor diameter	ΔU	Total velocity deficit in the wake based on second-order Larsen model
k	Jensen's Constant	ΔU_1	Larsen model's first-order velocity deficit in the wake
x	Downstream distance	ΔU_2	Second-order Larsen's model's velocity deficit
s	Downstream ratio (x/D)	$z(x,r)$, d_0, d_1, d_2, d_3, d_4	Larsen's second-order contributions
u	Velocity in the wake	D_{eff}	Effective rotor diameter
U_∞	Free-stream velocity	$R_{9.5}$	Wake radius at 9.5D downstream of the wind turbine
C_T	Thrust coefficient	R_{nb}	Larsen's Empricial Constant
R_w	Wake radius	H	Hub height
r	Radial distance from centre	I_a	Ambient turbulence intensity
c_1	Larsen's non-dimensional mixing length	β	Frandsen's model's constant
x_0	Larsen's first-order approximation Parameter	α	Frandsen's model's experimental constant
A	Rotor area	$\bar{x}$	Normalised chord-wise distance

5.3 Introduction

Wind turbines are often installed in dense clusters, mainly due to the limited number of quality sites, as well as the need to reduce the cost of transmission lines and maintenance. Grouping the wind turbines places the majority of them in the wake of upstream ones.

Working in the wake region of upstream turbines causes the following issues: (i) reduction in the turbine service life due to increased turbulence intensity in the incoming flow (Crespo *et al*., 1999); (ii) increased noise emission due to blade-vortex interaction (Larattro *et al*., 2014); (iii) reduction in the energy harvested due to the loss of available kinetic energy in the flow (Mo *et al*., 2013, Krogstad and Eriksen, 2013). Wake effects also pose a significant challenge for advanced wind plant-level control systems. In most cases, the upwind rows of turbines in a farm are forced to operate at a decreased efficiency to reduce the wake effects imposed upon downstream turbines (Churchfield *et al*., 2015, Aho *et al*., 2012).

Wind turbine wakes have been extensively investigated both experimentally and theoretically (Luo *et al*., 2015, Jimenez *et al.*, 2007, Sanderse *et al.*, 2011). The wake of a wind turbine can be categorized into two regions based on the distance over which the blade shape is influential; namely, near-wake and far-wake regions. The near-wake is the region immediately downstream of the turbine in which the effect of the rotating blades is dominant. This region is also characterised by the formation of helical tip vortices and a high velocity deficit. It was reported that the estimated length of the near-wake region is $0 \leq x/D \leq 5$, where D is the rotor diameter and x is the downstream distance (Schepers, 2003, Jimenez *et al*., 2008). On the other hand, the far wake starts where the actual rotor shape is less important, but the flow has less energy and carries an increased level of turbulence (Sanderse, 2012). Figure 1 schematically shows the typical wake expansion and velocity profiles downstream of a wind turbine. It can be seen that due to the velocity difference between the wake and the free stream, a shear layer including tip vortices is created between the free flow and wake region (Crespo *et al*., 1999, Blomhoff, 2012). Further downstream, the induced turbulent eddies inside the shear layer mix with the free stream and with the low-velocity region in the wake causing the shear layer to expand. The near-wake ends where

the shear layer spreads inwards and reaches the wake axis. At this point the tip vortices breakdown and the static pressure reaches the atmospheric pressure (Mo *et al*., 2013, Crespo *et al*. 1999).

The shape, structure and the breakdown distance of the wake are highly influenced by factors such as atmospheric turbulence, topographical features, and velocity gradients in the atmospheric boundary layer (ABL) (Liu et al., 1983, Sanderse, 2012). A laminar ABL with a low turbulence level results in longer far-wake regions, as well as a larger velocity deficit, compared to a highly turbulent boundary layer. The longer wake leads to a lower available energy for the downstream wind turbines. On the other hand, a higher turbulence intensity results in a faster wake recovery, although this may result in a higher rate of turbine blade fatigue due to the resulting fluctuating forces (Elliott, 1991).

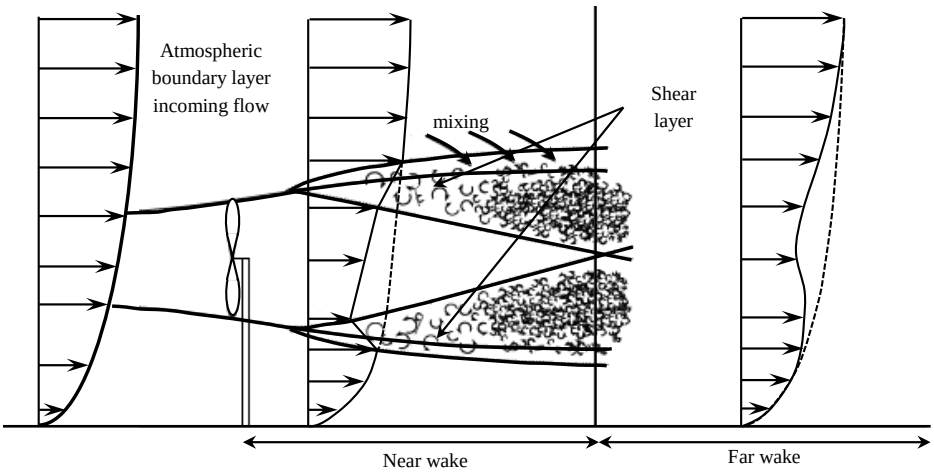

Figure 5.1 Schematic representation of wind turbine wake when turbine is placed in an atmospheric boundary layer.

Several *semi-empirical* models have been developed to study the wake regions behind horizontal-axis wind turbines. These wake models can be divided into two classes, namely *near-wake* models and *far-wake* models, according to their ability to predict the aerodynamic performance of the blades themselves and also in predicting the flow field in the far wake region. These semi-empirical models are explained in detail in the following sections.

5.3.1 Semi-empirical near-wake models

Semi-empirical *near-wake* models mainly calculate the flow-induced forces acting on the rotor in order to predict the power generated by the wind turbine. These models should be able to account for the shape of the blades due to its significant effect on the aerodynamic performance of the blades and the wake close to the rotor area. The *blade element method* (*BEM*) which is the simplest model in this category, calculates the blade loads by dividing the blade into several elements and using tabulated data of the airfoil sections (Troldborg *et al*., 2007, Sørensen *et al*., 2016). The *actuator disk* (*AD*) model is an extended version of the BEM which assumes the blades form a uniform disk at the rotor plane. Using the same approach as the BEM, the effects of the blades are applied through a uniform thrust over the rotor area, represented as a disk. The actuator disk is then coupled with CFD to calculate the flow field in the wake (Sørensen *et al*., 1998). Another wake model, considered as a near-wake model, due to its ability in calculating the aerodynamic behaviour of the blades and rotor, is the *vortex wake* model; the blades of the turbine are replaced by concentrated vortices which produce the equivalent amount of lift and dynamic forces using vorticity transport Biot-Savart equations (Green's function). This model can be extended to calculate the flow produced by the shedding vortices and their effect on the blades (Dixon, 2008). It can be concluded that the engineering (*semi-empirical*) near-wake models are primarily developed to provide an *estimate* of the forces acting on the rotor of a wind turbine, and are *unable to reveal flow features*. They also do not take the effect of different conditions such as yaw misalignment, wake of other turbines, ABL and incoming turbulence into consideration. This necessitates the development of a *precise full CFD model* which is capable of predicting the aerodynamic performance of the blades and flow features accurately; as done in this paper for the first time.

5.3.2 Semi empirical far-wake models

The far-wake begins after the transition region, which starts by the breakdown of the near-wake. At these distances, the aerodynamic properties of the rotor are less discernible compared to those of the near-wake region. Thus, the important factors which far-wake models should be able to predict are velocity deficit, turbulence intensity, and the expansion of the wake. The semi-empirical far-wake models can be divided into *kinematic wake* models (also called *explicit* models), *field* models (also called *implicit* models or *boundary layer* models), and *combined* models (Kloosterman, 2009).

Kinematic models, also known as explicit models, are relatively simple wake models that can be solved analytically; this makes them suitable to evaluate the wind speed deficits in large wind farms. These models use the momentum equation to model the velocity deficit of the wake behind a turbine. The wake descriptions do not consider the initial expansion region of the wake. Four well-known kinematic models are those by Jensen, Larsen (first order and second order), and Frandsen (Sanders, 2012, Frandsen *et al*., 2006, Larsen, 1988). Due to their application in industry, the results based on four *semi-empirical* far-wake kinematic models proposed by *Jensen*, *Larsen*, and *Frandsen* are compared to the CFD model developed in this study to compare their ability in predicting the wake development. Each of these models assumes an initial velocity profile in the near-wake region and calculates the velocity deficit and wake expansion using simplified momentum equations based on these velocity profiles. The original forms of these models are not capable of covering the change in the turbulence intensity in the wake and they need to be coupled with a turbulence model in order to calculate the contained turbulence intensity in the wake. Among the aforementioned models the Larsen model can account for the effect of the ambient

turbulence on the wake expansion. Table 1 represents the governing equations required for each of these kinematic far-wake models.

Table 5.1 Governing equations for velocity distribution and wake diameter

Wake model	Wake diameter and velocity distribution in the wake
Jensen model	$D_w = D(1+2ks)$ $u = U_\infty\left[1-\frac{1-\sqrt{1-C_T}}{(1+2ks)}\right]$
Larsen model (first order)	$R_w(x) = (\frac{35}{2\pi})^{1/5}(3c_1^2)^{1/5}(C_T A(x+x_0))^{1/3}$ $\Delta U_1(x,r) = -\frac{U_\infty}{9}(C_T A(x+x_0)^{-2})^{1/3}\left[r^{3/2}(3c_1^2 C_T A(x+x_0)^{-\frac{1}{2}} - \left(\frac{35}{2\pi}\right)^{3/10}(3c_1^2)^{-\frac{1}{5}}\right]^2$ $c_1 = \left[\frac{D_{\text{eff}}}{2}\right]^{\frac{5}{2}}\left(\frac{105}{2\pi}\right)^{-\frac{1}{2}}(C_T A x_0)^{-\frac{5}{6}}$, $x_0 = \frac{9.5D}{\left(\frac{2R_{9.5}}{D_{\text{eff}}}\right)-1}$, $D_{\text{eff}} = D\sqrt{\frac{1+\sqrt{1-C_T}}{2\sqrt{1-C_T}}}$ $R_{9.5} = 0.5[R_{\text{nb}} + \min(H, R_{\text{nb}})]$, $R_{\text{nb}} = \max\left(1.08D, 1.08D + 21.7D(I_a - 0.05)\right)$
Larsen Model (second order)	$\Delta U = \Delta U_1 + \Delta U_2$ (ΔU, ΔU_1, and ΔU_2 are total velocity deficit, first order velocity deficit, and second order velocity deficit respectively) $\Delta U_2 = U_\infty(C_T \times A \times (x+x_0)^{-2})^{2/3} \times \sum_{i=0}^{4}\left(d_i \times z(x,r)^i\right)$ $z(x,r) = r^{3/2}(C_T \times A \times (x+x_0))^{-1/2} \times \left(\frac{35}{2\pi}\right)^{-3/10} \times (3\times c_1^2)^{-3/10}$ $d_0 = \frac{4}{81}\varsigma_0\left(-1-3\left(4-12\left(6+27\left(-4+\frac{48}{40}\right)\frac{1}{19}\right)\frac{1}{4}\right)\frac{1}{5}\right)$ $d_1 = \frac{4}{81}\varsigma_0\left(4-12\left(6+27\left(-4+\frac{48}{40}\right)\frac{1}{19}\right)\frac{1}{4}\right)\frac{1}{5}$, $d_2 = \frac{4}{81}\varsigma_0\left(6+27\left(-4+\frac{48}{40}\right)\frac{1}{19}\right)\frac{1}{4}$ $d_3 = \frac{4}{81}\varsigma_0\left(-4+\frac{48}{40}\right)\frac{1}{19}$, $d_4 = \frac{4}{81}\varsigma_0\frac{1}{40}$, $\varsigma_0 = (\frac{35}{2\pi})^{1/5} \times (3\times c_1^2)^{-2/15}$
Frandsen	$\beta = \frac{1+\sqrt{1-C_T}}{2\sqrt{1-C_T}} = \left(\frac{D_{\text{eff}}}{D}\right)^2$, $D_w(x) = D(\beta^{k/2} + \alpha s)^{1/k}$ or $D_w(x) = D\max[\beta, \alpha s]^{1/2}$ $u = \frac{U_\infty}{2}\left(1 \pm \sqrt{1-2\frac{A}{A_w}C_T}\right)$

5.3.3 Contributions of the current study to the field

All of the semi-empirical wake models discussed in Section 1.3 are based on experimental data and cannot be used for general cases. The effect of an ABL and incoming turbulence are not considered in these models. These models are also incapable of calculating the turbulence intensity in the wake region and they need to be coupled with a turbulence model in order to calculate the resultant turbulence intensity. This paper, for the first time, develops a *full LES* model of wind turbine wakes, which produces accurate and detailed information about the *flow field* as well as the *wake development* downstream of the turbine *without requiring* any initial experimental data; the numerical results obtained using the model are validated by experiments from the literature. Moreover, the developed CFD model is used as a benchmark in order to compare the semi-empirical engineering models (explained in Section 1.3) and examine their accuracy in predicting the wake development and velocity field in the wake.

5.4 LES model developed for this study and its validation

In this section, a large eddy simulation (LES) model is developed and validated with experimental data available in the literature. The LES has been performed for the NREL Phase VI turbine and the wind tunnel with the same specifications as given by Hand *et al*., (2001); see Figure 5.2. The domain consists of two zones: 1) cylindrical zone around the blades; 2) rest of the domain. A sliding-mesh technique is applied to the cylindrical zone which allows the relative movement of the zones on the interface.

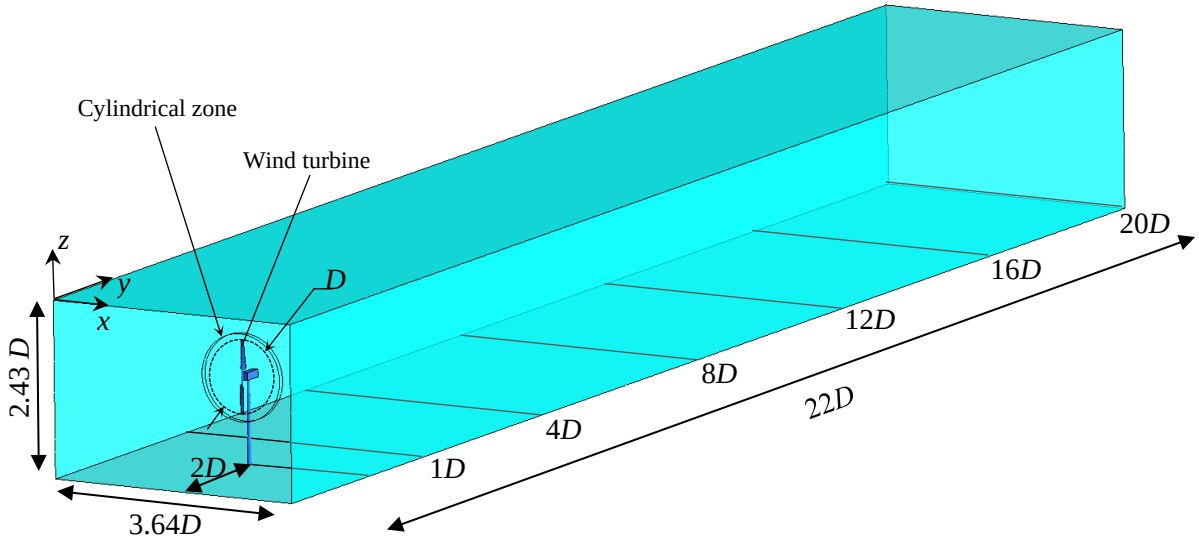

Figure 5.2 Dimensions of the computational domain used for numerical simulation of wind tunnel.

Figure 5.3 depicts the shape of the turbine blade, its twist and chord variation along the span as well as the experimental and computational wind tunnel model adopted from Hand et al. (2001). NREL phase VI is a stall-regulated wind turbine with a rated output power of 19.8 kW. The rotor diameter is D=10.058 m and the blade consists of S809 airfoil from root to tip. The nacelle and hub parts in computational domain are simplified in the current study to avoid the difficulties associated with the generation of high quality grid.

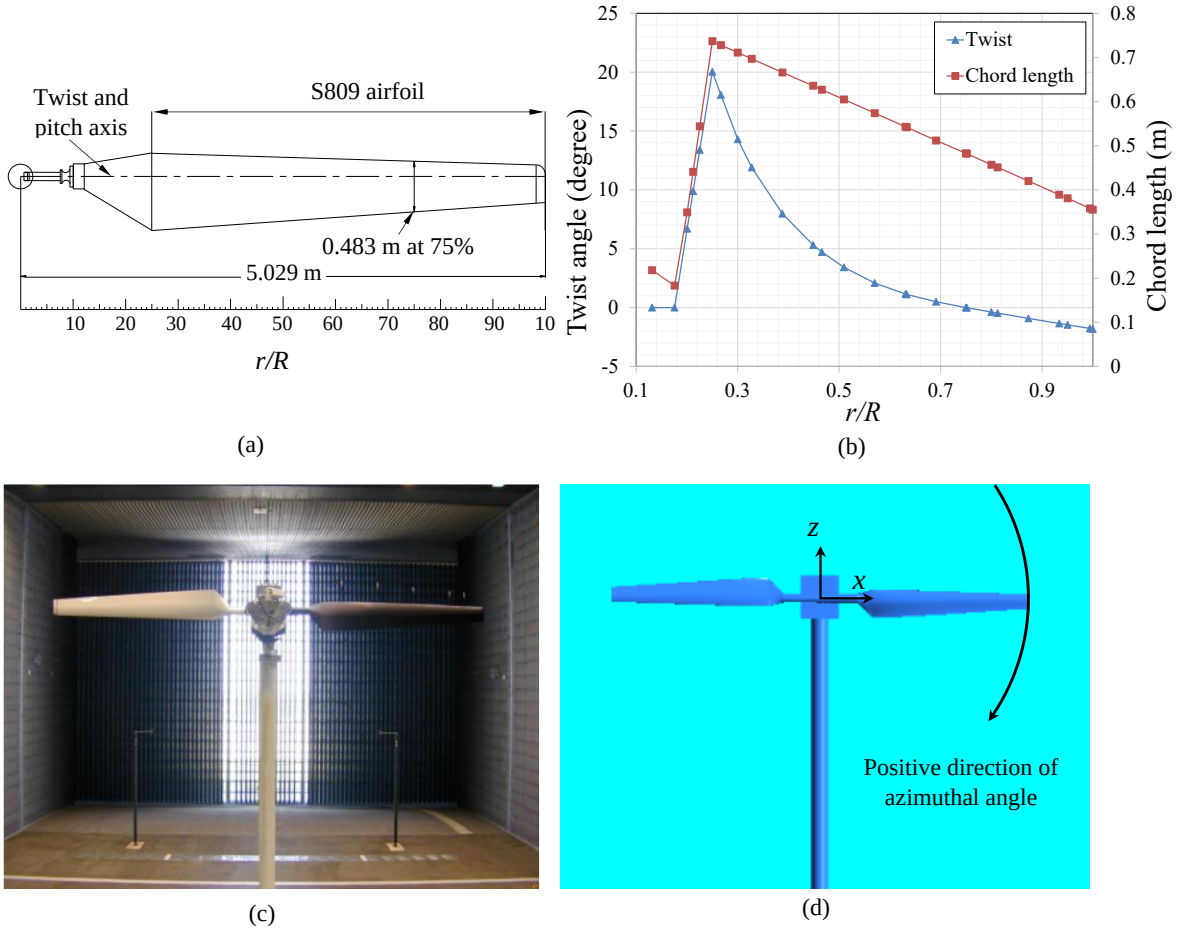

Figure 5.3 (a) Blade geometry and shape, (b) twist and chord variations along the blade, (c) experimental model (adopted from Hand et al., (2001)), (d) computational model used in the current study.

ICEM CFD was used to create a hexahedral mesh with twenty-one inflation layers on the blade in the cylindrical zone. The distance of the first node from the wall is small enough to ensure $y^+ = 1$ for the whole blade surface (Figure 5.4). Using Jensen estimation for wake expansion (1983), the wake region in computational domain was specified. The maximum element size inside this region is 0.15 m which is relatively finer in comparison with the rest of the domain. This grid configuration is finer compared to the previously published articles (Mo and Lee, 2012); hence it is expected that the current grid results in more accurate results. The total number of elements inside the computational domain is about 11 million, as shown in Figure 4. Due to the high computational cost of the simulation, the sensitivity analysis have been carried out for output power and pressure coefficients over 4 revolutions for two grid sizes. Results revealed only a difference of 1.5% between the calculated parameters

when the number of elements was increased from 11 million to 16 million. However, the computation time was increased by about 60%. Thus, the coarser mesh was chosen for the computation to reduce the computational time without a significant reduction in the accuracy of data. Moreover, since the flow structure in the near-wake zone is determined by the blades, sudden changes in flow patterns are not expected due if the pressure distribution on the blade is predicted accurately (Burton et al., 2001).

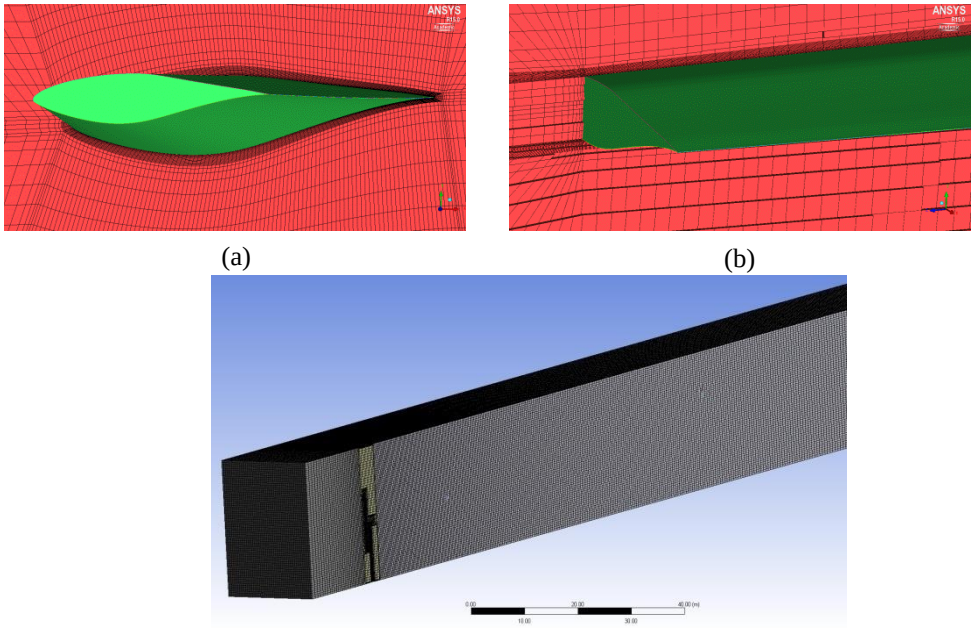

Figure 5.4 Generated mesh in computational domain, a and b) Sectional view of the mesh and the inflation layer around the blades, c) generated mesh in the wind tunnel.

ANSYS FLUENT, which is a general-purpose CFD code, was used to implement the calculations. FLUENT applies a finite-volume technique to discretise the partial differential equations. Computations were carried out using a uniform inlet velocity of 7 m/s for the wind speed and a rotational speed of 71.9 (rpm) for the blades. A pressure outlet with the ambient flow condition was selected for the outlet where the flow leaves the domain. Non-slip boundary condition was chosen for all solid surfaces such as: blades, tower, nacelle, ground and walls in the wind tunnel case. The time-step was selected as 0.0023 (sec), which corresponds to one degree of blade rotation. A small enough time step was chosen to

guarantee a Courant-Friedrich-Levy number in order of 1. Since the vortex shedding of a wind turbine is similar to vortex shedding of a disk in a uniform flow (Medici and Alfredsson, 2006). This vortex shedding is associated with the vortical structures in far-field ($x > 4D$) that have a significant effect on the wake development. The Strouhal number for these scales of instabilities are found to be around 0.3 which corresponds to very low frequencies (order of 1) (Chamorro et al., 2013). The chosen time-step in current study corresponds to a sample frequency of around 400 (Hz) that can capture most of the vortical structures with a significant effect on wake development. The smallest turbulent length scale and associated time scale can be calculated using Kolmogorov's theory as $\frac{L}{\eta} = Re^{3/4}$ and $\frac{t_L}{t_\eta} = Re^{1/2}$, respectively (Pope, 2000). Here, L represents the largest length scale (which can be estimated here equal to the rotor diameter) and η is the smallest length scale in the domain. Using these estimations the smallest length scale and associated time scale are approximately equal to $t_\eta \approx 7 \times 10^{-4}$ m and $t_\eta \approx 7 \times 10^{-4}$ s. Using current grid and time step, the majority of the length scales which have a significant effect on wake development can be resolved while the effect of smaller eddies are modelled. The LES calculations were carried out for a sufficiently long period of time (approximately 30 revolutions) to ensure the wake is fully developed and results are statistically stable. The SIMPLE algorithm was used in the present work for pressure-velocity coupling. The computational domain used in the wind tunnel case was modified to eliminate the effect of walls on wake development. Figure 5-5 shows the extended domain used to study the wake development in the uniform flow condition. As the turbine is exposed to a uniform flow, the boundary condition used for the extended domain is set as the inlet velocity condition.

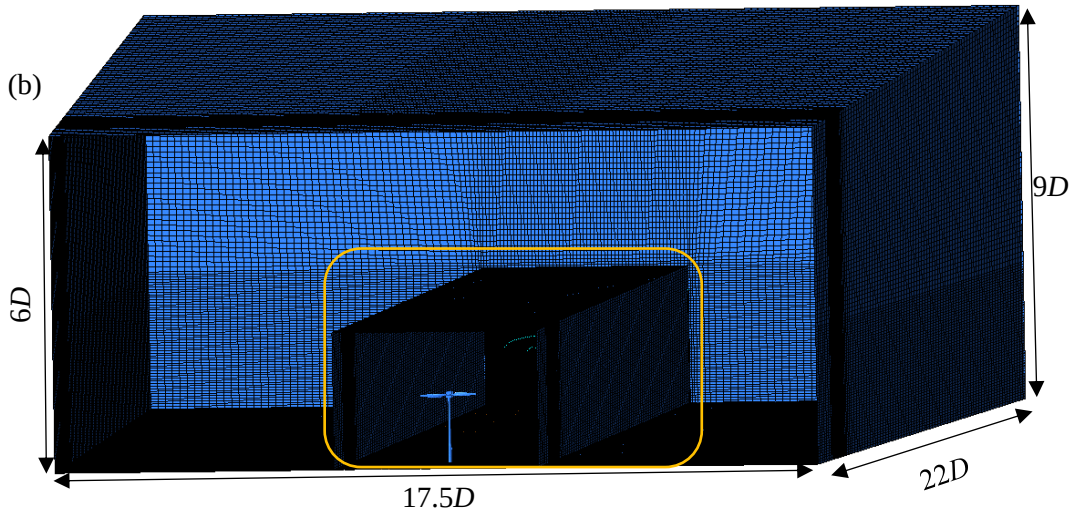

Figure 5.5 Computational grid used for numerical study of unconfined environment.

Large eddy simulation is a turbulent model which resolves turbulent eddies with the scale larger than the grid size directly and models the small scale eddies. This is the main advantage of the LES, since large scale eddies carry a large amount of the kinetic energy of the flow and hence, have a major effect on the flow behaviour. The large and small scales of the turbulence are filtered based on the grid size and the effect of smaller scales on flow behaviour is taken into account by utilization of a sub-grid scale model. This approach significantly reduces the computational cost when compared to a DNS method while still provides high resolution. Several sub-grid models have been proposed such as: Smagorinsky, WALE (Wall-Adapting Local Eddy viscosity), wall modelled large eddy simulation approach, dynamic Smagorinsky-Lilly and Dynamic Kinetic Energy Transport. More information about the LES approach, its fundamentals, and sub-grid models can be found in literatures (Berselli et al., 2005, Wilcox, 1998, Pope, 2000, Sagaut, 2006).The governing equations for large eddy simulations are filtered conservation and Navier-Stokes equations as follows:

$$\frac{\partial \rho}{\partial t} + \frac{\partial}{\partial x_i}\left(\rho \overline{u_i}\right) = 0 \quad , \tag{5.1}$$

$$\frac{\partial(\rho\overline{u_i})}{\partial t}+\frac{\partial(\rho\overline{u_j}\,\overline{u_i})}{\partial x_j}=\frac{\partial\sigma_{ij}}{\partial x_j}-\frac{\partial\overline{p}}{\partial x_i}-\frac{\partial\tau_{ij}}{\partial x_j}\,, \tag{5.2}$$

where $\bar{u}$, σ, and τ_{ij} are the resolved velocity, the stress tensor due to molecular viscosity and the subgrid scale stress defined as $\tau_{ij}=\rho\overline{u_iu_j}-\rho\overline{u_i}\,\overline{u_j}$, respectively. The subgrid scale stress can be decomposed as $\tau_{ij}=L_{ij}+C_{ij}+R_{ij}$ is the Leonard tensor which represents the effect of large eddies on each other. Interaction between the subgrid scales are manifested through the Reynolds subgrid tensor (R_{ij}) and cross-stress tensor (C_{ij}) represents the interaction between large and small scale eddies (Pope, 2000, Sagaut, 2006). The subgrid stress tensor is unknown and is modelled using subgrid scale models. In the current study, the dynamic Smagorinsky-Lilly model proposed by Lilly (1992) is used as the subgrid scale model in order to accurately capture the large scale fluctuations in the mean shear and transitional regimes.

An important parameter which can be used to show the interaction of the blade with flow and has been used in literatures for validation of the numerical studies, is the pressure coefficient which is given as:

$$C_p=\frac{P-P_\infty}{0.5\,\rho(U^2+r^2\omega^2)} \tag{5.1}$$

where P, P_∞, U, and ω are pressure on the blade surface, atmospheric pressure, free stream velocity and rotational speed, respectively. Figure 5.6 shows a comparison of pressure coefficients at different locations on the blade between the numerical simulations and the experimental results from the literature (Hand et al., 2001), showing very good agreement, hence confirming the applicability of the developed LES model for the wind turbine aerodynamics.

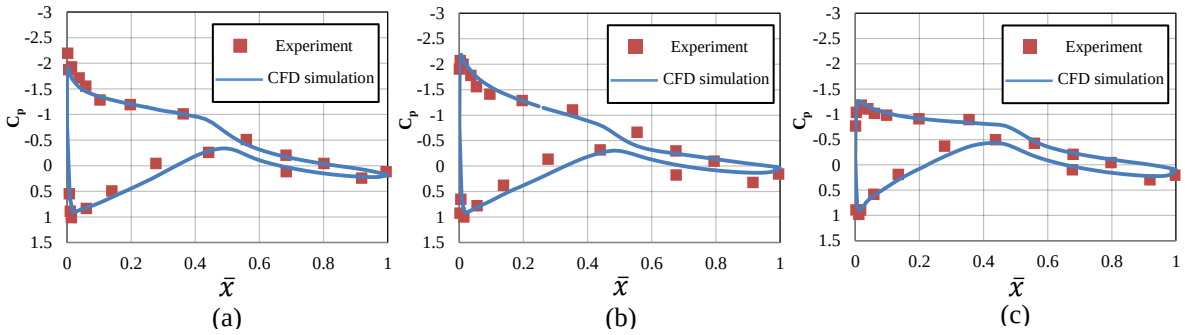

Figure 5.6 Comparison of the results of the computed pressure coefficient, C_p, on the turbine blades with experiment (Hand *et al.*, 2001) for three radii, (a) *r/R*=0.3, (b) *r/R*=0.63, (c) *r/R*=0.95.

The calculated output power using the computed torque of the blades is shown in Figure 5.7. The averaged value of the output power obtained from simulation is approximately 5.73 (kW), which differs by 4.6% when compared with the experimental data (Hand *et al.*, 2001, Simms *et al.*, 2001). As seen, the calculated pressure coefficient and the output power show a very good agreement with experimental data (Figures 5.6 and 5.7). Another parameter which can be used to further validate the model is the thrust coefficient. The calculated thrust coefficient from CFD is 0.495 which is 1.5% less than the experimental value of 0.487 (Hand *et al.*, 2001).

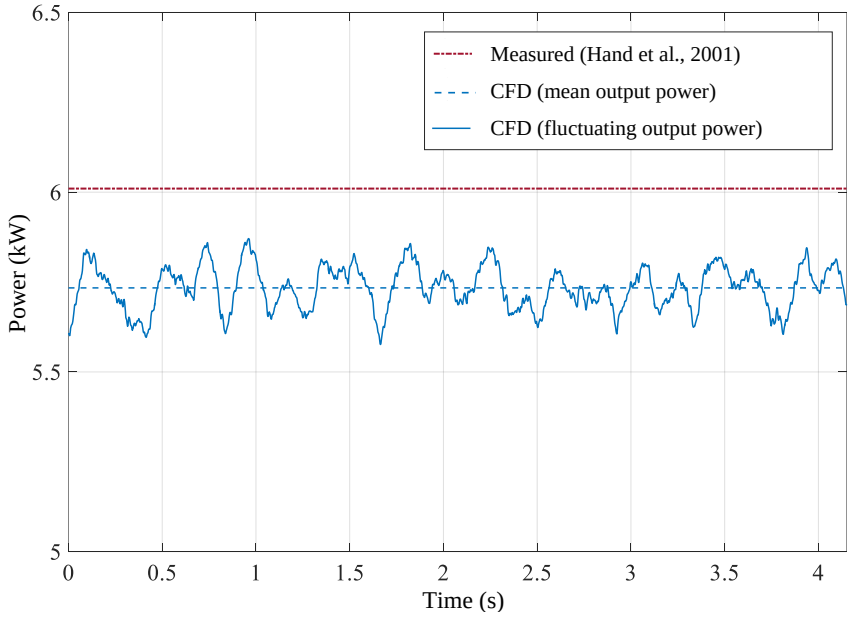

Figure 5.7 Calculated output power for confined environment compared to mean measured output power in the experiment by Hand et al., (2001). Note the non-zero origin on the power scale. The time period corresponds to 5 revolutions after starting recording the simulation results.

5.5 Results based on CFD model

In this section, some of the results obtained from the LES computation for the NREL Phase VI wind turbine are presented in order to highlight the capability of this method to capture the flow details and provide accurate information about wake development. Figure 5.8 shows the velocity profile downstream of the turbine. The W-shape of the velocity profile in the near-wake corresponds to the wake region with the largest velocity deficit at tip height. This structure, which is due to the presence of the concentrated tip vortices leading to the maximum velocity deficit, maintains its shape up to 8*D* downstream. The effect of the tower and nacelle is obvious immediately downstream of the wind turbine (1*D* downstream) and it vanishes by 4*D* downstream of the turbine. This momentum loss is recovered by mixing, while the momentum loss in the wake due to energy extraction extends up to 16*D* downstream.

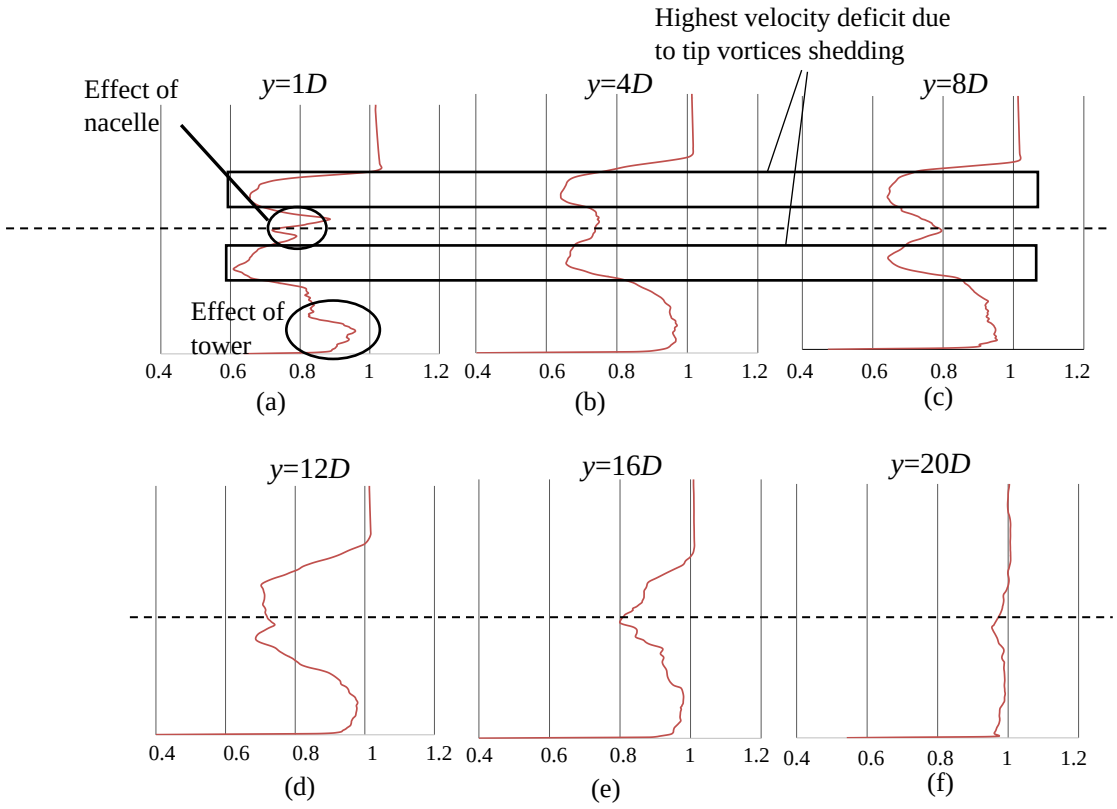

Figure 5.8 Axial normalised velocity profiles at various streamwise locations y=1*D*, 4*D*, 8*D*, 12*D*, 16*D*, 20*D*.

Figure 5.9 illustrates the vortical structures in the wake using the iso-surface of Q-criterion. The rings of tip vortices are shed up to 1.5*D* downstream. After this distance, these structures start to break down due to instabilities, shear between the ambient and wake region, and interactions between the various vortical structures in the wake. However, the effect of the vortical structures in the wake can be seen up to 20*D* downstream.

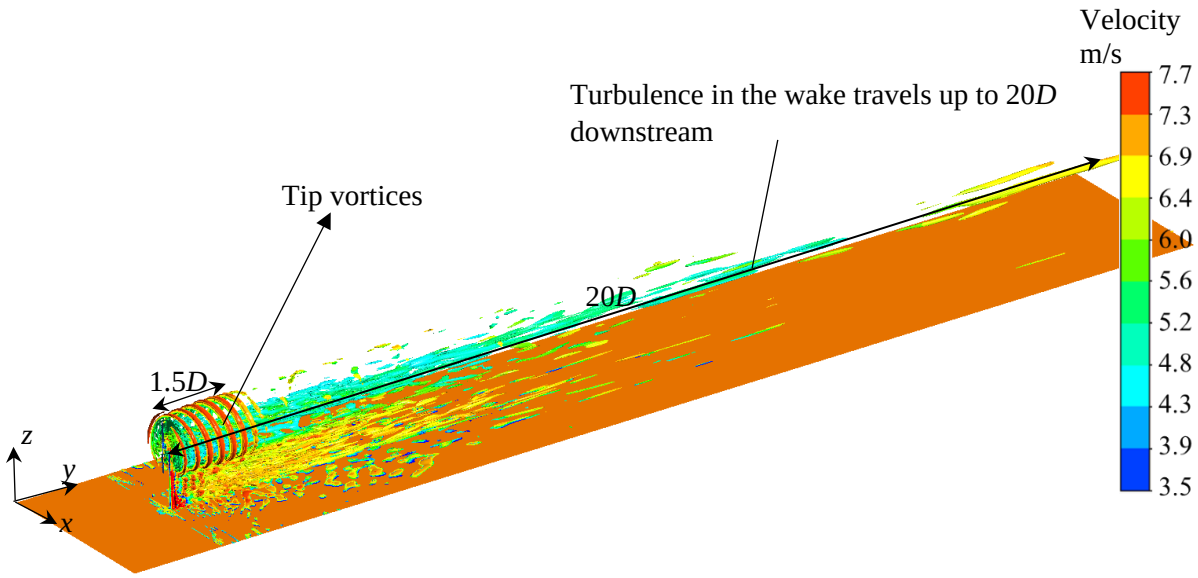

Figure 5.9 Iso-surface of instantaneous normalized Q-criterion coloured by axial velocity magnitude showing the vortical structures in the wake region.

The effect of the rings of tip vortices is present up to 7*D* in the vorticity contours depicted in Figure 5.10. These structures start to dissipate and mix with the ambient flow after 7*D*; while there is no sign of the effect of distinct tip vortices after 12*D*, there still exists vortical and turbulent structures in the region corresponding to the wake up to 20*D*.

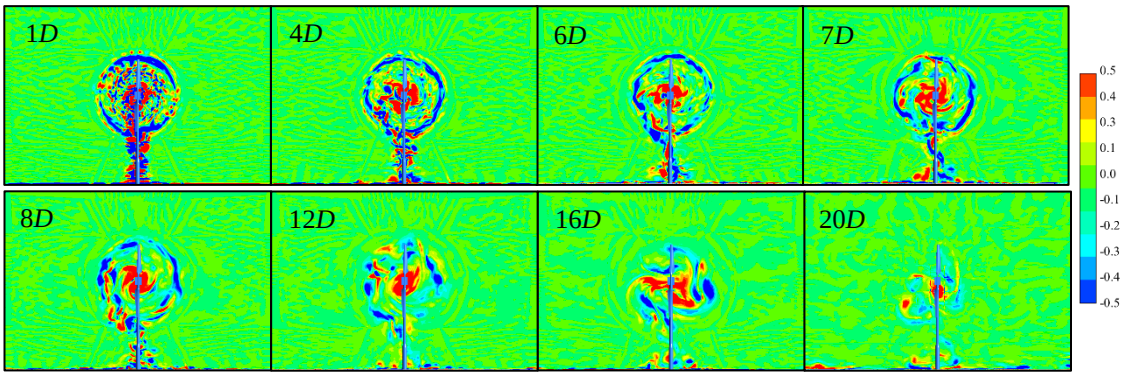

Figure 5.10 Vorticity contours at different locations downstream of the wind turbine for uniform flow.

5.6 Comparison of the models and discussion

The aim of this section is to assess the accuracy of the semi-empirical models available in the literature (*i.e.*, Jensen, Larsen, and Frandsen models) by means of comparing their results compared to those of the accurate CFD model developed in this paper. In other words, the full CFD model developed in this paper is used as a benchmark to evaluate the accuracy of the semi-empirical models used in the literature.

In order to compare these kinematic models with the developed LES model, the wake expansion and velocity contours are presented in figures 5.11 and 5.12, respectively. It should be noted that the wake diameter is calculated using the highest velocity gradient as it can be a good representative for the boundary between low velocity region in the wake and free stream (see also Figure 5.13). The LES was performed for an unconfined environment with a uniform incoming velocity profile to compare the prediction capability of all cases within the same environment. As seen in Figure 5.10, the semi-empirical engineering models overestimate the wake expansion rate as well as the wake diameter. It is shown that despite their simplicity in comparison with the Larsen models, models proposed by Jensen and Larsen can better predict the near wake expansion ($y < 4D$). For $4D < y < 7D$ models proposed by both Jensen and Larsen result in almost the same wake diameter. Further

downstream ($7D < y < 9D$) the deviation of the Jensen and Frandsen models from the LES becomes larger due to the higher expansion rate which is produced by these models. The wake diameter starts to decrease in the LES model after $9D$ downstream due to mixing of the wake with ambient flow. Moreover, a comparison between the velocity contours in Figure 5.12 reveals that the Larsen models can generally better represent the velocity field in the wake when compared to the LES model; this can be observed by comparing the wake areas associated with the velocities. Considering the velocity change in the wake region, it can be concluded that the Larsen models (Figure 5.21(d) and Figure 5.12(e)) also produce a more accurate velocity profile inside the wake region. These modes are less accurate in near wake region than the LES model since they use an empirical self-similar velocity profile as the starting profile in the near-wake. On the other hand, the computation time is also one of the factors which should be considered. The LES simulation took approximately 200 hours to complete using 40 CPU cores with a processor speed of 2.4 GHz, based on Linux operating system. In comparison, obtaining the velocity field using engineering models took only a few seconds using only a single CPU core.

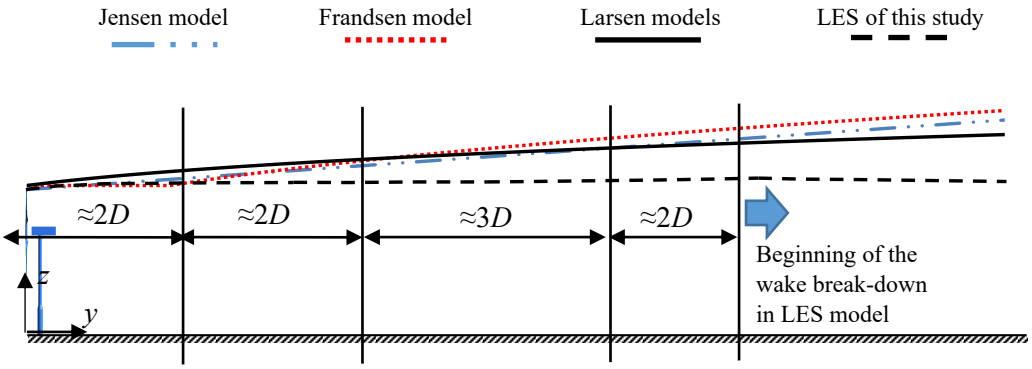

Figure 5.11 Wake diameter for studied models uniform unconfined environment; the wake diameter for the LES is calculated based on the location of the highest velocity gradient.

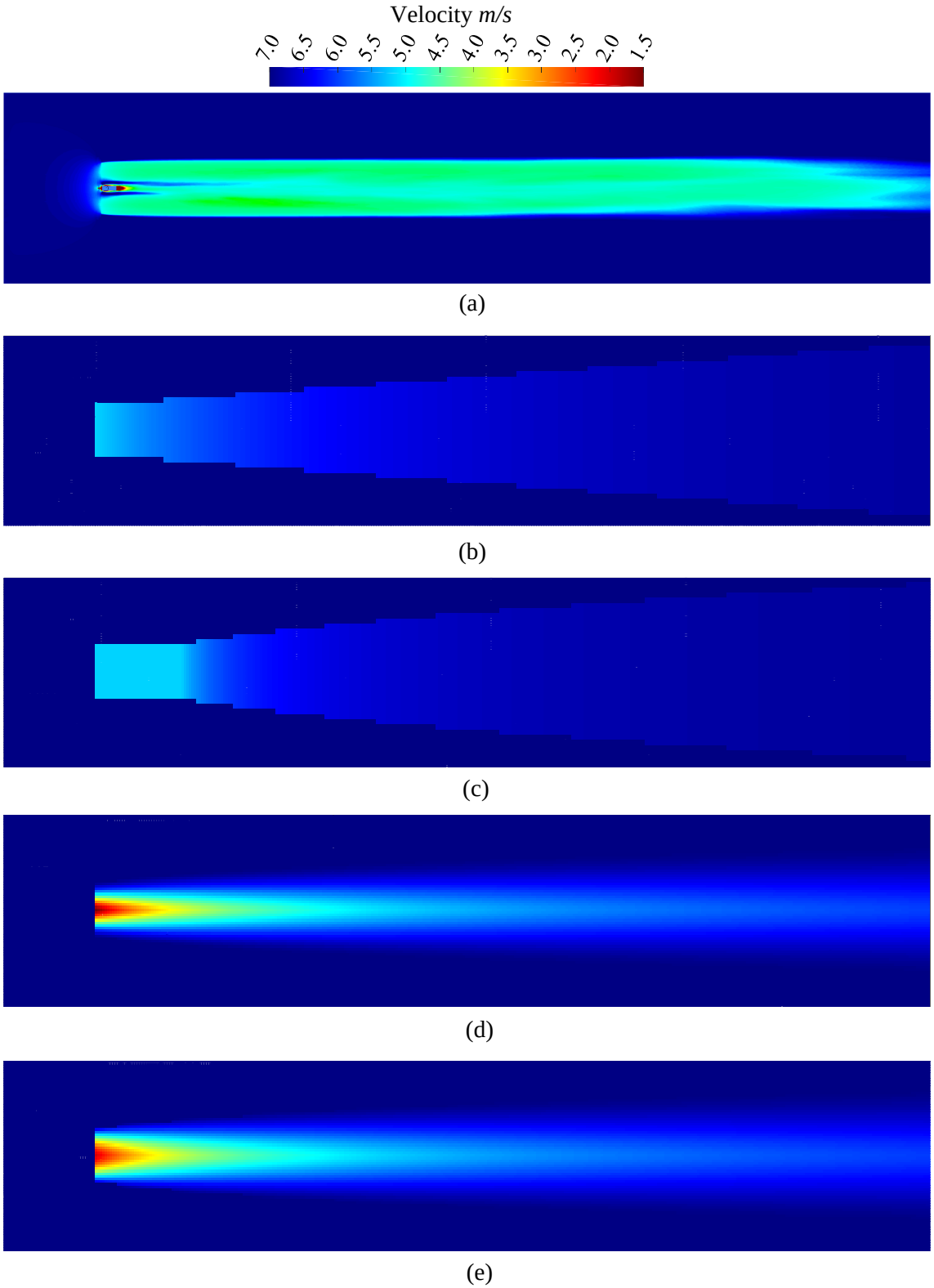

Figure 5.12 Velocity contour (m/s) through horizontal plane at hub height for several engineering models and LES model carried out for NREL phase VI located in and unconfined environment with a wind velocity of 7 m/s, up to 16*D* downstream of wind turbine: (a) current LES model, (b) Jensen model, (c) Frandsen model, (d) Larsen first order model, (e) Larsen second order model.

Figure 5.13 shows the velocity profiles downstream of the wind turbine. Although, the proposed models by Jensen and Frandsen are very simple, they can provide reasonable velocity profiles and wake diameters in the near field (up to 4*D*). Further downstream, the Jensen and Frandsen models deviates from the LES result and overestimates the wake expansion and recovery rates, while results produced by the Larsen models are closer to the LES results. This difference is more evident at 16*D* downstream where the velocity deficit predicted by the Larsen models is closer to the LES results. The velocity profiles produced by the engineering models are axisymmetric while the LES results shows a slight asymmetric behaviour. The asymmetry arises from rotation of the blades, which shows that the engineering models are not able to take the effect of rotation into account.

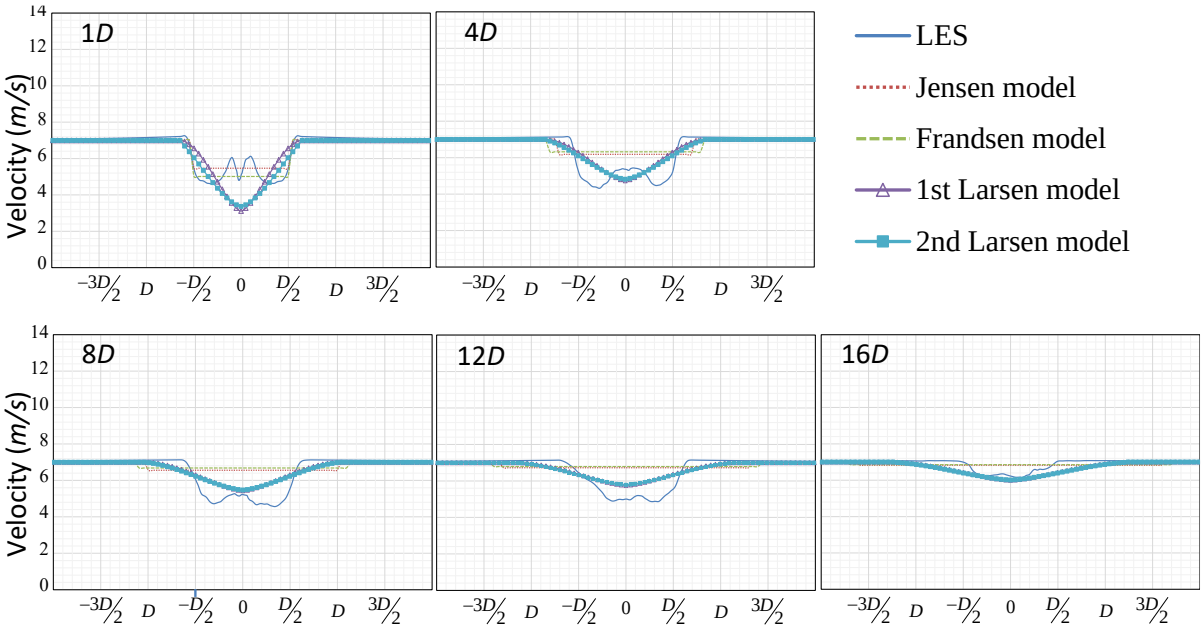

Figure 5.13 Comparison of velocity profiles on the horizontal plane passing through the axis of rotation at several locations downstream of the wind turbine.

5.7 Conclusion

In wind farms, most wind turbines operate in the wake regions of other turbines with increased turbulence intensity due to strong tip vortices and turbulence, induced by the

rotation and interaction of the blade and tower. The consequences are power loss and high fluctuating loads on the rotor blades. Thus, several semi-empirical wake models have been developed to predict wind turbines wakes, their interaction and their development in wind farms. When compared with experiment, many of these models can produce acceptable results in terms of predicting the velocity deficit and power loss in wind farms. However, the assumptions that these models are based on, may affect their application to real conditions, such as different wind profiles and incoming turbulence. They are essentially incapable of accounting for the effect of tip losses, yaw misalignment, effect of topography, atmospheric turbulence, stall and effect of increased turbulence due to neighbouring machines. Although some corrections have been introduced by researchers to modify these models, they are primarily based on experimental data under limited conditions.

The semi-empirical engineering models investigated in this study can be used to calculate the velocity deficit and wake expansion in uniform flow. However, none of these models can adequately reveal all wake details such as tip vortices, wake breakdown, vortices generated inside the wake and increased turbulence intensity. These models are widely used in industry for designing the layout of wind farms. They are able to produce relatively good estimates of the velocity deficit in wind farms (which can then be used to calculate the overall power production and optimize the positioning of the turbines), but they usually under-predict the total amount of the produced power. On the other hand, the simplicity of these models results in low computational cost in comparison with high fidelity CFD models. These factors (position optimization and computational cost) become more important in wake studies in large wind farms, where wake interaction is significant.

The engineering models were found to over-predict the wake expansion and under-predict the velocity recovery rate. Over-prediction of the wake expansion can result in a wind-farm

layout with fewer wind turbines and thus less energy extraction, while a denser layout could be constructed on the limited available sites to capture higher rate of wind power. Moreover, a higher recovery rate can lead to power loss and increased maintenance costs due to positioning the wind turbines in an area which is affected by a wake. On the other hand, the LES model can produce detailed information about the flow field which can be used to design a wind farm which operates under optimum condition in terms of power production and maintenance cost. Results showed that each of these models can perform better in particular regions in terms of predicting the wake diameter or velocity deficit. Based on the results, it can be concluded that a combination of these models can be used by dividing the computational domain into several regions and using the appropriate model for each region in order to increase the accuracy of the prediction.

5.8 References

Aho, J., Buckspan, A., Laks, J., Jeong, Y., Dunne, F., Pao, L., Fleming, P., Churchfield, M. & Johnson, K. 2012. Tutorial of wind turbine control for supporting grid frequency through active power control, National Renewable Energy (NREL).

Blomhoff, H. P. 2012. *An experimental investigation of wind turbine wakes.* Master of Science in Product Design and Manufacturing, Norwegian University of Science and Technology.

Choudhry, A., Mo, J. O., Arjomandi, M. & Kelso, R., 2014, Effects of wake interaction on downstream wind turbines, *Wind Engineering*, **38**, 535-548.

Churchfield, M. J., Moriarty, P. J., Hao, Y., Lackner, M. A., Barthelmie, R., Lundquist, J. & Oxley, G. S. 2015. A comparison of the dynamic wake meandering model, large-eddy simulation, and field data at the Egmond aan Zee Offshore Wind Plant preprint. National Renewable Energy Laboratory (NREL).

Crespo, A. 1985. Numerical analysis of wind turbine wakes. In Delphi workshop.

Crespo, A., Hernández, J. & Frandsen, S. 1999. Survey of modelling methods for wind turbine wakes and wind farms. *Wind Energy,* **2,** 1-24.

Dixon, K. R. 2008. *The near wake structure of a vertical axis wind turbine, including the development of a 3d unsteady free-wake panel method for VAWTs.* Master of Science, Delft University of Technology.

Elliott, D. L. 1991. Status of wake and array loss research. *Windpower Conference,* Palm Springs, California.

Frandsen, S., Barthelmie, R., Pryor, S., Rathmann, O., Larsen, S., Højstrup, J. & Morten Thøgersen 2006. Analytical modelling of wind speed deficit in large offshore wind farms. *Wind Energy,* **9,** 39-53.

Jensen, N. O. 1983. A note on wind generator interaction. Risø National Laboratory. Internal technical report.

Jimenez, A., Crespo, A., Migoya, E. & Garcia, J. 2007. Advances in large-eddy simulation of a wind turbine wake. *Journal of Physics: Conference Series,* **75,** 012041.

Jimenez, A., Crespo, A., Migoya, E. & Garcia, J. 2008. Large-eddy simulation of spectral coherence in a wind turbine wake. *Environmental Research Letters,* **3,** 015004.

Katz, J. & Plotkin, A. (eds.) 2001. *Low-speed aerodynamics*: Cambridge University Press.

Kloosterman, M. H. M. 2009. *Development of the near wake behind a horizontal axis wind turbine.* Master of Science, Delft University of Technology.

Krogstad, P.A. & Eriksen, P. E. 2013. "Blind test" calculations of the performance and wake development for a model wind turbine. *Renewable Energy*, **50**, 325-333.

Laratro, A., Arjomandi, M., Kelso, R. & Cazzolato, B. 2014, A discussion of wind turbine interaction and stall contributions to wind farm noise, *Journal of Wind Engineering and Industrial Aerodynamics,* **127**, 1-10.

Larsen, G. C., 1988. A simple wake calculation procedure, Technical report, Risø National Laboratory.

Lilly, D. K., 1992, A proposed modification of the Germano subgrid-scale closure method, *Physics of Fluids A,* **4**, 633-635.

Liu, M. K., Yocke, M. A. & Myers, T. L. 1983. Mathematical model for the analysis of windturbine wakes. *Journal of Energy*, **7,** 73-78.

Luo, K., Zhang, S., Gao, Z., Wang, J., Zhang, L., Yuan, R., Fan, J. & Cen, K. 2015. Large-eddy simulation and wind-tunnel measurement of aerodynamics and aeroacoustics of a horizontal-axis wind turbine. *Renewable Energy*, **77**, 351-362.

Mo, J. O., Choudhry, A., Arjomandi, M., Kelso, R. & Lee, Y.-H. 2013. Effects of wind speed changes on wake instability of a wind turbine in a virtual wind tunnel using large

eddy simulation. *Journal of Wind Engineering and Industrial Aerodynamics*, **117**, 38-56.

Sanderse, B. 2012. Aerodynamics of wind turbine wakes. Energy Research Centre of the Netherlands, Literature review.

Schepers, J. G. 2003. Endow: Validation and improvement of ECN's wake model. Energy Research Centre of the Netherlands, Technical report.

Sørensen, J. N. 2016. *General momentum theory for horizontal axis wind turbines*, Springer.

Sørensen, J. N., Shen, W. Z. & Munduate, X. 1998. Analysis of wake states by a full-field actuator disc model. *Wind Energy*, **1,** 73-88.

Troldborg, N., Sørensen, J. N. & Mikkelsen, R. 2007. Actuator line simulation of wake of wind turbine operating in turbulent inflow. *Journal of Physics: Conference Series,* **75,** 1-15.

Chapter 6 Wind turbine wake development in the atmospheric boundary layer

6.1 Chapter overview

In this chapter, the wake data of a wind turbine operating in a smooth boundary layer was acquired using the large eddy simulation approach detailed in Chapter 5. The effect of the atmospheric boundary layer on wake expansion, wake structure, velocity profiles and vorticity in the wake was implemented through a power-law wind velocity profile. For the modelling purposes, the turbulent features corresponding to a topography with moderate scrub or scattered trees were selected. The wake development of the wind turbine in the atmospheric boundary layer was compared with the wake of the same wind turbine exposed to uniform flow. It was found that a strong downwash is generated when the wind turbine operates in the atmospheric boundary layer. Increasing the turbulence intensity and incoming instabilities also reduced the wake length and increased the mixing rate in the wake region. The details of the method, results and the underlying mechanism of the downwash is presented in the following section. The section is represented in the paper format accepted for publication in the Journal of Wind Engineering and Industrial Aerodynamics.

Statement of Authorship

Title of Paper	The effect of boundary layer on the wake of a horizontal axis wind turbine
Publication Status	☐ Published ☐ Accepted for Publication ☑ Submitted for Publication ☐ Unpublished and Unsubmitted work written in manuscript style
Publication Details	Submitted to the Journal of Wind Engineering and Industrial Aerodynamics

Principal Author

Name of Principal Author (Candidate)	Nima Sedaghatizadeh		
Contribution to the Paper	- Research - Providing the data, writing of the manuscript and production of original figures - Correspondence with editor and reviewers including the production of all cover letters and rejoinder		
Overall percentage (%)			
Certification:	This paper reports on original research I conducted during the period of my Higher Degree by Research candidature and is not subject to any obligations or contractual agreements with a third party that would constrain its inclusion in this thesis. I am the primary author of this paper.		
Signature		Date	14/09/2017

Co-Author Contributions

By signing the Statement of Authorship, each author certifies that:

i. the candidate's stated contribution to the publication is accurate (as detailed above);

ii. permission is granted for the candidate in include the publication in the thesis; and

iii. the sum of all co-author contributions is equal to 100% less the candidate's stated contribution.

Name of Co-Author	Maziar Arjomandi		
Contribution to the Paper	- Supervision of the work, including the production of the manuscript - Participation in the development of the concepts and ideas presented in the manuscript - Evaluation and editing of the manuscript prior to submission		
Signature		Date	15/09/2017

Name of Co-Author	Richard Kelso		
Contribution to the Paper	- Supervision of the work, including the production of the manuscript - Conceptual explanation of the mechanism of wind turbine wake development and downwash and participation in the development of ideas presented in the manuscript - Evaluation and editing of the manuscript prior to submission		
Signature		Date	14/9/2017

Name of Co-Author	Benjamin Cazzolato		
Contribution to the Paper	- Supervision of the work, including the production of the manuscript - Participation in the development of the concepts and ideas presented in the manuscript - Evaluation and editing of the manuscript prior to submission		
Signature		Date	14/09/2017

Name of Co-Author	Mergen H. Ghayesh		
Contribution to the Paper	- Supervision of the work, including the production of the manuscript - Participation in the development of the concepts and ideas presented in the manuscript - Evaluation and editing of the manuscript prior to submission		
Signature		Date	14/09/2017

The effect of boundary layer on the wake of a horizontal axis wind turbine

Nima Sedaghatizadeh, Maziar Arjomandi, Richard Kelso, Benjamin Cazzolato, Mergen H. Ghayesh

School of Mechanical Engineering, University of Adelaide, Adelaide, SA, 5005

Revision under review: submitted to the Journal of Wind Engineering and Industrial Aerodynamics.

6.2 Abstract

This paper analyses the effect of a mean shear similar to an atmospheric boundary layer on the wake of a wind turbine by means of Large Eddy Simulation. More specifically, a comparison is made between the wake in the *presence* of the smooth boundary layer and that in the *absence* of a boundary layer (i.e., an unconfined uniform incoming flow). The numerical simulations show that the presence of the smooth boundary layer lowers the power output, however, the rings of tip vortices in the presence of a power-law incoming flow are more stable when compared to the case of a uniform incoming flow. More importantly, the length of the wake region for the case with the smooth boundary layer is about 12*D* which is much shorter than that of the case with a uniform incoming flow (namely 20*D*). Strong downwash observed at this distance in the presence of the smooth boundary layer results in a higher velocity magnitude and lower turbulence in the far wake of the wind turbine in the smooth boundary layer case when compared with the uniform flow. A mechanism explaining these observations is also proposed. This new knowledge may result in denser wind farms compared to wind farms established on smoother surfaces.

Nomenclature

x, y, z	Cartesian coordinate system	S_{ij}	Strain rate tensor (s^{-1})
D	Rotor diameter (m)	ρ	Fluid density (kg/m^3)
r	Radial distance (m)	μ	Dynamic viscosity (Pa.s)
R	Radius of the rotor (m)	μ_t	Subgrid turbulent viscosity (Pa.s)
T	Thrust (N)	υ	Kinematic viscosity (m^2s^{-1})
C_T	Thrust coefficient	L_s	Mixing length scale
P	Pressure (Pa)	α	Angle of attack (°)
u_i	Velocity component (ms^{-1})	κ	von Karman factor
$\overline{u}$	Resolved velocity (ms^{-1})	C_s	Smagorinsky factor
λ	Tip speed ratio	δ_{ij}	Kronecker delta function
σ	Stress tensor (N/m^2)	$\bar{x}$	Normalised chord-wise distance
τ	Subgrid scale stress (N/m^2)	h_0	Reference height (here equal to hub height)

6.3 Introduction

In wind farms, which typically consist of many turbines, the interaction of downstream turbines with the wakes from the upstream turbines results in a reduction in the overall efficiency of the wind farms. This is mainly due to the fact that the kinetic energy of the wind significantly decreases when the upstream turbine extracts energy from it. Turbine wakes are an inherent source of turbulence which may cause fluctuating loads on the blades of the downstream turbines. Fluctuating loads and increased turbulence intensity, in turn, may cause the generation of noise and fatigue on the turbine blades (Crespo et al., 1999, Cleijne, 1993). Moreover, since a wind turbine operates in an atmospheric boundary layer (ABL), its blades are subject to different wind speeds at different heights during each revolution which, consequently, affects the performance and wake development (Jimenez et al., 2007, Wharton and Lundquist, 2012).

In order to enable the extraction of energy in large wind farms, the loss of energy inside the wake should be recovered from the flow surrounding the wind turbine wake. Vertical and horizontal energy influx, which need to occur in order to recover the energy in the wake region, are highly affected by the ABL properties, in particular its velocity distribution and turbulence structure (Sørensen, 2016, Kinzel et al., 2015). Despite the fast growth in the number of wind farms, limited studies have been conducted to fully understand the effect of ABL parameters on the wind turbine performance and wake development; this paper is the first to do so.

Several numerical and experimental studies have been reported in the literature on the investigation of the wind turbine and its wake development. Most of the experimental investigations have been carried out using scaled wind turbines in small wind tunnels due to the difficulties associated with field experiments (e.g. setting up instruments and measuring

data in the wake) and the high cost of large-scale wind tunnel experiments. For instance, Chamorro et al. (2012) investigated the effect of turbulent scales on the wake of a miniature wind turbine. Their study suggested that wind turbines can act as a spatial and temporal high-pass filter with the ability of dampening the large-scale turbulence structures in the incoming flow. They also demonstrated that a wind turbine can act as an active source of turbulent energy, hence a wind turbine can result in the amplification of some frequencies (both spatial and temporal) in the turbulent flow field while dampening others (Chamorro et al., 2012, Chamorro et al., 2013). Particle Image Velocimetry (PIV) has been employed in a number of experiments to better specify the development of the generated wake (Grant and Parkin, 2000, Schepers and Snel, 2007, Sherry et al., 2013). For instance, Schepers and Snel (2007) performed PIV on a large-scale wind turbine with a 4.5 m rotor diameter in the MEXICO (Model experiments in Controlled Conditions) program. This was carried out in order to provide the required information about the wake aerodynamic for the model validation and improvement (Snel et al., 2007, Schepers and Snel, 2007). The focus of their investigation was on the structure of tip vortices around the rotor area, the performance of the wind turbine, as well as the dynamic loads on the blades. They found discrepancies between experimental and theoretical results of up to 20% and 30% in performance and dynamic loads, respectively, due to the complexity of the flow.

One of the concerns in wind tunnel experiments is blockage ratio and test section length which can affect the wake structure. McTavish et al. (2013) investigated the effect of blockage ratio on the wake expansion using PIV measurement of a scaled wind turbine in a water channel. Their results revealed that in order to eliminate the effect of walls on the wind turbine wake, the blockage ratio should be kept below 10%. One of the highly-cited experiments in this field was performed by Hand et al. (2001) using the NREL Phase VI

wind turbine with 10.058 m rotor diameter in a large wind tunnel with a blockage ratio less than 9%. The aerodynamic performance and loading on the blades were measured, along with some qualitative visualisation of the tip vortices using smoke. Similar to the current study the results of this study have been frequently used by different researchers for validation of the wake models (The interested reader is referred to Bai and Wang (2014) for more information regarding the experimental studies on the wind turbine wake.). Schümann et al. (2013) reported a low velocity region in the wake downstream of the wind turbine surrounded by the tip vortices (Figure 6.1). It was also found that there are strong rotational features within the central area of the wake. The wake of the tower is deflected by the rotational structures in the near wake. Tower effects also result in a deformation in the wake and the movement of the rotational centre; it also changes the distribution of turbulence intensity (Schümann et al., 2013).

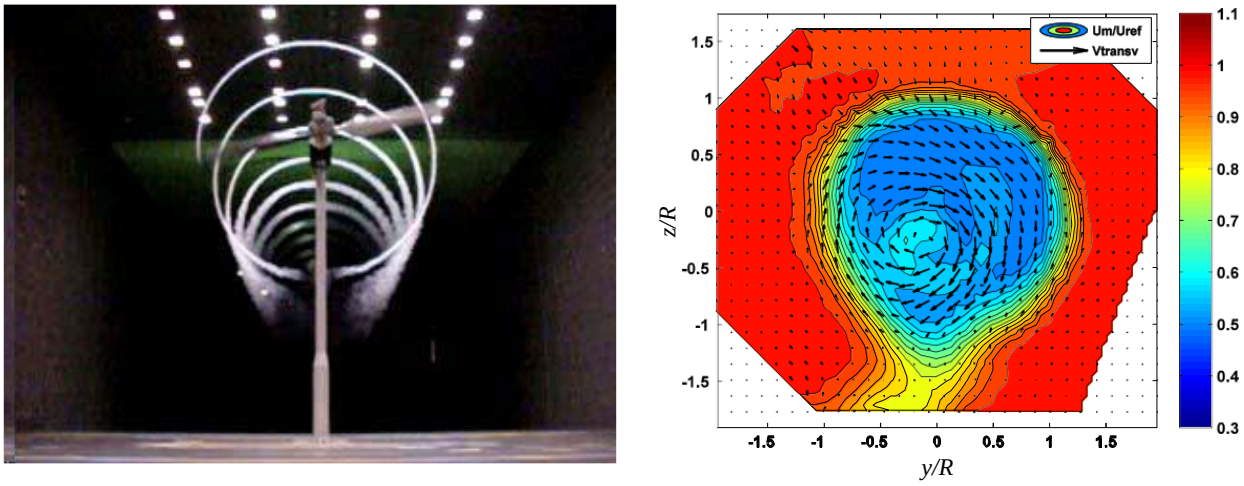

(a) (b)

Figure 6.1 (a) Visualization of the tip vortices of a large-scale wind turbine in a wind tunnel (Hand et al., 2001), (b) PIV visualization of the wake of a medium-sized wind turbine, showing the rotational core, with the effect of tower and tip vortices also evident (Schümann et al., 2013).

Regarding numerical simulations, advances in computational resources promote the application of the CFD methods to study wind turbine wakes. Four different approaches can be used in order to computationally investigate the wake of a wind turbine (Bai et al., 2014,

Jimenez et al., 2007), namely Direct Numerical Simulation (DNS), Reynolds Averaged Navier-Stokes (RANS), Large Eddy Simulation (LES), and Hybrid LES. Despite the advances in computer technology, DNS, which is the most accurate model, has not been chosen for simulating the wake of a wind turbine due to its high computational costs. RANS models, on the other hand, as the most affordable turbulent models, are not able to analyse the instabilities in the wake since they are based on time-averaged Navier-Stokes equations (Choudhry et al., 2014). Although LES models are computationally more affordable than DNS models, they still require a high computational power, especially in order to accurately resolve the boundary layer on the blade surface. In order to reduce the computational cost, hybrid models have been developed, replacing the blades with an actuator disk or actuator line (Troldborg et al., 2007, Watters et al., 2010). However, these models are sensitive to blade shape since they require experimental data based on blade profiles to account for dynamic forces on the actuator line and disk. Mo et al. (2013) developed for the first time a full LES model for NREL Phase VI wind turbine and validated their model against the experimental data. Their results revealed that the wake instabilities are a function of the upstream velocity magnitude and they presented a new description to identify the near-wake region based on these observations. Moreover, the velocity and vorticity contours in their study shows detailed information about the velocity field and wake structure. Their study showed that coherent vortical structures in the wake exist up to 20D downstream of the turbine.

Turbulence intensity (TI), velocity profile, and ground topology affect the wake development and its breakdown, and consequently the layout of a wind farm. Constructing wind farms in low TI environments (e.g. offshore wind farms) might require large spacing between wind turbines, while on the other hand, dense wind farms can be constructed on

land with moderate turbulent intensity in the incoming flow. In this study, the effect of a smooth boundary layer (SBL) on the development and structure of the wake of a wind turbine is investigated numerically for the first time. Based on the literature review, of all the turbulence models mentioned above, LES is the optimal choice when both the computational cost and accuracy are considered. Hence, the simulations of this paper are based on an LES model. The NREL Phase VI wind turbine was chosen for the numerical modelling and simulations. Full LES was employed to simulate the flow field in the near wake region as well as the far-wake up to 20*D* downstream of the wind turbine. Numerical simulations are performed in the *presence* and *absence* of the SBL so as to shed light on the effect of the SBL profile on the wind turbine wake development. Results show that the SBL in an unconfined flow has significant effect on the wake development and its expansion; the wake of the wind turbine starts to break down closer to the wind turbine in the presence of an SBL when compared to the uniform flow field (i.e., in the absence of SBL). Due to faster recovery of the wake, it's possible that downstream turbines can be installed closer to upstream turbines, which suggests that denser wind farm layouts may be possible.

6.4 Problem description and computational mesh

The NREL phase VI wind turbine, which is a two-bladed stall-regulated turbine with a 10.058 m rotor diameter, was selected for the numerical modelling and simulations. Figure 6.2 depicts the shape of the turbine blade, its twist and chord variation along the span as well as the experimental and computational wind tunnel model adopted from Hand et al. (2001). The wind turbine has a rated output power of 19.8 kW and the blades consist of the S809 airfoil from root to tip. The blades have a linear taper and an aspect ratio of 7.2. The turbine solidity is 5.8%. The nacelle and hub parts in the computational domain are simplified in the current study to avoid the difficulties associated with the generation of a high quality grid.

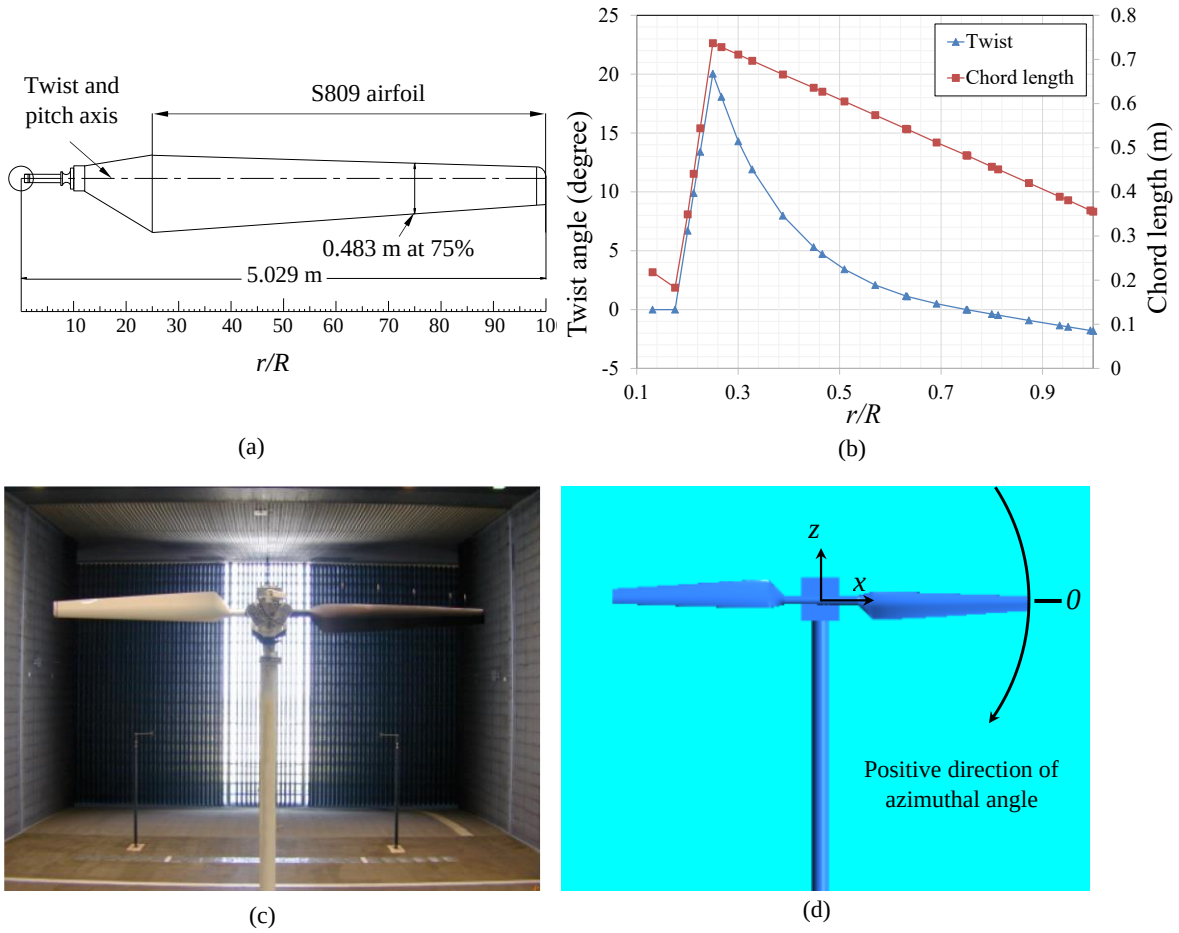

Figure 6.2 (a) Blade geometry and shape (Reproduced from Hand et al., 2001), (b) twist and chord variations along the blade, (c) experimental model (adopted from Hand et al., (2001)), (d) computational model used in the current study. Rotor rotates counter clockwise. The blade is at zero azimuthal angle at horizontal state and as shown in the figure.

In order to validate the developed numerical model, a comparison was conducted between the experimental data available in the literature and the results from modelling. The experimental results, which were adopted from Hand et al. (2001), were obtained in a *wind tunnel* with a 24.4 m × 36.6 m cross sectional area and a length of 221.3 m using the NREL Phase VI wind turbine with a D=10.058 m rotor diameter. The computational wind tunnel domain was chosen to have a similar geometry (i.e., 24.4 m × 36.6 m cross sectional area and 221.3 m length) as shown in Figure 3, with the wind turbine located at approximately 2D from the inlet boundary in the middle of the wind tunnel. A cylindrical rotary zone was created around the blade in order to simulate the rotation of the blades (Figure 6.3). A sliding

mesh technique was applied to this zone, using a mesh interface between the cylindrical zone and the rest of the domain.

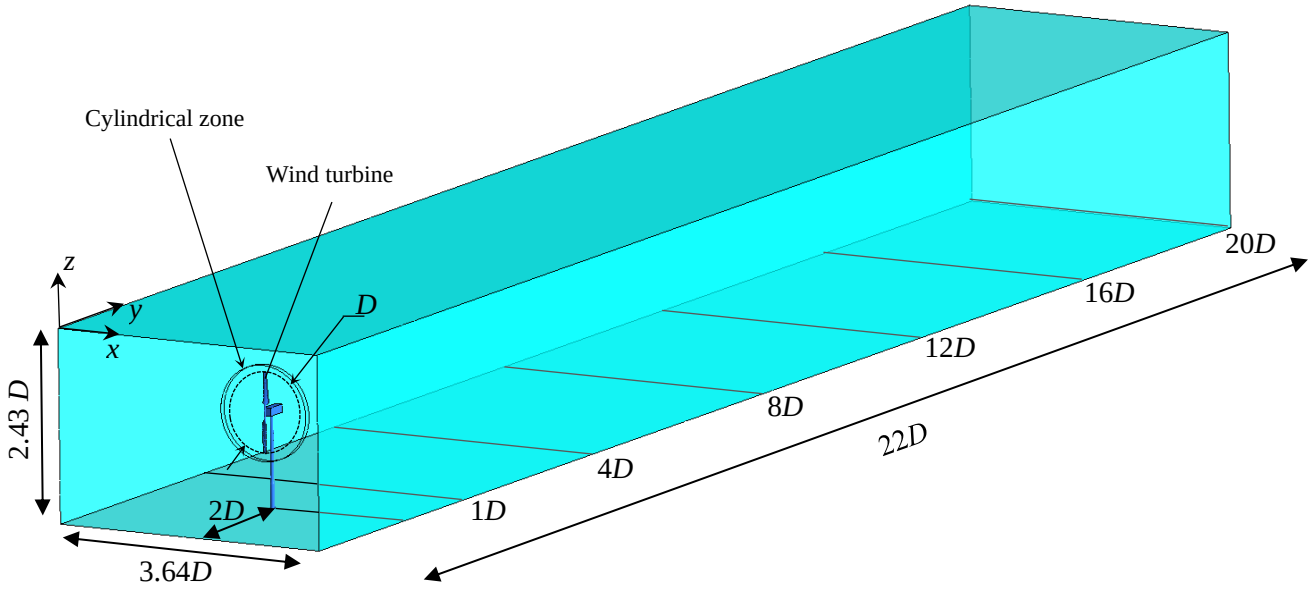

Figure 6.3 Dimensions of the computational domain used for numerical simulation of wind tunnel.

The computational grid for the wind turbine in the wind tunnel (which is used for validating the model) is depicted in Figure 6.4, as well as the computational domain for the SBL study. As shown in Figure 6.4(b), for the unconfined environment with an SBL profile, the computational domain (Figure 6.3) is extended to eliminate the wall effects and to implement the velocity profile of the SBL. For this purpose the domain used for modelling the turbine in the confined environment (Figure 6.4(a)) was inserted in the middle of the computational domain created for unconfined environment (Figure 6.4(b)). The computational domain is expanded in streamwise direction to minimize the effect of boundaries on the wake expansion.

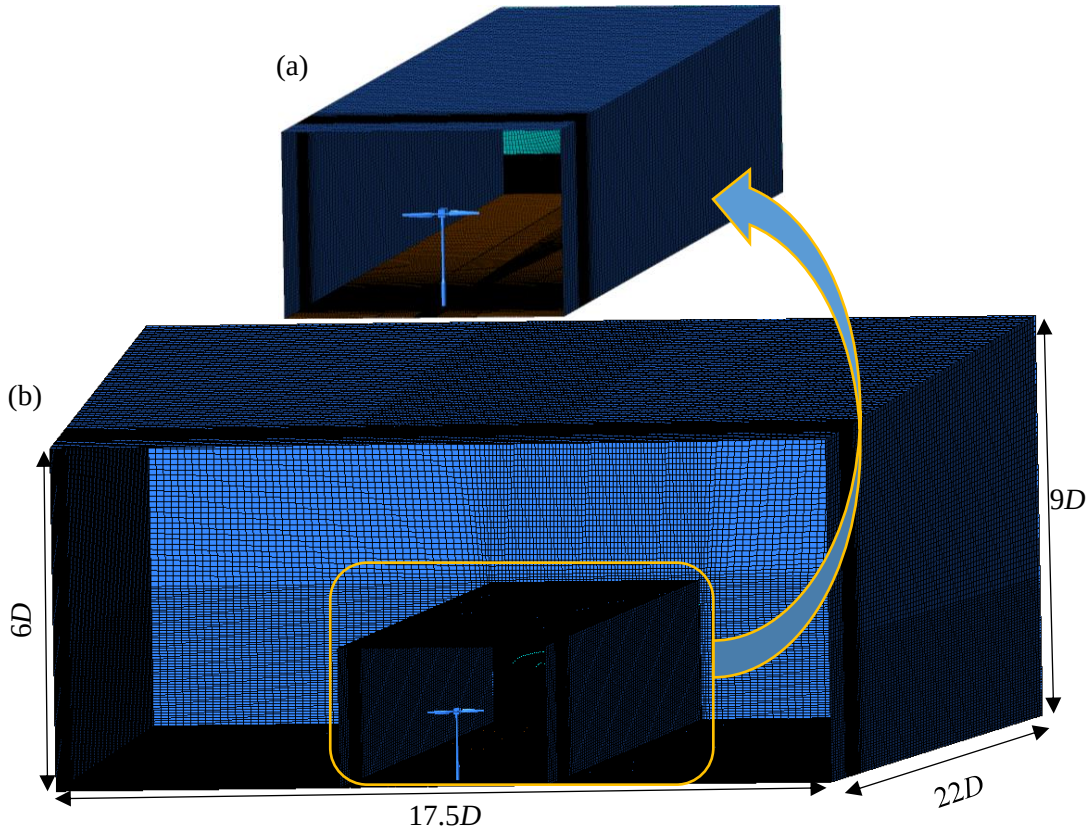

Figure 6.4 Computational grid used for numerical study. (a) Wind tunnel (used for validation), (b) Unconfined with ABL.

In order to accurately resolve the boundary layer, the first row of nodes of the computational grid around the blade is placed close enough to the blade surface to ensure a $y^+ \leq 1$. Twenty inflation layers with the growth rate of 1.1 were created adjacent to the blade surface to ensure that the boundary layer is captured precisely. Furthermore, each blade was meshed with 150 nodes in the spanwise direction and 110 nodes in the chordwise direction. Figure 6.5 shows the grid generated around the blades. Computational grids for all cases were composed of hexahedral elements. Since the blade of the NREL Phase VI turbine had a blunt trailing edge, the computational blade was also trimmed at 99% of the chord. The total number of elements within the domain is approximately 12.5 million for the unconfined environment (Figure 6.4(b)) and 11 million for the wind tunnel (Figure 6.4(a)). This mesh size and the maximum resolution were restricted by the available computer resources. The mesh size chosen in this work is finer compared to the previously published articles (Mo and

Lee, 2012); hence it is expected that the current grid produces more accurate results. Due to the high computational cost of the simulation, the sensitivity analysis has been carried out for output power and pressure coefficients over 4 revolutions for two grid sizes. Results revealed only an improvement of 1.5% in the accuracy of the calculated parameters when the number of elements was increased from 11 million to 16 million while the computation time was increased by about 60%. Thus, the coarser mesh was chosen for the modelling of the wake to reduce the computational time without a significant reduction in the accuracy of the computed data.

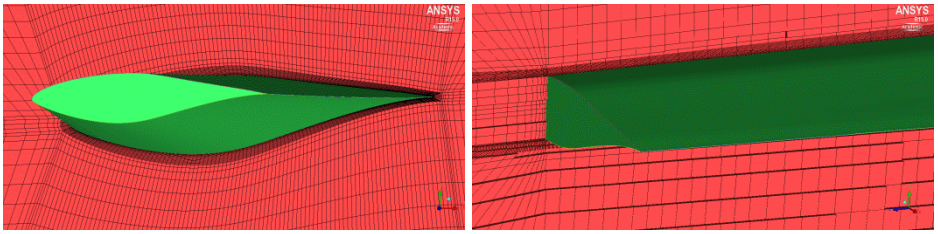

Figure 6.5 Sectional view of the mesh and the inflation layer around the

The effect of the smooth boundary layer is highlighted by comparing the results to those of the uniform flow profiles. Figure 6 shows the schematic arrangements of these cases for the uniform (a) and power-law velocity profiles (b). A thick boundary layer with the height of 2.4*D* (approximately twice the height of the turbine) is represented by the power-law velocity profile with power index of 0.2, which denotes a terrain with moderate scrub or scattered trees. To ensure an identical rotor speed for both uniform and boundary layer cases the velocity magnitude at the hub height was chosen to be equal.

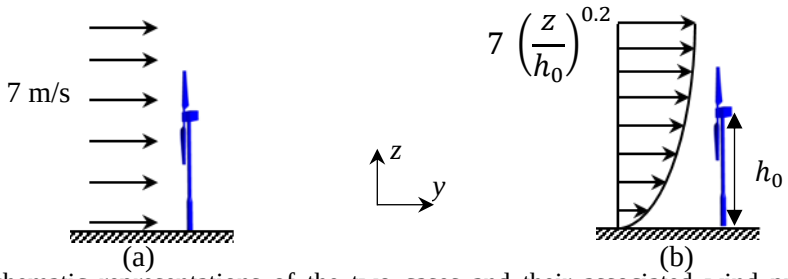

Figure 6.6 Schematic representations of the two cases and their associated wind profiles; (a) unconfined environment with 7 m/s uniform velocity profile, (b) SBL represented by power-law velocity profile with hub height velocity of 7 m/s.

Uniform velocity and power-law velocity profiles were applied as inlet boundary conditions for the uniform flow and SBL cases (as depicted in Figure 6.6), respectively. The free-stream turbulence intensity was set to 0.2% for all cases to emphasise the effect of the SBL profile. For the outlet, a pressure outlet with a zero gauge-pressure boundary condition was chosen. All the solid surfaces such as wind tunnel (for validation case), blades, nacelle, and tower are walls with no-slip boundary condition. Computations were carried out for the hub-height velocity profile of 7 m/s, resulting in a Reynolds number of approximately 5×10^6 based on the rotor diameter. The blades rotate at a constant rate of 71.9 rpm for all the cases studied. The time step was set to 0.002318 seconds corresponding to a 1 degree rotation of the blades per time-step. In order to have the same kinetic energy over the rotor area for both cases, the hub height velocity of the power-law profile should be 7.04 m/s rather than the chosen value of 7 m/s. Considering the small difference in the energy and velocity, no significant difference is expected to be caused by the difference in energy of the incoming flow. LES calculations were carried out using FLUENT 16.2. Simulations were performed for a sufficiently long time-period of time (30 revolutions) to ensure the wake was fully developed and the results were statistically stable. After ensuring that the wake was sufficiently developed, results were recorded over 10 revolutions of the wind turbine in order to calculate the time-average parameters.

6.5 Numerical method

Large Eddy Simulation (LES) was used to calculate the flow field in the wake of the wind turbine because of its greater ability to capture instabilities in the flow field caused by vortex shedding, in comparison to RANS models. This technique explicitly solves the large-scale turbulence and models the eddies smaller than grid scale using subgrid models.

The Navier-Stokes equations, together with energy and continuity equations, are solved with appropriate boundary conditions in order to provide the flow field for the computational domain. In this study, heat transfer and temperature gradients within the fluid domain are negligible, and the focus is on the fluid motion. As such, the energy equation is not considered. The conservation equations are presented by (Wilcox, 1998)

$$\frac{\partial \rho}{\partial t} + \frac{\partial}{\partial x_i}(\rho u_i) = 0, \tag{6.1}$$

$$\frac{\partial(\rho u_i)}{\partial t} + \frac{\partial(\rho u_j u_i)}{\partial x_j} = \frac{\partial \sigma_{ij}}{\partial x_j} - \frac{\partial p}{\partial x_i} + f_i, \tag{6.2}$$

where u is the velocity, p is the pressure, f represents the body forces, and σ is the stress tensor defined as

$$\sigma_{ij} = \mu\left(\left(\partial u_i\right)\Big/\left(\partial x_j\right) + \left(\partial u_j\right)\Big/\left(\partial x_i\right)\right) - \tfrac{2}{3}\mu\frac{\left(\partial u_l\right)}{\left(\partial x_l\right)}\delta_{ij} \tag{6.3}$$

The governing equations for LES are obtained by filtering the original continuum and Navier-Stokes equations as (Wilcox, 1998)

$$\frac{\partial \rho}{\partial t} + \frac{\partial}{\partial x_i}\left(\rho\overline{u_i}\right) = 0, \tag{6.4}$$

$$\frac{\partial(\rho\overline{u_i})}{\partial t}+\frac{\partial(\rho\overline{u_j}\,\overline{u_i})}{\partial x_j}=\frac{\partial\sigma_{ij}}{\partial x_j}-\frac{\partial\overline{p}}{\partial x_i}-\frac{\partial\tau_{ij}}{\partial x_j}. \tag{6.5}$$

In the above equations, $\overline{u}$ is the resolved velocity, σ is the stress tensor due to molecular viscosity (which is calculated from resolved velocity) and τ_{ij} is the subgrid scale stress defined as $\tau_{ij}=\rho\overline{u_iu_j}-\rho\overline{u_i}\,\overline{u_j}$. In order to close the set of equations, the Boussinsque hypothesis is used for calculating the stress tensor as (Wilcox, 1998)

$$\tau_{ij}-\frac{1}{3}\tau_{kk}\delta_{ij}=-2\mu_t\overline{S_{ij}}, \tag{6.6}$$

In above equation, μ_t is subgrid turbulent viscosity, calculated using Smagorinsky-Lilly model as $\mu_t=\rho L_s{}^2\left|\overline{S}\right|$; $\overline{S}$ is the resolved strain rate and L_s is the mixing length for subgrid length scale computed by (Wilcox, 1998)

$$\overline{S_{ij}}=\frac{1}{2}\left(\frac{\partial\overline{u_i}}{\partial x_j}+\frac{\partial\overline{u_j}}{\partial x_i}\right),$$

$$\left|\overline{S}\right|\equiv\sqrt{2\overline{S_{ij}}\,\overline{S_{ij}}}, \tag{6.7}$$

$$L_s=\min\left(\kappa d, C_sV^{1/2}\right).$$

In the above equations, κ is the von Karman factor, d is the closest distance to the walls, C_s is the Smagorinsky factor, and V denotes the volume of the computational cell. The value of the C_s has a significant effect on the large scale fluctuations in mean shear and transitional regimes. In order to address this issue, Germano et al. (1991), and then later Lilly (1992), proposed a method in which the Smagorinsky constant is calculated dynamically using the

resolved motion data. In this study, the dynamic Smagorinsky-Lilly model was applied in order to eliminate the limitations imposed by the traditional Smagorinsky-Lilly subgrid-scale model.

6.6 Validation of the model

As explained in Section 6.4, in order to validate the model, the computed pressure distribution on the blade was compared with experimental data reported by Hand et al. (2013) for a turbine inside a wind tunnel. The pressure distribution on the blade is caused by angular and axial momentum changes which characterise the wake. Thus, an accurate prediction of the pressure coefficients implies that the model can accurately estimate the near-wake pattern and its structure. Figure 6.7 shows a comparison between numerical simulations and experimental results. It is shown that the results from the LES model are a good match with the experimental data, with a maximum discrepancy of 8%. It should also be noted that in the experimental setup by Hand et al. (2001), there was a limited number of pressure taps located on the surface of the turbine blades, especially near the trailing and leading edges; hence the data is more limited than desirable. Higher discrepancies near the root of the blade can be attributed to the effect of the simplified hub and nacelle which can affect the flow and pressure field due to close proximity to these locations.

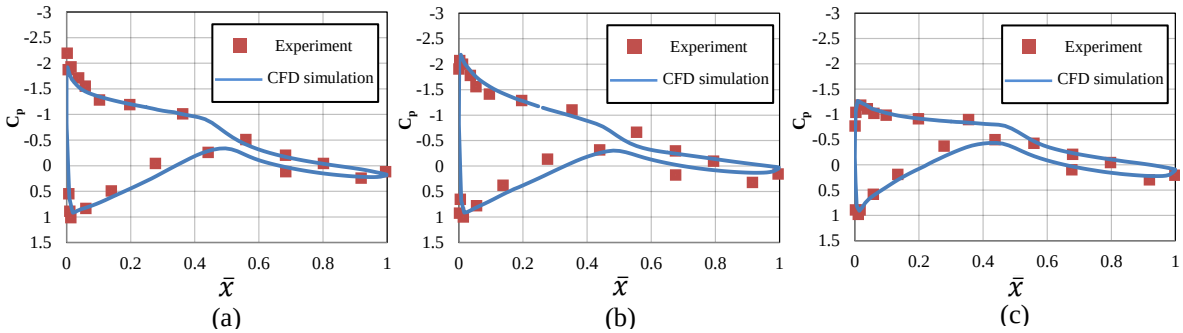

Figure 6.7 Comparison of the results of the computed pressure coefficient on the turbine blades with experiment (Hand *et al.*, 2001) for three radii, (a) *r/R*=0.3, (b) *r/R*=0.63, (c) *r/R*=0.95.

Another parameter which was used to validate the model is the total output power of the

blades. Figure 8 shows the fluctuating output power calculated using the computed torque of the blade. The averaged value of the output power obtained from simulation is approximately 5.73 (kW), which results in a 4.6% discrepancy when compared with the experimental data (Hand et al., 2001). Another indicator of the forces acting on the rotor and also extracted energy is the thrust coefficient. The momentum loss through the rotor plane is balanced by the thrust force which is manifested as a pressure drop across the rotor. The thrust coefficient is defined as $C_T = (\int (P_1 - P_2)\, dA)/(1/2\, \rho A U^2)$, with P_1, P_2, A, and U being the pressure in front of the rotor, pressure behind the rotor, area of the rotor, and velocity of the free stream, respectively ($(P_1 - P_2)$ represents the pressure difference across the rotor). The experimental thrust coefficient for the wind turbine at the wind speed of 7 m/s was found to be 0.487. The calculated thrust coefficient equals to 0.495 which shows 1.5% discrepancy from the experimental data (Hand et al., 2001).

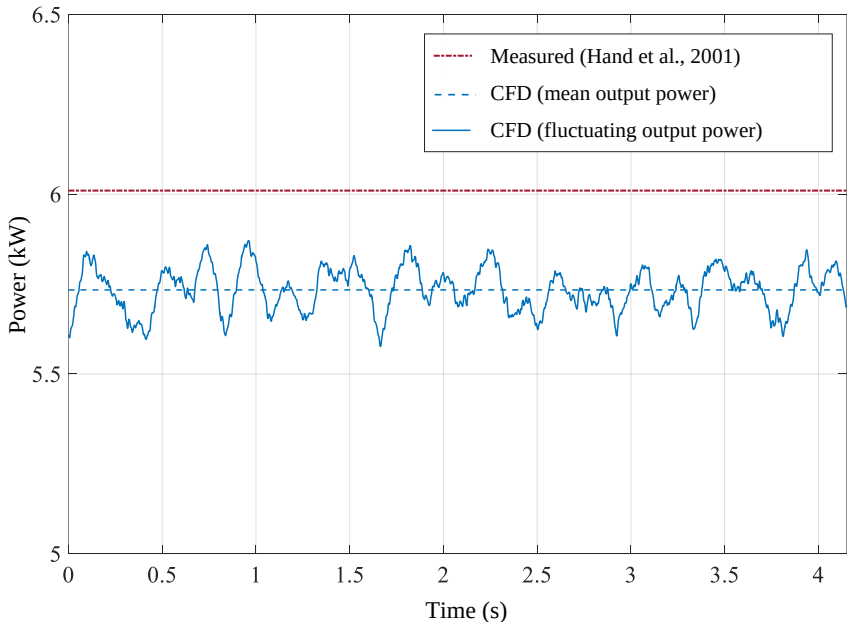

Figure 6.8 Calculated output power for confined environment compared to mean measured output power in the experiment by Hand et al., (2001). Note the non-zero origin on the power scale.

6.7 Results and discussion on SBL effects

6.7.1 Velocity in the wake region

Before presenting the results for the flow field in the wake region, it is beneficial to calculate the angle of attack along the blade length. This analysis can help to explain the interaction between the flow and the blade and the effect of partial separation of the flow on the wake development. The angle of attack along the blade varies because of the change in the relative velocity and also the twist angle from the root to the tip. The distributions of the angle of attack for both the SBL and the uniform flow cases, as well as the twist angle, are shown in Figure 6.9. Since the blade at 270° azimuthal angle (*x*-axis in Figure 2 shows the zero azimuthal angle) experiences higher velocities of the incoming flow with the power-law velocity profile, the calculated angle of attack for this blade is slightly larger than that of the blade at 90° azimuthal angle. This figure also reveals that for both the case with an SBL and for uniform flow profile, the blades work in a pre-stall condition, hence the flow is expected to be attached along the entire blade length (i.e. no stall occurs).

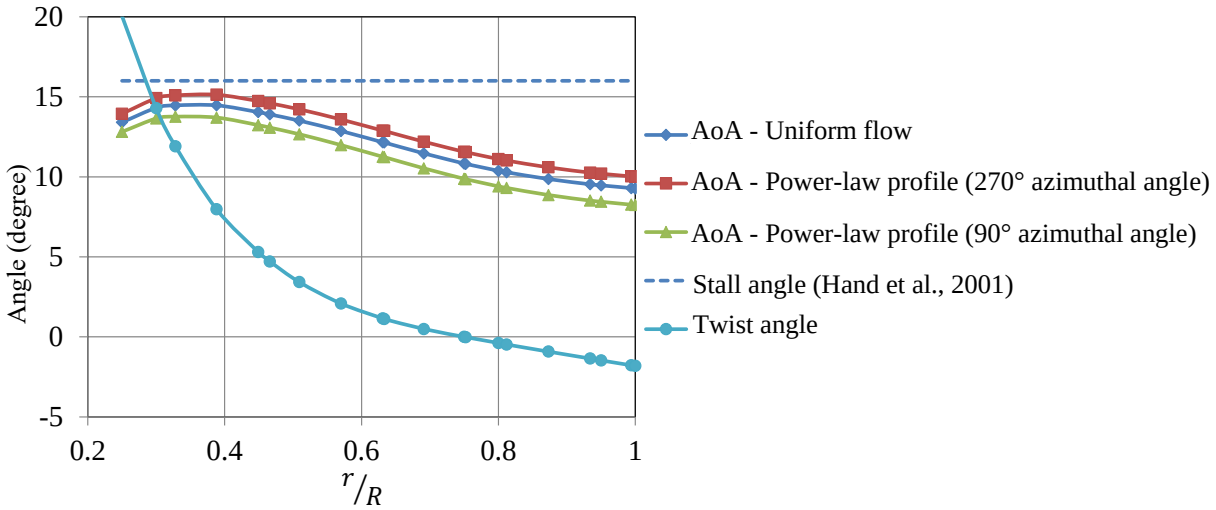

Figure 6.9 Variation of angle of attack and twist angle along wind turbine blade (*r/R*) compared to the stall angle for a S809 airfoil reported by Hand et al. (2001).

The vertical profiles of the time-averaged normalised axial velocities for several downstream locations behind the turbine are presented for both the SBL and uniform flow cases in Figure 6.10. It is evident from Figure 6.10 (b, c) that the effect of the tower exists for both cases up to 4*D* downstream, and this effect vanishes at larger distances due to wake growth and turbulent mixing. For the uniform flow profile the wake is almost axisymmetric with the axis of symmetry located close to the rotor's axis of rotation, especially for the region of the rotor itself. This phenomenon is in agreement with previously published data (Mo et al., 2013, Chamorro and Porté-Agel, 2009). The velocity profile at 1*D* (Figure 6.10 (b)) reveals an additional momentum deficit due to the existence of the tower, resulting in a lower flow velocity compared to the part of the profile above the tower ($z > 0$). Passing through the wind turbine, the flow loses its momentum showing that the turbine is extracting energy from the incoming flow and hence producing a wake. This can be observed from the regions of reduced velocity, or velocity deficit zones at *y/D*=1, where the W-shaped velocity profiles are apparent. It can also be seen that the maximum decay in velocity occurs around the blade tip location corresponding to the ring of tip vortices. A higher velocity gradient at $z > 0$ above the wake area and hence higher mixing due to the momentum influx in the SBL case results in a faster recovery when the turbine is placed in an atmospheric boundary layer. As can be seen in Figure 6-10, the effect of the wake exists up to 20*D* downstream (Figure 6.10 (f)) for the uniform flow, while the velocity deficit vanishes after 12*D* downstream for the SBL profile. In other words, the recovery occurs at 12*D* downstream when the turbine is subject to the SBL. Moreover, the smooth ground surface and mixing results in high velocity gradient close to the ground which causes a sharp change in the flow velocity in this region, hence the effect of ground boundary layer is limited to a small region close to the surface.

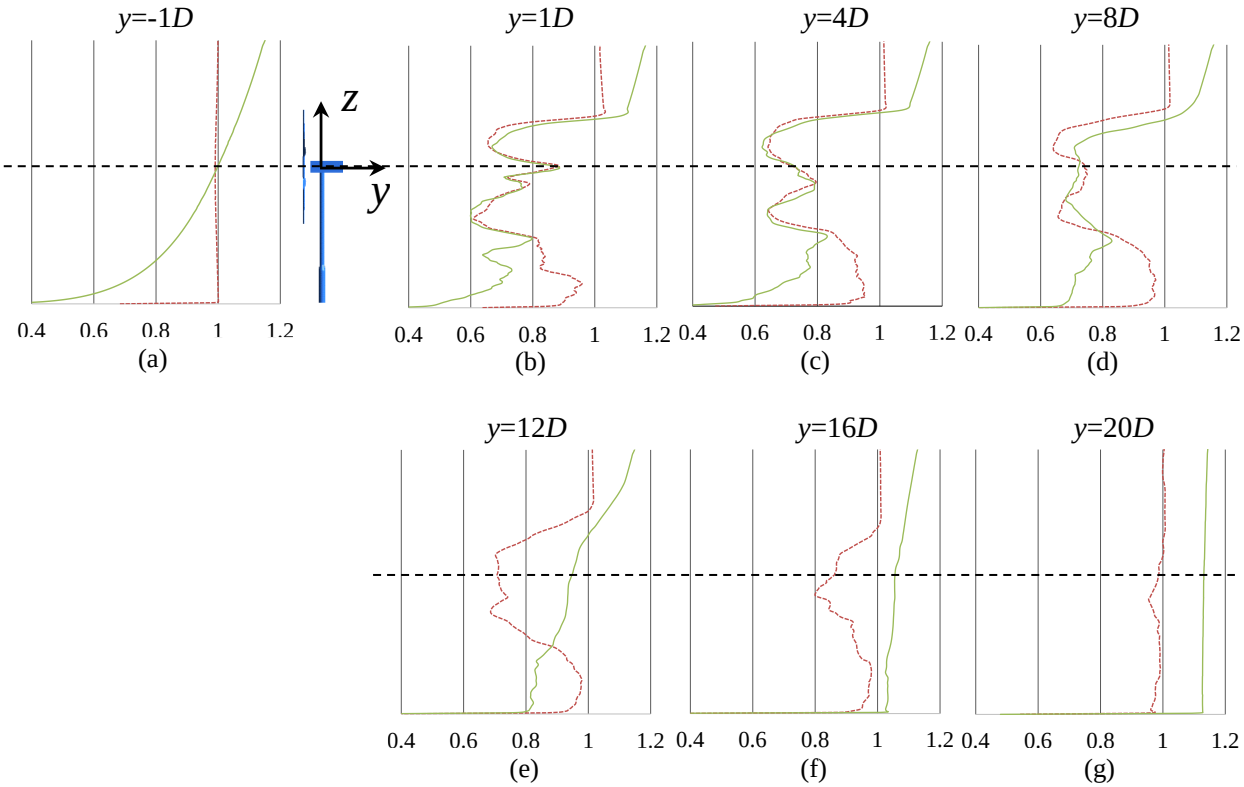

Figure 6.10 Axial normalised velocity profiles at various streamwise location (dashed line represents the uniform flow case, and solid line shows SBL case).

In order to verify that the velocity profile is present throughout the domain, the velocity profile at a distance of 12*D* longitudinal from the turbine and 8*D* lateral from the centre line as well as the velocity profile at the outlet are presented in Figure 6-11. As seen in the the velocity profile far from the wind turbine and in its wake shows power-law behaviour, with only a small deviation from the power-law velocity profile. As will be discussed later in section 5.2, the speed up in the velocity can be explained by the convection of the higher velocity fluid above the hub towards the ground due to the existence of longitudinal vortices in the boundary layer (Porteous et al., 2014, . This effect is identical to the findings by Porteous et al. (2014) who showed up to 20% speed up in the wake of a cylinder in boundary layer compared to the average velocity magnitude. As is shown on Figure 18, the downwash created due to longitudinal vortices can result in a vertical momentum influx from the high

momentum wind above the hub height into the low momentum flow in the wake and beneath the hub height.

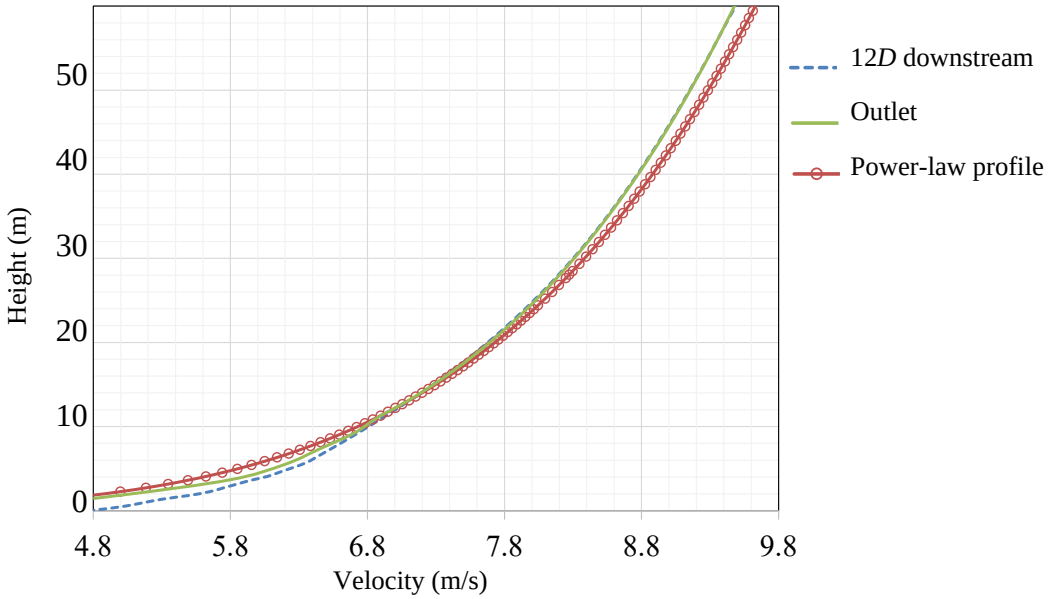

Figure 6.11 Velocity profile far from the wind turbine and at 8*D* lateral distance form center line.

Comparisons of the time-averaged axial (*y*-) velocity contours at different locations downstream of the wind turbine for both of the incoming flow profiles (i.e., uniform and SBL) are shown in Figure 6.12. Moreover, for both flow profiles the effects of the tower shadow can be observed by the relatively reduced velocities in the wake of the tower. The effect of the wake downstream of the wind turbine is evident for both cases through the low velocity circular region which corresponds to the wake surrounded by tip vortices. This structure breaks down in the SBL case much closer to the wind turbine compared to uniform flow case. It can be observed that the mixing in the flow continues after wake break-down in the SBL case (after 8*D* downstream) which results in higher axial velocity at the 20*D* section.

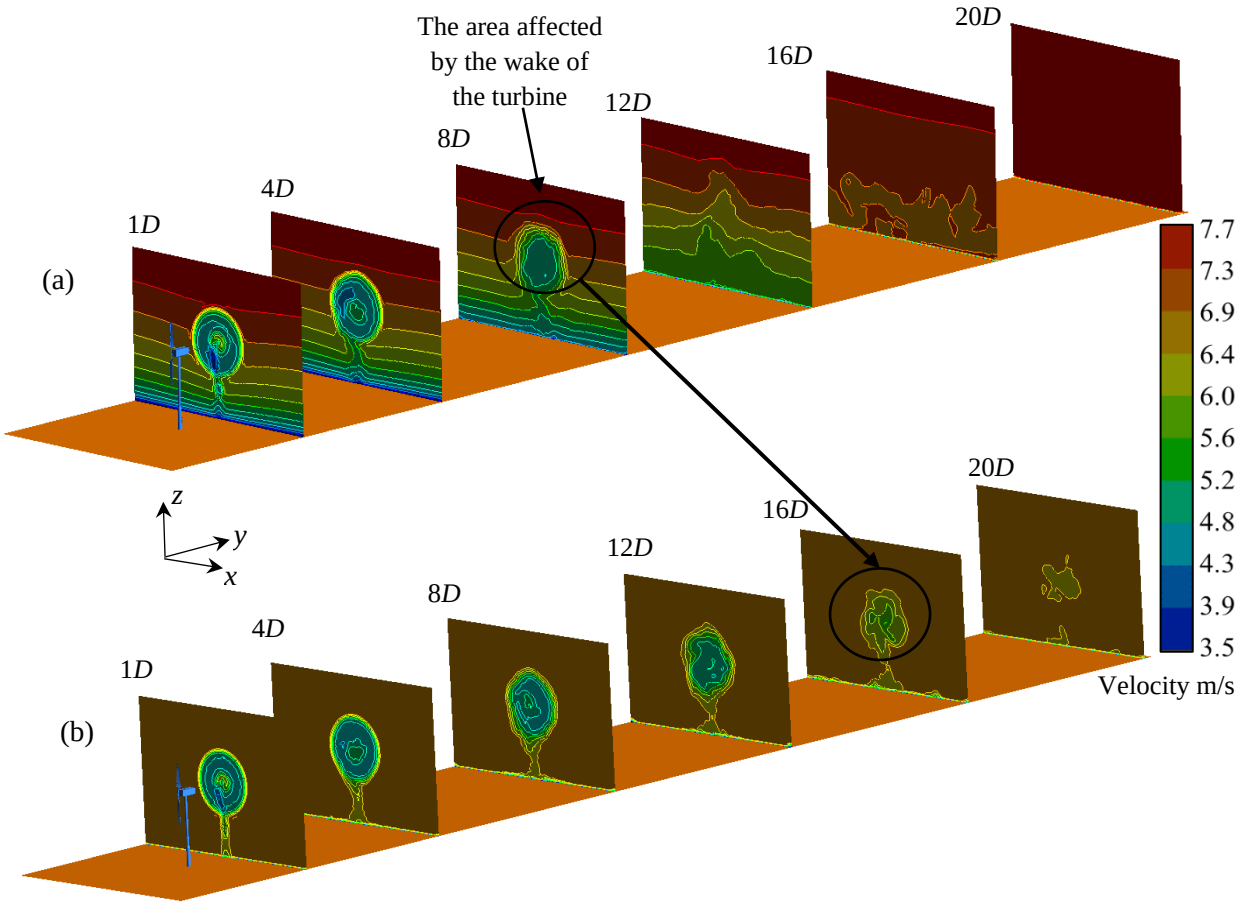

Figure 6.12 Mean axial velocity (m/s) contours, at different locations downstream of the wind turbine, a) power-law atmospheric boundary layer, b) uniform flow.

Fluctuating output power for both cases (uniform velocity profile and SBL) is shown in Figure 6.13. The average output power extracted from the blades is 5.2% higher for the uniform velocity profile when compared to the SBL case. The total fluctuating component about the mean value is calculated using the Root Mean Square (RMS) of fluctuating power. The RMS of power for the SBL profile is 13% greater than that for uniform flow, which can be attributed to the higher fluctuating loads on the blades due to the velocity gradient in the SBL. The calculated thrust coefficients in the current study are 0.47 and 0.465 for the uniform and SBL profiles, respectively. The higher thrust for the uniform velocity profile can be explained by the higher total velocity deficit, which results in a higher pressure drop across the rotor.

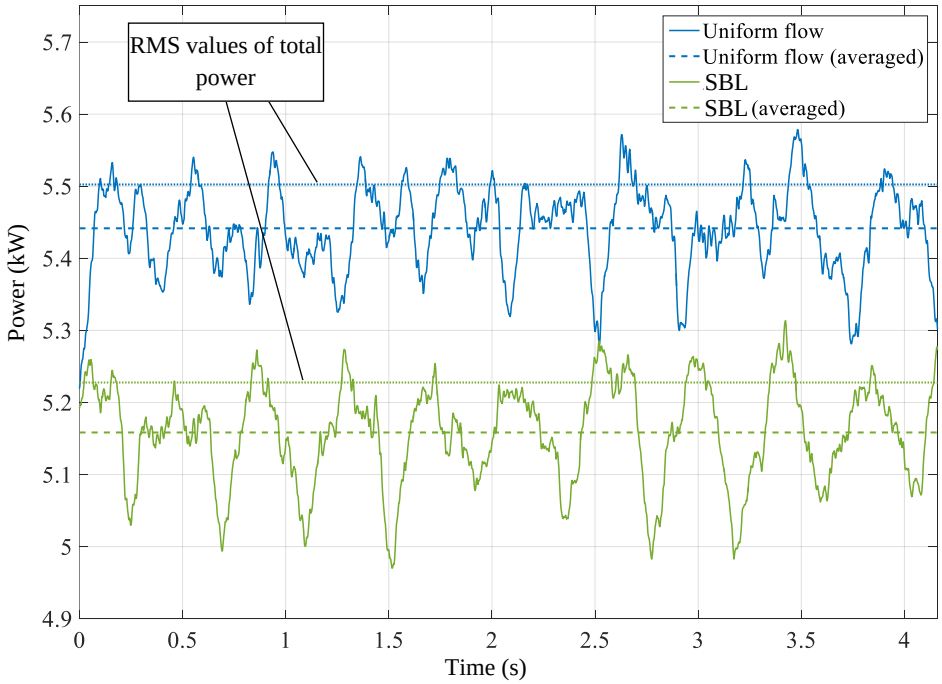

Figure 6.13 Instantaneous and average output power for uniform and ABL flow

The fast Fourier transform (FFT) of the fluctuating power is shown in Figure 6.14. The FFT analysis is conducted for the detrended (mean value removed) fluctuations of 1800 samples over 5 revolutions of the blade. Table 1 represents the fundamental frequency and the associated amplitude of the power. The fundamental frequency for both cases equals to the blade-pass frequency, showing that the fluctuations are related to the loads acting on the blade when the blade passes the region affected by the tower. The amplitude of the oscillation is 70% larger for the SBL case compared to the other case, which shows that the blades are experiencing higher fatigue loads when subject to the velocity gradient of the SBL.

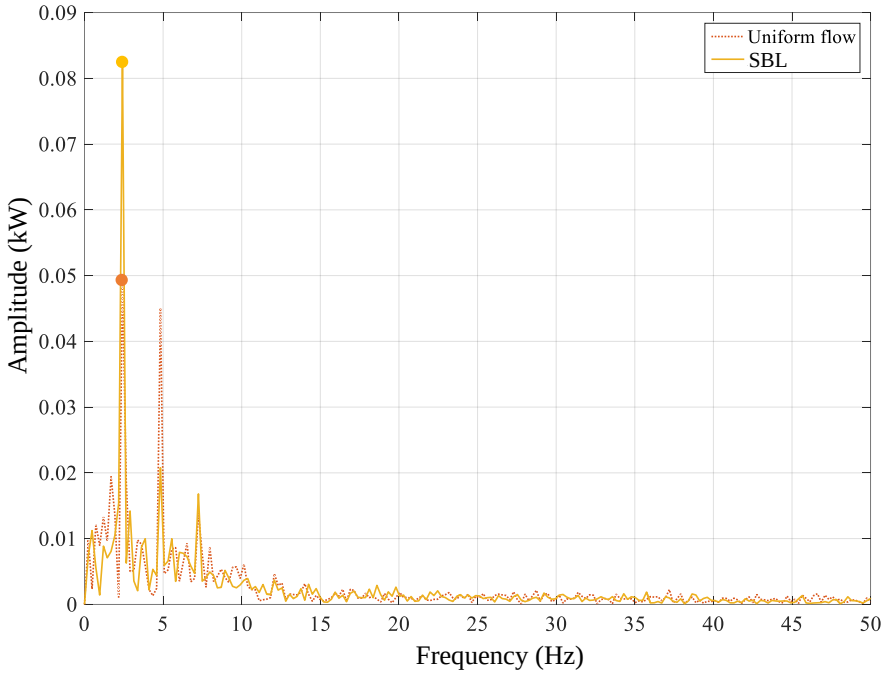

Figure 6.14 FFT of power fluctuations. Dots in the figure represent the first frequency for each case.

Table 6.1 Amplitude of the fluctuating power at the blade pass frequency.

Case	Blade pass frequency (Hz)	Amplitude (kW)
Unconfined environment	2.415	0.049
Atmospheric boundary layer	2.415	0.0825

6.7.2 Wake structure

Since wind turbines consist of rotating blades, a vortex system similar to a translating wing is expected to exist for each blade (Hansen, 2008). However, significant differences also exist due to the effect of the rotation and complex geometry of the blades (Sezer-Uzol et al., 2009). Generally, the wake region includes three types of vortices (as shown in Figure 6.15): a vortex sheet from the trailing edge of the rotor blades which travels in a helical path downstream of the rotor; strong tip vortices at the edge of the rotor wake and root or hub vortices which translate in a linear path along the rotor axis (Ivanell *et al*., 2009).

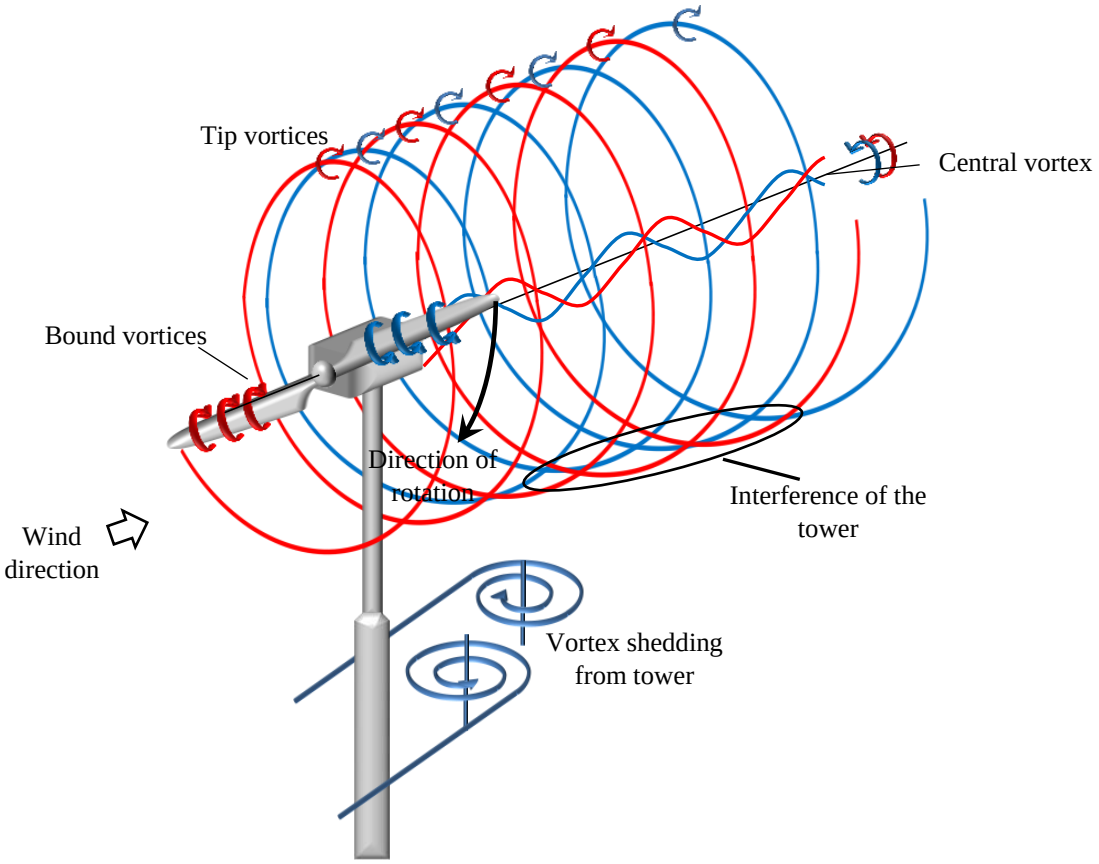

Figure 6.15 Schematic diagram of the typical vortex system downstream of a wind turbine.

The thick SBL can be considered to consist of a distribution of spanwise vortex lines which wrap around the wind turbine rotor and the tower. In the case of an obstacle of simple geometry and low aspect ratio, we can expect a pair of horseshoe vortices to form at the base of the structure and another pair to form at the free end of the structure (Adaramolaa, et al. 2006). In the case of a wind turbine, which consists of a "porous" actuator disc placed on top of a slender tower, the flow pattern can be expected to form from a similar mechanism, but the resulting flow pattern will clearly be more complex. Figure 6.16 shows a schematic diagram of the vortex lines approaching a wind turbine and wrapping around the wind turbine and tower.

The turbine rotor disc can be considered, from a macroscopic point of view, as a porous disc placed normal to the flow and immersed in a velocity gradient. The incoming vortex lines

embedded in the SBL flow will therefore wrap around the rotor disc, leading to turning and stretching of the vortex lines around the outside of the rotor's shear layer. The stretching of this vorticity will lead to a distribution of longitudinal (streamwise) vorticity on either side of the turbine wake, which in turn will induce a central downwash within the wake. The strength of the stretching will be related to the pressure drop across the rotor disc. The segments of the spanwise vortex lines impinging on the front of the turbine rotor will, of course, pass through the rotor and rotate with the rotor's wake flow downstream. The interaction of the spanwise SBL vorticity with the turbine's tower will lead to a horseshoe vortex system forming at the base of the tower, and potentially other longitudinal vortices above the base, as well as the junction between the tower and the nacelle.

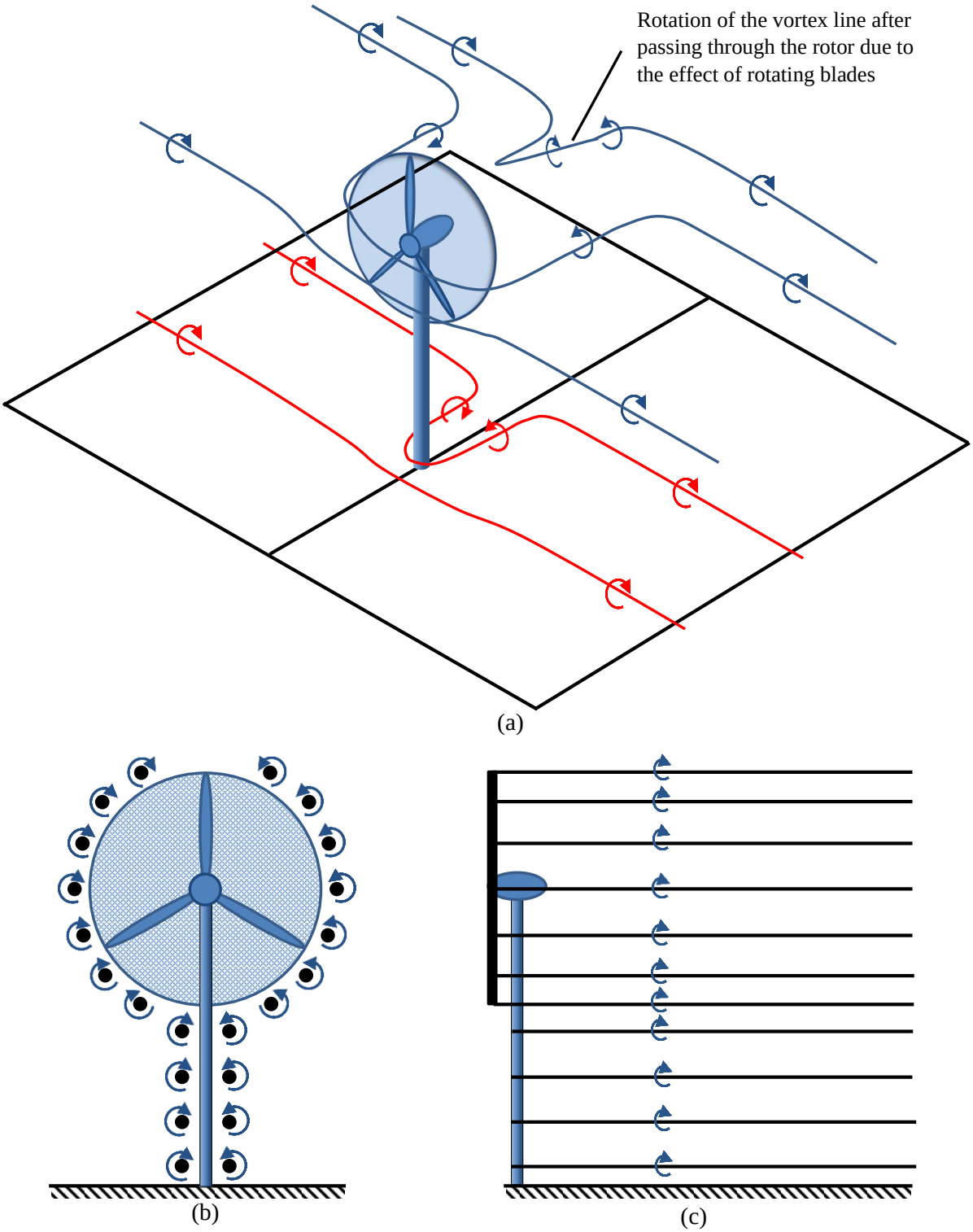

Figure 6.16 Distribution of the SBL vortex lines around the rotor and tower of the wind turbine, a) Schematic iso-view showing the spanwise vortex lines wrapping around the rotor and tower, b) Front view of the vortex line distribution, c) Side view of the turned and stretched SBL vortex lines.

It is anticipated that the effect of the turning and stretching of the SBL vortex lines will not be apparent in the near field of the turbine wake. The formation of any longitudinal vortices and the generation of a significant downwash will be affected by the gradual redistribution (by mutual induction and diffusion) and stretching of the vortex lines over a significant axial distance, and also the evolution and breakdown of the rotor shear layer. In fact, results reported below show that at y = 12*D* the SBL-generated longitudinal vortices become the dominant vortex structures within the wake, collectively leading to the rapid downward motion and lateral spreading of the wake pattern.

Figure 6.16 depicts the iso-surface of Q-criterion in the wake region. Tip, root, and bound vortices can be seen in the plots. A comparison between Figure 6.17(a) and Figure 6.17(b) shows that the tip vortices start to break down closer to the wind turbine in the case of uniform flow in comparison with the SBL conditions. Figure 6.17(a) shows fewer turbulent structures in the SBL domain compared to uniform flow case, especially within the region below the wake of the rotor. This can be explained by lower kinetic energy of the flow beneath the rotor in SBL case, which results in a lower velocity deficit by the wake of the tower and also lower velocity gradient in the shear layer created between the rotor wake and the ground. Figure 6.17(b) also shows that turbulent structures are present in the wake up to $y = 20D$ in the uniform flow case.

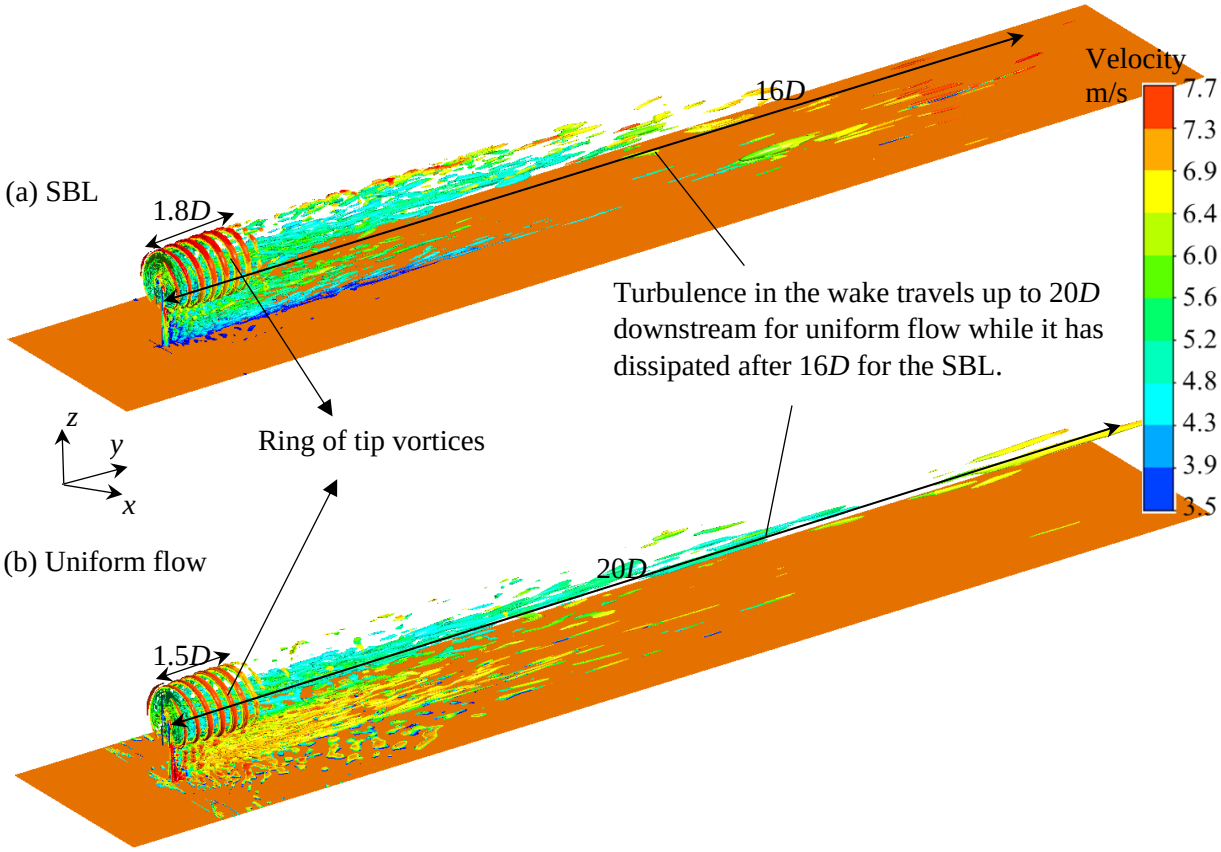

Figure 6.17 Iso-surface of instantaneous normalized Q-criterion, coloured by axial velocity magnitude, showing the vortical structures in the wake region.

The effect of the SBL on the vorticity pattern is depicted in Figure 6.18(a) and compared with the uniform flow case of Figure 6.18(b). For both cases, the vorticity contours show a strong ring of helical tip vortices immediately downstream of the turbine. The ring of tip vortices is visible up to 8*D* downstream for the uniform flow case. Further downstream, the pattern starts to break down so that there is no distinct ring of vortices visible, which can also be seen in Figure 6.17. The rings are more persistent and stronger in the SBL case in the near-wake region up to 4*D*, as shown in Figure 6.17. The expansion rate of the helical ring is higher for SBL case after 4*D*, resulting in a 20% larger diameter in this case when comparing the vorticity contours at 7*D*. The most significant difference between the flow structures can be seen after 12D in the SBL case, where the vortical structures in the wake are rapidly convected toward the ground, after which they spread and dissipate (most likely

through annihilation of vorticity of opposite sign), leaving little trace of any wake vorticity at 20*D*. This also explains higher velocity content at 20*D* and small changes in the axial velocity in Figure 6-12 (i.e. the velocity variation is not large enough which results in almost one colour band in the figure at this distance). In the uniform flow case, the vortical structures continue to convect downstream at approximately constant height while they dissipate at a significantly lower rate compared to the SBL case.

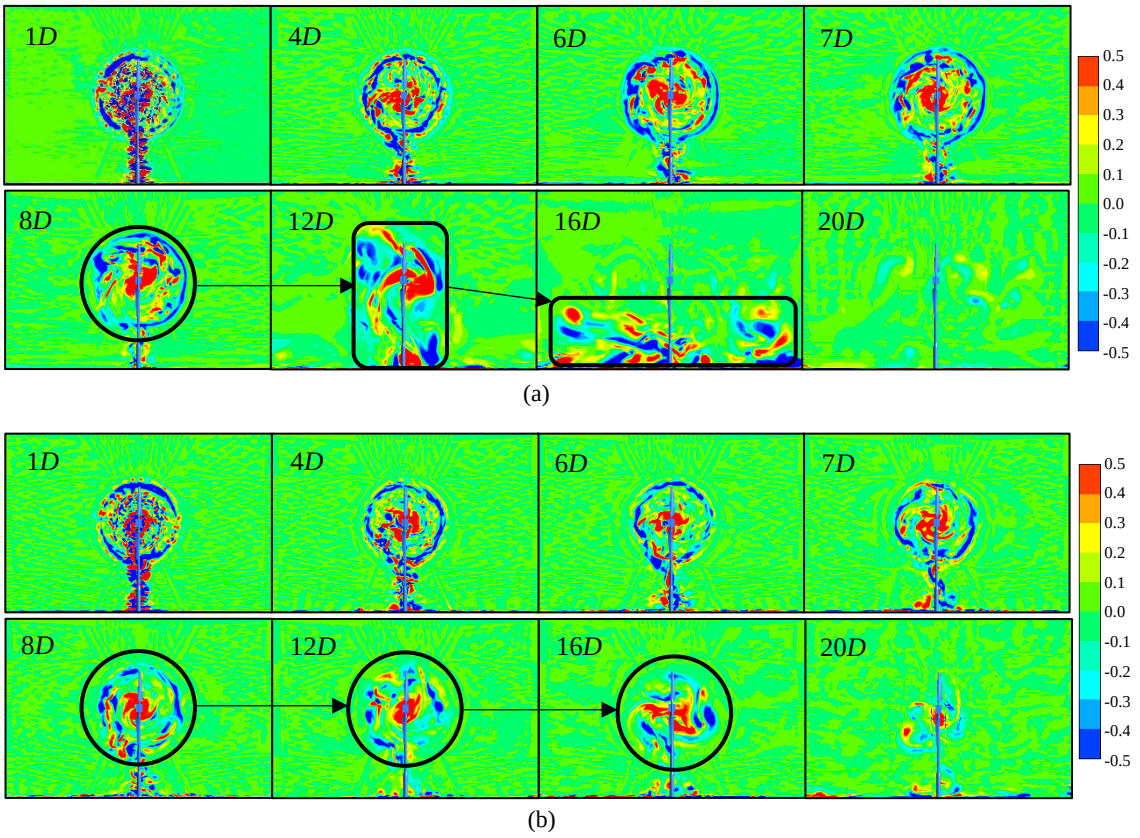

Figure 6.18 Contours of axial vorticity at different locations downstream of the wind turbine; (a) SBL; translation and collapse of the wake vortical structures, (b) Uniform flow; translation and dissipation of the wake vortical structures.

Further insights into this process are provided by the instantaneous (at the end of the fortieth revolution) and mean vertical velocity component (as mentioned in section 6.4, time averaged data is obtained over last 10 revolutions of the blade) on the axis of rotation, depicted in Figure 6.19 (a) and (b) respectively. Both of the figures show fluctuations in the vertical component of the velocity in the near-wake region which is caused by complex

vortical structures due to the effect of the nacelle, tower and rotating blades. These structures are apparent in Figure 6.18 for both cases up to 12D. However, the fluctuation for the SBL case vanishes further downstream, which is shown to be caused by fluid from above the wake being convected downwards into the wake region. It would appear that at $y = 12D$ the longitudinal vortices associated with the vorticity originating in the SBL become the dominant vortex structures within the wake, leading to the rapid downward motion and lateral spreading and dissipation of the vortical wake pattern further downstream.

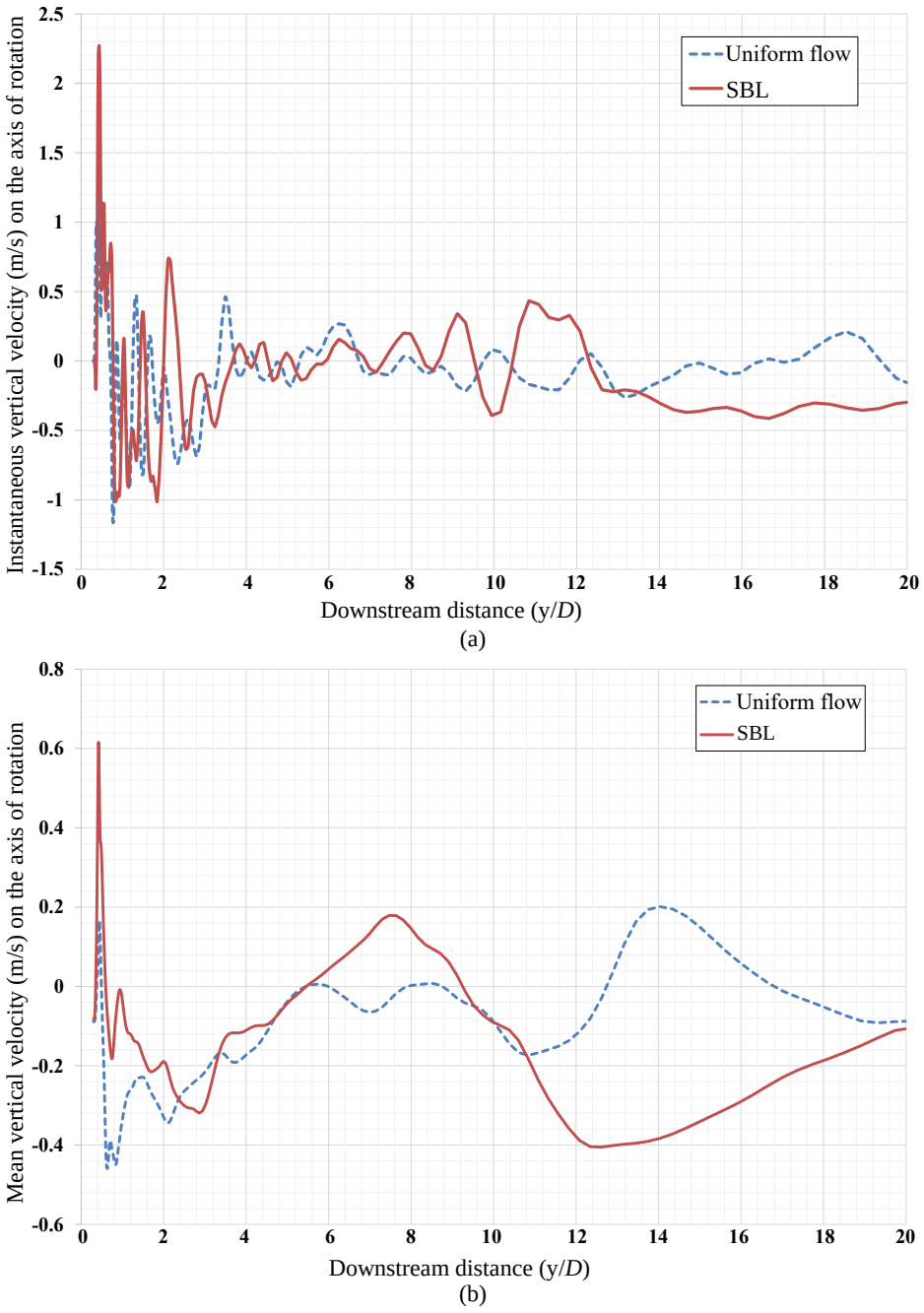

Figure 6.19 Vertical velocity component on the axis of rotation downstream of the wind turbine for both ABL and uniform flow cases, (a) Instantaneous vertical velocity, (b) Mean vertical velocity.

Figure 6.20 shows the vorticity contours overlaid with the in-plane velocity vector field 14*D* downstream of the wind turbine. The downwash is clearly visible in the SBL case at 14*D*, where there is a strong downward velocity component. As a result, the turbulent structures in the wake are convected towards the ground plane and high-momentum fluid is drawn downwards into the wake region from above. The significance of this process can be seen in

Figure 6.10 where the momentum in the wake is shown to exceed the momentum of the original SBL profile after 16*D*.

The axial circulation contained within the turbine wake at different cross sections is shown in Figure 6.21. This was evaluated within contours enclosing the wake on either side of the centreline of the flow. In this way, the macroscopic effect of the complex pattern of vortices in the wake can be assessed. The results show that the circulation is almost symmetrical for the left and right sides of the cross sections for both cases. The slight asymmetry in the near field (y < 4D) is probably caused by the rotation of the rotor. It can be seen in Figure 6.21 that the magnitude of the circulation on either side of the wake is almost constant for uniform flow case, and its sign indicates that a small downwash exists throughout the wake, which is broadly consistent with the downwash distributions presented in Figure 6.19. However, in the SBL case the initial circulation is consistent with a small but increasing upwash, followed by a sudden reversal in the sign of the circulation, beginning at y = 12*D*. The peak circulation occurs at y = 14*D*, after which the circulation decays rapidly. The sudden downwash and the subsequent annihilation of the wake vorticity are consistent with the observed behaviour of the wake described in Figure 6.18 and the downwash distributions of Figure 6.19. The process of annihilation is likely to be due to a viscous interaction of the wake vortices with the ground plane, leading to the generation of vorticity of opposite sign, as described by Harris and Williamson (2012) and Lim et al. (1991) for the canonical flow cases of axial and ring vortices.

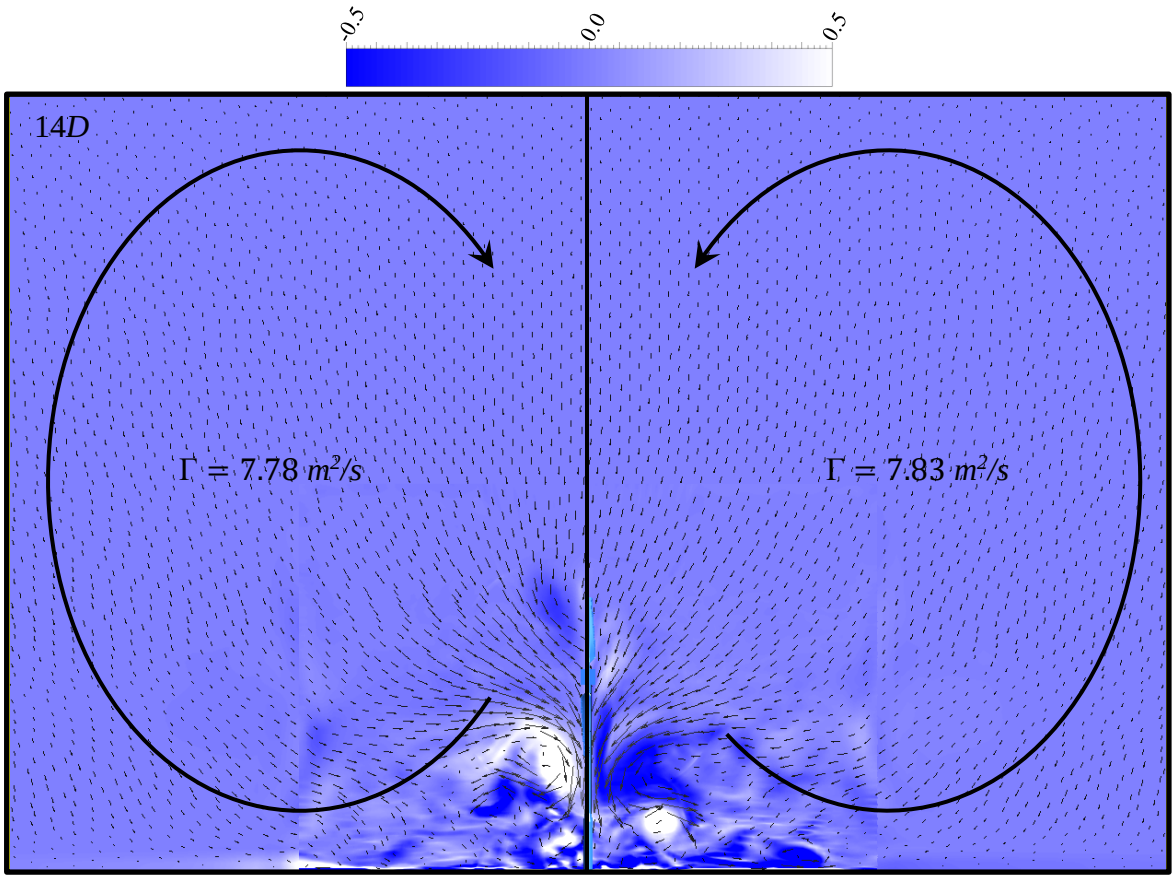

(a)

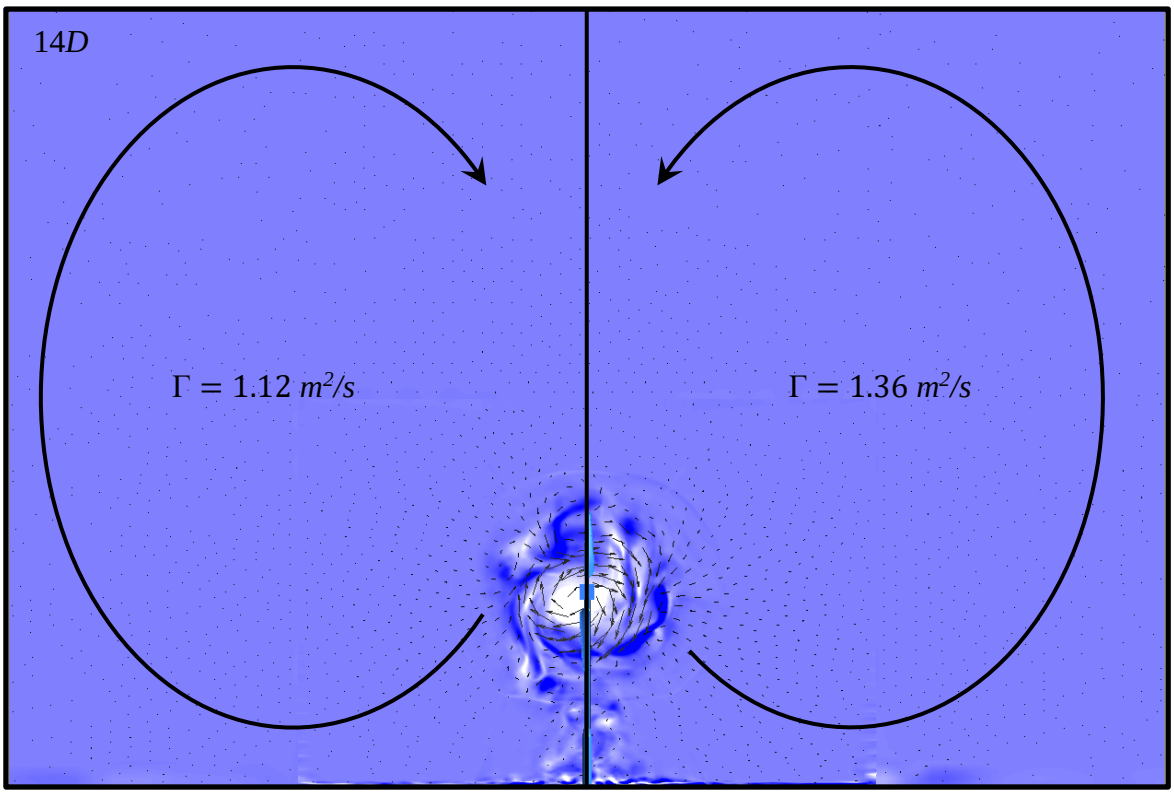

(b)

Figure 6.20 Overlapped vorticity contours with overlapped velocity vectors at several cross sections downstream of the wind turbine, (a) SBL, (b) Uniform flow. Existence of downwash in SBL case is evident when two cases are compared.

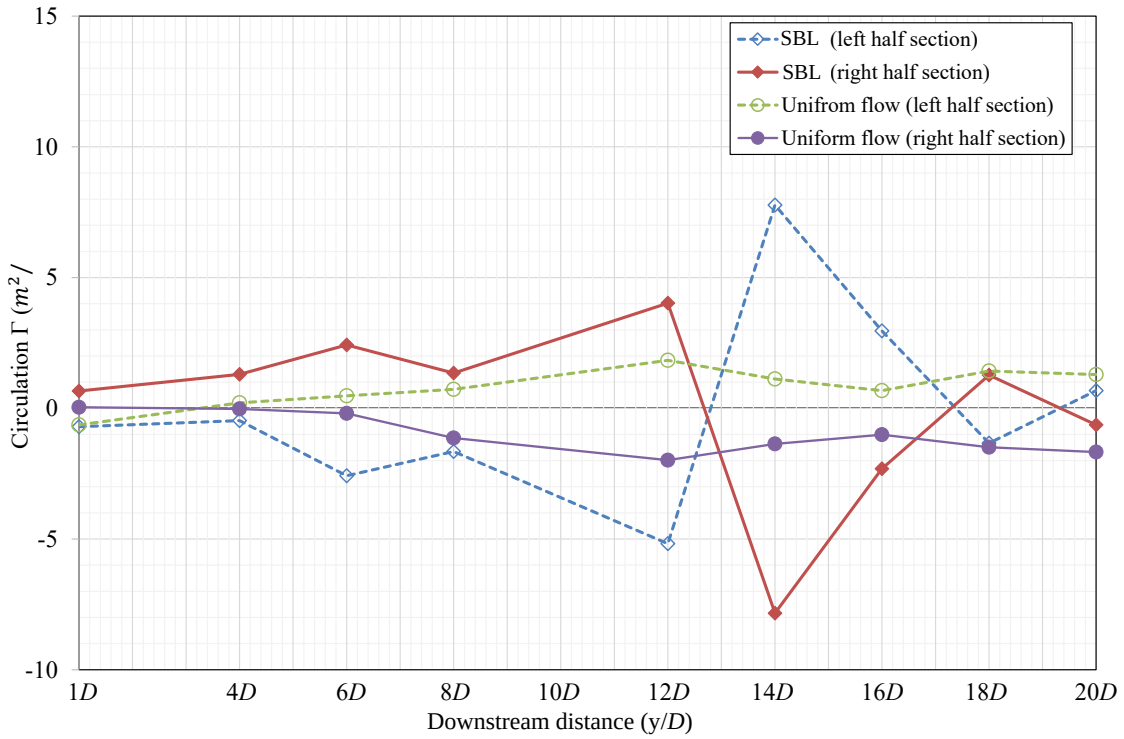

Figure 6.21 Axial circulation variation downstream of the wind turbine on a $\boldsymbol{7.3D \times 4.9D}$ section. This section is selected in a way to insure that all the vortical structures in the wake is included in the section in order to account for their effect in calculation.

Figure 6.22 shows the vorticity contours for both the SBL and uniform velocity profiles through the horizontal and vertical midsections. Although the helical tip vortices are distinct in the near field, they rapidly break down to form an incoherent pattern of axially-oriented vortices which can be traced up to 16*D* downstream for the uniform flow, while this trail vanishes after 12*D* downstream of the turbine in the SBL condition. These results are again consistent with the presence of a strong downwash in SBL case, leading to the rapid distortion and annihilation of the wake vorticity in the far field and the induction of high velocity fluid down into the wake.

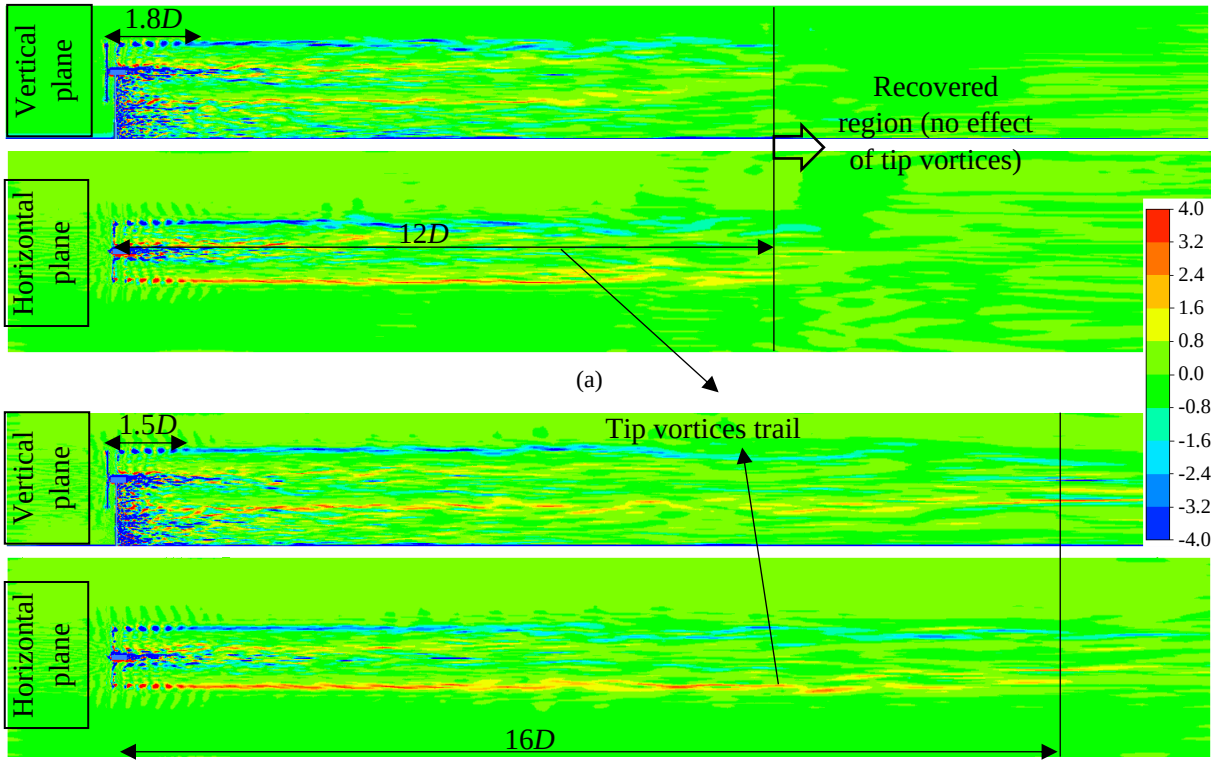

Figure 6.22 Vorticity contours on vertical and horizontal planes through the axis of rotation, showing the tip vortices convecting downstream; a) In the presence of the SBL profile, b) In the presence of uniform flow).

In the near field in Figure 6.22, the helical tip vortices (as illustrated schematically in Figure 6.15) are distinctly visible up to 1.5*D* downstream of the rotor plane in both cases when the horizontal mid-plane is considered. In the vertical plane the tip vortices at the top of the wake are seen to remain coherent for a larger distance in the SBL case, which is consistent with a higher velocity above the wake region in this case in comparison with uniform flow case. The wake expansion in the near field is depicted in Figure 6.23 using the locations of the tip vortices for the cases of the SBL and uniform profiles on the horizontal plane. The results show a 2% higher expansion rate for the uniform flow case when compared to SBL flow, which suggests that the incoming SBL velocity profile suppresses the wake development. Visual inspection of Figure 6.18 also shows this to be the case. This may be partially explained by the turning and differential stretching which occurs in the helical vortex pattern due to the velocity gradient in the smooth boundary layer. This is also consistent with the

larger computed C_t which leads to a larger axial velocity deficit and a greater shear, which in turn result in a higher expansion rate. The effect of the SBL velocity gradient on the rings of tip vortices is evident in the detailed view of Figure 6.24, where the rings of vortices in the SBL case are shown to rotate as they translate downstream as a result of the mean shear of the SBL profile.

The above observations also explain some of the differences in the measured axial circulation distributions of the wake as discussed earlier. The continued turning and stretching of the helical vortex pattern under the influence of the SBL velocity gradient will lead to components of rotor-tip vorticity aligned with the mean flow on either side of the wake, of a sign that is consistent with an upwash on the centreline of the wake. A similar process was described by Perry & Lim (1978) to explain the formation of streamwise vortices in a buoyant co-flowing wake. Referring to Figure 6.21, we see that the circulation strength increases monotonically up to y = 12*D*, consistent with the continuous realignment of the vorticity within the rotor shear layer. Vertical velocities in the wake are also consistent with this. Note that for $y < 4D$ in both the uniform flow and SBL cases, the vertical velocities in the wake are consistent in magnitude and sign, which suggests that they are due mainly to the wake behind the tower and nacelle.

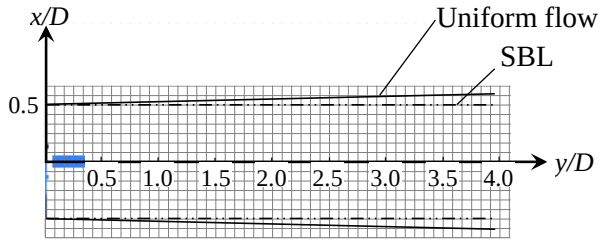

Figure 6.23 Comparison of wake expansion between SBL and uniform profiles, based on the location of tip vortices (wake expansion extended in order to better show the difference in wake expansion growth rate).

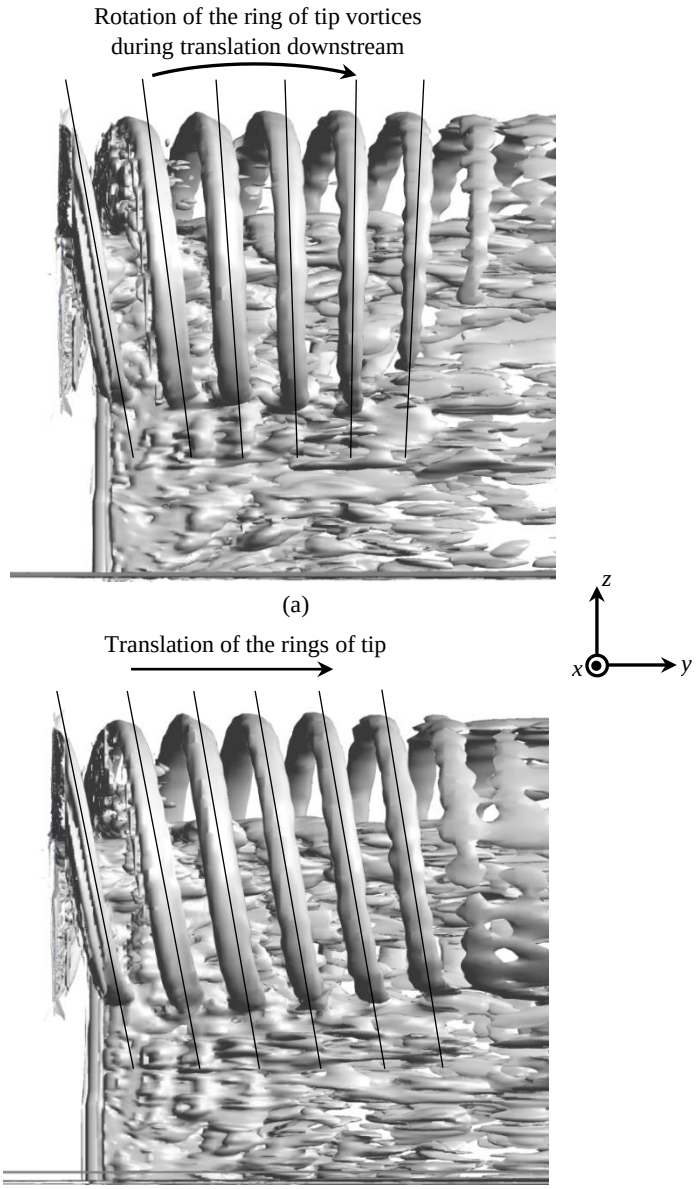

Figure 6.24 Iso-surface of instantaneous vorticity, a) Translation and rotation of the rings of tip vortices in the *presence* of the SBL, b) Translation of the rings of tip vortices in the *presence* of uniform flow.

6.8 Conclusions

A series of numerical simulations was performed in order to investigate the effect of an SBL profile on the wake of the NREL Phase VI wind turbine. A power-law velocity profile was used to model the atmospheric boundary layer. A Large Eddy Simulation model was developed in order to understand the wake development, its recovery and velocity deficit behind the wind turbine.

In the near field, the study has identified the effect of mean shear in the incoming ABL flow on the initial development of the helical vortex structure, whereby the helical vortices in the shear layer tilt in the direction of the mean shear. Qualitative observations of the helix visualized using the Q-criterion suggest that at hub height the distance to breakdown is the same for both flow cases, but at the top of the helix the higher velocity above the shear layer leads to the helix being stretched and a larger distance to breakdown in the SBL case. A higher rate of velocity decay is also observed on the upper side of the shear layer in the SBL case. In spite of these differences, the rate of growth in the wake diameter is suppressed by the mean shear in comparison to the uniform flow case.

Visualization of the initial tip vortex rollup (Figure 6.24) shows that the mean shear of the SBL leads to the rotation of the helical vortex pattern. The continued turning and stretching of the helical pattern leads to components of vorticity aligned with the mean flow on either side of the wake, leading to an upwash on the centreline of the wake up to $y = 12D$. The initial downwash in the near-wake region ($y < 4D$) is probably associated with the nacelle and tower.

In the far wake the effect of the shear in the SBL case is much more significant. In the uniform flow case the rotor shear layer, having broken down to a turbulent structure in the near field, continues to decay downstream by the mechanisms of turbulent mixing, dissipation and cross-annihilation of vorticity. However, in the SBL case the wake undergoes a significant change in structure at $y = 12D$, at which point the wake is driven downwards towards the ground plane by a strong downwash. Profiles of the mean and instantaneous vertical velocity component on the turbine centreline support this observation, as does the mean axial component of circulation on either side of the wake. The effect of the wake being driven towards the ground plane is twofold. Firstly, the interaction leads to a

reduction in the mean axial circulation on either side of the wake. This is likely to be due to a viscous interaction with the ground plane, leading to the generation of vorticity of opposite sign, and the resulting annihilation of the streamwise vorticity. Secondly, the downwash leads to high-momentum fluid from above the turbine being transported downwards into the wake region, leading to the wake momentum far exceeding that of the original SBL profile after 16*D*. It can be concluded from this study that a second downstream turbine can generate greater power in a smooth boundary layer if it is placed beyond 12*D* downstream of the first turbine, since it experiences equivalent or higher kinetic energy than the incoming flow.

A major outcome of this study is study is the proposed mechanism that explains how the SBL contributes to the significant differences in flow structure and recovery rate. The mechanism recognises that the SBL can be described as a layer containing a series of spanwise vortex lines, which are turned and stretched by the presence of the (porous) rotor, nacelle and tower, leading to the generation of additional axial vorticity in the wake. The evolution of the wake is governed by a balance between the turning and stretching of the helical vortices in the rotor shear layer, leading to upwash in the centre of the wake, and the turning and stretching of the boundary layer vortex lines, leading to a downwash in the centre of the wake. The axial location where the downwash becomes dominant will depend on the operating condition of the turbine, as this will control the relative strengths of the helical tip vortices and the circulation available from the SBL. Further study will, no doubt, shed more light on this complex interaction.

The present study also reveals that, despite the higher velocity magnitude above the hub height for the SBL case, the total output power is lower when compared to the uniform flow. This may be caused by the lower energy in the wind below the hub height which results in a lower total generated power. On the other hand, the amplitude of the fluctuating power was

70% larger when the turbine was placed in the atmospheric boundary layer, which suggests higher fluctuating load on the blades. This is due to the strong shear in the ABL case which causes the blade to face a fluctuating velocity magnitude during each revolution.

The results of this study can be used by researchers and wind farm designers to understand the effect of the environment and atmospheric boundary layer on the wind turbine operation and performance and to develop a “toolbox” which can take all of these parameters into account. These parameters were found to have a significant effect on the wake development and consequently will affect the performance of wind turbines and wind farms. However, further work is required prior to implication of the current outcomes, in order to account for different parameters in atmospheric boundary layer such as turbulent intensity, turbulent length scale, and temperature gradient.

6.9 References

Adaramola, M. S., Akinlade, O. G., Sumner, D., Bergstrom, D. J. & Schenstead, A. J., 2006, Turbulent wake of a finite circular cylinder of small aspect ratio, *Journal of Fluids and Structures*, **22**, 919-928.

Bai, C. J. & Wang, W. C., 2016, Review of computational and experimental approaches to analysis of aerodynamic performance in horizontal-axis wind turbines (HAWTs), *Renewable and Sustainable Energy Reviews,* **63**, 506-519.

Blomhoff, H. P. 2012. *An experimental investigation of wind turbine wakes.* Master of Science in Product Design and Manufacturing, Norwegian University of Science and Technology.

Chamorro, L. P., Guala, M., Arndt, R. E. A. & Sotiropoulos, F., 2012, On the evolution of turbulent scales in the wake of a wind turbine model, *Journal of Turbulence*, **13**, 1-13.

Chamorro, L. P., Hill, C., Morton, S., Ellis, C., Arndt, R. E. A. & Sotiropoulos, F., 2013, On the interaction between a turbulent open channel flow and an axial-flow turbine, *Journal of Fluid Mechanics*, **716**, 658-670.

Chamorro, L. P. & Porté-Agel, F. 2009. A wind-tunnel investigation of wind-turbine wakes: Boundary-layer turbulence effects. *Boundary-Layer Meteorology,* **132,** 129-149.

Choudhry, A., Mo, J. O., Arjomandi, M. & Kelso, R., 2014, Effects of Wake Interaction on Downstream Wind Turbines, *Wind Engineering*, **38**, 535-548.

Cleijne, J. W. 1993. Results of Sexbierum Wind Farm; single wake measurements. TNO Institute of Environmental and Energy Technology, Technical report.

Crespo, A., Hernández, J. & Frandsen, S. 1999. Survey of modelling methods for wind turbine wakes and wind farms. *Wind Energy,* **2,** 1-24.

Elliott, D. L. 1991. Status of wake and array loss research. *Windpower Conference,* Palm Springs, California.

Germano, M., Piomelli, U., Moin, P. & Cabot, W. H. 1991. A dynamic subgrid-scale eddy viscosity model. *Physics of Fluids A*, **3,** 1760-1765.

Grant, I. & Parkin, P., 2000, A DPIV study of the trailing vortex elements from the blades of a horizontal axis wind turbine in yaw, *Experiments in Fluids*, **28**, 368-376.

Hand, M. M., Simms, D. A., Fingersh, L. J., Jager, D. W., Cotrell, J. R., Schreck, S. & Larwood, S. M. 2001. Unsteady aerodynamics experiment phase VI: Wind tunnel test configurations and available data campaigns. National Renewable Energy Laboratory, Report of experiment.

Hansen, M. O. L., 2008, *Aerodynamics of Wind Turbines*, Second edition, Earthscan, London. Sterling, VA.

Harris D. M. & Williamson C. H. K., 2012, Instability of secondary vortices generated by a vortex pair in ground effect. *Journal of Fluid Mechanics*, **700**, 146-186.

Ivanell, S. S. A., 2009, Numerical computations of wind turbine wakes, Technical report, Royal Institute of Technology, Linn´e Flow Centre, Department of Mechanics, Stockholm, Sweden.

Jimenez, A., Crespo, A., Migoya, E. & Garcia, J. 2007. Advances in large-eddy simulation of a wind turbine wake. *Journal of Physics: Conference Series,* **75,** 012041.

Jimenez, A., Crespo, A., Migoya, E. & Garcia, J. 2008. Large-eddy simulation of spectral coherence in a wind turbine wake. *Environmental Research Letters,* **3,** 015004.

Kinzel, M., Araya, D. B. & Dabiri, J. O. 2015. Turbulence in vertical axis wind turbine canopies. *Physics of Fluids,* **27,** 115102.

Kloosterman, M. H. M. 2009. *Development of the near wake behind a horizontal axis wind turbine.* Master of Science Thesis, Delft University of Technology.

Lilly, D. K. 1992. A proposed modification of the Germano subgrid-scale closure method. *Physics of Fluids A,* **4,** 633-635.

Lim, T. T., Nickels, T. B. & Chong, M.S., 1991. A note on the cause of rebound in the head-on collision of a vortex ring with a wall. *Experiments in fluids*, **12**, 41-48.

Liu, M.-K., Yocke, M. A. & Myers, T. L. 1983. Mathematical model for the analysis of windturbine wakes. *Journal of Energy,* **7,** 73-78.

McTavish, S., Feszty, D. & Nitzsche, F., 2013, An experimental and computational Assessment of blockage effects on wind turbine wake development, *Wind Energy*, **17**, 1515-1529.

Mo, J. O., Choudhry, A., Arjomandi, M., Kelso, R. & Lee, Y.-H. 2013. Effects of wind speed changes on wake instability of a wind turbine in a virtual wind tunnel using large eddy simulation. *Journal of Wind Engineering and Industrial Aerodynamics,* **117,** 38-56.

Perry, A. E., and Lim, T. T., 1978, Coherent structures in co-flowing jets and wakes, *Journal of Fluid Mechanics,* **88**, 451–463.

Porteous, R., Moreau, D. J., Doolan, C. J. & Prime, Z. 2014. Wake dynamics of circular finite wall-mounted cylinders in different boundary layers. 19*th Australasian Fluid Mechanics Conference*. Melbourne, Australia.

Sanderse, B. 2012. Aerodynamics of wind turbine wakes. Energy research Centre of the Netherlands, Literature review report.

Schepers, J. G. & Snel, H., 2007, Model experiments in controlled conditions, The Energy Research Center of the Netherlands (ECN), Final repot, ECN-E-07-042.

Snel, H., Schepers, J. G. & Montgomerie, B. 2007. The MEXICO project (Model Experiments in Controlled Conditions): The database and first results of data processing and interpretation. *Journal of Physics: Conference Series*, 75, 012014.

Sezer-Uzol, N., Gupta, A. & Long, L. N., 2009, 3-D Time-Accurate Inviscid and Viscous CFD Simulations of Wind Turbine Rotor Flow Fields, in Parallel Computational Fluid Dynamics 2007, Springer Berlin Heidelberg, **67**, 457-464..

Sherry, M., Sheridan, J. & Jacono, D., 2013, Characterisation of a horizontal axis wind turbine's tip and root vortices, *Experiments in Fluids*, **54,** 1-19.

Schümann, H, Pierella, F & Sætran, L 2013, Experimental investigation of wind turbine Wakes in the wind tunnel, *Energy Procedia*, **35**, 285-296.

Sørensen, J. N. 2016. *General momentum theory for horizontal axis wind turbines*, Springer.

Troldborg, N., Sørensen, J. N. & Mikkelsen, R., 2007, Actuator line simulation of wake of wind turbine operating in turbulent inflow, *Journal of Physics*: Conference Series, **75**, 012063.

Watters, C. S., Breton, S. P. & Masson, C., 2010, Application of the actuator surface concept to wind turbine rotor aerodynamics, *Wind Energy*, **13**, 433-447.

Wharton, S. & Lundquist, J. K. 2012. Assessing atmospheric stability and its impacts on rotor-disk wind characteristics at an onshore wind farm. *Wind Energy,* **15,** 525-546.

Wilcox, D. C., 1998, *Turbulence modeling for CFD*, Second edition, DCW Industries.

Wilson, J. M., Davis, C. J., Venayagamoorthy, S. K. & Heyliger, P. R. 2014. Comparisons of horizontal-axis wind turbine wake interaction models. *Journal of Solar Energy Engineering*, **137,** 031001.

Chapter 7 Effect of wake on noise propagation

7.1 Chapter preview

The effect of noise propagation in the presence of the wake of a wind turbine operating in the atmospheric boundary layer is presented in this chapter. The CFD model explained in Chapters 5 and 6 was used to calculate the flow field and compute the pressure fluctuations on the blade surface. To calculate the sound pressure level and its propagation, the Ffowcs Williams Hawkings method was used as described in Chapter 4. The effect of atmospheric boundary layer on noise propagation was investigated by comparing the calculated dominant frequency of the noise signatures in far-field in the presence and absence of the smooth boundary layer. It was shown that the noise radiated from the blades was ducted by the wake of the wind turbine to the wake breakdown point at which the energy of the sound was transformed to the medium. Thus, based on the location of the observer in far-field, the noise might be amplitude modulated and perceived with a higher sound pressure level.

Statement of Authorship

Title of Paper	Atmospheric boundary layer effect on the wake of a wind turbine
Publication Status	☐ Published ☐ Accepted for Publication ☑ Submitted for Publication ☐ Unpublished and Unsubmitted work written in manuscript style
Publication Details	Submitted to the Journal of Renewable Energy

Principal Author

Name of Principal Author (Candidate)	Nima Sedaghatizadeh
Contribution to the Paper	- Research - Providing the data, writing of the manuscript and production of original figures - Correspondence with editor and reviewers including the production of all cover letters and rejoinder
Overall percentage (%)	
Certification:	This paper reports on original research I conducted during the period of my Higher Degree by Research candidature and is not subject to any obligations or contractual agreements with a third party that would constrain its inclusion in this thesis. I am the primary author of this paper.
Signature	Date: 14/09/2017

Co-Author Contributions

By signing the Statement of Authorship, each author certifies that:

i. the candidate's stated contribution to the publication is accurate (as detailed above);

ii. permission is granted for the candidate in include the publication in the thesis; and

iii. the sum of all co-author contributions is equal to 100% less the candidate's stated contribution.

Name of Co-Author	Maziar Arjomandi
Contribution to the Paper	- Supervision of the work, including the production of the manuscript - Participation in the development of the concepts and ideas presented in the manuscript - Evaluation and editing of the manuscript prior to submission
Signature	Date: 15/09/2017

Name of Co-Author	Richard Kelso		
Contribution to the Paper	- Supervision of the work, including the production of the manuscript - Participation in the development of the concepts and ideas presented in the manuscript - Evaluation and editing of the manuscript prior to submission		
Signature		Date	14/9/2017

Name of Co-Author	Benjamin Cazzolato		
Contribution to the Paper	- Supervision of the work, including the production of the manuscript - Participation in the development of the concepts and ideas presented in the manuscript - Evaluation and editing of the manuscript prior to submission		
Signature		Date	14/09/2017

Name of Co-Author	Mergen H. Ghayesh		
Contribution to the Paper	- Supervision of the work, including the production of the manuscript - Participation in the development of the concepts and ideas presented in the manuscript - Evaluation and editing of the manuscript prior to submission		
Signature		Date	14/09/2017

The interaction of self-noise and wake of a wind turbine

Nima Sedaghatizadeh, Maziar Arjomandi, Benjamin Cazzolato, Richard Kelso,

Mergen H. Ghayesh

School of Mechanical Engineering, the University of Adelaide, SA, 5005

Paper submitted to: Renewable Energy.

7.2 Abstract

Similar to any large structure erected in the atmospheric boundary layer, the blades of wind turbines experience varying velocity over their surface due to wind shear in the atmospheric boundary layer and incoming turbulence. Due to the temporal and spatial variation of flow structures, aerodynamically generated noise perceived from a wind turbine changes in terms of noise level and its directivity. In this study, the noise signature of an operating wind turbine in a smooth boundary layer was investigated numerically using Ffowcs Williams and Hawkings (FW-H) analogy. An embedded Large Eddy Simulation was used to computationally resolve the flow field. Results revealed that, the highest noise level in the vicinity of the wind turbine corresponds to the blade pass frequency and is due to amplitude modulation of the trailing edge noise caused by the rotation of the blade as well as blade tower interaction. However, further downstream the sound level associated with the blade pass frequency reduces and the frequency of highest noise level increases compared to blade-pass frequency. Results also showed peaks in the overall sound pressure level downstream of the wind turbine which is hypothesized to be related to the collapse of the wake and sudden release of sound energy. Moreover, there are greater fluctuations in the overall sound pressure level in the presence of the boundary layer when compared with the uniform flow case.

7.3 Introduction

Wind turbines are relatively new source of environmental noise which has been known to affect the attitude of communities towards wind farms and development of wind energy (Iachini et al. 2012; Pawlaczyk-Luszczynska et al. 2013; Pedersen, E. et al. 2008; Pedersen, E, Hallberg & Waye 2007; Shepherd, Hanning & Thorne 2012; Waye & Öhrström 2002). This typically becomes an issue when wind farms are constructed close to populated rural

areas (Sedaghatizadeh et al., 2017). Thus, accurate prediction of the noise generation and its propagation from wind turbines is of high importance for communities and wind farm developers.

Wind turbine noise can be divided into two main categories based on the nature of the generated noise: i) Mechanical noise, ii) Aerodynamic noise. Mechanical noise is often tonal in nature and is generated by the moving parts of a turbine. Mechanical noise is not considered as a major concern in modern wind turbines since the advancements in fabrication has eliminated most of mechanical noise generation. Moreover mechanical noise is tonal and attenuates significantly a short distance from the turbine. Aerodynamic noise is generated by the interaction of the turbine blade with the unsteady flow, resulting in pressure fluctuations which, in turn, lead to noise sources. Aerodynamic noise generation mechanisms can be divided into the following categories based on the cause of the pressure fluctuation on the blade surface: turbulent inflow, turbine blade stall, blade trailing edge, blade-tower interaction, blade tip and laminar boundary layer vortex shedding (Oerlemans, 2011). Directivity of the emitted noise from wind turbines is complex and the perceived noise is usually a combination of different mechanisms due to blade-flow interaction. The level of complexity increases since the propagation of the noise in a fluid medium is a function of several parameters such as the flow field, ground topology and temperature distribution.

Among all the factors, the wake of a wind turbine significantly affects the refraction of the sound and the propagation pattern of the generated noise due to its unsteadiness, velocity pattern and contained variety of vortical structures. Colonius et al. (1994) showed that the sound is refracted when the sound rays are comparable to the size of the vortices. Since a wide variety of vortices with different sizes and strengths exist in the wake region, the noise

generated by the wind turbine is affected by their presence. Moreover, it was shown that the downwind propagation of the wind turbine noise is affected by the velocity deficit in the wake (Heimann et al., 2011, Barlas et al., 2017). Lee (2015) used the parabolic equation method combined with an actuator disk-RANS CFD to study the effect of the wake on sound propagation for different values of incoming wind shear. Their results revealed that the far-field noise level increases when the incoming wind shear is small. Unlike results from the research conducted by Heimann et al. (2011), he reported that the far-field sound pressure level (SPL) could be reduced in the presence of the wind turbine wake and high wind shear. The study shows that the largest variation in noise signature occurs beyond 18D downstream of the turbine. Barlas et al. (2017) conducted a study on the effect of wind turbine wake on sound refraction and propagation in the presence of the atmospheric boundary layer. They used a combination of the parabolic equation method for acoustic calculations and actuator line/LES model for flow field prediction. Results showed a significant increase in the sound pressure level in the far-field, especially in neutral atmospheric boundary layer conditions. A 7.5 dB amplification in the SPL at the wake centre in the presence of the stable boundary layer at 15D downstream of the wind turbine shows the significant effect the wake flow can have on sound refraction and noise propagation (Barlas et al., 2017).

Although wake and flow field downstream of a wind turbine significantly affect the noise propagation and its perception, wind turbine noise radiation affected by wake and atmospheric boundary layer is not well understood. Thus, this study employs a hybrid approach by implementing a complete large eddy simulation of a two bladed wind turbine to compute the pressure fluctuations on the wind turbine blade surface and the Ffowcs-Williams and Hawkings analogy to calculate the sound pressure level arising from these fluctuations..

7.4 Methodology

In this study a hybrid method is utilised to calculate the effect of wake and atmospheric boundary layer on aerodynamic sound signature from a wind turbine. The noise signals are calculated in two steps: i) the pressure fluctuation on the blade surface is computed by the means of computational fluid dynamic, ii) the sound signature is computed from the calculated pressure fluctuations using FW-H analogy.

In order to accurately calculate the pressure fluctuation, a large eddy simulation approach was utilised. This technique is capable of providing sufficient spectral content for aeracoustic computations. The Ffowcs Williams and Hawkings (FW-H) analogy was used to calculate the sound signals arising from the pressure fluctuations. Compared to the direct computational acoustics, using the FW-H analogy reduces the computation cost significantly, since the sound signature is calculated indirectly from the CFD results. The FW-H analogy is an extension of Lighthill's theory, which takes into account the noise source related to surfaces in a relative motion. The FW-H equation is written as (Ffowcs Williams and Hawkings, 1969):

$$\frac{1}{a_0^2}\frac{\partial^2 \acute{p}}{\partial t^2} - \nabla^2 \acute{p} = \frac{\partial^2}{\partial x_i \partial x_j}\{T_{ij}H(f)\} - \frac{\partial}{\partial x_i}\{[P_{ij}n_j + \rho u_i(u_n - v_n]\delta(f)\} + \frac{\partial}{\partial t}\{[\rho_0 v_n + \rho(u_n - v_n]\delta(f)\} \quad (1)$$

where ρ_0 is the fluid density at the state of equilibrium, ρ is the instantaneous fluid density, u_i is the fluid velocity component in x_i direction, u_n is the fluid velocity component normal to the surface ($f = 0$), v_i is the surface velocity component in x_i direction, and v_n represents the velocity component normal to the surface. The terms $\delta(f)$ and $H(f)$ in the FW-H equation are the Dirac delta and Heavyside functions, respectively, where $f = 0$ corresponds to the

source surface and $f > 0$ denotes the exterior flow region. Here $\acute{p}$ is defined as the gauge hydrodynamic pressure, while a_0, P_{ij} and T_{ij} represent speed of sound, compressive stress tensor and Lighthill's stress tensor, respectively. Equation (1) reduces to Lighthill's theorem if there is no surface (i.e., $H = 1$).

The FW-H equation can be integrated analytically assuming a free-space flow without any obstacles between the sound source and the receiver. The solution to this is given in Equation (2), broken into quadrupole, dipole, and monopole terms.

$$H(f)\acute{p}(x,t) =$$

$$\underbrace{\frac{1}{4\pi}\int_V \frac{\partial^2}{\partial y_i \partial y_j}\left[\frac{1}{|1-M_r|}T_{i,j}\left(y, t-\frac{r}{a}\right)\right]\frac{dy}{r}}_{\text{Quadrupole}}$$

$$+\underbrace{\frac{1}{4\pi}\int_{f=0}\frac{\partial}{\partial y_i}\left[\frac{1}{|1-M_r|}F_i\left(y, t-\frac{r}{a}\right)\right]\frac{dy}{r|\nabla f|}}_{\text{Dipole}} \qquad (2)$$

$$+\underbrace{\frac{1}{4\pi a_0}\int_{f=0}\frac{\partial}{\partial t}\left[\frac{1}{|1-M_r|}Q_i\left(y, t-\frac{r}{a}\right)\right]\frac{dy}{r|\nabla f|}}_{\text{Monopole}}$$

where $F_i = P_{i,j}n_j + \rho u_i(u_n - v_n)$ and $Q_i = \rho v_n + \rho(u_n - v_n)$. The quadrupole term, which is represented by a volume integral, contributes to the unsteady stresses in the region outside the source surface, while surface integrals represented by the dipole and monopole terms are respectively related to the flow interaction with moving bodies and body thickness, respectively. The monopole part of the formulation contributes to the thickness noise or volume displacement noise, which originates from the relative motion of the air and surface. This explanation has been added to the text. Since the airfoil is stationary, the contribution of the monopole term is just associated with the relative motion of the fluid over the airfoil

surface. Monopole noise source is significantly affected by the compressibility of the medium. However, the effect of compressibility on the monopole term in the current study was neglected due to non-compressibility of the fluid medium. The quadrupole term is often negligible compared to the other two terms and becomes close to zero for subsonic flows. Although the Mach number is small for the cases considered in this study, Ghasemian and Nejat (2015) showed that the quadrupole term by eddies contributes significantly to the total sound pressure level at a receiver. Thus, all terms corresponding to monopole (thickness), dipole (loading) and quadrupole noise sources are considered in the present study. The flow parameters are obtained from LES calculations and used as inputs for the FW-H equations.

The fundamental governing equations for LES are the Navier-Stokes and continuity equations, solved with the appropriate boundary conditions. The Navier-Stokes equations are filtered to reduce the computational cost. The LES approach includes solving the filtered Navier-Stokes equations together with continuity equations with an appropriate boundary layer. Using these filters, turbulent eddies smaller than the grid size are filtered in the domain and are modelled, while larger eddies are resolved directly. In the current study, the Boussinsque hypothesis and the dynamic Smagorinsky-Lilly model are used to calculate the subgrid-scale stresses. Governing equations and detailed information about the large eddy simulation and subgrid models can be found in the literature related to this field (Sedaghatizadeh et al., 2017, Wilcox, 1998, Menter and Egorov, 2010).

7.5 Problem description and computational domain

The NREL phase VI wind turbine, which is a two-bladed stall-regulated turbine with a 10.058 m rotor diameter, was selected for the purpose of this study. In order to investigate the effect of the boundary layer on the aeroacoustic behaviour of the wind turbine, two cases were considered; one in the presence of a smooth boundary layer and another in the absence

of the boundary layer (uniform flow). Computations were carried out for the hub-height velocity profile of 7 m/s for both uniform and boundary layer flow, resulting in a Reynolds number of approximately 5×10^6 based on the rotor diameter. The boundary layer was represented by a power-law velocity profile with the hub height velocity of 7 m/s and power-law index equal to 0.2, corresponding to a terrain with moderate scrub or scattered trees. The computational domain and aerodynamic performance of the wind turbine have been explained in detail in previously published work about the effect of the boundary layer on the wake development of a wind turbine (Sedaghatizadeh et al., 2017). In this work the temporal resolution of the model was increased in order to provide sufficient spectral content. This was done based on the Nyquist–Shannon sampling theorem to cover the frequency range associated with important aerodynamic noise mechanisms. Interested researchers are encouraged to refer to the publically available articles (Sedaghatizadeh et al., 2017a, Sedaghatizadeh et al., 2017b) for description about the grid resolution and CFD domain.

7.6 Validation of the model

Due to the lack of experimental data about the perceived noise, the validation of the model was performed in two stages for both aerodynamic and aeroacoustic calculations. In order to aerodynamically validate the model, the computed pressure distribution on the blade was compared with experimental data reported by Hand et al. (2001) for a turbine inside a wind tunnel. The accurate prediction of pressure distribution on the blade is important for both aeroacoustic and aerodynamic calculations since it has a direct impact on both sound and flow fields. Thus, a good agreement with experimental data and accurate calculation of pressure distribution on the blade surface is the first step and prerequisite for calculating the aeroacoustic and aerodynamic results. The integral of the calculated pressure distribution on

different sections of the blade shows a good agreement, with a maximum of 8% deviation from the experimental data of Hand et al. (2001) who used a limited number of pressure taps on the blade surface (Sedaghatizadeh et al., 2017). Other parameters used in the validation of the aerodynamic model, are the total output power and thrust coefficient. The averaged value of the output power obtained from the simulation is approximately 5.73 kW, which results in a 4.6% discrepancy when compared with the experimental data (Hand et al., 2001). The thrust coefficient, C_t, which is a representative of the forces acting on the rotor, axial velocity deficit and wake expansion rate, also shows only 1.5% deviation from the experimental data. Further details of the aerodynamic verification can be found in the previously published article by the authors (Sedaghatizadeh et al., 2017).

To confirm the aeroacoustic calculations, the sound pressure level calculated by the FW-H analogy is plotted in Figure 7.1 compared with the results presented by Tadamasa and Zangeneh (2011) who investigated the far-field noise signature from a wind turbine. They used both impenetrable and permeable FW-H formulations in conjunction with a RANS turbulent model to predict the noise emitted from a wind turbine. Outcomes show that the trend of the current results is in a reasonable agreement with the ones presented by Tadamasa & Zangeneh. The discrepancy between the results in the low frequency range can be explained by the different CFD approaches for modelling the turbulent flow. Tadmasa & Zangeneh used SST $k-\omega$ based CFD approach and their predicted pressure distribution on the blade sows inaccuracies when compared with experimental results (Tadamasa and Zangeneh, 2011, Ghasemian and Nejat, 2015). In addition to this, another source of the difference between the current study and study carried out by Tadamasa and Zangeneh (2011), especially at low frequencies, might emerge from inclusion of the volumetric integral in the current study while it was neglected in previous work.

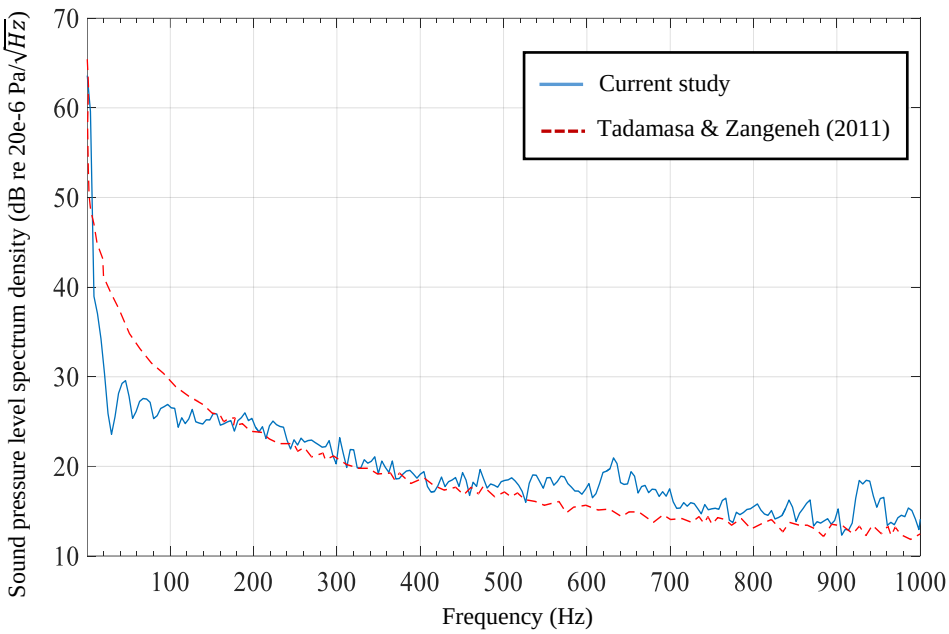

Figure 7.1 Validation of the aeroacoustic results against the data published by Tadamasa and Zangeneh (2011) using FW-H/RANS approach for a receiver at reference point downstream of the NREL Phase VI wind turbine (Reference distance from a wind turbine is defined as: $l_{Ref} = h_0 + D/2$, where l_{Ref}, h_0, and D are reference distance from wind turbine, hub height and rotor diameter, respectively.

7.7 Aerodynamic and aeroacoustic results

Figures 7.2 shows the instantaneous velocity contours of the wind turbine wake in a smooth boundary layer and for uniform flow. As shown, the wake length is shorter in the case of smooth boundary layer. This is due to the downwash formed in the presence of the boundary layer which results in convection of the high momentum flow towards the ground.

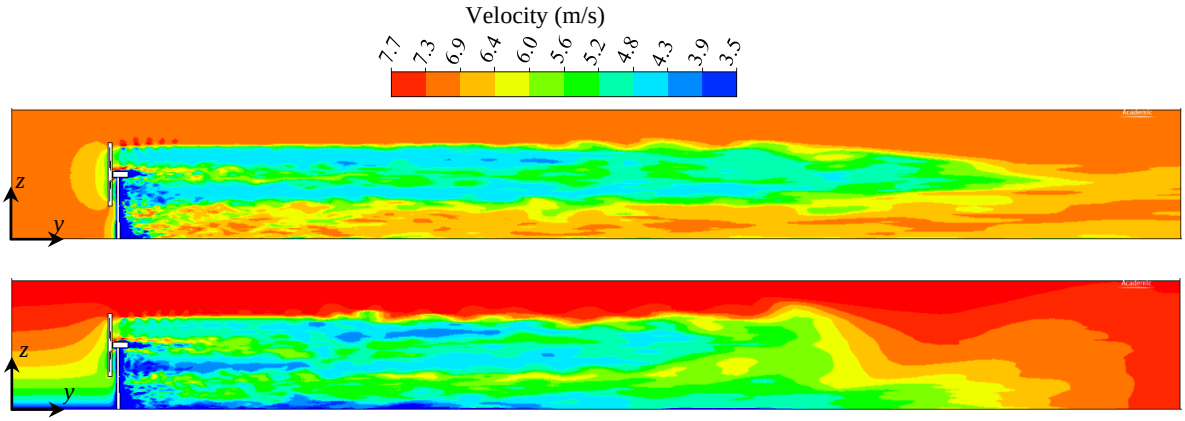

Figure 7.2 Instantaneous streamwise velocity contours showing the wake development in the absence (upper) and presence of a smooth boundary layer (lower).

The overall sound pressure level variation with respect to the distance from the wind turbine is presented in Figure 7.3, as well as the iso-surfaces of the vorticity for both cases. The sound pressure level generally decreases as the distance increases due to spreading, absorption and dissipation in the medium. The sound pressure level in the presence of the boundary layer in close proximity of the turbine is generally in the same order of the sound in the presence of uniform flow. This could be explained by the higher shear velocities and higher pressure fluctuation levels in the presence of the boundary layer. This figure also shows the overall sound pressure level at the different distances from the wind turbine where the receiver is located at a height of 2 m from the ground. Whilst the SPL generally decreases as the distance from the wind turbine increases, there are some peaks visible for both cases. These peaks are related to the effect of the wake, which results in an increased sound level at several locations. Results also reveal a slightly lower sound pressure level in the presence of the wake. This behaviour can be explained by the scattering effect of the wake on the sound. As seen in Figure 3, the presence of the boundary layer results in more fluctuations in the diagram. This can be explained by the convection of the turbulence in the presence of the boundary layer due to the downwash generated by the longitudinal vortices. These structures refract the sound which results in an increased sound pressure level at these

locations. As shown in the figure, the peaks in the sound pressure level can be related to the sound energy release in the medium due to break-up of the wake at different locations.

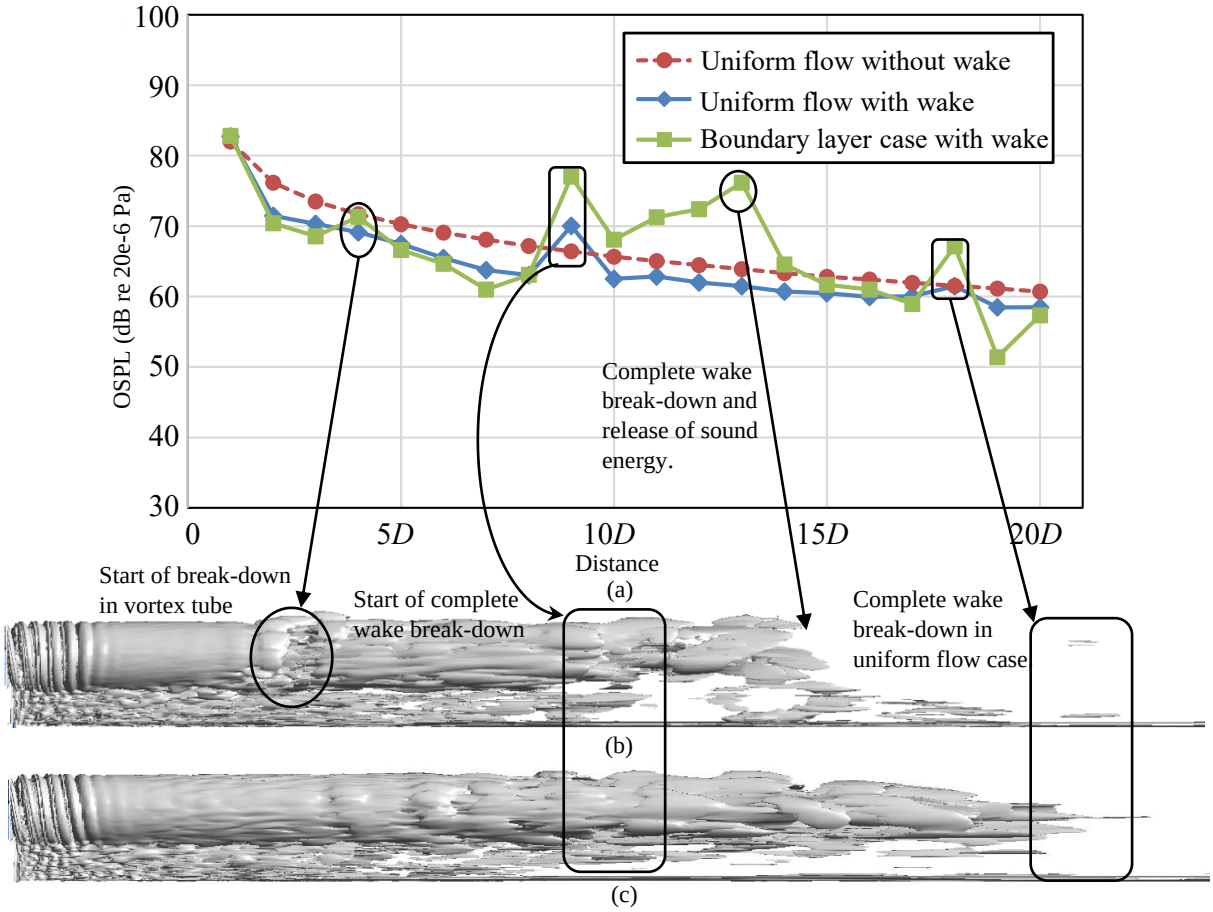

Figure 7.3 a) Overall sound pressure level (OSPL) at 2 m height downstream of the wind turbine in the presence and absence of the boundary layer as well as for the no-wake condition, b) Iso-surface of the vorticity field in the presence of a smooth boundary layer, c) Iso-surface of the vorticity field in the absence of the boundary layer (uniform flow).

Figure 7.4 depicts the sound power spectral density corresponding to the locations of the peaks observed in the SPL plot of Figure 7.3. The results show that the highest acoustic energy content generally corresponds to the frequencies lower than 500 Hz. This could be related to the interaction turbulent eddies with the blades and also with each other. The frequency content of the noise is lower in the presence of the smooth boundary layer when compared with the uniform flow case. This could be explained by the interaction of the blade with varying velocity magnitudes which occurs in the range of blade pass frequency and

increases the low frequency noise level. Moreover, the sound spectrum of the uniform flow case contains higher frequency content when compared to the case in the presence of the boundary layer.

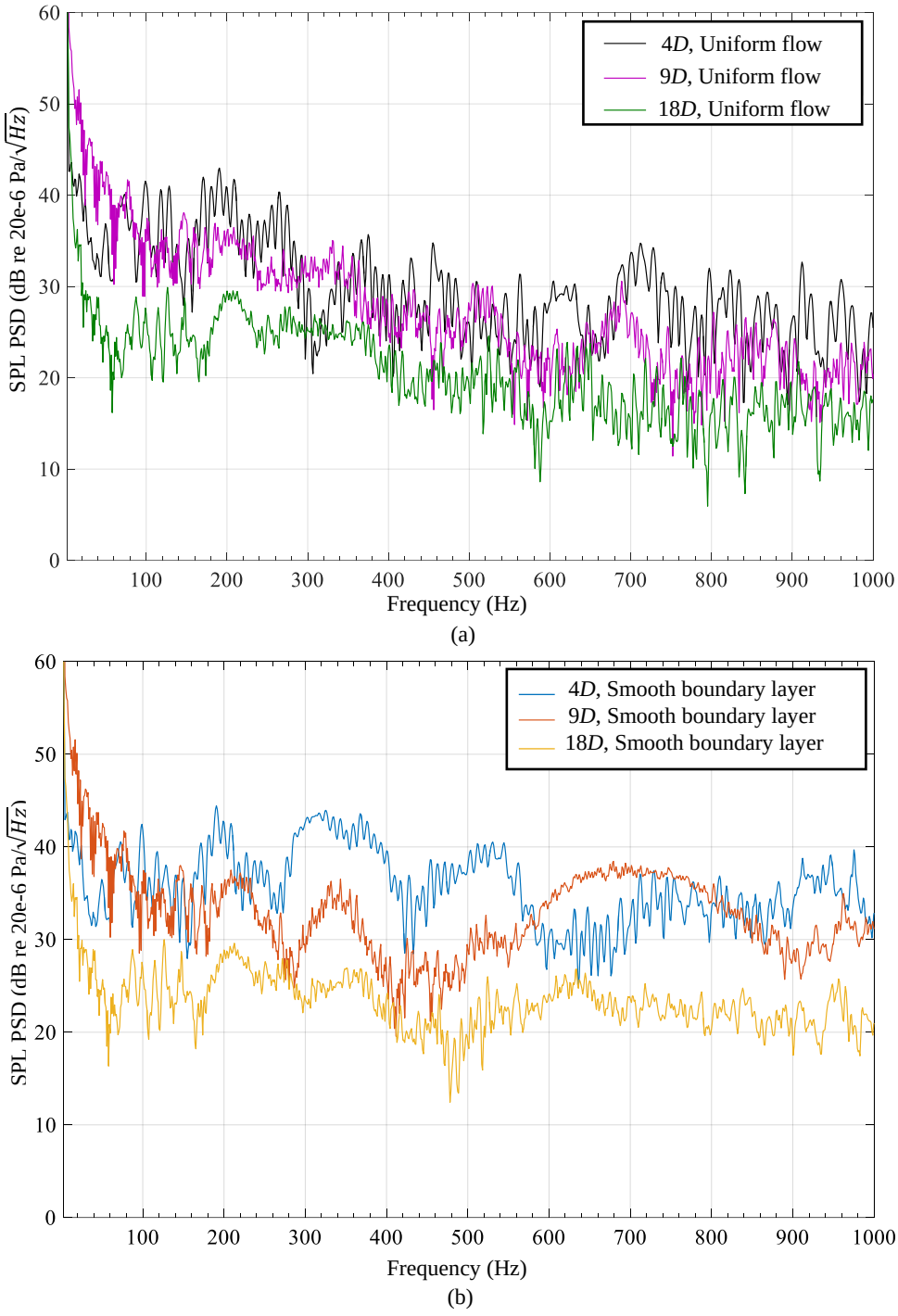

Figure 7.4 Sound power spectral density downstream of the wind turbine where peaks in amplitude are observed, a) in the presence of uniform flow, b) in the presence of the smooth boundary layer.

In order provide an insight about the source of the noise, the pressure fluctuations on surface

of the wind turbine blade for different frequency bands is presented in Figure 7.5. The pressure fluctuation distribution on the blade shows a similar trend for both cases in the presence and absence of the smooth boundary layer. However, higher pressure levels are visible on the leading edge of the blade in the presence of the smooth boundary layer due to interaction of the wind turbine blade with the varying wind velocity when compare d with the uniform flow case. In addition, the existence of the higher sound pressure level at low frequencies in the spectrum suggests that the noise associated with the interaction of eddies is more pronounced in the presence of the boundary layer.

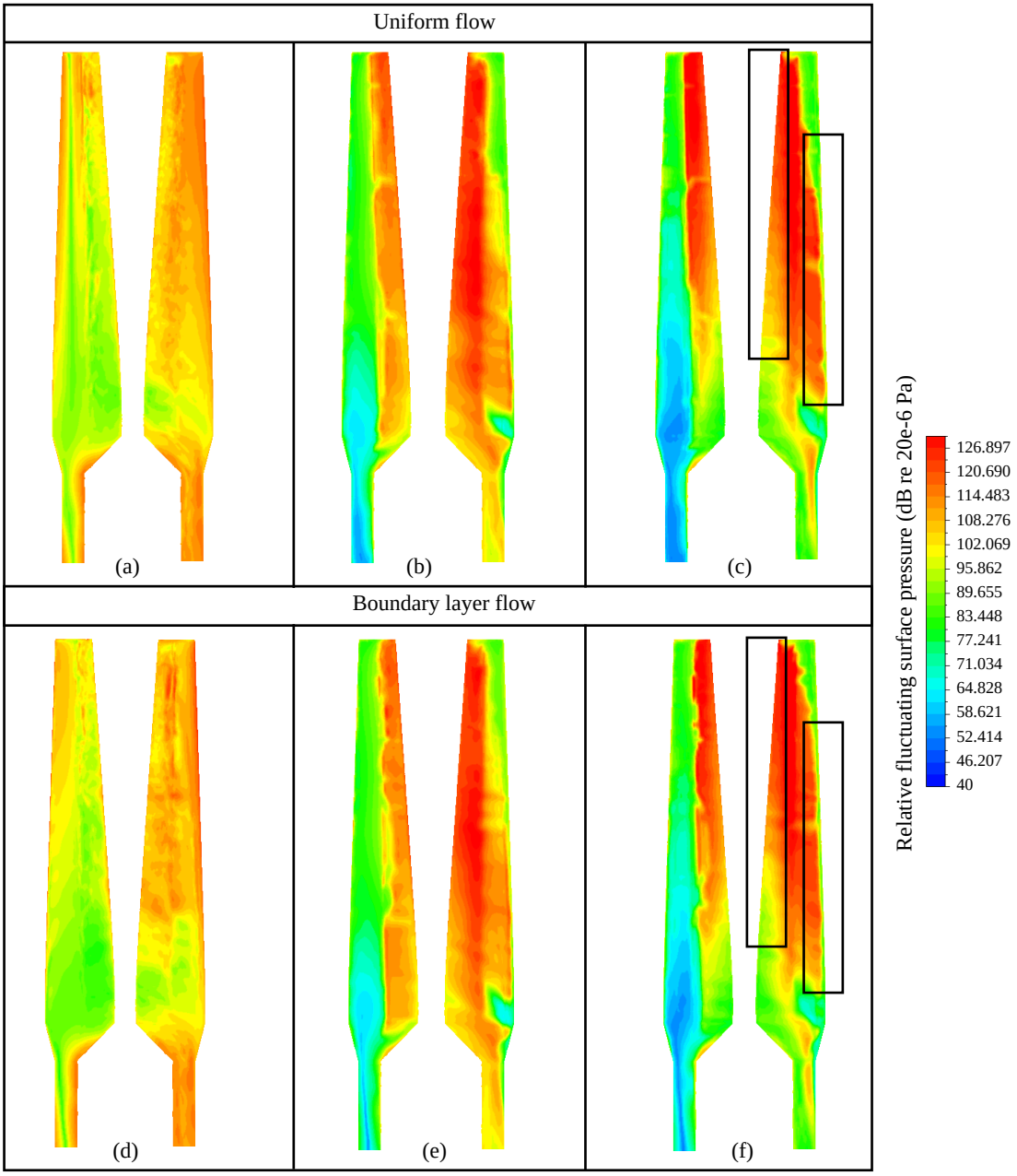

Figure 7.5 Contours of relative fluctuating pressure on the blade surface associated with several octave bands in the presence and absence of the boundary layer, a) uniform flow at the 2 Hz octave band, b) uniform flow at the 63 Hz octave band, c) uniform flow at the 250 Hz octave band, d) boundary layer flow at the 2 Hz octave band, e) boundary layer flow at the 63 Hz, d) boundary layer flow at the 250 Hz octave band.

Since the pressure fluctuation on the blade surface does not show significant difference in the presence and absence of the incoming boundary layer flow, it can be concluded that the main difference between the perceived noises from the two cases arises from the wake effect. The contribution of the noise sources from the wind turbine blade is similar in the presence

and absence of the boundary layer. Thus, the refraction of the sound due to wake effect is the main contributor to the peaks observed in the sound pressure level plots. This happens at break points of the wake and at 4*D*, 10*D*, 13*D*, and 18*D* in the presence of boundary layer and at 10*D* and 18*D* in the absence of the boundary layer. To further study the effect of wake on wind turbine noise, more detailed analysis will need to be performed using more accurate models for propagation as well as investigating different wind velocity profiles, terrain categories as well as employing models which account for reflection and refraction of the noise.

7.8 Conclusion

The aeroacoustic behaviour of a two-bladed horizontal axis wind turbine was investigated numerically. A large eddy simulation was used in conjunction with Ffowcs Williams and Hawkings analogy to calculate the flow field parameters and far-field sound signature. It was found that the varying velocity magnitude in the incoming wind of a smooth boundary layer does not significantly affect the pressure fluctuation on the blade and thus noise generated by blades. This is due to higher fluctuating pressure on the blade surface when the blade interacts with the varying wind velocity. Moreover, the overall sound pressure level downstream of the wind turbine at different distances showed an increased noise level at around 10*D*. The noise level gradually decreases in presence of a uniform flow. However, the overall sound pressure level fluctuates after 10*D* in the presence of the boundary layer. This is due to the convection of the turbulent eddies in the wake toward the ground by the strong downwash. This study reveals the effect of the wind turbine wake on sound downstream of the turbine.

As discussed, the wake affects the sound propagation and can result in amplitude modulation of the noise in far-field even at 18*D* distance from the wind turbine. These findings can explain the noise perception by the communities far from wind turbines. Based on the preliminary results, the exclusion distance from wind turbines to prevent noise disruption might not be sufficient. Since wind turbines are erected on different terrains and operate in different atmospheric conditions, more investigations should be carried out in order to identify the effect of different parameters such as terrain, wind condition, and temperature distribution on the wake and noise propagation.

7.9 References

Barlas, E., Zhu, W. J., Shen, W. Z., Kelly, M. & Andersen, S. J. 2017. Effects of wind turbine wake on atmospheric sound propagation. *Applied Acoustics*, **122**, 51-61.

Colonius, T., Lele, S. K. & Moin, P. 1994. The scattering of sound waves by a vortex: Numerical simulation and analytical solution. *Journal of Fluid Mechanics*, **260**, 271-298.

Ghasemian, M. & Nejat, A. 2015. Aerodynamic noise prediction of a horizontal axis wind turbine using improved delayed detached eddy simulation and acoustic analogy. *Energy Conversion and Management*, **99**, 210-220.

Hand, M. M., Simms, D. A., Fingersh, L. J., Jager, D. W., Cotrell, J. R., Schreck, S. & Larwood, S. M. 2001. Unsteady Aerodynamics Experiment Phase VI: Wind Tunnel Test Configurations and Available Data Campaigns. National Renewable Energy Laboratory, Report of Experiment.

Heimann, D., Käsler, Y. & Gross, G. 2011. The wake of a wind turbine and its influence on sound propagation. *Meteorologische Zeitschrift*, **20**, 449-460.

Iachini, T., Maffei, L., Ruotolo, F., Senese, V. P., Ruggiero, G., Masullo, M. & Alekseeva, N. 2012. Multisensory assessment of acoustic comfort aboard metros: A virtual reality study. *Applied Cognitive Psychology*, **26**, 757-767.

Lee, S. 2015. Prediction of far-field wind turbine noise propagation with parabolic equation. 21st AIAA/CEAS Aeroacoustics Conference. *American Institute of Aeronautics and Astronautics.*

Menter, F. R. & Egorov, Y. 2010. The scale-adaptive simulation method for unsteady turbulent flow predictions. Part 1: Theory and model description. *Flow, Turbulence and Combustion*, **85**, 113-138.

Pawlaczyk-Luszczynska, M., Dudarewicz, A., Zaborowski, K., Zamojska, M. & Waszkowska, M. Assessment of annoyance due to wind turbine noise. ICA 2013 Montreal, 2-7 June 2013 Montreal, Canada. Acoustical Society of America through the American Institute of Physics.

Pedersen, E., Bouma, J., Bakker, R. & Van Den Berg, F. 2008. Response to wind turbine noise in the Netherlands. *The Journal of the Acoustical Society of America*, **123**, 3536-3536.

Pedersen, E., Hallberg, L.-M. & Waye, K. P. 2007. Living in the vicinity of wind turbines — A grounded theory study. *Qualitative Research in Psychology*, **4**, 49-63.

Sedaghatizadeh, N., Arjomandi, M., Cazzolato, B. & Kelso, R. 2017a. Wind farm noises: Mechanisms and evidence for their dependency on wind direction. *Renewable Energy*, **109**, 311-322.

Sedaghatizadeh, N., Arjomandi, M., Kelso, R., Cazzolato, B. & Ghayesh, M. H. 2017b. Modelling of wind turbine wake using large eddy simulation. *Renewable Energy*, Accepted manuscript.

Sedaghatizadeh, N., Arjomandi, M., Kelso, R. M., Cazzolato, B. S. & Ghayesh, M. H. 2017c. Atmospheric boundary layer effect on the wake of a wind turbine. *Revision submitted for review to the Journal of Wind Engineering and Industrial Aerodynamics*.

Shepherd, D., Hanning, C. & Thorne, B. 2012. Noise: Windfarms. *Encyclopedia of Environmental Management*.

Tadamasa, A. & Zangeneh, M. 2011. Numerical prediction of wind turbine noise. *Renewable Energy*, **36**, 1902-1912.

Waye, K. P. & Öhrström, E. 2002. Psycho-acoustic characters of relevance for annoyance of wind turbine noise. *Journal of Sound and Vibration*, **250**, 65-73.

Wilcox, D. C. 1998. Turbulence modeling for CFD, Second edition, DCW Industries.

Williams, J. E. F. & Hawkings, D. L. 1969. Sound generation by turbulence and surfaces in arbitrary motion. *Philosophical Transactions of the Royal Society of London. Series A, Mathematical, Physical and Engineering Sciences*, **264**, 1151, 321-342.

Chapter 8 Conclusion and future work

The work presented in this thesis investigated a number of phenomena related to the wake generated by wind turbines, the sound production and the subsequent radiation. More specifically, this thesis has investigated wind turbine wake development, the aerodynamic noise emitted from wind farms and wind turbines, and the effect of wake on noise propagation. The noise from wind turbines span a wide range of frequencies, which often makes it perceptible even in the presence of other environmental noise sources. The sound pressure level, spectral content and directivity of the emitted noise from wind turbines are highly affected by the interaction of the turbine with wakes from upstream turbines and incoming flow features in the atmospheric boundary layer. During the course of this research, several numerical studies were conducted to develop a better understanding of the aerodynamic noise generation and wake development by wind turbines.

8.1 Significance of the present work

In spite of vast scientific research in the area of wind turbine aeroacoustics, the underlying mechanism of the perceived noise in particular at far distances, is still a subject of discussion. Much research into wind turbine noise, has been focused on the application of semi-empirical models and experiments in the near field region, which cannot reliably relate the perceived noise to the known aerodynamic noise mechanisms. In addition, the incoming flow features affect the noise emission, especially when the wind turbine operates in a dense cluster and is subjected to the wake of one or more upstream turbines. This may also result in changes of directivity, level and frequency of the noise due to the partial stall on the blade. Studies on noise propagation also revealed that shear layers and vortical structures in the

flow can refract the sound and change the directivity of the noise in the fluid medium. Therefore, it is desirable to establish a framework to find the underlying mechanism of perceived noise and understand the effect of different incoming flow features, especially for turbines in the wake of an upstream turbine. The main outcomes and significance of this research can be described as:

a) A metadata analysis of previous noise surveys was carried out to find the principal mechanism associated with the perceived noise by residents adjacent to wind farms. Noise reports from communities have been used to find the correlation between the wind direction and directivity associated with different noise mechanisms. It was observed that the directivity and the location of the perceived noise are better aligned with the sudden change in sectional angle of attack which can be caused by turbulence and vortical structures in the incoming flow. Moreover, the locations of noise perception are within the region affected by the turbine wake, showing the direct effect of wake on noise propagation.
b) The aeroacoustic behaviour of an airfoil in pre-stall and stall conditions was investigated numerically using a coupled CFD simulation with the Ffowcs Williams and Hawkings analogy. The directivity of the noise was calculated using the noise signature in far-field. It was found that as the angle of attack increases the noise radiates more strongly in the direction perpendicular to the chord. Results also revealed that at some frequencies in pre-stall conditions, the noise is greater towards the leading edge, which is in contrast with trailing edge noise theory. Thus it can be concluded that additional noise mechanisms exist which cannot be described by trailing edge noise theory.

c) A CFD model of a wind turbine wake using the LES approach was developed for a wind turbine and validated against experimental data. The wake of the same wind turbine was predicted using three semi-empirical models and their results were compared with the developed high fidelity CFD model. Results revealed that each engineering model is best suited for modelling a specific part of the wake. Thus, in order to predict the wind turbine wake expansion and velocity profile in the wake, it is required to use a combination of models that are applied to different parts of the wake. Moreover, in the engineering wake models the effect of incoming turbulence intensity, the interaction of incoming unsteady structures and flow features in the wake of upstream turbines are not considered. Although engineering models can provide a relatively good estimate of velocity deficit and wake expansion, which can be used to calculate the power loss in a given wind farm layout or to optimise the power output from a farm, their spatial and temporal resolutions are not sufficient for noise prediction.

d) The validated CFD model was further developed to account for the effect of an atmospheric boundary layer corresponding to a moderate scrub terrain. It was found that the length of wake is shorter when the turbine is exposed to the atmospheric boundary layer. The velocity profiles revealed that after 12D the wake momentum in the far-field is greater than that of a turbine exposed to a uniform velocity profile. This suggests that a downstream turbine can generate greater power in an atmospheric boundary layer if it is placed beyond 12D downstream of a turbine. A strong downwash was detected in the presence of the atmospheric boundary layer, which results in a reduction in the mean axial circulation on either side of the wake. This significant difference in the flow behaviour in the presence and absence of the

atmospheric boundary layer was described based on the bending and interaction of the spanwise vortices in the atmospheric boundary layer by the operating turbine.

e) Noise propagation from a wind turbine in the presence of atmospheric boundary layer and turbine wake was investigated numerically. Results revealed that the wind turbine wake acts as a duct which channels the sound energy along the wake to the breakdown point.

8.2 Future work

Wind turbines are large structures installed in the atmospheric boundary layer and wide variety of factors affect their performance. The operation of wind turbines also has significant impacts on the environment that they are operating in. Therefore, several avenues of future research are available that can be used to further investigation on the operation of wind turbines operation, their performance and environmental impact. Some of these areas are:

1) Wind turbines are erected on different surfaces; from smooth open coasts to hilly terrains. The incoming flow features, such as turbulent intensity and length scale vary in the incoming flow with regard to different surface topology. This results in different wake structures which, in return, result in different aeroacoustic behaviour and noise propagation. The developed model can be further modified and used for the investigation of the effect of different terrain categories on the wake development and noise emission from wind turbines.
2) The developed CFD model can be used to investigate the effect of wind turbine and its wake on the surface temperature distribution downstream of the turbine. Wind turbines can act as large mixers in the atmospheric boundary layer, and their wake and contained vortical structures can disturb the formation of inversion layers and stratified and

stratified atmospheric boundary layer. Since wind turbines are usually erected in rural areas and next to farms, there is some evidence they can affect the crop growth and yield.

3) Modifications to the CFD model developed in this work can be used for the investigation of the effect of temperature gradient on wake development and noise propagation. Since the temperature gradient has a significant effect on both the turbine wake and noise propagation.
4) The quadrupole term in FW-H analogy, which accounts for the noise generated due to the interaction of vortices with each other is usually neglected. In complex flows such as the flow over the blade of a wind turbine the role of quadrupole can be significant. Hence, integrating the full FW-H analogy with the CFD model developed in this work can provide more accurate aeroacoustic results.
5) Developing and incorporating the aeroacoustic analogies such as the parabolic equation methods and the linearized Euler model which are able to account for the effect of refraction and scattering can be beneficial since the wind turbine wake contains complex vortical structures which affects noise propagation.

Appendix A: On the requirements for the wind turbine experiment in a wind tunnel

---

Effect of Wall Confinement on a Wind Turbine Wake

N. Sedaghatizadeh, M. Arjomandi, R. Kelso, B. Cazzolato, M. H. Ghayesh

School of Mechanical Engineering, the University of Adelaide, Adelaide, SA, 5005

Paper accepted in AFMC conference: Sedaghatizadeh, N., Arjomandi, M., Kelso, R. M., Cazzolato, B. S. & Ghayesh, M. H. Effect of wall confinement on a wind turbine wake. 20th Australasian Fluid Mechanics Conference, 2016 Perth, Australia.

Statement of Authorship

Title of Paper	Effect of Wall Confinement on a Wind Turbine Wake
Publication Status	☑ Published ☐ Accepted for Publication ☐ Submitted for Publication ☐ Unpublished and Unsubmitted work written in manuscript style
Publication Details	Sedaghatizadeh, N., Arjomandi, M., Kelso, R. M., Cazzolato, B. S. & Ghayesh, M. H. Effect of wall confinement on a wind turbine wake. 20th Australasian Fluid Mechanics Conference, 2016 Perth, Australia.

Principal Author

Name of Principal Author (Candidate)	Nima Sedaghatizadeh		
Contribution to the Paper	- Research - Providing the data, writing of the manuscript and production of original figures - Correspondence with editor and reviewers including the production of all cover letters and rejoinder		
Overall percentage (%)			
Certification:	This paper reports on original research I conducted during the period of my Higher Degree by Research candidature and is not subject to any obligations or contractual agreements with a third party that would constrain its inclusion in this thesis. I am the primary author of this paper.		
Signature		Date	14/09/2017

Co-Author Contributions

By signing the Statement of Authorship, each author certifies that:

i. the candidate's stated contribution to the publication is accurate (as detailed above);

ii. permission is granted for the candidate in include the publication in the thesis; and

iii. the sum of all co-author contributions is equal to 100% less the candidate's stated contribution.

Name of Co-Author	Maziar Arjomandi		
Contribution to the Paper	- Supervision of the work, including the production of the manuscript - Participation in the development of the concepts and ideas presented in the manuscript - Evaluation and editing of the manuscript prior to submission		
Signature		Date	15/09/2017

Name of Co-Author	Richard Kelso		
Contribution to the Paper	- Supervision of the work, including the production of the manuscript - Participation in the development of the concepts and ideas presented in the manuscript - Evaluation and editing of the manuscript prior to submission		
Signature		Date	14/9/2017

Name of Co-Author	Benjamin Cazzolato		
Contribution to the Paper	- Supervision of the work, including the production of the manuscript - Participation in the development of the concepts and ideas presented in the manuscript - Evaluation and editing of the manuscript prior to submission		
Signature		Date	14/09/2017

Name of Co-Author	Mergen H. Ghayesh		
Contribution to the Paper	- Supervision of the work, including the production of the manuscript - Participation in the development of the concepts and ideas presented in the manuscript - Evaluation and editing of the manuscript prior to submission		
Signature		Date	14/09/2017

Abstract

This study investigates the effect of wall confinement on a wind turbine wake as a means to guide future wind-tunnel-based wake studies. Large Eddy Simulation was utilised to simulate the wake region for two cases. The first case simulated the NREL phase VI wind turbine in a wind tunnel with 9% blockage. The reason behind selecting this case is the availability of the experimental data in the literature which enabled us in validating the model. The second case was the same turbine located in an unconfined environment, with the same flow upstream velocity. The results show that the wind tunnel walls significantly affect the wake development and its stability, even with a blockage of less than 10%. Tip vortices in the unconfined environment start to break down closer to the turbine compared to the wall-bounded case, resulting in a shorter wake recovery length for the unconfined flow. Vorticity contours reveal coherent vortical structures in the confined wake up to 20 turbine diameters downstream, while these structures dissipate after 16 diameters in an unconfined environment. The calculated power also showed that the turbine in the wind tunnel generates 5.5% more power than that in the unconfined flow. Collectively, these results provide an insight into the effect of walls on the turbine wake in both numerical and experimental studies, offering guidance on how wind tunnel studies relate to real, unconfined flows.

Introduction

Most experimental studies on wind turbine wakes have been conducted in wind tunnels under controlled conditions to avoid the difficulties associated with experiments conducted in actual wind farms (Vermeer et al., 2003). One of the concerns in wind turbine experiments, especially those with full-sized turbines, is the effect of walls and blockage

ratio. Excessive blockage in a closed-section wind tunnel results in accelerated flow around the turbine and changes in the wake development compared to the open field case.

Two approaches are generally used to minimise the effects of wall confinement on the results of wind tunnel experiments. The first is to apply correction factors on some aerodynamic parameters, and the second is to keep the blockage ratio small enough to avoid the wall interactions. In wind turbine wake studies, where the structure and development of the wake is important, the second approach should be used. McTavish et al. (2013) stated that the wind turbine wake is not affected by the walls when the blockage ratio is less than 10%. However, the blockage effect in wind turbine wake studies is a function of several parameters such as the blockage ratio (based on rotor swept area), tip speed ratio, number of blades, pitch angle and even the shape of the blades.

In this study, the wake development of the NREL phase VI wind turbine is investigated numerically to test the validity of the 10% limit for blockage ratio by comparing its wake development in a wind tunnel with the development in an unconfined environment.

Problem Description and Computational Mesh

The NREL phase VI, a two-bladed stall-regulated wind turbine with a rotor diameter of 10.058 m, was selected due to availability of the experimental data in the literature for validation of the numerical model developed in this paper. The NREL experiment was carried out in a large open-loop wind tunnel with a 24.4 m x 36.6 m cross section area (Hand et al., (2001). Figure 9.1 shows the experimental arrangement which was replicated in the computational model. The hub and nacelle in the computational model are simplified in order to reduce the complexity of the model which makes high quality grid generation difficult.

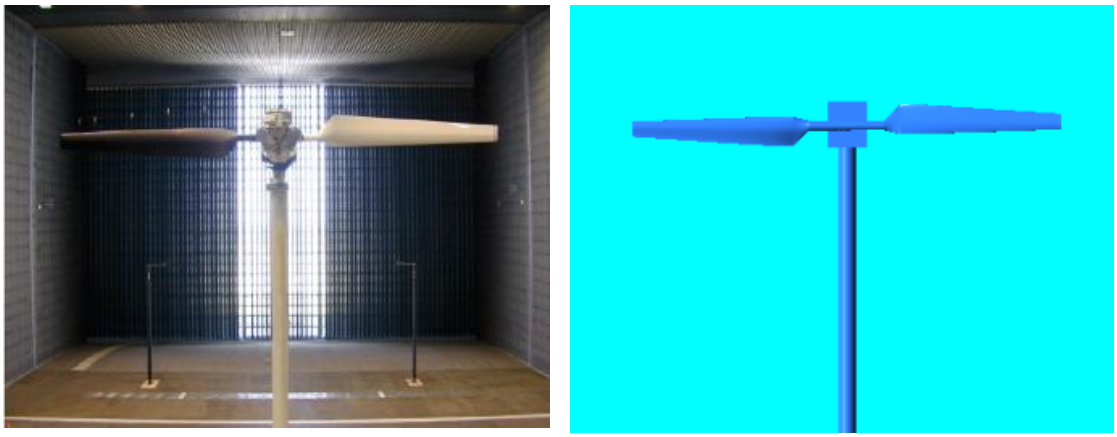

Figure 0.1 Wind turbine in wind tunnel (left) (Hand et al., (2001) and computational model (right).

Two computational domains were created, one for the wind tunnel and one for an unconfined environment. The computational domain for the wind tunnel is 24.4m high and 36.6m wide to replicate the experimental wind tunnel. The length of the tunnel is 221.3 m which is equals to twenty-two rotor diameters (see Figure 9.2). The turbine is placed at a position two diameters downstream from the inlet, in the middle of the wind tunnel. The blockage ratio is 9%.

For the unconfined environment with a uniform wind velocity profile, a larger domain was considered with the wind tunnel computational domain placed in the middle of the computational space. A $y^+ \leq 1$ was used to accurately resolve the boundary layer on the blade surface which resulted approximately 11 and 12.5 million hexahedral cells for wind tunnel and unconfined environment respectively. The computational domains for wind tunnel and unconfined environment are shown in Figure 9.2.

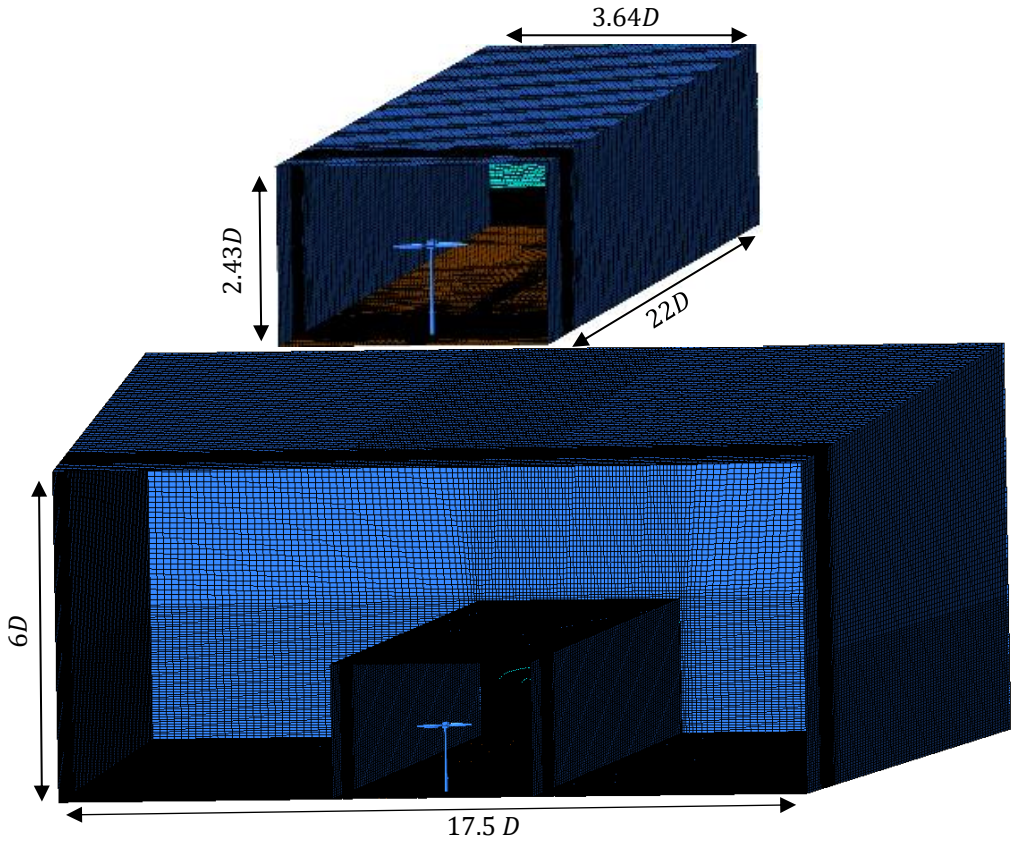

Figure 0.2 Computational domain for wind tunnel (top) and unconfined environment (bottom). *D* is the diameter of the rotor.

Figure 3 shows the schematic layouts of the cases which were studied.

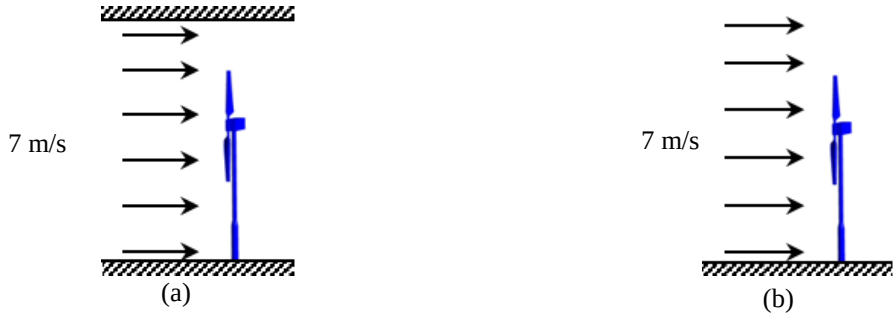

Figure 0.3 Schematic layout of the two test cases and wind profiles; a) wind tunnel, b) unconfined environment.

Computations were carried out for uniform wind velocity profiles of 7 m/s resulting in Reynolds number of approximately 5 million based on rotor diameter. The blades rotate at a constant speed of 71.9 rpm in both cases. The time step was set to 0.002318 seconds corresponding to a 1 degree rotation of the blade per time-step. LES calculations were carried

out using FLUENT 16.2 which is a general-purpose CFD code. Simulations were performed for a sufficiently long period of time (30 revolutions), to ensure the wake was fully developed and the results are statistically stable. After ensuring that the wake was sufficiently developed, results were recorded over 10 revolutions of the wind turbine to calculate the time-average parameters.

Numerical Method

Large Eddy Simulation (LES) was used to computationally calculate the flow field in the wake of wind turbine. The basic governing equations are the Navier-Stokes, energy and continuity equations which are solved together with appropriate boundary conditions to provide the flow field for the computational domain. In this study, heat transfer and temperature gradients within the fluid domain are negligible, and the focus is on fluid motion, so the energy equation is not considered. Conservation equations are presented below as:

$$\frac{\partial \rho}{\partial t} + \frac{\partial}{\partial x_i}(\rho u_i) = 0 \tag{9.1}$$

$$\frac{\partial (\rho u_i)}{\partial t} + \frac{\partial (\rho u_j u_i)}{\partial x_j} = \frac{\partial \sigma_{ij}}{\partial x_j} - \frac{\partial p}{\partial x_i} + f_i \tag{9.2}$$

The governing equations of LES are obtained by filtering the original continuum and Navier-Stokes equations as:

$$\frac{\partial \rho}{\partial t} + \frac{\partial}{\partial x_i}(\rho \overline{u_i}) = 0 \tag{9.3}$$

$$\frac{\partial (\rho \overline{u_i})}{\partial t} + \frac{\partial (\rho \overline{u_j}\ \overline{u_i}\ )}{\partial x_j} = \frac{\partial \sigma_{ij}}{\partial x_j} - \frac{\partial \bar{p}}{\partial x_i} + \frac{\partial \tau_{ij}}{\partial x_j} \tag{9.4}$$

In the above equations, $\overline{u}$ is the resolved velocity, σ is the stress tensor due to molecular viscosity, obtained from resolved velocity, and τ_{ij} is the subgrid scale stress defined as $\tau_{ij} = \rho\overline{u_i u_j} - \rho\overline{u_i}\,\overline{u_j}$. To close the set of equations, the Boussinsque hypothesis is used for calculations as:

$$\tau_{ij} - \frac{1}{3}\tau_{kk}\delta_{ij} = -2\mu_t\overline{S_{ij}} \tag{9.5}$$

where μ_t is subgrid turbulent viscosity, calculated using Smagorinsky-Lilly model as $\mu_t = \rho L_s^2 \left|\overline{S}\right|$. Here $\overline{S}$ is the resolved strain rate and L_s is the mixing length for subgrid length scale computed by:

$$\overline{S_{ij}} = \frac{1}{2}\left(\frac{\partial\overline{u_i}}{\partial x_j} + \frac{\partial\overline{u_j}}{\partial x_i}\right) \tag{9.6}$$

$$|\bar{S}| \equiv \sqrt{2\overline{S_{ij}}\,\overline{S_{ij}}} \tag{9.7}$$

$$L_s = min\left(\kappa d, C_s V^{1/2}\right) \tag{9.8}$$

In the above equations, κ is the von Karman factor, d is the closest distance to the walls, C_s is the Smagorinsky factor, and V is the volume of the computational cell. The value of the C_s has a significant effect on large-scale fluctuations in mean shear and transitional regimes. In order to address this problem, Germano et al. (1991) and following them Lilly (1992) proposed a method in which the Smagorinsky constant is calculated dynamically using the resolved motion data (Gemano et al., 1991, Lilly, 1992). In this study, the dynamic Smagorinsky-Lilly model is applied in order to eliminate limitations imposed by the traditional Smagorinsky-Lilly subgrid-scale model.

Validation of the Model

To validate the model, the computed pressure distribution on the blade was compared with experimental data from the wind tunnel experiment (Hand et al., 2001). The pressure distribution on the blade is caused by angular and axial momentum changes which characterises the wake. Thus, accurate prediction of the pressure coefficient provides information which is required to validate the model. Figure 9.4 shows a comparison between numerical simulations and experimental results for wind tunnel case. The results show that the developed LES model is a good match with experimental data, having a maximum difference of 8% between the experimental and computational data. It should also be noted that there was a limited number of pressure taps located on the surface of the physical blades and their uncertainty in accurately measuring the surface pressure, especially near the trailing and leading edges, should be taken into account. Higher discrepancies near the tip of the blade could be due to the effect of tip vortices and higher centrifugal forces which creates radial flow towards the tip.

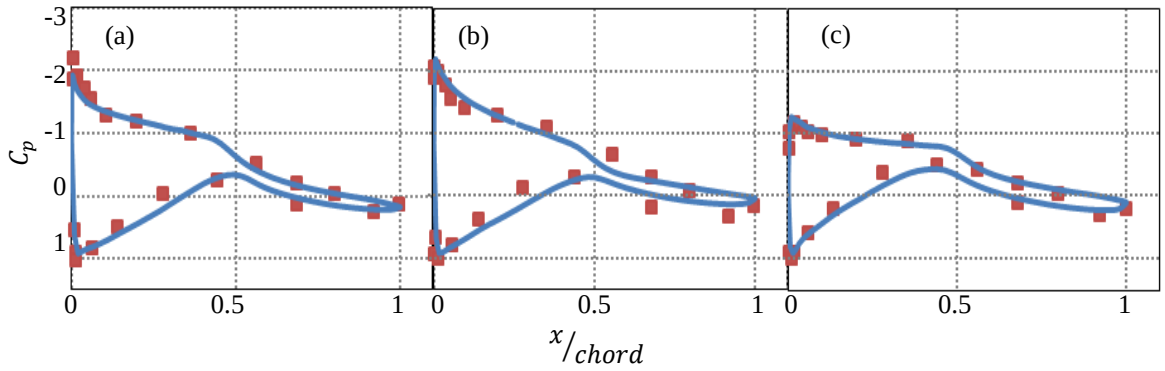

Figure 0.4 Comparison of the results of the computed pressure coefficient with experiment [3], a) $\frac{r}{R} = 0.3$, b) $\frac{r}{R} = 0.63$, c) $\frac{r}{R} = 0.95$.

Another parameter which can be used to validate the model is the total output power of the blades. Figure 5 shows the fluctuating output power calculated using the computed torque

of the blade. The averaged value of the output power obtained from the simulation is 5.73 (kW) which results in 4.6% discrepancy compared with the experimental data (Hand et al., 2001).

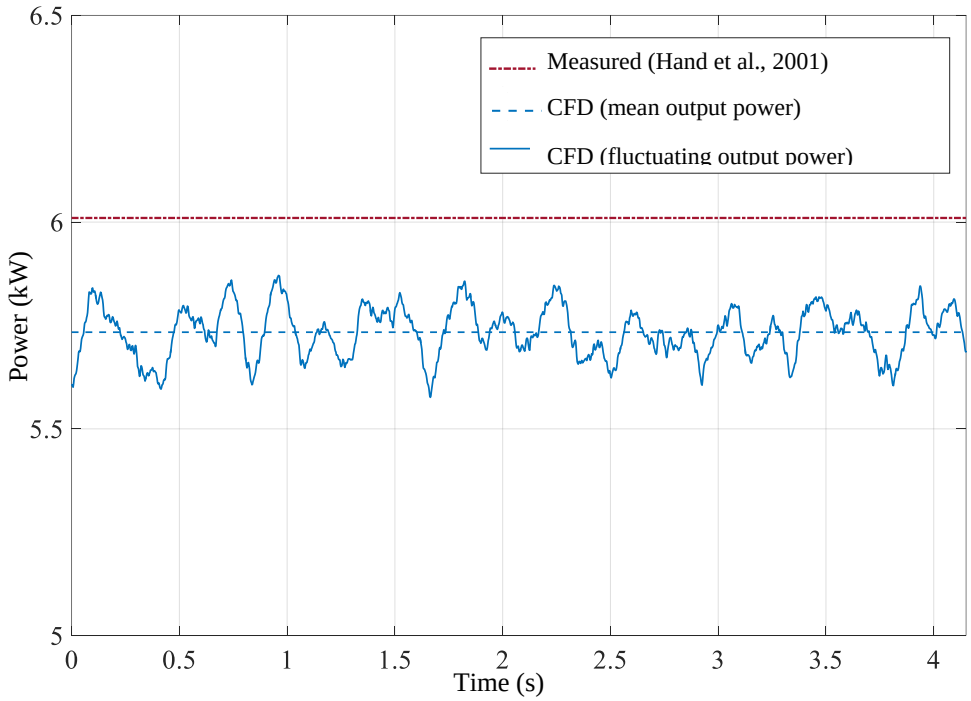

Figure 0.5 Fluctuating output power for wind tunnel case.

Results and Discussion

Figure 9.6 shows the vertical profiles of the normalised axial velocities averaged over time for several normalised locations downstream of the turbine. The effect of the tower is evident for both cases up to 4*D* downstream. This effect vanishes due to wake growth and turbulent mixing. For both cases the wake is almost axisymmetric about the axis of symmetry located close to the blade axis of rotation, especially for the region corresponding to the rotor blade. This observation is in agreement with previously published data and studies (Mo et al., 2.013). Passing through the wind turbine, airflow clearly loses its momentum, showing that the turbine is extracting energy from the incoming flow and hence producing a wake. This can be observed from the regions of reduced velocity, or velocity deficit, at *y/D*=1 where the

W-shaped velocity profiles are apparent. Velocity profiles show that the maximum decay occurs around the blade tip location, which corresponds to the helical ring of tip vortices. Moreover, the wake is spatially constrained by the walls in the wind tunnel, which results in an acceleration in the flow around the outside of the turbine. The velocity profiles also show that the difference between the velocity outside the wake for two cases increases with downstream distance. The velocity increase in the wind tunnel case is caused by both the wake growth and the confinement of the tunnel walls.

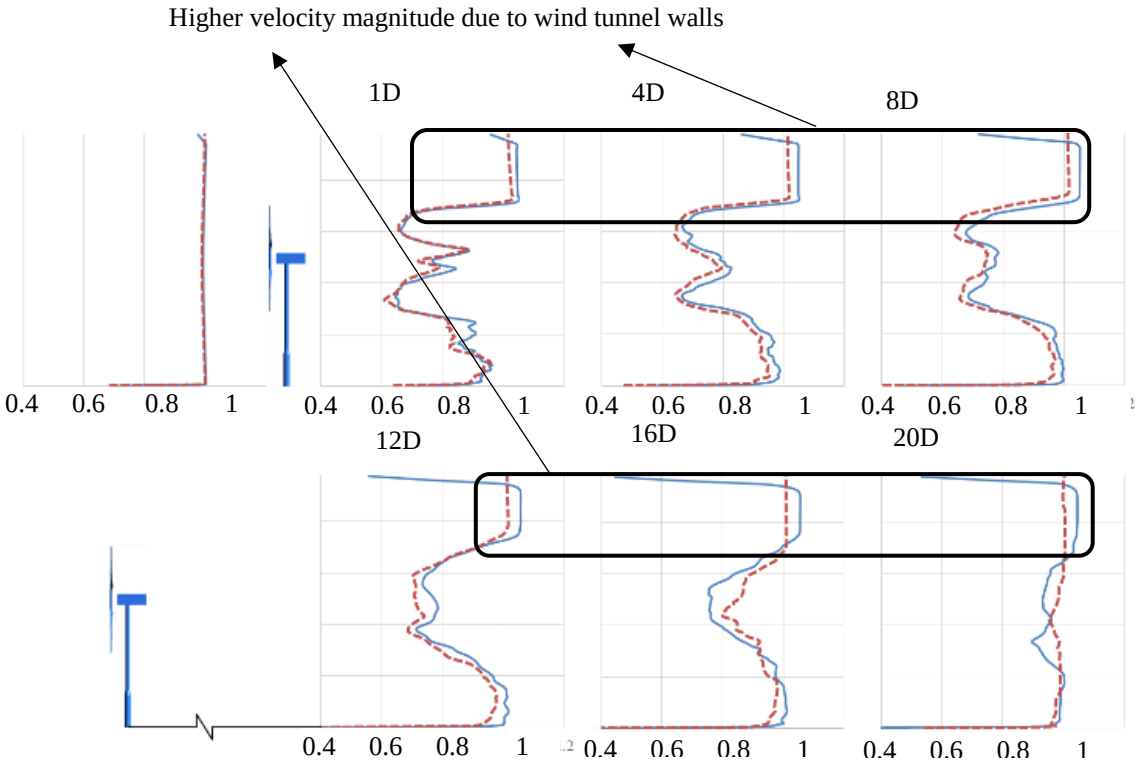

Figure 0.6 Normalised axial velocity profile downstream of wind turbines (dashed line represents the unconfined environment; solid line represents wind tunnel case).

Time-averaged axial velocity contours for the wind tunnel and unconfined environment are compared in Figure 9.7. The contours show significant differences in terms of velocity magnitude, wake growth and also wake length between the two cases. Additionally, the effects of the tower shadow can be observed in the region with relatively-reduced velocities

in the wake of the tower. In the wind tunnel case this effect dominates closer to the wind turbine by the higher velocity magnitude around the wake area. Whereas the effects of the wake exist for up to 20*D* downstream of the turbine in the wind tunnel simulation, in the unconfined case it vanishes by about 16*D* downstream.

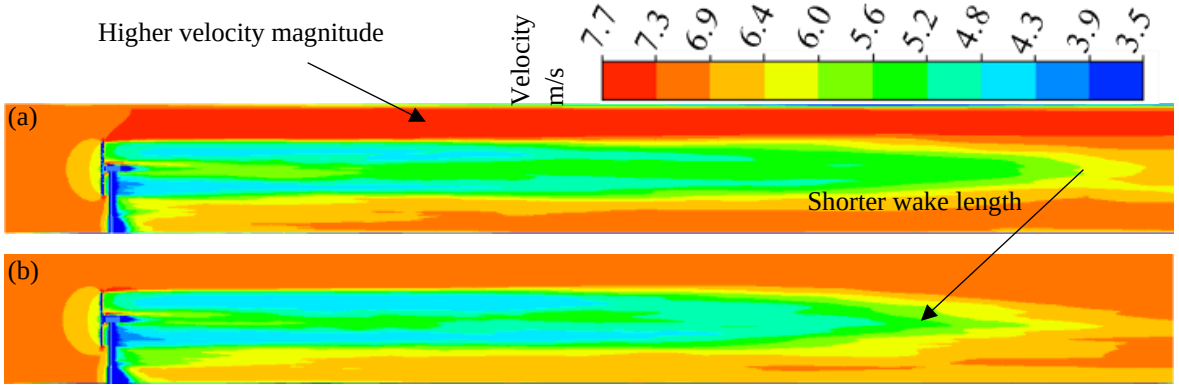

Figure 0.7 Axial velocity contour on midsection plane in, a) Wind tunnel, b) Unconfined environment.

The fluctuating output power for both cases is shown in Figure 9.8. The average output power extracted from the blades is higher when turbine is placed in the tunnel. This is due to the blockage effect which increases the velocity deficit, as can be seen in velocity contours (Figure 9.7). The higher axial-momentum gradient results in higher extracted power in wind tunnel case. Another indicator of the rotor performance is the thrust coefficient. The momentum loss through the rotor plane is balanced by thrust force which is manifested through pressure drop across the rotor. Thrust coefficient can be calculated as $C_T = \frac{\int (P_1 - P_2)\, dA}{\frac{1}{2}\rho A V^2}$, where P_1, P_2, A, and V are pressure in front of the rotor, pressure behind the rotor, area of the rotor, and velocity of the free stream respectively. The experimental thrust coefficient for the wind turbine at a wind speed of 7 m/s was found to be 0.487. The calculated thrust coefficients are 0.4945 and 0.4757 for wind tunnel and unconfined environment cases, respectively. The higher thrust in the wind tunnel can be explained by the flow acceleration due to confinement effect which results in higher pressure drop through

the rotor. Thrust coefficient can also be used as a validating parameter which shows only 1.5% deviation from the experimental data.

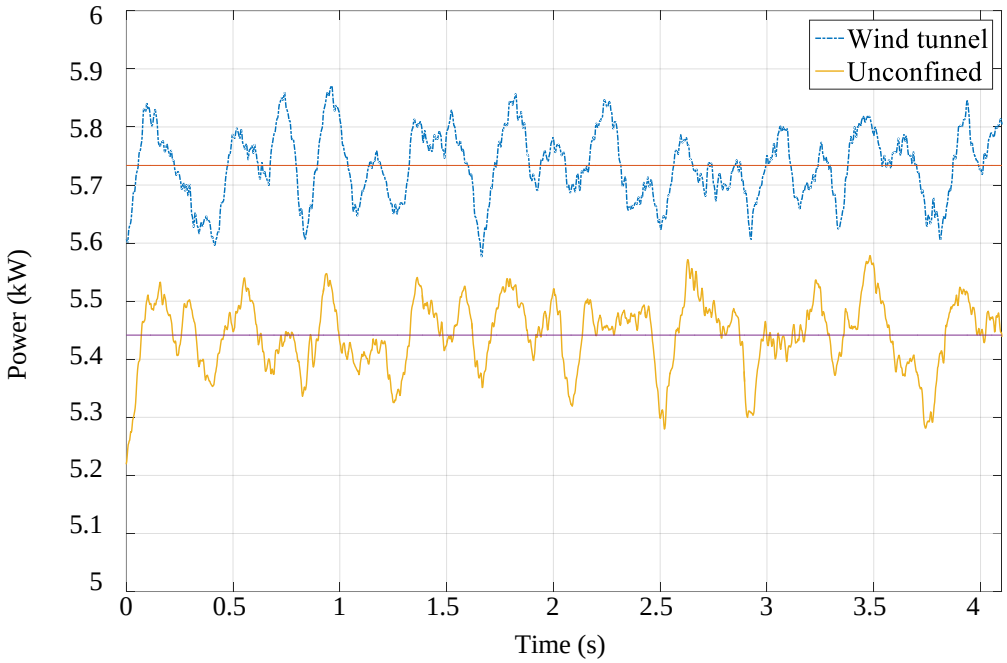

Figure 0.8 Instantaneous output power for a period of five revolutions of the blades.

The fast Fourier transform (FFT) of the fluctuating power is shown in Figure 9.9. The FFT was computed for the de-trended fluctuations for 1800 samples over 5 revolutions of the blades. The frequency of the first peak for both cases is equal to blade pass frequency, showing that the fluctuations are related to loads when the blade passes the region affected by the tower. The amplitude of the oscillation is 7.5% larger when the turbine is placed in unconfined environment, which shows that the blades are experiencing higher fatigue loads when there is no closed section around the turbine. It can be concluded that higher momentum and increased velocity due to confinement suppresses the effect of the tower when the turbine is located in the wind tunnel.

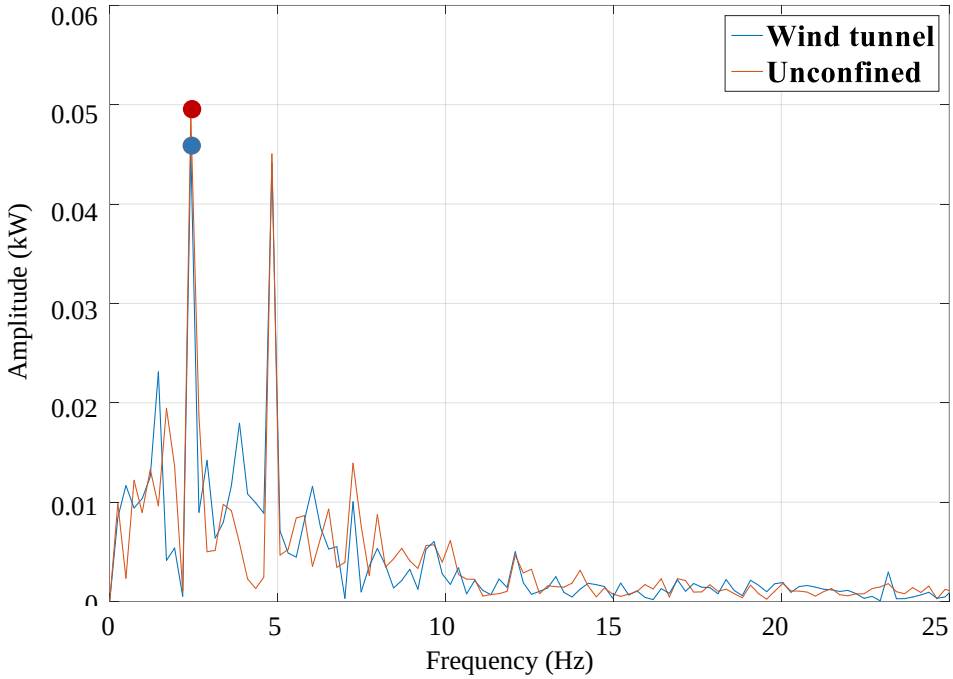

Figure 0.9 Fast Fourier Transform of power fluctuations.

Vorticity contours in Figure 10 show strong helical rings of tip vortices immediately downstream of the turbine. The ring of vortices is visible up to 4*D* downstream for wind tunnel case. Further downstream the ring starts to break down, and after 6*D* there is no distinct ring of vortices visible. A similar trend is observed for the unconfined environment, with the ring structure being visible up to 7*D* for this case, suggesting that the structure is more stable in the unconfined flow. This difference can be explained by the higher velocity gradient due to flow acceleration in wind tunnel case. In contrast, by 12*D* downstream the mixing rate in the unconfined environment exceeds the wind tunnel case. From this point the vortical structures become unstable, and without wall confinement, the wake expands faster and the rate of turbulent mixing increases. At 20*D* from the rotor the flow structure has substantially dissipated more in the unconfined flow case.

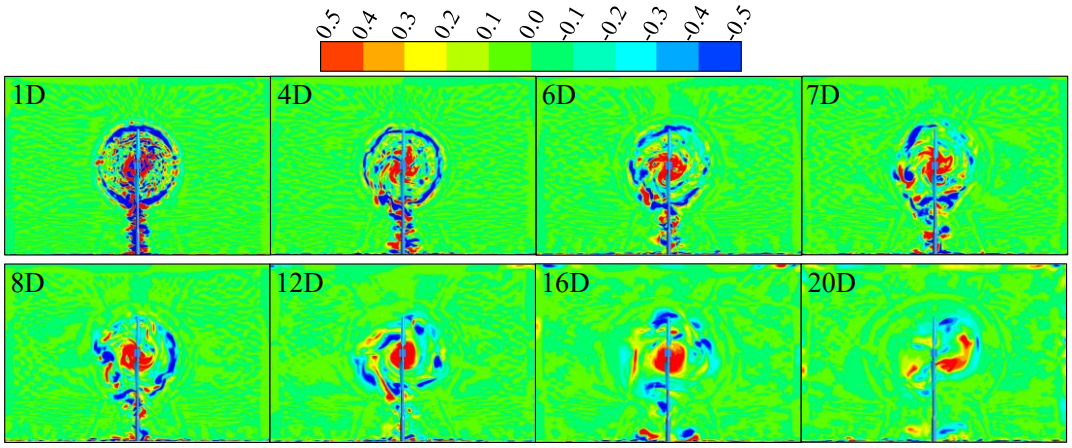

(a) Wind tunnel

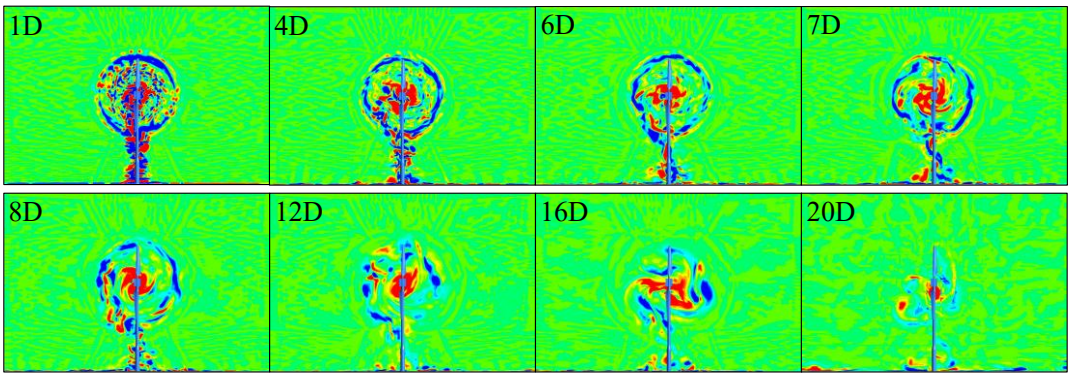

(b) Unconfined environment

Figure 0.10 Vorticity contours at several locations downstream of turbine.

Figure 9.11 shows the vorticity contour on the horizontal and vertical midsections. Tip vortices are distinctly visible up to 1.5*D* downstream. However, the trail of tip vortices can be traced far downstream almost up to 20*D* in the wind tunnel and 16*D* in the unconfined flow.

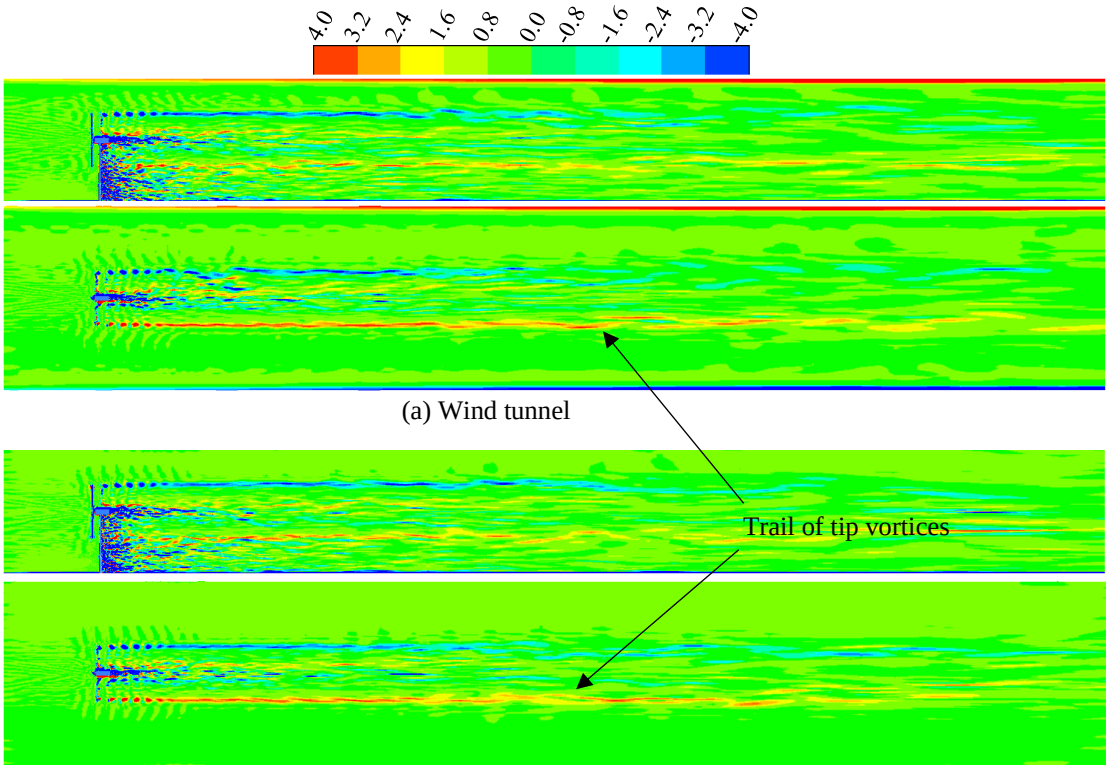

Figure 0.11 Vorticity contour showing the tip vortices downstream of the rotor.

The wake expansion is depicted in Figure 9.12 using the locations of the tip vortices to define the shear layer width. The wake expansion rate for the unconfined case is slightly higher than that of the wind tunnel case. These effects are attributed directly to the effects of confinement.

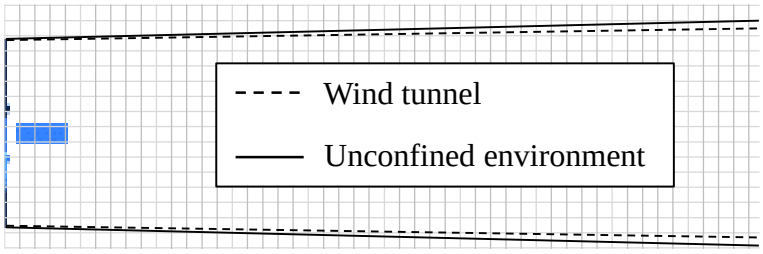

Figure 0.12 Comparison of wake expansion based on the locations of the tip vortices.

Conclusion

Large Eddy Simulation was used to investigate the effect of confinement on the wake of an NREL phase VI wind turbine.

Simulation results revealed that confinement has a significant effect on the spatial distribution of the mean velocity profile, wake structure and its development, even when the blockage ratio is less than 10%. The uniform incoming flow in the unconfined environment led to a relatively smaller length of the wake region. The results showed that the wake effect extends up to 20*D* downstream in wind tunnel case and up to 16*D* in unconfined case. Comparing wake expansion based on the location of the tip vortices showed that the unconfined environment has a higher expansion rate compared to wind tunnel case.

A W-shaped velocity profile was observed for all cases immediately behind the wind turbine, with the maximum velocity decay at a tip distance from the axis of rotation. It was observed that removing the surrounding walls results in slightly lower velocity in the wake region up to 12D downstream of the wind turbine. Further downstream the wake velocity recovers after 16D in unconfined case while region with reduced velocity extends to 20D for the wind tunnel.

This study reveals that the 10% limit for blockage ratio reported in previously-published literature is not sufficient to eliminate the effect of wind tunnel walls. Further studies should be carried out in order to specify the effective parameters and their role on blockage effect.

References

Vermeer, L.J., Sørensen, J.N. & Crespo, A., Wind Turbine Wake Aerodynamics, *Progress in Aerospace Sciences*, **39**, 2003, 467-510.

McTavish, S., Feszty, D. & Nitzsche, F., An Experimental and Computational Assessment of Blockage Effects on Wind Turbine Wake Development, *Wind Energy*, **17**, 2013, 1515-1529.

Hand, M.M., Simms, D.A., Fingersh, L.J., Jager, D.W., Cotrell, J.R., Schreck, S. & Larwood, S.M., Unsteady Aerodynamics Experiment Phase VI: Wind Tunnel Test Configurations and Available Data Campaigns, National Renewable Energy Laboratory, U.S Department of Energy Laboratory, 2001.

Germano, M., Piomelli, U., Moin, P. & Cabot, W.H., A Dynamic Subgrid-Scale Eddy Viscosity Model, *Physics of Fluids A*, **3**, 1991, 1760-1765.

Lilly, D.K., A Proposed Modification of the Germano Subgrid-Scale Closure Method, *Physics of Fluids A*, **4**, 1992, 633-635.

Mo, J.O., Choudhry, A., Arjomandi, M., Kelso, R. & Lee, Y.H., Effects of Wind Speed Changes on Wake Instability of a Wind Turbine in a Virtual Wind Tunnel Using Large Eddy Simulation, *Journal of Wind Engineering and Industrial Aerodynamics*, **117**, 2013, 38-56.